THE UNIVERSITY OF QUEENSLAND

AUSTRALIA

The role of calcium transporting proteins in the acquisition of resistance to trastuzumab

Elena Pera

MSc, MPhil

A thesis submitted for the degree of Doctor of Philosophy at

The University of Queensland in 2015

School of Pharmacy

Abstract

HER2-positive breast cancers represent approximately 20-25% of all breast cancers and are characterized by an overexpression of the growth factor receptor HER2. Trastuzumab, a monoclonal antibody, is a molecularly targeted therapeutic used in the treatment of this subtype of breast cancer. However, 30% of eligible patients have intrinsic resistance to trastuzumab and approximately 60% of patients who initially responded to this therapeutic, develop resistance within one year. Calcium transporters and modulators are known to be involved in breast cancer and in chemoresistance. However, their role has not been evaluated in HER2-positive trastuzumab resistant breast cancer cells. The aim of this project was to identify possible calcium related proteins associated with trastuzumab resistance.

In the first part of this thesis, the expression of Ca^{2+} transporters and modulators and their role in trastuzumab activity was assessed in the HER2-positive breast cancer cell line SKBR3. Ca^{2+} signaling profiling was also assessed using fluorescence imaging plate reader (FLIPR) assays. Inhibition of the expression of the Ca^{2+} channels TPC2, TRPV1 and the Ca^{2+} channel modulator STIM1 using siRNA decreased SKBR3 cellular proliferation. Silencing of STIM1, the Ca^{2+} pump SPCA1 and the Ca^{2+} permeable ion channel TRPM7 increased the anti-proliferative effects of trastuzumab in SKBR3 cells.

In the second part of this thesis, trastuzumab resistant and age-matched control cell lines were established from parental SKBR3 cells through seven months of continuous culturing in the presence of trastuzumab. Two trastuzumab treated colonies were selected for their resistance to trastuzumab (RT1 and RT2). Two other colonies were selected from age-matched controls because of their development of *de novo* resistance to trastuzumab (RV1 and RV2). Two age-matched cell lines that retained their sensitivity to trastuzumab were selected as controls (SV1 and SV2). Levels of mRNA expression of 45 Ca^{2+} channels, pumps and channel modulators were evaluated using quantitative RT-PCR. An siRNA screen of selected targets to identify targets that when silenced could restore trastuzumab sensitivity was also performed. Additionally Ca^{2+} signaling profiling and the quantitation of HER2, EGFR and IGF1R protein expression were conducted. All trastuzumab resistant cell lines maintained their overexpression of the HER2 receptor. Significantly increased mRNA levels of the voltage-gated calcium Ca^{2+} channel $Ca_V3.2$ was observed in both *de novo* resistant cell lines RV1 and RV2 compared to control cell lines SV1 and SV2. Acquired resistant

cell lines RT1 and RT2 showed altered sensitivity to the purinergic receptor activator ATP, indicating a possible remodeling of Ca^{2+} signaling in these trastuzumab resistant cell lines.

In the third part of this thesis, specific experiments were conducted to further evaluate two selected targets, the Ca^{2+} permeable ion channels $Ca_V3.2$ and TRPM7 channel. Pharmacological inhibition and silencing of $Ca_V3.2$ channel did not reverse trastuzumab resistance. However, $Ca_V3.2$ mRNA levels were higher in the basal HER2-positive trastuzumab resistant HCC1569 breast cancer cell line compared to the luminal HER2-positive trastuzumab sensitive SKBR3 cell line. Partial siRNA-mediated silencing of TRPM7 or pharmacological inhibition of TRPM7 channel activity did not reverse trastuzumab resistance in the trastuzumab resistant cell line RV1. However, the TRPM7 kinase inhibitor NH125 was able to promote trastuzumab activity in the trastuzumab resistant cell line RV1. Further studies are required to definitively associate TRPM7 kinase with trastuzumab resistance, given the reported sensitivity of other atypical α-kinases to NH125.

In the last part of this thesis publically available data was mined to identify other potential calcium related proteins associated with trastuzumab resistance. These data sets included cDNA microarray analysis of trastuzumab resistant and sensitive SKBR3 cell lines and trastuzumab resistant breast cancer clinical samples and proteomic analysis of trastuzumab resistant and sensitive SKBR3 cell lines. These analyses indicated that the Ca^{2+} ATPase pump SERCA3 and galectin-3 may be associated with trastuzumab resistance.

Results presented in this thesis suggest that the acquisition of trastuzumab resistance may be associated with the expression and/or activity of specific Ca^{2+} channels and pumps, including SERCA3, $Ca_V3.2$ channel and TRPM7 and the Ca^{2+}-related protein galectin-3. Further studies of these proteins may help identify new approaches to reverse trastuzumab resistance and/or identify new biomarkers for predicting trastuzumab sensitivity in HER2-positive breast cancers.

Declaration by author

This thesis is composed of my original work, and contains no material previously published or written by another person except where due reference has been made in the text. I have clearly stated the contribution by others to jointly-authored works that I have included in my thesis.

I have clearly stated the contribution of others to my thesis as a whole, including statistical assistance, survey design, data analysis, significant technical procedures, professional editorial advice, and any other original research work used or reported in my thesis. The content of my thesis is the result of work I have carried out since the commencement of my research higher degree candidature and does not include a substantial part of work that has been submitted to qualify for the award of any other degree or diploma in any university or other tertiary institution. I have clearly stated which parts of my thesis, if any, have been submitted to qualify for another award.

I acknowledge that an electronic copy of my thesis must be lodged with the University Library and, subject to the policy and procedures of The University of Queensland, the thesis be made available for research and study in accordance with the Copyright Act 1968 unless a period of embargo has been approved by the Dean of the Graduate School.

I acknowledge that copyright of all material contained in my thesis resides with the copyright holder(s) of that material. Where appropriate I have obtained copyright permission from the copyright holder to reproduce material in this thesis.

Elena Pera
MSc, MPhil

Publications during candidature

Conference abstracts

- **E Pera**, AA Peters, SJ Roberts-Thomson, GR Monteith. *Profiling of calcium transporters and modulators in trastuzumab resistant SKBR3R breast cancer cells*. TPTR Conference. Boston, USA. March 2014.
- **E Pera**, AA Peters, SJ Roberts-Thomson, GR Monteith. *Calcium transporters and modulator profiling in trastuzumab resistant SKBR3R breast cancer cells*. The Australian Society of Clinical and Experimental Pharmacologists and Toxicologists (ASCEPT) Conference, Melbourne, VIC, Australia. December 2013.
- **E Pera**, AA Peters, SJ Roberts-Thomson, GR Monteith. *Calcium pumps, channels and channel modulator profiling in trastuzumab resistant SKBR3R breast cancer cells.* Ca^{2+} signaling Gordon Conference, Lucca, Italy. June 2013.
- **E Pera**, AA Peters, SJ Roberts-Thomson, GR Monteith. *Alteration of SKBR3 cancer cell proliferation by silencing specific calcium pumps, channels and channel modulators.* The Australian Society of Clinical and Experimental Pharmacologists and Toxicologists (ASCEPT) Conference, Sydney, NSW, Australia. December 2012.
- **E Pera**, AA Peters, SJ Roberts-Thomson, GR Monteith. *Consequences of the silencing of specific calcium pumps, channels and channel modulators on the proliferation of SKBR3 HER2-positive breast cancer cells.* EMBO conference, Nice, France. September 2012.
- **E Pera**, AA Peters, SJ Roberts-Thomson, GR Monteith. *Calcium channels, pumps and channel modulators and proliferation of SKBR3 HER2-positive cancer cells.* European Calcium Society (ECS) meeting, Toulouse, France. September 2012.

Publications included in this thesis

No publications included

Contributions by others to the thesis

This PhD research was conceived, designed and performed by me under the supervision of my advisory team: Prof Gregory Monteith, Prof Sarah Roberts-Thomson, Dr Amelia Peters.

Quantitative RT-PCR experiments to evaluate TRPM7 silencing (Figure 5.3) were performed by Dr Amelia Peters at the School of Pharmacy. Dr Peters used RNA samples from the trastuzumab resistant breast cancer cell line RV1 that I isolated.

Microarray data incorporated into the chapter 4 (Figure 4.3 and Figure 4.4) and the analysis on the gene expression profile dataset of clinical patients resistant to trastuzumab in chapter 6 (Table 6.4) were supplied by A/Prof Paraic Kenny.

Statement of parts of the thesis submitted to qualify for the award of another degree

None

Acknowledgements

I would like to express my special appreciation and thanks to my advisor Professor Greg Monteith, you have been a tremendous mentor for me. I would like to thank you for encouraging my research and for allowing me to grow as a research scientist. Your advice on both research as well as on my career have been priceless. I would also like to thank my advisory team members: Professor Sarah Roberts-Thomson, thank you for your advice and guidance and Dr Amelia Peters, thank you for all the patience you have shown me throughout my PhD. You have helped make my PhD an enjoyable experience and for your brilliant comments and suggestions, thank you.

I would like to thank the Calcium Signaling in Cancer Research Laboratory for their support, feedback and suggestions during my PhD. In particular, I would like to thank Dr Diana Ross for her support and friendship in and out of the laboratory; I could not have done it without your help! To Kunsala Yapa, thank you not only for being a great lab member, but also for your friendship.

A special thanks goes to my family. Words cannot express how grateful I am for all the sacrifices that you have made on my behalf since I moved to Australia. Thank you. Thank you for being so understanding, supporting and loving even from the other side of the world. Special thanks to my sister, who is also my best friend; she has been always there for me.

I would also like to thank all of my friends who supported me in writing, and motivating me to strive towards my goal. I would like to thank my dog Nerone, for keeping me company throughout my Australian journey. You have been the perfect audience for all my practice presentations. I would also like to express my appreciation to my beloved partner Simone, who has given me great support and encouragement, thank you for being at my side.

Lastly, I would like to express my gratitude to The University of Queensland and the Australia Government for supporting my PhD candidature with a University of Queensland Centennial Scholarship and International Postgraduate Research Scholarship.

Keywords

breast, cancer, trastuzumab, resistance, calcium signaling, calcium transporters, gene expression.

Australian and New Zealand Standard Research Classifications (ANZSRC)

ANZSRC code: 060111, Biochemistry and Cell Biology, Signal Transduction, 20%
ANZSRC code: 111201, Medical and Health Sciences, Oncology and Carcinogenesis, Cancer Cell Biology, 40%
ANZSRC code: 111207, Medical and Health Sciences, Oncology and Carcinogenesis, Molecular Targets, 40%

Fields of Research (FoR) Classification

FoR code:0601, Biochemistry and Cell Biology, 80%
FoR code: 0699, Other Biological Sciences, 20%

TABLE OF CONTENTS

LIST OF FIGURES

LIST OF TABLES

LIST OF ABBREVIATIONS AND FULL GENE NAMES

ER	Endoplasmic Reticulum
$[Ca^{2+}]_i$	Intracellular free Ca^{2+} Concentration
A8MYK9	Putative Uncharacterized Protein ATP2A3 (SERCA3)
AA	Acetic Acid
ABCC2	ATP-Binding Cassette Sub-Family C Member 2
ADA	Adenosine Deaminase
ADCC	Antibody-Dependent Cellular Cytotoxicity
ADM	Adrenomedullin
ADORA2A	Adenosine A2a Receptor
AM	Acetoxymethyl
AMPK	5' AMP-activated Protein Kinase
ANKRD58	Ankyrin Repeat Domain Family Member D
ANKS6	Ankyrin Repeat And Sterile Alpha Motif Domain Containing 6
ANXA11	Annexin A11
ANXA2	Annexin A2
ANXA7	Annexin A7
AQP3	Aquaporin 3
ASPH	Aspartate Beta-Hydroxylase
ASPHD1	Aspartate Beta-Hydroxylase Domain Containing 1
ATCC	American Type Culture Collection
ATP	Adenosine Triphosphate
ATP1B1	Sodium/Potassium-Transporting ATPase Subunit Beta-1
ATP2A3	ATPase, Ca^{2+} Transporting (SERCA3)
Bad	Bcl-2-Associated Death Promoter
Bak	Bcl-2 Homologous Antagonist/Killer
Bax	Bcl-2–Associated X Protein
Bcl-2	B-Cell Lymphoma 2 Protein
Bcl-XL	Bcl-2 And B-Cell Lymphoma-Extra Large
BDKRB1	Bradykinin Receptor B1
BDKRB2	Bradykinin Receptor B2
BSA	Bovine Serum Albumin

CACNA1I	Calcium Channel Voltage-Dependent T-Type Alpha 1I Subunit ($Ca_V3.3$)
CACNB1	Calcium Channel Voltage-Dependent Beta 1 Subunit
CACNB2	Voltage-Dependent Calcium Channel Beta 2 Subunit
CALM1	Calmodulin 1
CaMK	Ca^{2+}-CaM-Dependent Protein Kinase
CAMK2G	Calcium/Calmodulin-Dependent Protein Kinase II Gamma
CAPN1	Calpain 1
CAPN2	Calpain 2
Catsper 1	Cation Channels of Sperm 1
Catsper 2	Cation Channels of Sperm 2
Catsper 3	Cation Channels of Sperm 3
Catsper 4	Cation Channels Of Sperm 4
Ca_Vs	Voltage-Gate Ca^{2+} Channels
$Ca_V1.1$	Voltage-Gate Ca^{2+} L-Type 1.1 Channel
$Ca_V1.2$	Voltage-Gate Ca^{2+} L-Type 1.2 Channel
$Ca_V1.3$	Voltage-Gate Ca^{2+} L-Type 1.3 Channel
$Ca_V1.4$	Voltage-Gate Ca^{2+} L-Type 1.4 Channel
$Ca_V2.1$	Voltage-Gate Ca^{2+} P-Type 2.1 Channel
$Ca_V2.2$	Voltage-Gate Ca^{2+} N-Type 2.2 Channel
$Ca_V2.3$	Voltage-Gate Ca^{2+} R-Type 2.3 Channel
$Ca_V3.1$	Voltage-Gate Ca^{2+} T-Type 3.1 Channel
$Ca_V3.2$	Voltage-Gate Ca^{2+} T-Type 3.2 Channel
$Ca_V3.3$	Voltage-Gate Ca^{2+} T-Type 3.3 Channel
CCDC109B	Coiled-Coil Domain Containing 109B (MCU)
CCL2	Chemokine (C-C Motif) Ligand 2
CCL21	Chemokine (C-C Motif) Ligand 21
CCL5	Chemokine (C-C Motif) Ligand 5
CCR5	Chemokine (C-C Motif) Receptor 5
CD40	CD40 Molecule, TNF Receptor Superfamily Member 5
CDH24	cDNA FLJ25193 Fis
Cdk2	Cyclin-Dependent Kinase 2
CHRNA4	Cholinergic Receptor Nicotinic Alpha 4
CLCA2	Chloride Channel Accessory 2

CLIC4	Chloride Intracellular Channel 4
CORO1A	Coronin Actin Binding Protein 1A
CPA	Cyclopiazonic Acid
CRAC	Ca^{2+}-Release Activated Ca^{2+} Channel
CT	Comparative Threshold Cycle
CTGF	Connective Tissue Growth Factor
CX3CL1	Chemokine (C-X3-C Motif) Ligand 1
CXCR3	Chemokine (C-X-C Motif) Receptor 3
CXCR4	Chemokine (C-X-C Motif) Receptor 4
DAPI	4',6-Diamidino-2-Phenylindole
DENND2D	cDNA Dkfzp667i053
DHRS2	Dehydrogenase/Reductase (SDR Family) Member 2
DHRS3	Dehydrogenase/Reductase (SDR Family) Member 3
dNTPs	Deoxynucleotide Triphosphates
dsRNA	Double-Stranded Molecules
DUSP6	Dual Specificity Phosphatase 6
ECM	Extracellular Matrix
EDN2	Endothelin 2
EDTA	Ethylenediaminetetraacetic Acid
eEF2	Eukaryotic Elongation Factor 2
eEF2K	Eukaryotic Elongation Factor 2 Kinase
EGF	Epidermal Growth Factor
EGFR	Human Epidermal Growth Factor Receptor 1
EMT	Epithelial-Mesenchymal Transition
FAK	Focal Adhesion Kinase
FAM26B	Calcium Homeostasis Modulator 2
FBS	Fetal Bovine Serum
FDA	Food and Drug Administration
FLIPR	Fluorometric Imaging Plate Reader
FYN	FYN Oncogene
GAL	Galanin/GMAP Prepropeptide
GIMAP5	GTPase IMAP Family Member 5
GNAS	GNAS Complex Locus

GPCR	G Protein Coupled Receptor
GRB2	Growth Factor Receptor-Bound Protein 2
GSTO1	Glutathione S-Transferase Omega 1
HDPP	HER2-Derived Prognostic Predictor
HER1	Human Epidermal Growth Factor Receptor 1
HER2	Human Epidermal Growth Factor Receptor 2
hERG	Human Ether-A-Go-Go Potassium Channel
HIF-1α	Hypoxia-Inducible Factor-1 A
HRP	Horseradish Peroxidase
IGF	Insulin-Like Growth Factor
IGF1R	Insulin-Like Growth Factor Receptor
IGFBP	IGF Binding Protein
IKK	Iκb Kinase
IL1R1	Interleukin 1 Receptor Type I
IP_3	Inositol Triphosphate
IP3Rs	Inositol Triphosphate Receptor Ca^{2+} Channels
IP3R1	Inositol 1,4,5-Trisphosphate Receptor Type 1
IP3R2	Inositol 1,4,5-Trisphosphate Receptor Type 2
IP3R3	Inositol 1,4,5-Trisphosphate Receptor Type 3
ITPR1	Inositol 1,4,5-Trisphosphate Receptor Type 1
JPH2	Junctophilin 2
KCNMA1	Potassium Large Conductance Calcium-Activated Channel Subfamily M Alpha Member 1 ($K_{Ca}1.1$)
KCNN4	Potassium Intermediate/Small Conductance Calcium-Activated Channel Subfamily N Member 4 ($K_{Ca}3.1$)
LCK	Lymphocyte-Specific Protein Tyrosine Kinase
LGALS3	Galectin-3
LGALS3BP	Galectin-3-Binding Protein
LILRB1	Leukocyte Immunoglobulin-Like Receptor Subfamily B Member
LogFC	Logarithm Fold Change
MAPK	Mitogen-Activated Protein Kinases
MCU	Mitochondrial Calcium Uniporter
MGB	Minor Groove Binder

MMPs	Matrix Metalloproteinases
MMP9	Matrix Metalloproteinase 9
MTS	[3-(4,5-Dimethylthiazol-2-Yl)-5-(3-Carboxymethoxyphenyl)-2-(4-Sulfophenyl)-2H-Tetrazolium
MUC4	Mucin-4
MYB	Myb Oncogene
NAADP	Nicotinic Acid Adenine Dinucleotide Phosphate
NCKX	$Na^+/Ca^{2+}/K^+$ Exchangers
NCX	Na^+/Ca^{2+} Exchangers
ND	Non Detected
NF-κB	Nuclear Factor Kappa-Light-Chain-Enhancer Of Activated B-Cells
NFAT	Nuclear Factor of Activated T-Cells
NMB	Neuromedin B
NMDA	N-Methyl-D-Aspartate
Orai1	Calcium release-activated calcium channel protein 1
Orai2	Calcium release-activated calcium channel protein 2
Orai3	Calcium release-activated calcium channel protein 3
P2RX5	Purinergic Receptor P2X Ligand-Gated Ion Channel 5
PACSIN1	Protein Kinase C And Casein Kinase Substrate In Neurons 1
PANTHER	Protein ANalysis THrough Evolutionary Relationships
PBS	Phosphate Buffer Saline
pCR	Pathological Complete Response
PI3K	Phosphatidylinositol 3-Kinase
PIP_2	Phosphatidylinositol 4,5-Bisphosphate
PIP_3	Phosphatidylinositol (3,4,5)-Triphosphate
PKD1	Polycystic Kidney Disease 1
PMCAs	Plasma Membrane Ca^{2+} ATPase
PMCA1	Plasma Membrane Ca^{2+} ATPase 1
PMCA2	Plasma Membrane Ca^{2+} ATPase 2
PMCA4	Plasma Membrane Ca^{2+} ATPase 3
PP2A	Protein Phosphatase 2A
PRKCB	Protein Kinase C Beta
PRNP	Prion Protein

PSEN1	Presenilin 1
PSS	Physiological Salt Solution
PTEN	Phosphatase And Tensin Homolog
PTGS1	Prostaglandin-Endoperoxide Synthase 1 (Prostaglandin G/H Synthase And Cyclooxygenase)
PTPN21	Protein Tyrosine Phosphatase Non-Receptor Type 21
PTPRC	Protein Tyrosine Phosphatase Receptor Type C
PVDF	Polyvinylidene Difluoride
QIMR	Queensland Institute of Medical Research
RASA3	RAS P21 Protein Activator 3
RCVRN	Recoverin
RD	Residual or Recurrent Disease
REIs	Reactive Oxygen Intermediates
RLGS	Restriction Landmark Genomic Scanning
RNAi	RNA Interference
ROCs	Receptor-Operated Ca^{2+} Channels
RT1	Resistant Trastuzumab 1
RT2	Resistant Trastuzumab 2
RTK	Tyrosine Kinase Receptors
RV1	Resistant Vehicle 1
RV2	Resistant Vehicle 2
RyR	Ryanodine Receptors
S100A10	S100 Calcium Binding Protein A10
S100A3	S100 Calcium Binding Protein A3
S100A4	S100 Calcium Binding Protein A4
S100A5	S100 Calcium Binding Protein A5
S100A6	S100 Calcium Binding Protein A6
S100A7	S100 Calcium Binding Protein A7
S100A8	S100 Calcium Binding Protein A8
S100A9	S100 Calcium Binding Protein A9
S100P	S100 Calcium Binding Protein P
SAA1	Serum Amyloid A1
SCAMP5	Secretory Carrier Membrane Protein 5

SERCAs	Sarcoendoplasmic Reticulum Ca^{2+} ATPases
SERCA1	Sarcoendoplasmic Reticulum Ca^{2+} ATPase 3
SERCA2	Sarcoendoplasmic Reticulum Ca^{2+} ATPase 2
SERCA3	Sarcoendoplasmic Reticulum Ca^{2+} ATPase 1
SERPINA3	Serpin Peptidase Inhibitor
SILAC	Stable Isotope Labeling By Amino Acids In Cell Culture
siNT	Non-Targeting siRNA
siRNA	Small Interfering RNA
SLC24A1	Solute Carrier Family 24 (Sodium/Potassium/Calcium Exchanger) Member 1 (NCKX1)
SLC24A3	Solute Carrier Family 24 (Sodium/Potassium/Calcium Exchanger) Member 3 (NCKX3)
SLC24A6	Solute Carrier Family 8 (Sodium/Lithium/Calcium Exchanger) Member B1 (NCKX6)
SLC25A4	Solute Carrier Family 25 (Mitochondrial Carrier; Adenine Nucleotide Translocator) Member 4
SOCs	Store-Operated Ca^{2+} Channels
SOCE	Store Operated Calcium Entry
SPCAs	Secretory Pathway Ca^{2+}- ATPases
SPCA1	Secretory Pathway Ca^{2+}- ATPase 1
SPCA2	Secretory Pathway Ca^{2+}- ATPase 2
SRI	Sorcin
ssRNA	Single-stranded RNA
STAT3	Signal transducer and activator of transcription 3
STIM	Stromal Interacting Molecule
STIM1	Stromal Interacting Molecule 1
STIM2	Stromal Interacting Molecule 2
SV1	Sensitive Vehicle 1
SV2	Sensitive Vehicle 2
TFNα	Tumor Necrosis Factor α
TG	Thapsigargin
TG2	Transglutaminase-2
TGFBI	Transforming Growth Factor Beta 1

TGM1	Transglutaminase 1
TMBIM1	Transmembrane BAX Inhibitor Motif Containing 1
TMC6	Transmembrane Channel-Like 6
TMEM165	Transmembrane Protein 165
TNF	Tumor Necrosis Factor
TPC	The Two-Pore Channel
TPC1	The Two-Pore Channel 1
TPC2	The Two-Pore Channel 2
TRAIL	TNF-Related Apoptosis-Inducing Ligand
TRIM27	Tripartite Motif-Containing 27
TRP	Transient Receptor Potential Ca^{2+} Channels
TRPC1	Transient Receptor Potential Cation Channel Canonical 1
TRPC4	Transient Receptor Potential Cation Channel Canonical 4
TRPC5	Transient Receptor Potential Cation Channel Canonical 5
TRPC6	Transient Receptor Potential Cation Channel Canonical 6
TRPM2	Transient Receptor Potential Cation Channel Melastatin 2
TRPM3	Transient Receptor Potential Cation Channel Melastatin 3
TRPM4	Transient Receptor Potential Cation Channel Melastatin 4
TRPM7	Transient Receptor Potential Cation Channel Melastatin 7
TRPM8	Transient Receptor Potential Cation Channel Melastatin 8
TRPV1	Transient Receptor Potential Cation Channel Vanilloid 1
TRPV2	Transient Receptor Potential Cation Channel Vanilloid 2
TRPV3	Transient Receptor Potential Cation Channel Vanilloid 3
TRPV4	Transient Receptor Potential Cation Channel Vanilloid 4
TRPV5	Transient Receptor Potential Cation Channel Vanilloid 5
TRPV6	Transient Receptor Potential Cation Channel Vanilloid 6
TUBB3	Tubulin Beta 3 Class III
TUBB4	Tubulin, Beta 4A Class Iva
TUBB6	Tubulin Beta 6 Class V
VAMP5	Vesicle-Associated Membrane Protein 5
VOCs	Voltage-Operated Ca^{2+} Channels
WNT5A	Wingless-Type MMTV Integration Site Family Member 5A
ZP3	Zona Pellucida Glycoprotein 3 (Sperm Receptor)

1 Introduction

1.1 Calcium Homeostasis

Calcium is abundant in nature and is an essential element of the body; it has great versatility and is involved in almost every cellular process (1, 2). The concentration of this ion is tightly regulated within the cell via processes that are often classed as “on” or “off” mechanisms. Multiple mechanisms can increase or decrease cytosolic Ca^{2+} to maintain correct homeostasis (3) (Fig. 1.1).

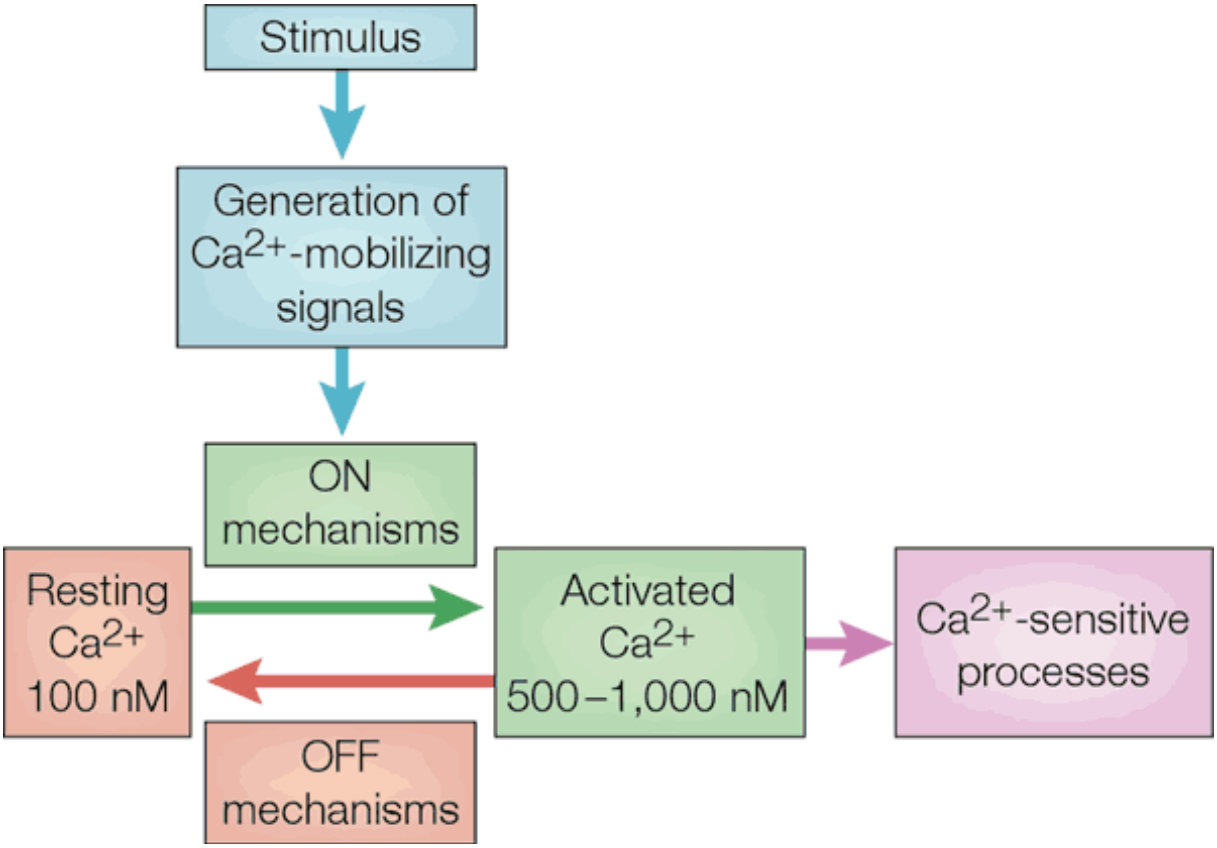

Figure 1.1 Calcium homeostasis

Stimulation of the cell generates Ca^{2+} mobilizing signals that act as ON mechanisms to trigger an increase in the intracellular concentration of free Ca^{2+} leading to a cellular response. The response is terminated by OFF mechanisms that restore Ca^{2+} to its resting level. (Taken from Berridge MJ, Lipp P and Bootman MD, 2000 (3))

At rest the calcium concentration in the cytosol is maintained at low levels (~ 100 nM range) mainly due to the work of active calcium transporters located on the endoplasmic reticulum (ER) and the plasma membrane, which allow the translocation of Ca^{2+} ions (4). The extracellular concentration of free Ca^{2+} is much higher and is in the range of 1-2 mM. Lipid bilayers are impermeable to calcium ions, thus their transit across membranes occurs mainly via channels and pumps (1). Stimulation of the cell can cause an influx of Ca^{2+} into the cytoplasm through channels on the plasma membrane or the activation of Ca^{2+} channels on the ER resulting in Ca^{2+} release from internal stores. These events can increase free Ca^{2+} in some cases to the μM range triggering a variety of cellular responses (3).

1.1.1 Calcium processes

Ca^{2+} controls numerous cellular processes such as fertilization, proliferation, development, learning and memory, contraction, secretion and cell death (3). This is due to the great versatility in the nature of Ca^{2+} increases in terms of speed, amplitude and spatio-temporal patterning (3, 5). Ca^{2+} signals can be highly localized to small regions surrounding the mouth of a channel (6), or can be manifested as Ca^{2+} release waves that spread through the entire cell or even across populations of cells (3). Deregulation of Ca^{2+} signaling may lead to altered cellular mechanisms, which may cause or promote cardiovascular disease, neuropathies, inflammation, endocrinological disorders, osteopathy and cancer (7).

Sections 1.1.1.1 – 1.1.1.4 will focus on the role of calcium in vital processes in cancers in particular proliferation, cell death, migration and metastasis.

1.1.1.1 Cell proliferation

The cell cycle is a series of events that allow cells to divide and duplicate. In eukaryotic cells, this includes four phases: two growth phases (G1 and G2) interspaced by the DNA synthesis phase (S) and the cell division phase (M); cells that are not undergoing cell division leave the normal cycle and remain in a quiescence state (G0) (8). The progression of the cell cycle is monitored by key points, which verify the status of the cell, in order to avoid aberrant cell proliferation (8).

Ca^{2+} signals are involved at various stages of the cell cycle and manipulation of Ca^{2+} signaling could affect cellular proliferation and gene transcription (9). Ca^{2+} transients have been detected during early G1 and G1-S transition and at other stages during the mitotic process (10).

Calmodulin (CaM), a Ca^{2+}-binding protein that works as a major intracellular receptor for Ca^{2+}, and Ca^{2+}-CaM-dependent protein kinases (CaMKs), appear to be involved in cell cycle progression (10, 11). Indeed, it has been shown that CaM levels change during the cell cycle, mostly during the G1-S transition and progression into G1 and M phases (12, 13) (Fig. 1.2). CaM has been linked in numerous studies to cell proliferation (13) and transformation (10), while CaMKs are required during G1, G2, M phases and during the metaphase to anaphase transition (10, 11, 14) (Fig. 1.2).

Calcineurin is a Ca^{2+}-dependent serine-threonine phosphatase regulated by the Ca^{2+}/calmodulin complex and, as for CaMKs (10), it has been shown to promote accumulation of cyclin D1 in the G1 phase (15) (Fig. 1.2). Cyclins act as growth factor sensors in mammalian cells and are often implicated in oncogenesis (16).

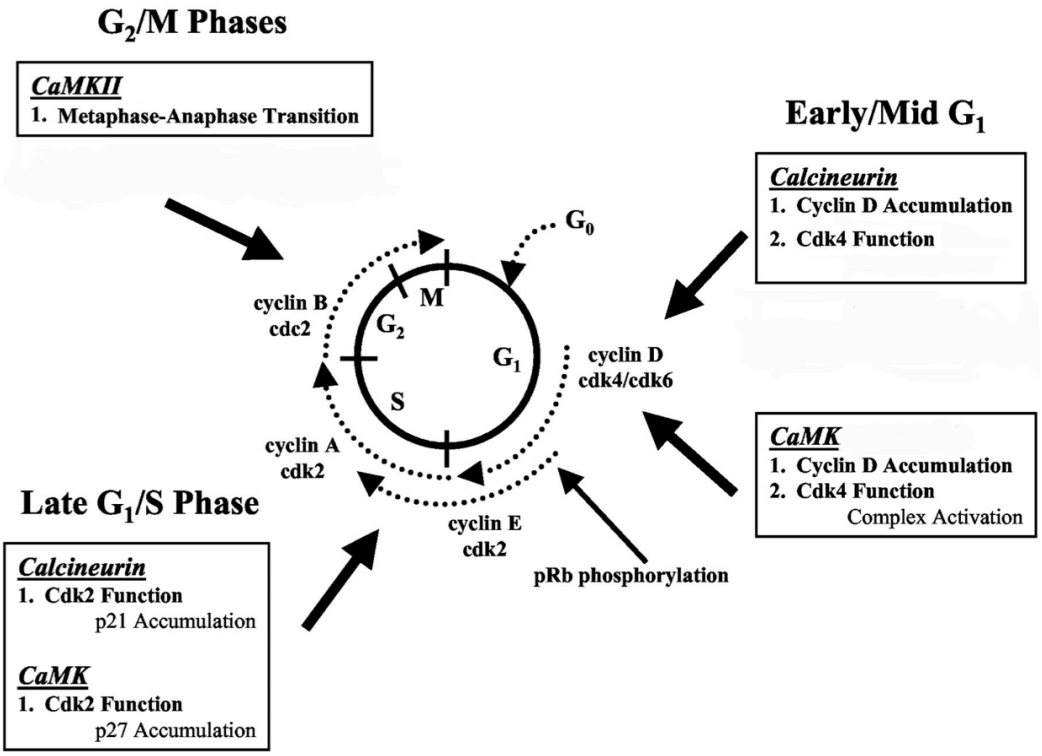

Figure 1.2 Regulation of cell cycle by Ca^{2+} effectors

During G1 phase, calcineurin and CamKs produce accumulation of cyclin D1. In late G1 or S phase, inhibition of calcineurin and CaMK leads to p21 and p27 accumulation, respectively, leading to cell cycle block (10). CaMKs are the targets of Ca^{2+}/CaM-dependent pathways at the G2/M and anaphase to metaphase transitions. Inhibition or loss of CaMKs function leads to a G2 arrest. (Adapted from Kahl et al., 2003 (10))

It is also well established in T-cells that Ca^{2+} signals induce cell cycle re-entry of quiescent T-cells following antigen stimulation. Indeed, T-cell stimulation leads to release of Ca^{2+} from intracellular stores through the activation of intracellular channels such as inositol triphosphate (IP_3) receptor Ca^{2+} channels (IP3R) and ryanodine receptors (RyRs) (17). Store depletion then activates Ca^{2+}-release activated Ca^{2+} (CRAC) channels on the plasma membrane in order to produce a sustained Ca^{2+} influx essential for the activity of the nuclear factor of activated T-cells (NFAT) protein, which is a key transcriptional regulator (17). NFAT is activated through dephosphorylation by calcineurin, a Ca^{2+}-calmodulin dependent phosphatase. In order to avoid NFAT rapid phosphorylation, a sustained Ca^{2+} signal is required through Ca^{2+} influx (17).

The significance of calcineurin/NFAT activity is not only confined to T-lymphocytes, but is also an important mechanism in neurons (18) cardiomyopathies (19) and several cancers including leukemia, pancreatic, prostate and breast cancer. In cancer, NFAT increases cellular proliferation, promotes angiogenesis, stimulates invasion/motility and appears to reduce cell death via apoptosis (20).

1.1.1.2 Cell Death

Cell death can be classified according to its morphological appearance as apoptosis, necrosis, autophagy or anoikis. Ca^{2+} appears to be involved in all of these processes (21, 22) (Fig. 1.3).

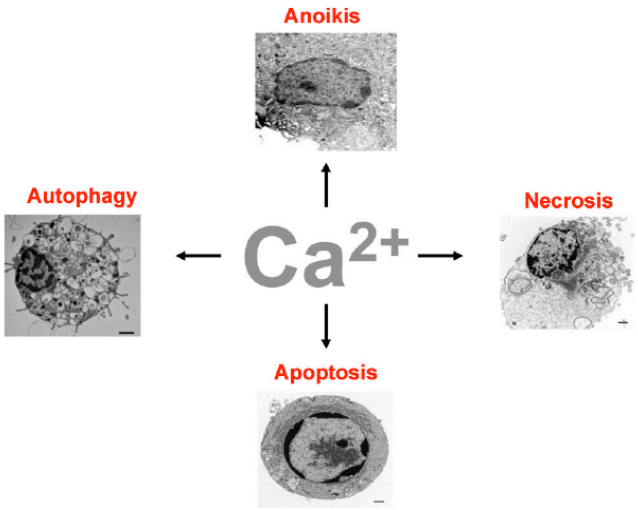

Figure 1.3 Calcium involvement in various type of cell death

Calcium is involved in morphologically different types of cell deaths, such as autophagy, apoptosis, necrosis and anoikis. (Taken from Zhivotovsky et al., 2011 (21))

The apoptotic process may be induced by extracellular stress signals, such as lethal ligands binding specific transmembrane receptors, but also by intracellular stress conditions such as DNA damage, oxidative stress, cytosolic Ca^{2+} overload, mild excitotoxicity and accumulation of unfolded proteins in the ER (23).

It has also been shown that increases in $[Ca^{2+}]_i$, due to Ca^{2+} release from the ER and Ca^{2+} influx from plasma membrane, promote apoptosis (24). However, it appears that more complex signals are involved in the changes in Ca^{2+} homeostasis that occur during apoptotic progression and that additional organelles are involved (25). Indeed, during intracellular stress conditions not only the ER and the mitochondria but also their cross-talk plays an important role in apoptosis (25). Overall, Ca^{2+} appears to be a leading actor in the complex mechanisms associated with apoptosis (26).

Proteins of the B-cell lymphoma 2 (Bcl-2) family are known to regulate cell death (22); they are both pro-apoptotic (Bcl-2–associated X protein (Bax), Bcl-2 homologous antagonist/killer (Bak) and Bcl-2-associated death promoter (Bad)) and anti-apoptotic (Bcl-2 and B-cell lymphoma-extra large (Bcl-XL)) proteins (22). Bcl-2 overexpression in cells results in a phenotype associated with resistance to pro-apoptotic drugs (27).

Bcl-2 protein expression also modifies Ca^{2+} homeostasis (28, 29), however this regulation has not been fully clarified. Bax and Bak are pro-apoptotic proteins located on both the mitochondria and the ER and the lack of expression of these two proteins confers significant resistance to various pro-apoptotic stimuli (30) underling the importance of Bcl-2 family members in the apoptotic process.

The main role of mitochondria in apoptosis is the release into the cytoplasm of caspase cofactors that are important key factors in this type of cell death (23). This process is mediated by the oligomerization of Bax and Bak proteins on the mitochondrial outer membrane (31). The release of pro-apoptotic proteins from the mitochondria is, however, inhibited by Bcl-2 expression (27).

Ca^{2+} is also involved in apoptosis through the activity of key Ca^{2+} binding proteins. For example, calpain, a Ca^{2+}-dependent protease, during the execution of apoptosis is able to cleave anti-apoptotic proteins such as members of Bcl-2 family proteins (32, 33) and caspase-12, which prevents activation of procaspase (34), in order to favor the progression of apoptosis.

As mentioned above, Ca^{2+} is not only involved in apoptosis, but its activity is relevant also in other types of cell death such as necrosis, autophagy and anoikis (21). In contrast to apoptosis, necrosis has been considered an uncontrolled type of cell death (35). However, specific mechanisms have been shown to occur during necrotic death, leading some investigators to now define necrosis as a different type of controlled cell death (23, 35). The critical point during necrotic death is the loss of function of the mitochondria due, in many cases, to a large accumulation of Ca^{2+}, adenosine triphosphate (ATP) loss and production of reactive oxygen intermediates (REIs) (36). These events further increase Ca^{2+} overload (37).

Autophagy can be considered a survival mechanism as it allows the cell to better cope with stress through the degradation and recycling of cellular components to produce nutrients. However, autophagy is also an alternative cell death mechanism (23). Indeed, autophagy has been shown to cause death in different cancer cells, especially in the absence of pro-apoptotic elements such as Bax and Bak or caspase (38, 39). Ca^{2+} appears to be involved in this type of cell death due to $[Ca^{2+}]_i$ increases and activation of CaMK (25). Localized Ca^{2+} signaling has also been reported as an important sensor for autophagy (40).

Anoikis is a type of cell death, which depends on integrins that mediate attachment to other cells. Anoikis is usually deregulated in epithelial cancer cells sustaining invasiveness and metastasis (23). One of the features of this type of cell death is an overexpression of Bcl-2 family members; alteration in Ca^{2+} signals has been reported to be involved in anoikis (21). Indeed, Ca^{2+} and reactive oxygen species (41, 42) as well as Ca^{2+}-activated chloride channels are shown to be involved in anoikis (43).

1.1.1.3 Metastasis

In general, cell migration is a non-pathological process during cell development, wound healing and immune response; however, malfunction of this process may promote processes important in disease such as metastasis (44).

Metastasis, in cancer, is the mechanism by which malignant cells migrate through the circulation from the primary location of the tumor to establish tumor growth in a secondary distant organ (45). Metastasis is the main cause of mortality in cancer and a key hallmark of aggressive tumors (46). The Ca^{2+} signal has been recently identified as a crucial regulator of this process (45, 47).

A tumor becomes invasive through degradation of the extracellular matrix (ECM), which is part of the connecting tissue and provide structural support and anchorage to cells (48). The ECM is a store for growth factors (44), chemokines and cytokines (49). The matrix metalloproteinases (MMPs), a family of proteases capable of the cleavage of cell surface receptors and degradation of many kinds of ECM components, release apoptotic ligands and modulate chemokines/cytokines activity (44). Expression of MMPs is usually correlated to connective tissue remodeling and migration (44).

An important element in cell migration is the activity of the focal adhesion kinase (FAK), a non-receptor tyrosine kinase, capable of coordinating signals between integrins and growth factor receptors (45). This kinase is a target for several extracellular stimuli including those mediated by an increase in $[Ca^{2+}]_i$ such as CAMKs pathways (50, 51).

Local increases in Ca^{2+} correlate with the activity of FAK inducing disruption of focal adhesions (52). Calpain activity is also involved in the regulation of adhesion in normal and pathological condition (53). S100 proteins are a family of Ca^{2+} binding proteins, which are implicated in several intracellular and extracellular functions including metastasis and epithelial-mesenchymal transition (EMT) (54, 55); the latter is a morphological transformation event that is a feature of cell development and cell migration characterized by a loss of cell adhesion (56).

In conclusion, intracellular and extracellular Ca^{2+} signals play a pivotal role, not only in normal cell development, but also in tumor progression and metastasis.

1.1.2 Calcium transporters

In order to maintain Ca^{2+} homeostasis, the cell uses a complex network of signals mediated by several Ca^{2+} transporters on the plasma membrane and intracellular organelles (Fig. 1.4).

As the plasma membrane lipid bilayer is impermeable to Ca^{2+} ions, specific proteins are expressed on the cell surface to enable the transport of Ca^{2+} into and out of the cytoplasm. Extracellular Ca^{2+} can be transported across the plasma membrane through three main transporting mechanisms: channels, ATPase pumps and exchangers (Fig. 1.4). These mechanisms have different characteristics in terms of affinity for Ca^{2+}, rate of Ca^{2+} transport and activation (57).

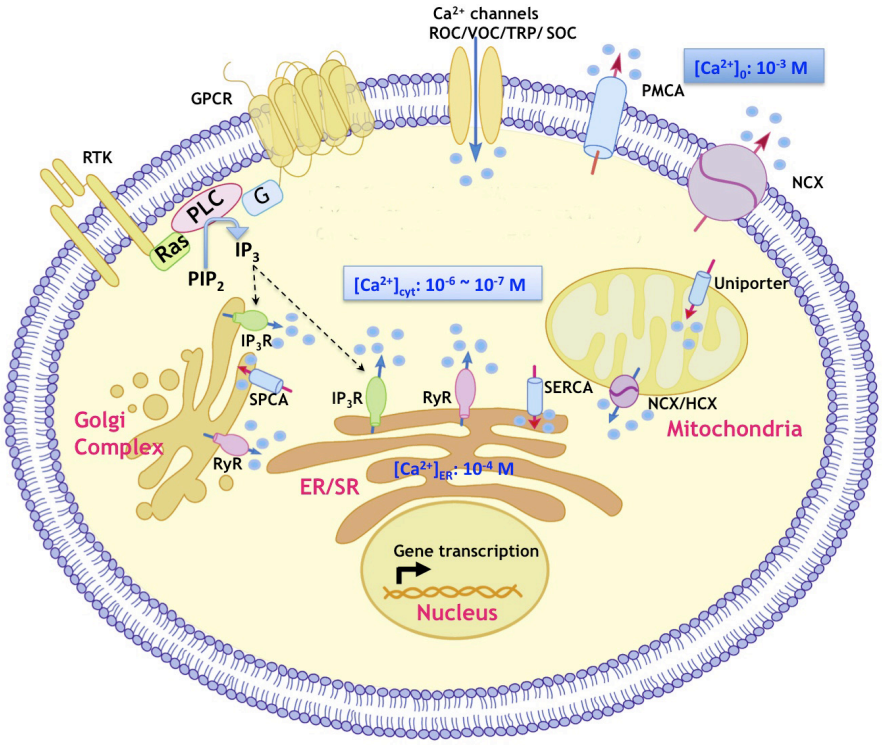

Figure 1.4 Ca^{2+} homeostasis in eukaryotic cell

In order to maintain low levels of intracellular Ca^{2+} in the cytosol and trigger specific Ca^{2+} signals, several Ca^{2+} transporters are involved in regulating Ca^{2+} homeostasis in the cell. Specific Ca^{2+} transporters control the transit of Ca^{2+} ions into organelles and across plasma membrane. Ca^{2+} signaling can also be indirectly regulated by G protein coupled receptors (GPCRs) and tyrosine kinase receptors (RTKs). (Adapted from Zhou Y, Xue S and Yang JJ, 2013 (58))

1.1.2.1 Ca^{2+} channels

Ca^{2+} can enter cells through different types of channels, which can be divided into four major categories: voltage-operated Ca^{2+} (VOCs) channels, receptor-operated Ca^{2+} channels (ROCs), store-operated Ca^{2+} channels (SOCs) and transient receptor potential (TRP) channels (59) (Fig. 1.4).

Voltage-gated Ca^{2+} channels (Ca_Vs) are found in excitable cells (neurons, skeletal muscle, heart), but can also be expressed in non-excitable cells (1). These channels are activated upon membrane depolarization; they are highly selective for Ca^{2+} ions and characterized by rapid and large Ca^{2+} entry (1). Six classes of Ca_Vs have been identified (L-, N-, P-, T-, R- and Q-type). They are made up of different subunits encoded by at least 26 different genes of the *CACN* superfamily. These channels are all tightly regulated: L-type Ca^{2+} channels are modulated by phosphorylation, while others are regulated by G proteins (60).

Among the ROC channels there are: N-methyl-D-aspartate (NMDA) receptors, nicotinic, acetylcholine, purinergic and glutamate receptors. They are encoded by several different genes: NMDA receptors are encoded by *GRIN* genes, nicotinic receptor by *CHRN* genes, purinergic receptors by *P2RY* and *P2RX* genes and glutamate receptors by *GRM* genes (61). These channels are activated by specific ligands to modulate the Ca^{2+} influx (60).

SOCs are activated in response to depletion of intracellular Ca^{2+} stores (59). The CRAC channel is the most studied in this category and the components of this channel have recently been identified (62). The main role of SOC channels is to assure supply of Ca^{2+} ions to the ER, indeed, CRAC channels are activated by decreases in Ca^{2+} levels in the ER (5).

CRAC channels are made up of four-transmembrane domain plasma membrane proteins (Orai1, -2 or -3), which constitute the channel-forming subunits of the channel (63, 64). Stromal interacting molecules (STIM1 or -2) are single transmembrane-spanning domain proteins located in the ER that function as Ca^{2+} sensors (65). Changes in Ca^{2+} levels in the ER are associated with a change in STIM protein conformation and self-aggregation adjacent to Orai subunits in the plasma membrane (66). Through their cytoplasmic C-terminus STIM proteins interact with specific domains on the N and C termini of Orai subunits and cause channel opening (67, 68). The close localization of STIM and Orai proteins causes an accumulation of Ca^{2+} ions in a narrow region that permit specific Ca^{2+} responses (5).

STIM and Orai activities have been linked to immunodeficiency (69, 70). Orai1 has also been linked to breast cancer invasion and metastasis (71). Alteration of Orai-mediated Ca^{2+} influx has also been linked to breast cancers with a poor prognosis (72).

TRP channels are a large family of proteins which all share similarities to *Drosophila* trp channels. They have six putative transmembrane domains (73) and are divided into seven classes (TRPC, TRPV, TRPM, TRPA, TRPN, TRPP, TRPML) amongst which TRPC (canonical), TRPV (vanilloid) and TRPM (melastatin) channels have been the most investigated (73). They are usually weakly voltage-sensitive and have a diverse selectivity of cations conductance (74). TRP channels are modulated by different stimuli such as: GPCRs, ligand activation, temperature, IP3R coupling and phosphorylation (75). Although, TRP channels may participate in store-operated Ca^{2+} entry, it is now incorrect to define them as SOCs channels as their main activation has been established as being not due to Ca^{2+} store depletion (75). TRP channels are particular important in the proliferation of some cell types and some have been shown to be involved in tumorigenesis in different cancer types (4).

Several TRP channels may also mediate release Ca^{2+} from intracellular stores (76), however, the major intracellular Ca^{2+} channels involved in Ca^{2+} store release are the IP3R and the ryanodine receptor. These store release channels share structural similarities. Their Ca^{2+} conductance is 10 times greater than voltage-gate Ca^{2+} channels (1). They are mainly located in the ER membrane and they are co-expressed in several cell types (77, 78).

Three IP3R subtypes are known (IP3R1, IPR3R2 and IP3R3) (79), and they can be co-expressed in the same type of cell (1). They are activated by IP_3 (80), but also by cytosolic Ca^{2+} (81). IP_3 is considered to tune the sensitivity of the channel to cytosolic Ca^{2+}, while luminal Ca^{2+} appears to regulate the affinity of the IP3R to IP_3 (79). Three isoforms of the ryanodine receptor (RyR1-3) are known; RyR1 and RyR2 are expressed in several tissues, RyR1 is mainly expressed in skeletal muscle, while RyR2 is mostly present in cardiac muscle and in Purkinje cells; RyR3 is expressed in several organs (77). Ca^{2+}, Mg^{2+} and ATP and other second messengers can modulate Ca^{2+} release via RyRs (77).

The two-pore channels (TPC) are recently discovered voltage-gate ion channels made up of 12 putative transmembrane segments (82) and they are activated by nicotinic acid adenine dinucleotide phosphate (NAADP) (82). There are three TPC isoforms (TPC1-TPC3) encoded by *TPCN* genes and they function as a dual sensor for luminal pH and Ca^{2+} (83). They show different localization

within the endolysosomal system: TPC1 is mainly located on the endosomal membranes and TPC2 is mostly expressed on the lysosomes and late endosomes, while TPC3 may be present primarily on recycling endosomes (82). Recently, a controversy on the TPC channels has arisen, claiming that TPC channels are Na^{2+} selective rather than Ca^{2+} selective (84) as previously stated (83).

Finally the mitochondrial calcium uniporter (MCU) is a highly selective inwardly rectifying Ca^{2+} channel that allows Ca^{2+} influx into the mitochondria driven by the negative charge of the membrane potential produce by the respiratory chain (85-87). MCU is encoded by the *CCDC109A* gene (87) and recently an accessory protein has been discovered, the MCUb encoded by the *CCDC109B* gene, which appears to produce a dominant-negative effect on MCU that drastically reduces Ca^{2+} influx into the mitochondria (88). MCU has recently been investigated in breast cancer cells and the silencing of MCU in MDA-MB-231 breast cancer cells potentiates ionomycin-induced cell death (89).

1.1.2.2 Ca^{2+} pumps

Another large class of Ca^{2+} transporters is the Ca^{2+} ATPases also referred to as Ca^{2+} pumps. Free Ca^{2+} levels in the cytosol need to be maintained at low levels, thus, Ca^{2+} is extruded from the cell or sequestered into the ER through an active transport mechanism that involves ATP cleavage (90). Ca^{2+} ATPase pumps are divided into three major classes: sarcoendoplasmic reticulum Ca^{2+} ATPases (SERCAs), plasma membrane Ca^{2+} ATPases (PMCAs) and secretory pathway Ca^{2+}-ATPases (SPCAs) (Fig. 1.4). The SERCA pumps are found mostly in the ER, but also in the nuclear envelop and on the Golgi apparatus; PMCA pumps are found on the plasma membrane and finally the SPCA pumps are usually present in the Golgi (90).

Ca^{2+} pumps are considered a large superfamily as they share similar basic properties and conserved regions and these pumps have high affinity for Ca^{2+} ions (91). Upon binding of Ca^{2+} on their cytosolic side, pumps undergo several conformational changes, which permit ATP to phosphorylate their catalytic residue and change their affinity for Ca^{2+} allowing the release of Ca^{2+} across the membrane (91).

SERCA pumps remove two Ca^{2+} ions from the cytoplasm through the hydrolysis of ATP (91). Three genes (*ATP2A1*, *ATP2A2*, *ATP2A3*) encode for SERCA proteins, which can undergo tissue type-dependent alternative splicing (91). Specific inhibitors of these pumps are: thapsigargin (TG) which has an irreversible action and cyclopiazonic acid (CPA), a reversible inhibitor that has a

lower affinity than TG (91). Malfunction of SERCA pumps have been associated with heart failure and cancer development (91). In several different cancers, such as colon, lung, gastric, prostate, pancreatic cancer and leukemia, mutations or altered expression of SERCA pumps have been linked directly or indirectly with the disease (91).

PMCA pumps have high affinity for Ca^{2+} and they transport one ion out of the cell for each ATP hydrolyzed (92). Four genes encode (*ATP2B1*, *ATP2B2*, *ATP2B3*, *ATP2B4*) for the different PMCA pumps and several alternative splicing variants have been identified for each gene (92). The expression of PMCA isoforms is tissue-specific (93): while PMCA1 and 4 are expressed in most tissues, the expression of PMCA2 and 3 is mostly limited to the brain and striated muscle (90). However, PMCA2 is also found in specialized cells such as the mammary gland during lactation (94). PMCA pumps not only hold the housekeeping role of maintaining basal Ca^{2+} levels (95), but they are also important in several specific functions. Indeed, their activity is associated with hearing (96), cardiac function (97) and male fertility disorders (95) and processes important in tumorigenesis (4). Expression of specific PMCA isoforms is increased in breast cancer cells (98, 99) and during differentiation of colon cancer cells (100).

SPCA pumps are usually located in the Golgi membranes and are the most recently identified and characterized human p-type Ca^{2+}-ATPase. The main distinct characteristic of SPCA pumps is their ability of transport also Mn^{2+} (101), which may be important for the activity of several enzymes present in the Golgi (91).

SPCA pumps have two isoforms, SPCA1 and SPCA2, encoded by the *ATP2C1* and *ATP2C2* genes, respectively. Alternative splicing isoforms are known for SPCA1, while SPCA2 alternative splicing has not been reported (91). SPCA pumps have a higher affinity for Ca^{2+} compared to SERCA and PMCA pumps. SPCA is inhibited by La^{3+}, a general Ca^{2+} transport blocker, and orthovanadate, an ATPase inhibitor, but not by concentrations of TG or CPA that inhibit SERCA (91).

SPCA1 mutations have been associated with Hailey-Hailey's disease, which is an autosomal dominant benign skin disorder (102). SPCA pumps have also been associated with ischemia (103), speech and language impairment (104), colon cancer (105) and breast cancer (106, 107).
In breast cancer, it has been shown that inhibition of SPCA1 expression produces an alteration in cell morphology in matrigel (a gelatinous mixture that resembles the complex extracellular environment) and reduces cell proliferation (106). SPCA1 silencing in basal-like MDA-MB-231

breast cancer cells alters the processing of insulin-like growth factor receptor (IGF1R) possibly through the regulation of calcium sensitive pro-protein convertases that reside in the Golgi lumen (106). IGF1R is associated with cancer initiation, proliferation, and resistance and also can be a predictor of poor survival (108-110). SPCA2 has also been associated with some breast cancers, and silencing of SPCA2 reduces the proliferation of breast cancer cell lines that overexpress this protein (107).

1.1.3 Ca^{2+} exchangers

On the plasma membrane other Ca^{2+} transporters are present to maintain Ca^{2+} homeostasis that function as Ca^{2+} exchangers. Na^{+}/Ca^{2+} exchangers (NCXs) are important for Ca^{2+} extrusion working with a 3:1 stoichiometry. Another exchanger is the $Na^{+}/Ca^{2+}/K^{+}$ exchanger (NCKX), which works with a 4:1:1 stoichiometry (111). Three members of the NCX and five members of the NCKX family are known and they belong to a larger superfamily of Ca^{2+}/cation antiporters (111).

NCX1 is present in the heart, brain, kidney and in other tissues at lower levels; NCX2 is mainly expressed in the brain, while NCX3 expression is limited to skeletal muscle and at lower levels in some brain regions. NCX exchangers can be regulated by Ca^{2+}, Na^{2+}, phosphatidylinositol 4,5-bisphosphate (PIP_2) and pH, and these transporters are associated with cardiovascular disease (111).

NCKX exchangers are present in the retinal epithelium and most of the isoforms are also present in the brain, with isoform-specific expression in particular regions. So far this type of exchanger has not been linked with cancer. Second messengers and protein-protein interaction may regulate this family of exchangers, however, further studies are needed (111).

1.2 Breast Cancer

Breast cancer is a malignant neoplasm of the breast tissue and it is the most commonly diagnosed cancer and leading cause of cancer death in women worldwide (112-114) (Fig. 1.5).

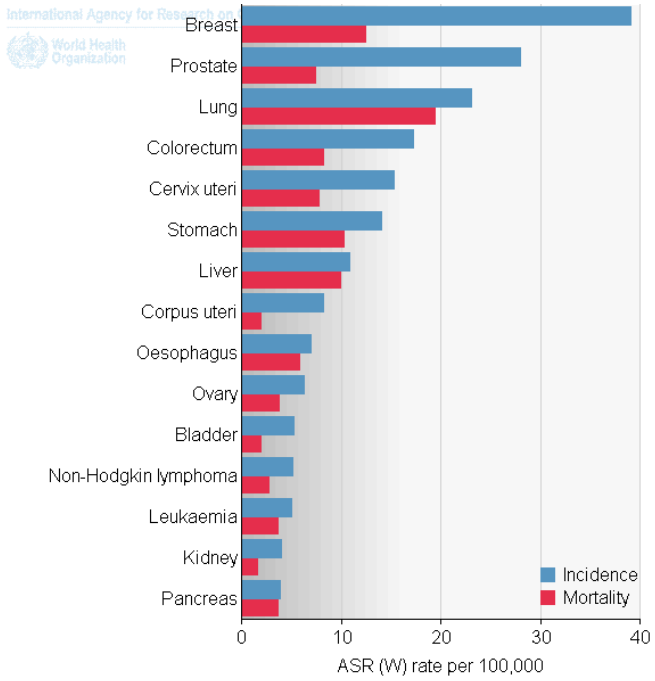

Figure 1.5 Incidence and mortality rates in cancer in women

Most frequent cancers in women worldwide GLOBOCAN 2012. (Taken from IARC website (114))

Breast cancer can be caused by a combination of genetic and environmental factors, in particular, genetic modifications, dietary, behavioral habits and environmental exposure. Gender, ageing, BRCA mutations, a family history of breast cancer, race and ethnicity are all risk factors for breast cancer (115). Obesity, alcohol consumption, hormone therapy and smoking have also been shown to increase the risk of breast cancer, while physical activity may reduce this risk (115, 116). The size, the stage of the tumor and the receptor status determine the type of treatment, which may include surgery, hormonal therapy, chemotherapy, radiation and/or immunotherapy (117).

Different types of breast tumors can be more sensitive to estrogen and progesterone hormones, while others can be driven by growth factors (118, 119). These characteristics are part of the biological heterogeneity of breast tumors and greatly influence the treatment outcome (119). Thus, pathological markers such as the estrogen receptor, progesterone receptor and the human epidermal growth factor receptor 2 (HER2) and expression of other prognostic factors such as the marker of proliferation Ki67 are taken into consideration in order to select an appropriate targeted therapy (120).

Based on their global gene expression, breast tumors have been classified into six hierarchal clusters using cDNA microarray: luminal A, luminal B, HER2-positive, basal-like and normal breast-like, and claudin-low (119). Different types of breast cancers have shown differences in incidence, prognosis and response to treatment (119). The luminal A type has a better disease-free prognosis, while the basal-like and HER2-positive have the worst outcome (121).

1.2.1 HER2-positive breast cancer subtype

HER2-positive breast tumors represent approximately 20-25% of all breast cancers (122-124) and they are among the most aggressive types of breast cancer. This type of tumor is associated with an overexpression of the HER2 receptor, which is used as a diagnostic marker. HER2 status is associated with disease relapse and low overall patient survival (125, 126). Incidence of positive lymph nodes has been correlated with HER2 overexpression and this type of tumor is often associated with metastasis (125).

The HER family includes other growth factor receptors such as HER1 (EGFR), HER3 and HER4 receptors encoded by the *ERBB1-4* genes (127). These receptors are located on the plasma membrane where they can form homodimers or heterodimers. The dimerization of these proteins arises from the binding of a ligand that causes a conformational change and induces the formation

of dimers (127, 128). Heterodimerization can occur among the HER family members but also with other proteins such as IGF1R (129).

HER receptor family signaling is performed primarily by phosphatidylinositol 3-kinase (PI3K) and mitogen-activated protein kinases (MAPK) pathways (128). HER2-positive breast cancers are associated with an up-regulation of PI3K and nuclear factor kappa-light-chain-enhancer of activated B cells (NF-κB) signaling, which protect cells against death stimuli (130, 131). Since HER2-positive breast cancers are associated with a more malignant phenotype, targeting members of the HER family, IGF1R and their downstream signaling is a potential therapeutic strategy in this type of breast tumors.

1.2.2 Trastuzumab

Most of the drugs that have been developed for HER2-positive tumors have as their target the HER2 receptor. Trastuzumab (Herceptin®) is a recombinant humanized monoclonal antibody directed against an extracellular region of the HER2 protein (132). It was the first agent approved for the specific treatment of HER2-positive tumors as adjuvant therapy in early-stage or metastatic breast cancer (133, 134). In HER2-positive metastatic breast cancer, trastuzumab is usually given as part of a treatment program that includes chemotherapy drugs such as paclitaxel (134-136).

At least 5 different mechanisms of action have been suggested for trastuzumab, these are: a) activation of antibody-dependent cellular cytotoxicity (ADCC), b) inhibition of signal transduction and cell cycle arrest, c) inhibition of proteolytic cleavage, d) inhibition of tumor angiogenesis and e) inhibition of DNA damage repair (128) (Fig. 1.6).

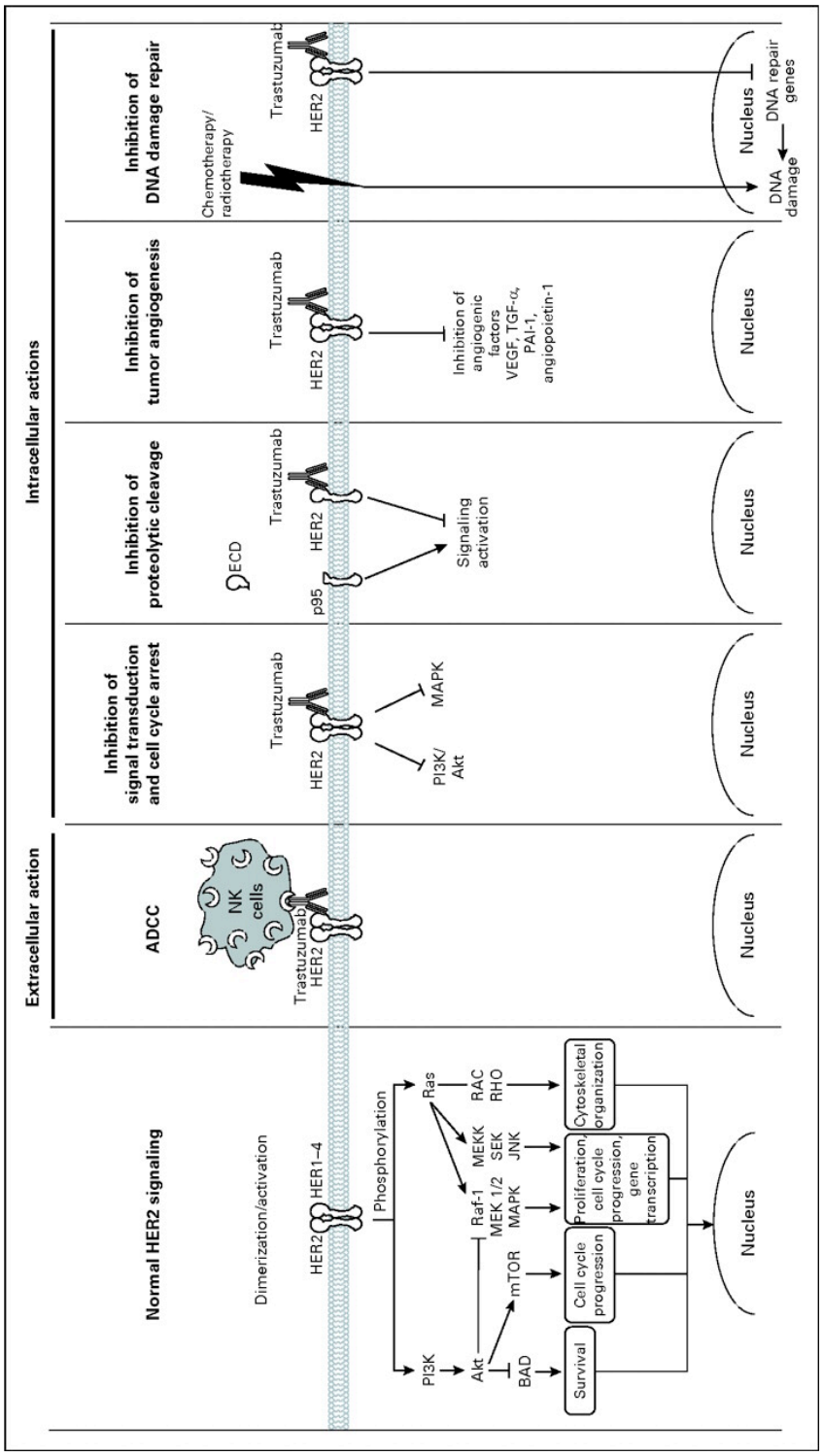

Figure 1.6 Mechanism of action for trastuzumab on HER2-positive breast cancer

Normal HER2 signaling includes the phosphorylation of PI3K and MAPK pathways producing cell survival and proliferation, cell cycle progression, gene transcription and cytoskeletal organization. Trastuzumab produces ADCC, inhibition of signal transduction and cell cycle arrest, inhibition of proteolytic cleavage, angiogenesis and inhibition of DNA damage repair. (Taken from Spector NL and Blackwell KL, 2009 (128))

Trastuzumab inhibits the activation/phosphorylation of the HER2 receptor with a consequential inhibition of PI3K and MAPK pathways with an overall decrease in cell proliferation and promotion of apoptosis (128). Moreover, trastuzumab may down-regulate signaling via cyclin D and increase the half-life of p27 promoting cell-cycle arrest in G1 phase (128).

Other anti-HER2 agents have been more recently developed such as pertuzumab and lapatinib. In some cases these are used in combination with trastuzumab therapy in order to achieve clinical benefits through total HER2 blockade (128). Recently, a new therapeutic trastuzumab emtansine showed a significant increases in progression-free survival in phase III trial (137) and it is now approved by the United States Food and Drug Administration (FDA) (138). This therapeutic agent is an antibody-drug conjugate composed by trastuzumab and a cytotoxic agent, which is delivered into the cells (139).

Despite the improved prognosis of HER2-positive breast cancers due to the development of trastuzumab, treatment is sometimes compromised due to trastuzumab resistance (140).

1.3 Drug Resistance In Cancer

Drug resistance is the reduction of efficacy of a drug for a certain treatment. The resistance can be a *de novo* resistance where the patient does not respond to the treatment from the beginning, or acquired, where resistance develops with prolonged exposure to the drug (141). Drug resistance can lead to therapy failure and consequent disease progression. Among the multiple factors that can determine the response to anticancer treatment, drug resistance is considered to be the major factor that limits the positive outcome of anticancer therapy (141, 142).

1.3.1 Mechanisms of resistance

Several different mechanisms result in resistance against anticancer drugs. These may be due to patient and genetic characteristics as well as epigenetic and environmental factors (141). Characteristics that may influence the response to a particular treatment in different patients may include poor absorption, rapid metabolism or excretion of the drug and these factors can results in a drug concentration that is not sufficient to reach therapeutic levels (141, 143). Poor tolerance may be another issue, particularly in elderly patients; this can lead to a requirement for dosage reduction, which may result in an ineffective therapeutic outcome. Another cause of ineffective therapy may be the inability to deliver the drug to the tumor site due to a large tumors size or low tissue penetration (141, 143).

Other important mechanisms of resistance can be due to molecular alterations within the tumor in order to trigger a survival mechanism to elude the effect of a single drug. These methods include decreased expression of cell surface receptors for the drug and mutation of the drug target (141, 143). Resistance to multiple drugs is common in cancer and may be due to an increased efflux or decreased entry of drugs or an alteration of membrane lipids which results in an overall decreased accumulation of drugs into the cells (141, 143) (Fig. 1.7). A study has shown that SPCA1, which is localized on the Golgi membrane, is important for the processing of proteins within the Golgi and alteration to its activity may involve modification in the trafficking of proteins directed to the plasma membrane (144), thus it may have a role in anticancer resistance.

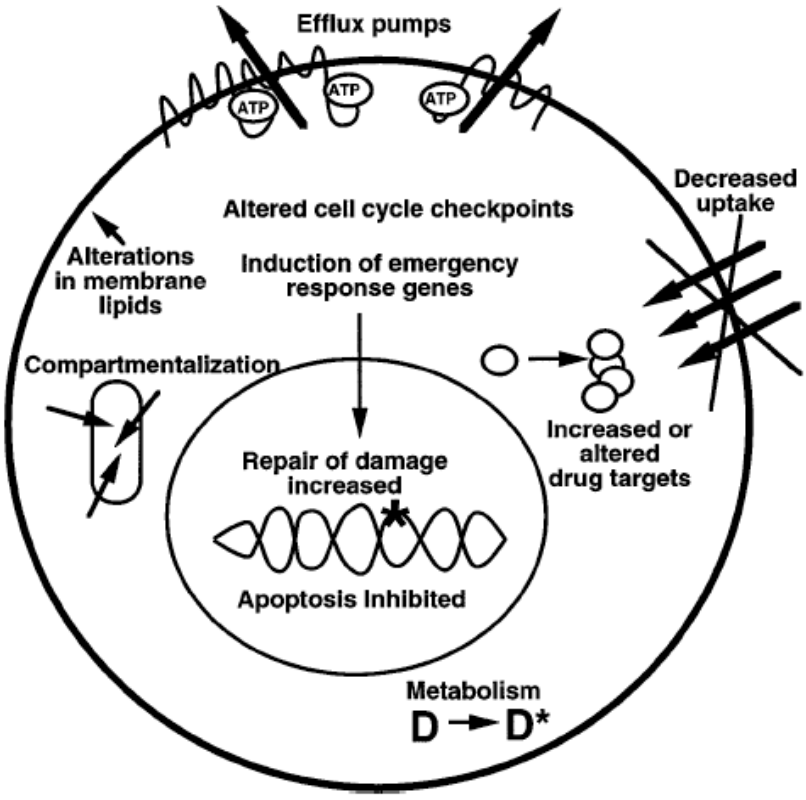

Figure 1.7 Different mechanism of anticancer drug resistance reported in cancer cells

Many mechanisms of resistance to anticancer drugs have been shown in cancer cells. The acquisition of resistance can be caused by lowered accumulation of the drug within the cells due to enhanced efflux, alteration in membrane lipids or decreased uptake produced by a loss of surface receptor or transporter for a drug. Other mechanisms can be cause resistance, such as modification of the specific target of the drug, altered cell cycle checkpoints, increased DNA repairs, compartmentalization or increased metabolism of the drug. (Taken from Gottesman MM, 2002(143))

Alteration of specific pathways can occur to favor cell proliferation and progression of the tumor. In some cases, such as the establishment of resistance, cancer cells may activate alternative pathways to overcome the death response given by an anticancer drug to promote cell survival (145).

1.3.2 Mechanism of trastuzumab resistance

Clinical studies show that trastuzumab is active against HER2-positive breast cancer and is well tolerated. Its response rate as a monotherapy is in the range of 12 to 34% for a median treatment duration of 9 months (146). The response rate significantly increases up to 82% when trastuzumab is given in association with other anticancer drugs and/or chemotherapy (147). However, most patients, who initially responded to the treatment, acquire resistance within 1 year (146). Approximately 25-30% of patients do not respond to trastuzumab at the commencement of therapy (148). An *in vitro* example of this type of *de novo* resistance is the JIMT-1 cell line, which was established from a patient who did not respond to the initial trastuzumab treatment despite HER2 overexpression (149).

Several potential mechanisms of resistance have been proposed for trastuzumab, which include: altered receptor-antibody interaction, up-regulation of HER2 downstream signaling, altered IGF1R and vascular endothelial growth factor (VEGF) signaling, extracellular HER2 cleavage and polymorphism and/or post-translational modification (glycosylation) of the Fc receptor (150, 151). Mutations in the region encoding the extracellular domain may be present on the *ERBB2* gene altering the interaction of trastuzumab with the receptor (146). The disruption of the interaction between trastuzumab and HER2 in resistant cells could also arise from the overexpression of the glycoprotein mucin-4 (MUC4), which is able to bind HER2 preventing its interaction with trastuzumab. Indeed, overexpression of MUC4 is associated with cancer progression, inhibition of apoptosis and HER2 activation (129).

Altered signaling by members of the HER family has been described in trastuzumab resistance. Ligands for EGFR, HER3 and HER4, when these receptors are overexpressed, cause heterodimerization of HER2 with these proteins favoring proliferation and inhibition of apoptosis (152). In these cases, trastuzumab is unable to block ligand-mediated activation of EGFR/HER2 and HER2/HER3 dimers (153).

Interestingly, increased IGF1R signaling may be a characteristic of some trastuzumab resistant cell lines. The overexpression of this receptor is generally associated with proliferation, metastasis and

inhibition of apoptosis (146, 151, 154). Moreover, a particular interaction and cross-talk between IGF1R and HER2 appears to only occur in trastuzumab resistant cells (155).

In sensitive cells, trastuzumab can inhibit the PI3K/Akt pathway leading to the inhibition of the cell cycle and promotion of apoptosis. However, in trastuzumab resistant cells, higher levels of phosphorylated Akt have been found to promote cell survival (156). A possible explanation could be related to defective or decreased expression of phosphatase and tensin homolog (PTEN), a phosphatase that acts as an antagonist of PI3K in the synthesis of phosphatidylinositol (3,4,5)-triphosphate (PIP_3) (157). However, alternative pathways, such as increased IGF1R signaling, are also considered as possible causes of PI3K/Akt pathway activation and subsequent trastuzumab resistance (158).

Trastuzumab decreases cyclin E/cyclin-dependent kinase 2 (cdk2)-mediated phosphorylation of p27 and increases p27-cdk2 complexes resulting in G1 arrest. Trastuzumab resistant cells have lower levels of p27 compared to sensitive cells, which contributes to cell survival (146).

HER2 is a 128 kDa protein, which can be cleaved by MMPs into a 110 kDa extracellular domain released into the serum, and a 95 kDa truncated fragment on the plasma membrane with increased kinase activity. Trastuzumab may interact with the circulating 110 kDa fragments reducing its therapeutic effect, and hence increased MMP-mediated cleavage of HER2 has been suggested as a potential resistance mechanism (129).

In conclusion, several mechanisms of trastuzumab resistance have been proposed and the next section discusses how Ca^{2+} signaling could contribute to trastuzumab resistance or how modulation of Ca^{2+} signaling could potentially offer a mechanism to avoid or overcome trastuzumab resistance is discussed.

1.4 Calcium signaling in cancer

Ca^{2+} signaling is a vital element in several cell processes and an alteration in Ca^{2+} homeostasis may lead to cell malfunction and disease (7). Changes in Ca^{2+} signaling have been linked to cellular mechanisms important in cancer progression (4, 45, 47, 99, 159). In particular, altered expression and/or activity of some Ca^{2+} transporters have been associated with different types of tumors (4, 45, 47, 99, 159). Moreover, Ca^{2+} signaling is involved in several types of drug resistance in cancer (45, 47, 99).

1.4.1 Ca^{2+} signaling and drug resistance in cancer

Tumor cells in order to escape drug-mediated death may activate alternative survival pathways, which may be induced by the reprogramming of particular receptor activities and/or expression. This may lead to the development of resistance for a particular anticancer drug. Ca^{2+} homeostasis may therefore be altered in resistant tumors and promote survival (160).

SOC channels have a role in resistance to apoptosis (161). In human prostate cancer, the down-regulation of Orai1 reduces Ca^{2+} influx and consequently protects cells from apoptosis induced by thapsigargin, tumor necrosis factor α (TNFα) and cisplatin and rescue via Orai1 transfection can restore a normal response to apoptotic stimuli (161). Similarly, leukemia cells that are resistant to the drug tipifarnib show a down-regulation of Orai3, which may attenuate Ca^{2+} influx and also drug-mediated induction of apoptosis (162).

Other Ca^{2+} transporters such as TRPV6 and TRPV2 are overexpressed in advanced and castration-resistant prostate cancer cells, respectively (163, 164). Indeed, TRPV6 expression enhances proliferation and survival via Ca^{2+} entry perhaps through Ca^{2+}-dependent NFAT activation. Small interfering RNA (siRNA)–mediated silencing of the channel increases apoptosis (163). In castration-resistant prostate cancer cells TRPV2 expression enhances cell migration and the expression of invasion markers and thus progression to a more aggressive tumor stage (164). Down-regulation of the calcium sensing receptor correlates with cytotoxic drug resistance in colon cancer and also with increased survivin and tymidylate synthetase expression, which are linked to inhibition of apoptosis and cell proliferation, respectively (165).

IP3R expression also appears to be involved in drug resistance, however, its activity may be isoform subtype and/or cancer specific. For example, IP3R1 is down-regulated in cisplatin resistant bladder cancer cells and increasing its expression reverses resistance and sensitizes cells to

cisplatin-mediated apoptosis (166), whereas IP3R1 is up-regulated in cisplatin resistant lung cancer cells (167).

Ca^{2+}-activated-K^+ channels are correlated with anticancer drug resistance in different tumors. Up-regulation of this channel correlates with malignancy in gliomas (168), while in epidermoid cancer cells, Ca^{2+}-activated-K^+ channels are expressed only in cispatin resistant cells (169). A single-nucleotide polymorphism of this channel is found in selenium resistant prostate cancer cells (170). Ca^{2+} binding proteins, such as calbindin 2, annexins, S100s, sorcin and calpain, are also involved in resistance in different types of cancer. Decreased levels of calbindin 2 correlate with 5-Fluoroacil resistance in colorectal cancer cells (171). Annexins are overexpressed in adriamycin resistant leukemia cells (172). S100 family proteins are down-regulated in several resistant cell lines such as, bladder, colon and ovarian cancer cells (55, 166). Sorcin expression is increased in drug resistant gastric (173) and lung cancer (174) cells, while its decrease in colorectal cells correlates with resistance (175).

Other proteins involved in Ca^{2+} signaling are also linked to drug-resistance in cancer. As described earlier, expression of Bcl-2 contributes to resistance in leukemia cells (176). The overexpression of the Ca^{2+}-dependent enzyme transglutaminase-2 (TG2) also appears to be responsible for TNF-related apoptosis-inducing ligand (TRAIL) resistance in lung cancer cells (177).

1.4.2 Ca^{2+} signaling and drug resistance in breast cancer

In addition to its association with drug-resistance in several types of cancers, Ca^{2+} is also involved in drug-resistance in breast cancer. For example, in two different types of breast cancer cell lines, luminal A and HER2-positive, a subpopulation of cells resistant to paclitaxel do not express the calcium-sensing receptor and this promotes malignancy (178). Moreover, CaM and CaMKs are involved in doxorubicin resistance in luminal A and basal breast cancer cell lines (179). Indeed, EBB (O-(4-Ethoxyl-Butyl)-Berbamine), a CaM antagonist induces marked G_2/M arrest and apoptosis in doxorubicin resistant breast cancer cells (179). Doxorubicin can induce the CaMK pathway leading to anti-apoptotic signaling due to the activation of ERK and Akt pathways in breast cancer cells, and CaMK is overexpressed in different drug resistant breast cancer cells (180). As shown for other types of drug resistance in cancer, S100 proteins are also involved in drug resistance in luminal breast cancer cell lines (181).

Interestingly, expression of the PMCA2 pump correlates with poor outcome and its overexpression protects cells from ionomycin-mediated cell death (182). Moreover, tissue microarray analysis shows a correlation between PMCA2 levels and higher tumor grades and HER2-positive status (182). PMCA2 appears to also interact with calcineurin to confer resistance to apoptosis in some breast cancer cells (183).

The Ca^{2+}-sensitive enzymes transglutaminase-2 and calpain can activate NF-κB contributing to cancer progression and also drug resistance in the basal breast cancer cell line MDA-MB-231 (184). Similarly, in HER2-positive breast cancer cell lines, BT474 and SKBR3, resistance to lapatinib appears to be due to the phosphorylation of RelA, a Ca^{2+} dependent subunit of the NF-κB complex (185).

Ca^{2+} signaling has been investigated in several models of drug resistance in breast cancer cell lines, resulting in the identification of potential targets to overcome resistance to drug treatments. Its role in trastuzumab resistant HER2-positive breast cancer cell lines has not yet been clarified, however, as discussed below some indirect evidences points to its potential involvement.

1.5 Trastuzumab resistance and Ca^{2+} signaling

To date, no studies have been conducted to evaluate a possible direct link between calcium transporters and trastuzumab resistance. Indirect evidence that calcium transporters are potentially involved in trastuzumab resistance is discussed below.

1.5.1 IGF1R

IGF1R is part of the tyrosine kinases receptor family; it is a transmembrane receptor, which can be activated by insulin-like growth factors IGF1 and IGF2 (186) and it is reported to be expressed in normal and malignant tissue (187). The receptor has an important role in growth and its activity is implicated with cancer development, progression and resistance to cytotoxicity treatments (188). Thus, IGF1R appears to be an attractive target to regulate breast cancer therapy.

IGF1R can be present as a homodimer or heterodimer by association with other receptors such as tyrosine kinase receptors of the HER family (155, 187). MAPK and PI3K/Akt pathways can be activated upon IGF1R ligand stimulation, this induces an increased expression of several factors that promote survival and proliferation such as cyclins, survivin, p27, Bcl-2, Bax and others (189).

Increased IGF1R signaling is associated with trastuzumab resistance (108-110). Heterodimerization has been observed in trastuzumab resistant breast cancer cells derived from the SKBR3 cell line but not in the parental cell line (189). Heterotrimerization of HER2, IGF1R and HER3 has also been suggested as a mechanism of trastuzumab resistance (158). This study described that the three receptors interact directly, activating unique downstream signaling pathways in a trastuzumab resistant cell line. Moreover, silencing one of the receptors does not influence the association of the remaining two, which are able to maintain activation of multiple signaling pathways (158).
Trastuzumab resistant BT474 and SKBR3 cells have increased IGF1R expression *in vitro* and inhibition of IGFR1 activity significantly increases the response to trastuzumab (190). However, clinical studies using immunohistochemical analysis conducted on breast cancer samples from patients with metastatic HER2-positive tumors receiving trastuzumab therapy concluded that IGF1R may not be relevant as a trastuzumab response predictor (191).

Trastuzumab has been reported to regulate the IGF binding proteins, IGFBP-2 and IGFBP-3, which form complexes with IGFs in order to regulate their interaction with the receptor. Interestingly, IGFBP-3, which promotes anti-proliferative and pro-apoptotic effects is down-regulated in

trastuzumab resistant cell lines, while IGFBP-2, which appears to have the opposite effect, is up-regulated (192).

It has been shown that the Golgi calcium pump SPCA1 is a key regulator of IGF1R processing in basal-like MDA-MB-231 breast cancer cells. Silencing of SPCA1 produces an alteration of the IGF1R processing, with a pronounced reduction in the active form and accumulation of pro-IGF1R in the trans-Golgi network (106). Mitochondria stress-activated calcineurin also appears to be critical for increased IGF1R expression and activity leading to resistance to apoptosis and tumor proliferation (193).

Hence, changes in calcium signaling may result in changes in IGF1R expression and activity. The consequence of these could be changes in trastuzumab resistance associated with IGF1R in breast cancer cells.

1.5.2 NF-κB

A Ca^{2+} dependent pathway that may be important in trastuzumab resistance is NF-κB, which is a protein complex that regulates DNA transcription (194). It controls the expression of many genes linked to proliferation and survival and thus it has an important role in the development and progression of cancer (195).

The NF-κB complex is made up of two subunits, which belong to two different classes of proteins: Rel proteins (RelA or p65, RelB and c-Rel) and p50, p52 subunit. These proteins may form homo- or heterodimers (194, 195) (Fig. 1.8). The complex is kept active by specific IκB inhibitor proteins. Upon activation of the complex, IκB kinase (IKK) phosphorylates IκB protein, which releases the activated RelA-p50 complex (194) (Fig. 1.8). However, other non-canonical pathways, which activate different NF-κB complex, may also occur (195).

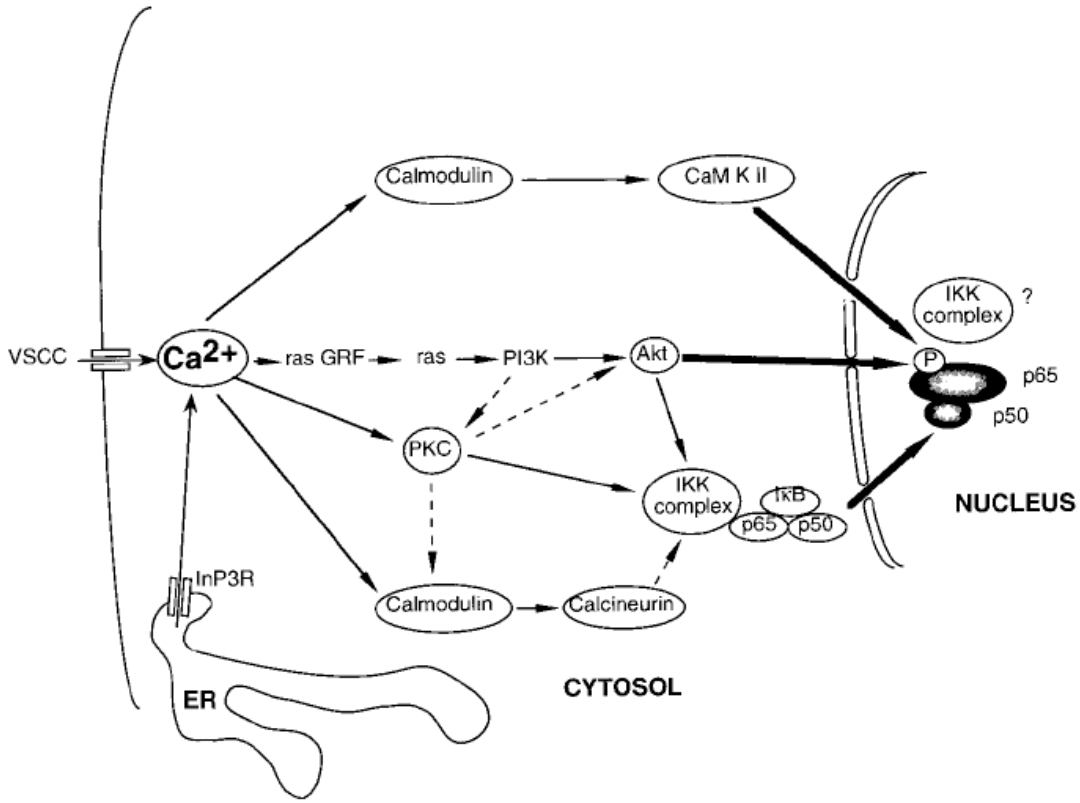

Figure 1.8 Ca^{2+} signaling and NF-κB pathway

Upon activation of the inhibitor of κB kinase (IKK), the NF-κB complex is phosphorylated and the p65-p50 subunits can translocate into the nucleus to promote DNA transcription. Ca^{2+} can modulate NF-κB activity through the activation of Ca^{2+} binding proteins such as calmodulin and calcineurin, or by activation of the Akt pathway. (Taken from Lilienbaum et al., 2003 (196))

NF-κB can be activated by several stimuli, such as TNFα, epidermal growth factor (EGF), interleukins, bacteria, viruses and stress. NF-κB can also be activated by overexpression of the HER2 receptor, which has been demonstrated to activate IKK (197). NF-κB activity is linked with Ca^{2+}, indeed, the RelA subunit has Ca^{2+} dependent activity and it mediates resistance to lapatinib in HER2-positive breast cancer cells (185).

Orai1 expression can induce NF-κB activation and translocation into the nucleus in lung cancer cells (198), while TRPM7 has been associated with hypoxia-inducible factor-1 α (HIF-1α) activity through NF-κB modulation (199). HIF-1α, plays a central role in tumor progression by regulating genes involved in cancer cell survival, proliferation and metastasis (199).

An association between TG2 overexpression and constitutive activation of NF-κB in various types of cancer cells has been also reported (200). Transglutaminases are activated by an increase in cytosolic Ca^{2+} and various tumor promoters (195) and altered expression of TG2 is also linked to drug resistance in cancer (177).

In conclusion, NF-κB activity has been linked with Ca^{2+} and HER2 expression, however the role of NF-κB in trastuzumab resistant breast cancer cells has not yet been investigated in the context of calcium signaling.

1.5.3 Calpain

Calpains are Ca^{2+} binding proteins involved in the proteolysis of several specific substrates and their activity is linked to cancer and several other diseases (201). In cancer calpains are involved in cell migration and survival through the proteolysis of focal adhesion proteins and IκB, respectively (201). They are also linked to apoptosis due to their effects on Bcl-2 family proteins, caspases and pro-apoptotic factors (201). The two most extensively studied subunits of this family are calpain-1 and calpain-2. Calpain-1 activation depends on physiological Ca^{2+} levels, while caplain-2 can be activated by ERK/MAPK pathways signaling (202).

HER2 overexpression activates Akt and ERK/MAPK pathways both of which are involved in calpain activation. The ERK/MAPK pathway activates calpain-2, while Akt induces the activation of NF-κB mediated by calpain activity (203). Recently, the role of calpain in trastuzumab resistant breast cancer was investigated and a correlation between calpain-1 expression and relapse-free survival in breast cancer patients treated with trastuzumab was demonstrated (202). Calpain-1

regulates the cleavage and activity of HER2 and the activity of the Akt1 pathway, and the deregulation of calpain-1 and its activation promotes trastuzumab resistance (204). Trastuzumab sensitive cells have higher calpain-1 activity than resistant cells; however, this resistance is associated with a requirement for calpain-1 activity for survival (204). It has also been reported that activation of calpain leads to degradation of PMCA1, which mediates apoptosis in breast cancer cells, possibly due to a disruption of Ca^{2+} homeostasis (205).

Calpain can be activated in adult skeletal muscle fiber by increased Ca^{2+} influx through the TRPC ion channel family. In particular, it has been shown that TRPC1 channels produce transient increases in Ca^{2+} influx leading to calpains activation in myoblasts (206). Calpain critically regulates cell migration in cervical cancer and it has been shown that the silencing of the Orai1 calcium influx activator STIM1 inhibits EGF-induced calpain activation in this cancer cell type (207).

Overall, calpain appears to be involved in trastuzumab resistance and its activity in cancer is affected by different Ca^{2+} transporters. It would be interesting to evaluate if the involvement of calpain in trastuzumab resistance is related to alteration of specific Ca^{2+} transporters.

1.6 Research hypothesis and aims

1.6.1 Hypothesis 1

Silencing of specific calcium channels, channel regulators and pumps can increase the effects of trastuzumab in HER2-positive trastuzumab sensitive SKBR3 breast cancer cells.

1.6.1.1 Aims

a. To assess mRNA levels of specific calcium channels, channel regulators and pumps in SKBR3 cells.
b. To characterize Ca^{2+} signaling in SKBR3 cells.
c. To silence specific calcium channels, channel regulators and pumps in SKBR3 cells.
d. To assess the proliferation of SKBR3 cells treated with trastuzumab after silencing of specific calcium channels, channel regulators and pumps.

1.6.2 Hypothesis 2

The acquisition of trastuzumab resistance is associated with alterations in the expression of specific calcium channels, channel regulators and pumps.

1.6.2.1 Aims

a. To develop trastuzumab resistant cell lines using SKBR3 breast cancer cells.
b. To compare calcium signaling in SKBR3 trastuzumab sensitive and SKBR3 resistant cells.
c. To compare levels of specific calcium channels, channel regulators and pumps in SKBR3 trastuzumab sensitive and SKBR3 resistant breast cancer cells.

1.6.3 Hypothesis 3

Alterations of specific calcium channels, channel regulators and pumps are a characterizing feature of the development of trastuzumab resistance in SKBR3 breast cancer cells and their inhibition reverses resistance to trastuzumab.

1.6.3.1 Aims

a. To assess the mRNA levels of specific calcium channels, channel regulators and pumps, identified as of interest in Aim 1.d and Aim 2.c, in normal breast cells, basal-like and luminal breast cancer cell lines.
b. To assess the ability of siRNA-mediated silencing of specific calcium channels, channel regulators and pumps identified as of interest in Aim 1.d and Aim 2.c to reverse trastuzumab resistance in trastuzumab resistant SKBR3 cells.
c. To assess the ability of pharmacological inhibitors of specific calcium channels, channel regulators and pumps identified as of interest in Aim 1.d and Aim 2.c to reverse trastuzumab resistance in trastuzumab resistant SKBR3 cells.

1.6.1 Hypothesis 4

Alteration of specific calcium related proteins is a characteristic of trastuzumab resistance in HER2-positive breast cancer cell lines and in HER2-positive clinical breast cancers.

1.6.1.1 Aims

a. To assess changes in mRNA levels of calcium related proteins in SKBR3 sensitive and resistant cell lines using cDNA microarray data.
b. To assess changes in protein levels of calcium related proteins in SKBR3 sensitive and resistant cell line using SILAC data.
c. To assess changes in mRNA levels of calcium related proteins in clinical breast cancers resistant to trastuzumab using cDNA microarray data.

2 Characterization of Ca^{2+} channels, pumps and channel modulator profiles of the HER2-positive SKBR3 cell line

2.1 Introduction

HER2-positive breast cancer, as discussed in section 1.2.1, represent 20-25% of all breast cancers (128). These breast cancers are characterized by an overexpression of HER2 receptors. The HER2 molecular subtype shows a different gene expression profile compared to other breast cancer molecular subtypes (118). Numerous HER2-positive breast cancer cell lines have been established (208) (Table 2.1) including luminal, estrogen and progesterone receptor negative cell lines such as SKBR3 and AU565, and hormone receptor positive cell lines such as the BT474, MDA-MB-361, UACC732, UACC812 and ZR-75-30 cell lines (Table 2.1). There are also some HER2-positive breast cancer cell lines that show basal characteristics, such as HCC1419, HCC1569, HCC1954, HCC202, JIMT-1, SUM190 and SUM225 (156). These HER2-positive basal-like breast cancer cell lines appear to be more likely to be resistant to trastuzumab (208). However, this trastuzumab resistance can be lost *in vivo*. For example, the basal JIMT-1 cell line, which was established from a patient who did not respond to trastuzumab at the commencement of therapy (149), shows insensitivity to trastuzumab *in vitro*, but not *in vivo*, using a xenograft model (209) (Table 2.1).

The SKBR3 cell line is one of the most commonly used HER2-positive breast cancer cell lines. It was established from a white Caucasian 43 years old woman at the Memorial Sloan–Kettering Cancer Center in 1970. The cell line was derived from a pleural effusion derived from an adenocarcinoma (210).

As discussed in section 1.1.1.1 of this thesis, Ca^{2+} signaling is an important regulator of the cell cycle (9, 10), and a remodeling of Ca^{2+} signaling and the expression of specific Ca^{2+} channels and pumps has been reported in a variety of cancer cell lines, including those of the breast. However, very few studies have assessed the expression and role of Ca^{2+} pumps, channels and modulators in HER2-positive breast cancer cell lines or their role in the sensitivity of such cells to trastuzumab. In this chapter, I evaluated the mRNA level of Ca^{2+} channels, pumps and channel modulators in SKBR3 cells. I also examined their potential roles in the proliferation of SKBR3 cells in the presence and absence of trastuzumab.

Table 2.1 List of available HER2-positive breast cancer cell lines

Characteristics of the HER2-positive breast cancer cell lines available with their responsiveness to trastuzumab (+ = expressed, - = not expressed, S = sensitive, R = resistant).

Cell line	Gene Cluster	ER	PR	HER2	Morphology	Tumour type	Donor	Trastuzumab response	Ref
AU565	Luminal	-	-	+	epithelial	Adenocarcinoma	White Caucasian female 43	S	(211)
BT474	Luminal	+	+	+	epithelial	Invasive ductal carcinoma	White Caucasian female 60	S	(212)
HCC1419	Basal	-	-	+	epithelial	Primary Ductal Carcinoma	Hispanic female 42	R	(213)
HCC1569	Basal	-	-	+	epithelial	Metaplastic carcinoma	Black female 70	R	(213)
HCC1954	Basal	-	-	+	epithelial	Ductal Carcinoma	East Indian female 61	R	(213)
HCC202	Basal	-	-	+	epithelial poorly differentiated	Ductal Carcinoma	White Caucasian female 82	R(2D) S(3D)	(213)
JIMT-1	Basal	-	-	+	epithelial	Ductal Carcinoma	White Caucasian female 62	R (*in vivo*)	(149)
MDA-MB-361	Luminal	+	-	+		Adenocarcinoma	White Caucasian female 40	R	(214)
SKBR3	Luminal	-	-	+	epithelial	Adenocarcinoma	White Caucasian female 43	S	(210)
SUM190	Basal	-	-	+		Inflammatory carcinoma		R(2D) S(3D)	(215)
SUM225	Basal	-	-	+		Invasive ductal carcinoma		R	(216)
UACC732	Luminal	-	+	+	epithelial	Inflammatory carcinoma	White Caucasian female 33	R	(217)
UACC812	Luminal	+	-	+	epithelial	Invasive ductal carcinoma	Female 43	S	(218)
ZR-75-30	Luminal	+	-	+	epithelial	Invasive ductal carcinoma	Black female 47	S	(219)

2.2 Chapter Hypothesis

Silencing of specific calcium channels, channel regulators and pumps increase the effects of trastuzumab in HER2-positive trastuzumab sensitive breast cancer cells (SKBR3).

2.2.1 Aims

a. To assess mRNA levels of specific calcium channels, channel regulators and pumps in SKBR3 cells.
b. To characterize Ca^{2+} signaling in SKBR3 cells.
c. To silence specific calcium channels, channel regulators and pumps in SKBR3 cells.
d. To assess the proliferation of SKBR3 cells treated with trastuzumab after silencing of specific calcium channels, channel regulators and pumps.

2.3 Methods

2.3.1 Materials and Cell Culture

All materials and solutions used in this thesis are cataloged in the Appendix 1 and 4. Trastuzumab was purchased from Roche Products, aliquoted and dissolved in sterile water to obtain 10 mg/mL stock solution. The solution was kept at 4°C and used within 1 month.

The HER2-positive human breast cancer cell line SKBR3, a gift from a collaborator at the Garven Institute, Sydney, was cultured in McCoy's A5 media (Invitrogen) supplemented with 10% fetal bovine serum (FBS) and 5% Penicillin-Streptomycin mixture (Invitrogen) as recommended by American Type Culture Collection (ATCC), and maintained at 37°C humidified atmosphere containing 95% O_2 and 5% of CO_2, and passaged twice a week. Cells were passaged as recommended by ATCC (210), media was removed and the cell monolayer was washed with 5 mL of phosphate buffer saline (PBS) and ethylenediaminetetraacetic acid (EDTA) buffer. Trypsin (1.5 mL) was then added to detach the cell monolayer from the flask and incubated at 37°C for 3-5 min. In order to stop the action of trypsin, 5 mL of fresh culture media was added to the flask, this mixture of media and cells was then transferred to a 10 mL tube. The cell suspension was centrifuged for 2 min at 400 g at room temperature. The cell pellet was re-suspended in 10 mL of fresh media and 5 mL of this cell suspension was then added to a new T75 flask with 5 mL of fresh culture media.

SKBR3 cells were periodically tested for mycoplasma using MycoAlert™ Mycoplasma Detection Kit (Lonza) and they were genotyped to authenticate the cell line using the STR Promega StemElite™ ID Profiling Kit. For the STR protocol, cells were collected and centrifuged in cold sterile PBS, cells were then diluted to 1 X 10^6 cells/mL with cold PBS. Cells (20 µL) were placed onto a FTA card, which was dried for 30-60 min before overlaying the spot on the card with 20 µL of methanol to fix the sample. The card was allowed to dry for 30 min and analyzed by the Queensland Institute of Medical Research (QIMR) as described by Reid and colleague (220).

2.3.2 Quantitation of RNA Expression

The expression of Ca^{2+} transporters was examined using quantitative RT-PCR. The amplification was measured using a StepOnePlus quantitative RT-PCR instrument (Applied Biosystem).

Quantitative RT-PCR was used to validate siRNA-mediated silencing and also to evaluate the relative mRNA level of specific targets.

2.3.2.1 RNA isolation and purification

RNA was isolated from SKBR3 cells grown in culture using the RNeasy™ Plus Mini kit (Qiagen), as per the manufacture's protocol. Briefly, RLT Plus buffer with 1% β-mercaptoethanol (Sigma Aldrich) (350 µL) was added to the wells of a 96-well plate. Cells were detached from the bottom of the well by scratching the monolayer with a tip, then the cell lysate was vortexed for 60 s and stored at -80°C overnight. Each sample was then added to a genomic DNA eliminator spin column and centrifuged for 30 s at 8000g, then the column was discarded and 350 µL of 70% ethanol was mixed with the flow-through. The solution was added to an RNeasy spin column and centrifuged at 8000g for 15 s. The column was first washed with 700 µL RW1 buffer and centrifuged at 8000g for 15 s and the flow-through discarded. Then the spin column was washed twice with 500 µL of RPE buffer and centrifuged each time at 8000g for 15 s first and then for 2 min; flow-through was discarded each time. The RNeasy spin column was then placed into a fresh 2 mL tube and centrifuged at 8000g for 1 min. Finally, the column was placed into a clean 1.5mL tube and 30 µL of RNase/DNase-free water was added to the membrane, incubated for 3 min then centrifuged at 8000g for 1 min. The column was discarded and flow-through containing RNA was collected. RNA was determined by measuring the absorbance at 260 nm using a UV spectrophotomer (Nano Drop 2000, Thermo Scientific)

2.3.2.2 Reverse transcription and Real Time PCR

A reverse transcription of RNA to obtain cDNA was performed using the Omniscript RT kit (Qiagen). As per manufacture protocol a reaction mix was prepared, which contained 2 µL/sample of RT Buffer (10X), 2 µL/sample deoxynucleotide triphosphates (dNTPs), 2 µL/sample random primers and 1 µL/sample of RNase inhibitor (Promega, Australia) and Omniscript Reverse Transcriptase enzyme. RNase inhibitor was previously diluted 1:4 with 1X RT buffer and the random primers were diluted 1:2.52 with RNase/DNase-free water. Samples (12 µL) were added to produce a total volume of 20 µL reaction mix. The initial sample concentration was adjusted in order to have 4.8 ng/µL of RNA in the final reaction mix. The cDNA produced was then used to perform the quantitative RT-PCR assay. The cDNA was diluted with RNase/DNase-free water 1:100 for 18s RNA quantification (Applied Biosystems) a ribosomal RNA used as control housekeeping gene (221, 222).

Five µL of cDNA was added to a master mix containing 10 µL /sample of TaqMan Universal Master Mix (4324018, Applied Biosystems), 1 µL /sample of the target specific primer-probe assay (Applied Biosystems) and 4 µL/sample of RNase/DNase-free water. The assays contained gene-specific primers and a dye-labeled TaqMan minor groove binder (MGB) probe (223). The primers (Applied Biosystem) used are reported in appendix 6.

The thermal cycling conditions comprised of a 95 °C AmpliTaq Gold® enzyme activation, and 40 cycles of 95 °C for 15 s for denaturation and 60 °C for 1 s for the anneal/extension step.
RNA expression was quantified using the comparative threshold cycle (C_T) method by reference with the endogenous control 18s rRNA as previously described (222, 224). The delta C_T value (ΔC_T) was calculated as the difference between the C_T value of the target and the 18s rRNA as shown in the equation below:

$$\Delta C_T = (\text{Target gene } C_T) - (18s \text{ rRNA } C_T)$$

The average of the ΔC_T value for the RNA sample used as control within a specific experiment was used to calculate the delta delta C_T ($\Delta\Delta C_T$) as shown in the equation below:

$$\Delta\Delta C_T = \text{target } \Delta C_T - \text{average control } \Delta C_T$$

Finally, the fold change of the target gene expression relative to the RNA sample used as a control was given by the formula $2^{-\Delta\Delta CT}$ (225).

2.3.3 siRNA-mediated silencing

Small interfering RNA (siRNA) technology was used to silence specific calcium channels and pumps. siRNA is a class of double-stranded molecules (dsRNA), involved in the RNA interference (RNAi) pathway, where they interfere with the expression of specific genes (226). The siRNA used in these studies are commercially available: siGENOME and ON-TARGET*plus* (SMARTpool, Dharmacon). The SMARTpool siRNA is a mixture of 4 siRNA provided as a single reagent and it provides advantages in both potency and specificity. In contrast to siGENOME siRNA, ON-TARGET*plus* siRNA has an antisense strand seed region that is modified to destabilize off-target activity and enhance target specificity. These siRNA can be easily transfected into mammalian cells *in vitro* for highly specific silencing of target genes (227).

The RNAi pathway is initiated by the enzyme Dicer, which cleaves long dsRNA into short fragments, that are then unwound into two pieces of single-stranded RNA (ssRNA): the passenger strand and the guide strand. The passenger strand is then degraded. The siRNA then specifically pairs with the guide strand, in order to degrade any nascent pre-mRNA transcript (226). In these studies, the siRNA was introduced into the cytoplasm of cells through a lipid based transfection reagent DharmaFECT (Dharmacon).

In order to identify siRNAs capable of inducing a change in proliferation, an optimized 8 day protocol was developed to use with the Click-iT® EdU assay (Invitrogen, described in section 2.3.4) in SKBR3 cells. The length of the protocol was chosen in order to allow comparison with drug treatments (e.g. trastuzumab). Seeding density was optimized in order to achieve 80% confluence at the end of the protocol. The optimal seeding density was 2 X 10^4 cells/well.

Initial experiments were conducted to optimize siRNA transfection using three different transfection reagents from Dharmacon (DharmaFECT 1, 2 and 4). Each reagent was tested at 2 different volumes 0.1 μL/well and 0.05 μL/well in the absence of siRNA treatment to examine the effect on cell viability. Moreover, 24h after the addition of the transfection reagent, the media was changed to further lower the possible toxicity caused by the transfection reagent as suggested by the manufacturer. Using 0.1 μL/well cells showed cell toxicity visible under the microscope 48-72 h after the addition of the transfection reagent (Fig. 2.1a).

An MTS proliferation assay (described in section 2.3.5) performed at the end of the 8 days protocol, demonstrated that lower volumes of the DharmaFECT transfection agent was associated with less effects on SKBR3 cell viability. DharmaFECT 2 and 4 resulted in less cell toxicity compared to DharmaFECT 1 even at the higher volume (Fig. 2.1a).

In order to validate which transfection reagent was best suited to the 8 day protocol in SKBR3 cells, a quantitative RT-PCR assay was performed on samples obtained from the isolation of RNA from SKBR3, 7 days after PMCA1 siRNA treatment. PMCA1 siRNA was selected as PMCA1 is expressed in a wide variety of breast cancer cell lines (228).

PMCA1 siRNA stock solution (20 μM) was diluted 1:10 to a 2 μM solution using 1x siRNA buffer (Thermo Scientific). The siRNA buffer was previously diluted 1:5 with RNAse-free water. In two

microfuge tubes, 5 µL/well of 2 µM PMCA1 siRNA solution was added to 5 µL/well of media with no added FBS. In two separate tubes 0.05 µL/well of DharmaFECT 2 or 4 were added to a 9.95 µL/well of media with no added FBS. The tubes containing PMCA1 siRNA and the tubes containing the transfection reagent were incubated for 5 min at room temperature. A 10 µL/well volume of the tubes containing DharmaFECT 2 or 4 was then added to the tubes containing PMCA1 siRNA, each tube was then incubated for 20 min at room temperature. Finally, 80 µL/well of culture media with 10% FBS was added to the mixture and was immediately added to each well.

From the results obtained, DharmaFECT 4 had superior silencing efficiency compared to DharmaFECT 2 at 0.05 µL/well (Fig. 2.2b). Thus, DharmaFECT 4 at 0.05 µL/well was selected as the optimal transfection reagent for these studies (Fig. 2.1b).

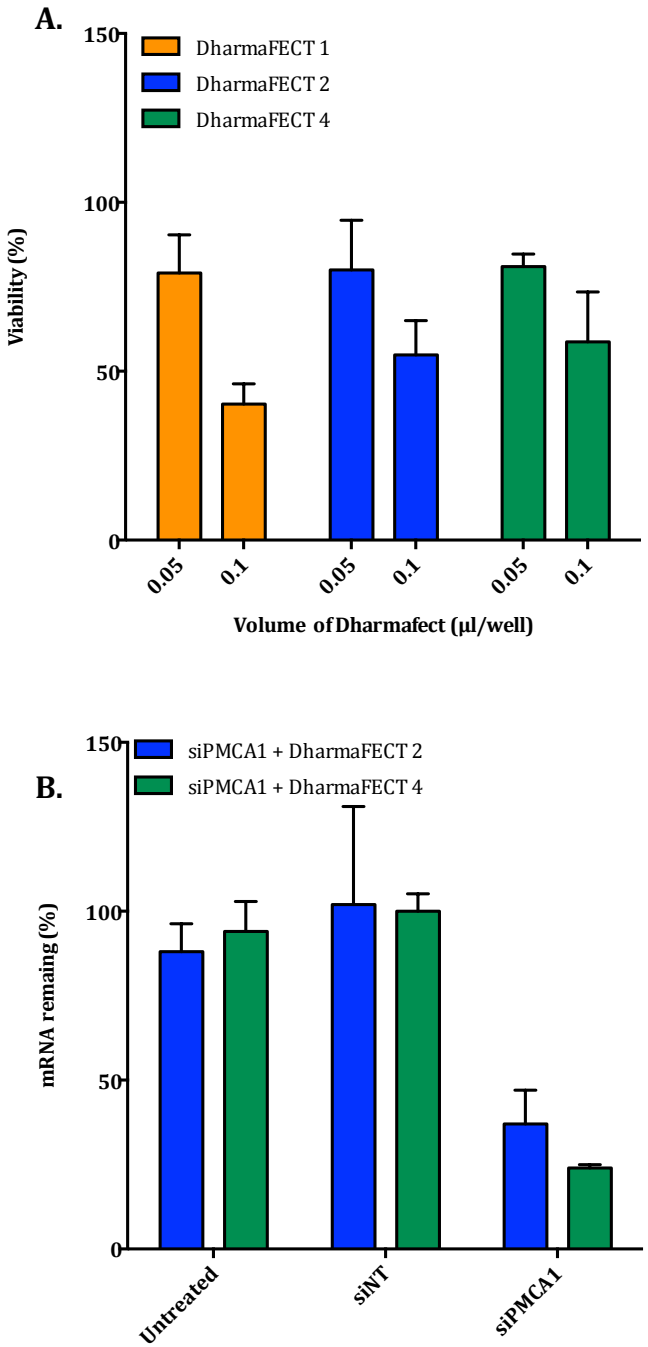

Figure 2.1 siRNA optimization for the SKBR3 cell line

A. An MTS assay showed that a lower volume of DharmaFECT was associated with less cellular toxicity. The results were normalized to absorbance values from untreated cells. DharmaFECT 2 and 4 were associated with less toxicity at the high volume (n=3, ± S.D.). **B**. Quantitative RT-PCR for PMCA1 mRNA levels showed that after 7 days, DharmaFECT 4 was associated with better silencing of PMCA1 (n=3, ± S.D.).

The siRNA screening using this optimized protocol (Fig. 2.2) included 19 Ca^{2+} pumps, channels and channel modulators. These targets were selected due to their representation of diverse classes of Ca^{2+} pumps, channels and modulators and their availability in the Calcium Signaling in Cancer Research Laboratory at the time of these studies. A Non-Targeting ON-TARGET*plus* siRNA (siNT) was used as a control in SKBR3 cells to evaluate possible off-target effects. The ON-TARGET*plus* siRNA-mediated silencing was validated by measuring the level of mRNA, using quantitative RT-PCR. Results were excluded if the silencing of a target showed less than 50% of silencing efficacy.

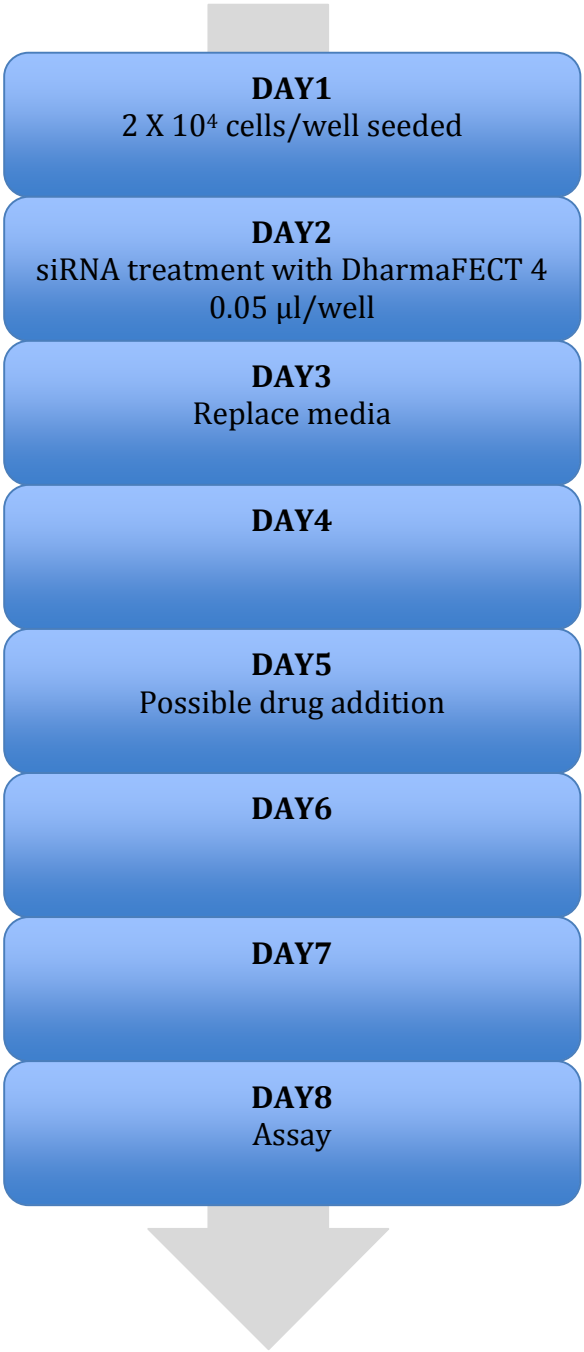

Figure 2.2 Schematic overview of optimized protocol

The optimized protocol involved 8 days of culture. No evidence of toxicity due to the transfection reagent was observed under these conditions. This protocol enabled the testing of cells treated with trastuzumab (48 h).

2.3.4 Cell Proliferation assay

The Click-iT® EdU Alexa Fluor® 555 Imaging Kit (Invitrogen) was used to assess cell proliferation. EdU (5-ethynyl-2'-deoxyuridine) is a nucleoside analog to thymidine and is incorporated into DNA during active DNA synthesis. Detection is based on a "click" reaction, a copper-catalyzed covalent reaction between EdU and the Alexa Fluor® dye (229).

For this assay, 2 X 10^4 cells/well were seeded into a 96-well plate and cultured as per section 2.3.1. After 7 days the Click-iT® EdU assay was performed. Briefly, 50 µL of media was removed from each well and replaced with 50 µL of growth media containing 20 µM EdU solution. After 1 h incubation at 37°C, the media was removed and 50 µL of 3.7% formaldehyde in PBS was added to each well, and incubated at room temperature for 15 min (for cell fixation). The fixative was then removed and each well washed twice with 50 µL of 3 % bovine serum albumin (BSA) in PBS. After this wash step, the cells were permeabilised with 50 µL of 0.5% Triton® X-100 in PBS for 20 min at room temperature.

A reaction mix able to detect EdU was then prepared as outlined in table 2.2. After fixation the wells were washed three times with 50 µL of 3 % BSA in PBS, then 50 µL of the reaction mix was added to each well and incubated at room temperature for 30 min protected from light.

Table 2.2 Click-iT® EdU reaction mix composition

Reaction components	**Volume per well**
1X Click-iT® reaction buffer	43 µL
$CuSO_4$ (Component E)	2 µL
Alexa Fluor® azide	0.12 µL
Reaction buffer additive	5 µL
Total volume	50 µL

Cells were then washed once with 50 µL of 3% BSA in PBS and once with PBS. Cells were then incubated for 1.5 h with 50 µL of 400 nM 4',6-diamidino-2-phenylindole (DAPI) protected from light. DAPI binds to DNA (230) and stains each cell nuclei. After incubation with DAPI, wells were finally washed with 50 µL PBS twice and then maintained in PBS during the acquisition of images.

Four images per well were acquired and analyzed using a multi-wavelength analysis module (Alexa Fluor® azide was detected using a Cy3-4040B (Semrock) filter, DAPI was detected using a DAPI-1160A (Semrock) filter) with an ImageXpress Micro (Molecular Devices) Imaging system in order to determine the percentage of EdU positive cells. The data were exported using a multi-wavelength setting and analyzed in Microsoft Excel to determine percentage of Edu positive cells.

This method was used to detect changes in the percentage of cells in the S phase of the cell cycle with siRNA treatment and/or by different concentrations of trastuzumab.

2.3.5 Approximation of viable cell number using [3-(4,5-dimethylthiazol-2-yl)-5-(3-carboxymethoxyphenyl)-2-(4-sulfophenyl)-2H-tetrazolium (MTS) assay

Approximate viable cell number was assessed using a CellTiter 96® AQueous Non-Radioactive Cell Proliferation Assay (Promega), which is a colorimetric method for determining the number of viable cells in proliferation or cytotoxicity assay (231). It utilizes a tetrazolium compound [3-(4,5-dimethylthiazol-2-yl)-5-(3-carboxymethoxyphenyl)-2-(4-sulfophenyl)-2H-tetrazolium, commonly referred to as MTS (231). MTS is bioreduced by living cells into a formazan product that is soluble in tissue culture medium (231).

Cells were seeded at 2 X 10^4 cells/well in a 96-well plate and after 24 h trastuzumab was added at different concentrations (0.1 µg/mL, 0.3 µg/mL, 1 µg/mL, 3 µg/mL, 10 µg/mL, 30 µg/mL, 100 µg/mL), media was replaced after 72 h with fresh trastuzumab-containing media. After a further 72 h, 20 µL of MTS was added to the plate and incubated at 37°C in a humidified atmosphere containing 95% O_2 and 5% of CO_2. After 2 h the absorbance of the formazan at 490 nm was measured using a microplate reader (iMark, microplate reader, Bio-Rad). A higher absorbance reading is indicative of increased viable cell number (231). The MTS assays described in this chapter were used to evaluate the anti-proliferative activity of trastuzumab in SKBR3 cells and to optimize the conditions for siRNA transfection.

2.3.6 Ca^{2+} measurement assay

Calcium measurement assays were performed using a fluorometric imaging plate reader ($FLIPR^{TETRA}$, Molecular Biosciences), which is a high-throughput platform to measure intracellular Ca^{2+}. This assay used a visible wavelength Ca^{2+} indicator dye (232). The indicator used in this project was Fluo-4 AM (Invitrogen), a molecule that exhibits an increase in fluorescence upon binding Ca^{2+} (233).

The Fluorometric Imaging Plate Reader (FLIPR) has been developed to perform quantitative optical detection of receptor/ion channel–mediated changes in cellular membrane potential or intracellular calcium using fluorescent indicator dyes (234). In this chapter, cytoplasmic Ca^{2+} levels were measured in SKBR3 cells to evaluate the nature of ATP or EGF induced Ca^{2+} transients and store operated calcium entry (SOCE).

Cells were seeded at 2 x 10^4 cells/well in a 96-well black-walled imaging plate (Corning). Media was changed every two days and after 10 days cells were loaded with Fluo-4 AM (4 μM) for 30 min at 37°C, then washed 3 times in physiological salt solution (PSS) (Appendix 1). Cells were then incubated for 15 min at room temperature to allow hydrolysis of the acetoxymethyl (AM) ester. Fluorescence was measured at an excitation wavelength of 470–495 nm and 515–575 nm emission. As $[Ca^{2+}]_i$ levels increase, Ca^{2+} ions complex with Fluo-4 AM resulting in an increased fluorescence emission (235). Data analysis was performed using ScreenWorks Software (v2.0.0.27, Molecular Devices). Relative increases in $[Ca^{2+}]_i$ were compared using response over baseline (fluorescence divided by starting fluorescence) (221, 236, 237). For ATP and EGF experiments, the relative maximum $[Ca^{2+}]_i$ was used to generate concentration response curves.

SOCE was assessed using external BAPTA (500 μM) to chelate extracellular Ca^{2+} and CPA (10 μM) to empty intracellular Ca^{2+} stores through SERCA inhibition. Then 2 mM $CaCl_2$ was added to allow Ca^{2+} influx through channels present on the plasma membrane (238, 239). Nominal Ca^{2+} solution (Appendix 1) was used to prepare the solution of BAPTA and CPA.

The increase in $[Ca^{2+}]_i$ caused by CPA produced the first peak in fluorescence. A second increase in $[Ca^{2+}]_i$ was produced by the re-addition of Ca^{2+}. The ratio between the influx and the store release was calculated as peak 2 maximum/peak 1 maximum as previously described as a measure of SOCE (238).

2.3.7 Immunoblotting

Immunoblotting uses antibodies to identify and quantify specific proteins. It involves separating the denatured proteins by their molecular weight by using a sodium dodecyl sulfate polyacrylamide gel electrophoresis (SDS-PAGE) technique. In order for the antibody to detect the protein of interest, the separated proteins from the gel are transferred to a polyvinylidene difluoride (PVDF) membrane using an electric current (240).

The protocol used for the detection of proteins in this thesis was as follows.

2.3.7.1 Protein sample preparation

Cells were seeded at 2 X 10^4 cells/well in a 96-well plate and cultured for 24 h before siRNA treatment. Protein was isolated 8 days after siRNA treatment. Cells were washed in cold PBS. Whole cell lysates were prepared by scraping wells with a pipette tip in the presence of 25 µL of lysis buffer containing protease and phosphatase cocktail inhibitor (Roche Applied Science). This protocol was performed on four consecutive wells and cell lysates were pooled from these four wells. Cell lysates were then vortexed for 60 s then incubated on ice for 20 min. The samples were then centrifuged at 14,000 rpm for 20 min at 4 °C to remove cellular debris. The supernatant was transferred into a new microfuge tube and stored at -80 °C.

2.3.7.2 Bradford Assay

Protein concentration was determined by a Bradford assay using a Bio-Rad protein assay kit. BSA in deionized water was used to generate a standard curve at concentrations of 0.1, 0.2, 0.3, 0.4, 0.5, 0.6, 0.7, 0.8 mg/mL. BSA solutions (10 µL/well) or protein samples were added to an individual well of a 96-well plate. As per the manufacturer's instructions, the Bio-Rad Coomassie brilliant blue G-250 based reagent (500-0006, Bio-Rad) was prepared by adding 1 part of reagent to 4 parts of water. The diluted reagent (200 µL) was added to each well of the 96-well plate, which contained either standards or sample. Absorbance at 595 nm for each well was determined using a microplate reader (iMark, microplate reader, Bio-Rad). Linear regression analysis was used to generate the standard curve (Microplate Manager 6 software, v6.1, Bio-Rad) and calculate the protein concentration of samples.

2.3.7.3 Electrophoresis and Immunoblotting

Approximately 20 µg of total protein was used in a 25 µL final volume for electrophoresis. The sample for electrophoresis contained 6.25 µL of NuPAGE LDS Sample Buffer (4x) (Invitrogen),

2.5 µL of NuPAGE Reducing Agent (10x) (Invitrogen), the volume corresponding to 20 µg of protein sample and sufficient deionized water to achieve a final volume of 25 µL. The sample was then heated for 10 min at 70°C for protein denaturation. Samples (25 µL) or PageRuler Plus Prestained Protein Ladder (5 µL; ~10-250 kDa) (Thermo Scientific) were loaded in separate lanes on a NuPAGE® Novex® 4-12% Bis-Tris Protein Gel (Invitrogen). The gels were then positioned in an Xcell SureLock® Mini-Cell (Invitrogen) electrophoresis system in order to create an internal and external chamber. NuPAGE MOPS SDS running buffer (Invitrogen) was added to both chambers, and the buffer for the internal chamber also contained 500 µL of NuPAGE antioxidant solution (Invitrogen). Gels were run at 50 V for 10 min to stack proteins then the voltage was increased to 190 V for approximately 60 min for protein separation.

Proteins were then transferred to a PVDF membrane using an iBLOT Dry Blotting device (Invitrogen). After the transfer, membranes were blocked for 1 h in PBS-T, a PBS solution containing 0.1% of Tween20 (Sigma Aldrich). Depending on the antibody used, either 5% skim milk powder or 5% BSA was added (see below). The membranes were then incubated for approximately 1 h with the primary antibody (see conditions below) at room temperature. After primary antibody the blot was washed 3 times (15 min each wash) with PBS-T buffer, membranes were then incubated for 1 h with the secondary antibody (see conditions below).

In this chapter, the primary antibodies used were: IGF1R-β rabbit polyclonal C-20 (SantaCruz Technologies) and IGF1R monoclonal XP® rabbit (IGF-I Receptor β, D23H3) (Cell Signaling) (Table 2.3). Each antibody was diluted 1:1000 in PBS-T buffer containing BSA (5%) (Table 2.3). Horseradish peroxidase (HRP) conjugated goat anti-rabbit IgG (H&L) (Bio-Rad) was the secondary antibody (1:10,000 dilution) (Table 2.3). As a loading control, β-actin levels were assessed using a monoclonal anti-mouse β-actin antibody (Sigma–Aldrich) in PBS-T (5% skim milk powder) at a 1:10,000 dilution (Table 2.3). Horseradish peroxidase (HRP) conjugated goat anti-mouse IgG (Bio-Rad) at 1:10,000 was the secondary antibody (Table 2.3).

Table 2.3 Antibodies used in this chapter for immunoblotting

Primary antibody				Secondary Antibody				Solution
Name	**type**	**Catalog number, Company**	**dilution**	**name**	**type**	**Catalog number, Company**	**dilution**	
IGF1R-β	rabbit polyclonal	sc-713 (C-20) SantaCruz Technologies	1:1000	Horseradish peroxidase (HRP) conjugated	goat anti-rabbit IgG (H&L)	#172-1019, Bio-Rad	1:10,000	PBS-T + BSA 5%
IGF1R	monoclonal XP® rabbit	#9750 β D23H3, Cell Signaling	1:1000	Horseradish peroxidase (HRP) conjugated	goat anti-rabbit IgG (H&L)	#172-1019, Bio-Rad	1:10,000	PBS-T + BSA 5%
β-actin	Monoclonal anti-mouse	AC-15, Sigma Aldrich	1:10,000	Horseradish peroxidase (HRP) conjugated	goat anti-mouse IgG	170-6516, Bio-Rad	1:10,000	PBS-T + Milk 5%

2.3.7.4 Image acquisition and analysis

Membranes were incubated with SuperSignal West Dura Extended Duration Substrate (Thermo Scientific) for 3 min, and then images were acquired using a Bio-Rad Versadoc MP400 Imaging System. Colorimetric imaging was used to acquire images of the ladder, and involved exposure for 5 s under white light. Images of protein bound secondary antibodies were acquired using chemiluminescent imaging, the length of exposure varied between 1 to 10 min depending on the target.

2.3.7.5 Densitometry.

Densitometry was used to compare target protein levels. This was measured using Quantity-One® 1-D imaging software (Bio-Rad). Using the volume tool, each band had background intensity subtracted and this value was compared with the corresponding β-actin loading control band.

2.4 Results

2.4.1 Ca^{2+} pumps, channel and modulator mRNA levels in SKBR3 cells

Quantitative RT-PCR assays were performed for 17 Ca^{2+} pumps, channels and modulators to evaluate mRNA levels in SKBR3 cells normalized to an endogenous control, 18s rRNA (Fig. 2.3). The targets chosen included different type of Ca^{2+} pumps such as PMCAs located on the plasma membrane or SPCAs located on the Golgi membrane. Different types of Ca^{2+} channels were also assessed including Orai channels that together with the STIM proteins produce SOCE, and several TRP channels located on the plasma membrane.

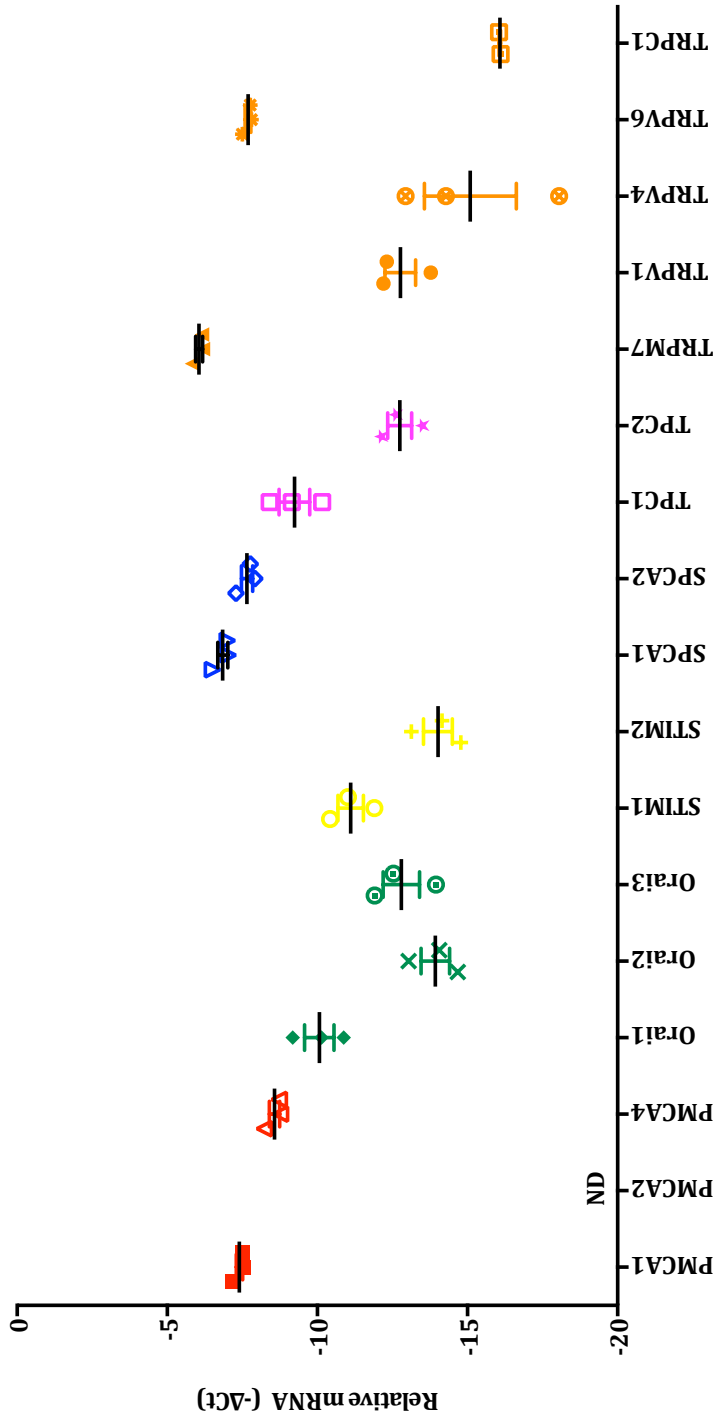

Figure 2.3 Relative mRNA levels of 17 Ca^{2+} pumps, channels and channel modulators in SKBR3 cells

The C_T values obtained for each target have been normalized to a control gene, 18s rRNA. The results are shown as $-\Delta C_T$. Each point represents an independent experiment (n=3). Different colors represent a different type of Ca^{2+} transporter. PMCA2 was not-detected (ND). Mean $-\Delta$Ct values for each target can be found in appendix 3.

SKBR3 cells showed no detectable mRNA expression for PMCA2 (Fig. 2.3), in contrast with some other luminal breast cancer cell lines such as ZR-75-1 (98). PMCA1 and PMCA4 mRNA were abundant in SKBR3 cells (Fig. 2.3) consistent with their reported ubiquitous expression in a variety of cell types, including breast cancer cell lines (228) and their reported "housekeeping" roles (241).

Ca^{2+} channels present on the plasma membrane such as the Orai channels showed large variations in mRNA levels. Orai1 mRNA was present at higher levels in SKBR3 cells than Orai2 and Orai3 mRNA (Fig. 2.3). The high levels of Orai1 compared to other Orai isoforms are consistent with previous studies by McAndrew et al (72). However, in contrast to McAndrew et al, my studies found similar levels of Orai2 and Orai3, this may be due to different culture conditions or the confluence of the SKBR3 used in this study.

The two Ca^{2+} sensors STIM1 and STIM2 showed different mRNA levels with a higher mRNA level of STIM1 compared to STIM2. This is in accordance with McAndrew and colleagues (72), who described a higher STIM1/STIM2 ratio in SKBR3 cells. Moreover, the relative mRNA level between STIM1 and STIM2 appears to be higher in SKBR3 cells compared to other breast cancer cell lines (72).

Assessment of mRNA expression levels of SPCA pumps, located on the Golgi complex, indicated that SPCA1 and SPCA2 had similar mRNA levels in SKBR3 cells (Fig. 2.3). The presence of SPCA2 mRNA in SKBR3 cells is in contrast to the basal-like MDA-MB-231 breast cancer cell line where very low to no SPCA2 is present, but was similar to the luminal like MCF-7 breast cancer cell line where high levels of SPCA2 have been reported. (107).

TPC channels have not been extensively studied in breast cancer cells. However, it has been previously reported that TPC1 is expressed in SKBR3 breast cancer cells (242) and that TPC1 and TPC2 mRNA is present in MDA-MB-231 and MDA-MB-468 cells (243). Consistent with the work of Brailoiu et al., mRNA levels of TPC1 were higher than TPC2 in SKBR3 cells (242).

TRP channel mRNA levels have not been extensively assessed in SKBR3 breast cancer cells. However, studies have reported that TRPM7 is expressed in MCF-7 cells (244), MDA-MB-231 cells (245) and in MDA-MB-468 cells (221). A study has also shown that TRPV1, TRPV4 and TRPV6 are expressed in MCF-7 cells (244), and another has reported TRPV6 and TRPV4 in T47D cells (246, 247). TRPV4 mRNA levels are higher in MDA-MB-468 cells compared to MDA-MB-

231 and HCC1569 cells (248). Low levels of TRPC1 mRNA have also been reported in MCF-7 and MDA-MD-231 cell lines, but not in T47D cells (249). The SKBR3 cells assessed in this study appear to have high levels of TRPM7 and TRPV6 mRNA compared to the other TRP channels assessed (Fig. 2.3), with lower levels of TRPV1, TRPV4 and TRPC1.

2.4.2 Characterization of Ca^{2+} signaling in SKBR3 cells

In order to better understand calcium signaling in SKBR3 cells, cytoplasmic Ca^{2+} levels were assessed using the Ca^{2+} indicator Fluo-4 AM and a fluorescent imaging plate reader, FLIPR. The response to ATP and EGF and also SOCE were assessed in SKBR3 cells to represent different potential regulators of $[Ca^{2+}]_i$.

Purinergic receptors are activated by ATP, and have been reported to increase $[Ca^{2+}]_i$ in a variety of breast cancer cell lines (250). Increases in $[Ca^{2+}]_i$ were assessed after stimulation with different concentrations of ATP (Fig. 2.4). In the presence of the Ca^{2+} chelator BAPTA, to remove extracellular Ca^{2+}, the ATP response was still present, indicative of Ca^{2+} store release. However, the EC_{50} for ATP in the presence of BAPTA was 4.7 μM, 9-fold higher than in the absence of BAPTA (Fig. 2.4b) suggesting that Ca^{2+} influx is also important in the ATP response in these cells. The EC_{50} values were similar to that reported in the basal like MDA-MB-468 breast cancer cell line (224), and the luminal MCF-7 breast cancer cell line (251), suggesting that there is no major difference in ATP-mediated $[Ca^{2+}]_i$ responses in these different breast cancer cell lines.

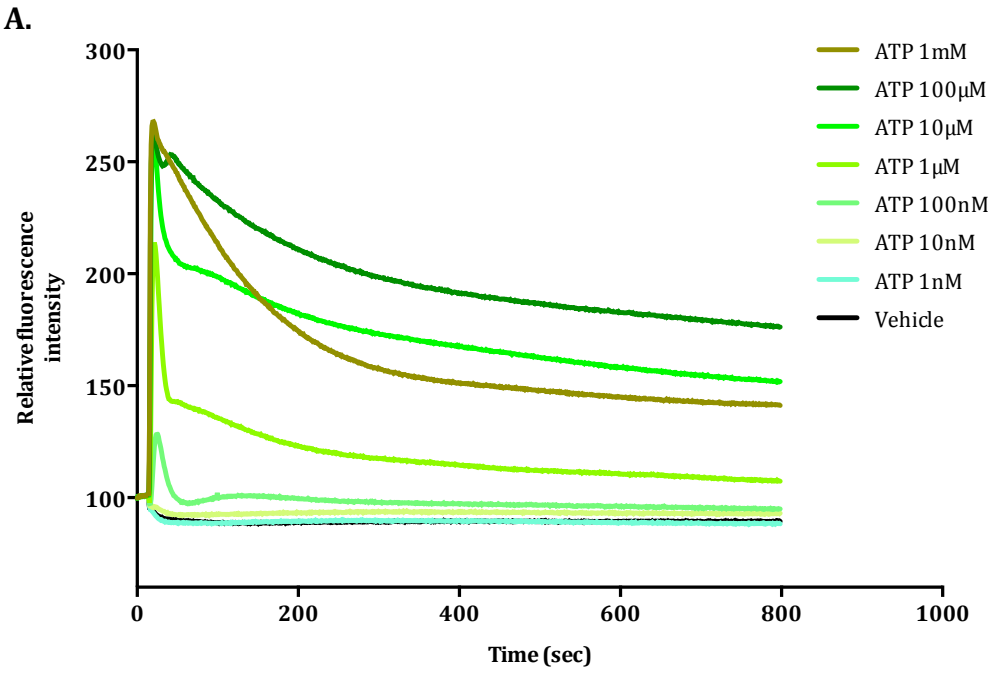
A.
Relative fluorescence intensity
300
250
200
150
100
0
200
400
600
800
1000
Time (sec)
ATP 1mM
ATP 100µM
ATP 10µM
ATP 1µM
ATP 100nM
ATP 10nM
ATP 1nM
Vehicle

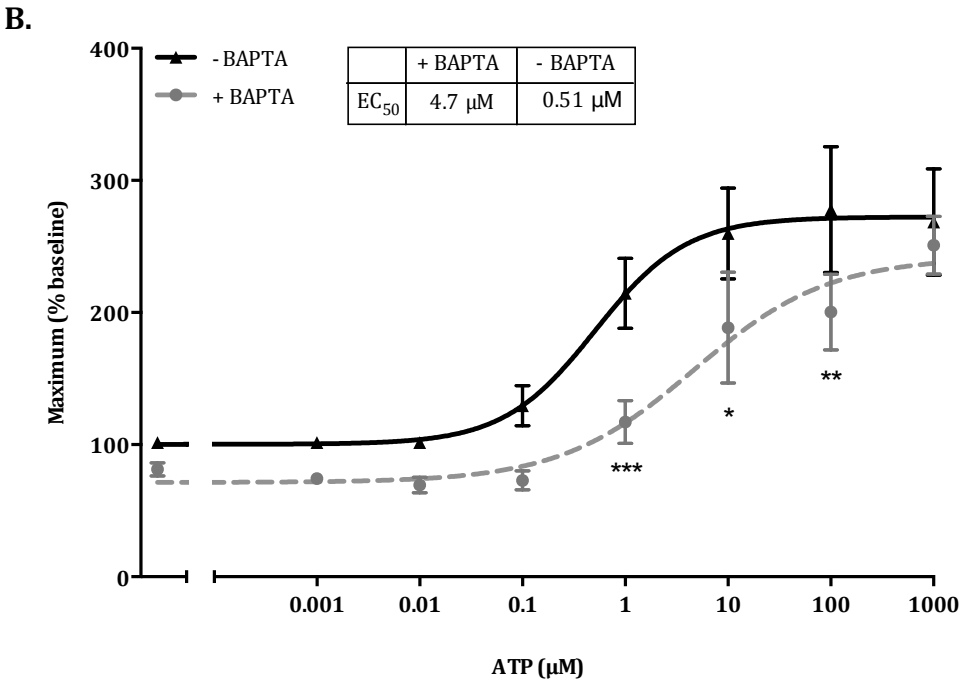
B.
- BAPTA
+ BAPTA
+ BAPTA
- BAPTA
EC50
4.7 µM
0.51 µM
Maximum (% baseline)
400
300
200
100
0
0.001
0.01
0.1
1
10
100
1000
ATP (µM)
***
*
**

Figure 2.4 Assessment of $[Ca^{2+}]_i$ in SKBR3 cells following stimulation with different concentrations of ATP

A. Average of Ca^{2+} traces from three independent experiments showing the increase of $[Ca^{2+}]_i$ due to different concentration of ATP. ATP traces are shown as compared to the vehicle. **B**. The graph represents the dose response curves for measurements of maximum $[Ca^{2+}]_i$ assessed using 0.001 μM, 0.01 μM 0.1 μM, 1 μM, 10 μM, 100 μM and 1 mM of ATP in the presence or absence of BAPTA (0.5 mM) and are shown ± S.D. (n=3). The EC_{50} value without BAPTA was 0.51 μM, while in its presence the EC_{50} value was 4.7 μM. Statistical analysis was performed using two-way ANOVA with Bonferroni post-tests (* $p \leq 0.05$, ** $p \leq 0.01$, *** $p \leq 0.001$).

EGF, the EGFR endogenous ligand, increases intracellular Ca^{2+} in several cell lines (252). EGF (50 ng/mL) is known to phosphorylate EGFR and activate downstream signaling such as Akt (253). However, EGF did not increase $[Ca^{2+}]_i$ in SKBR3 cells (Fig. 2.5).

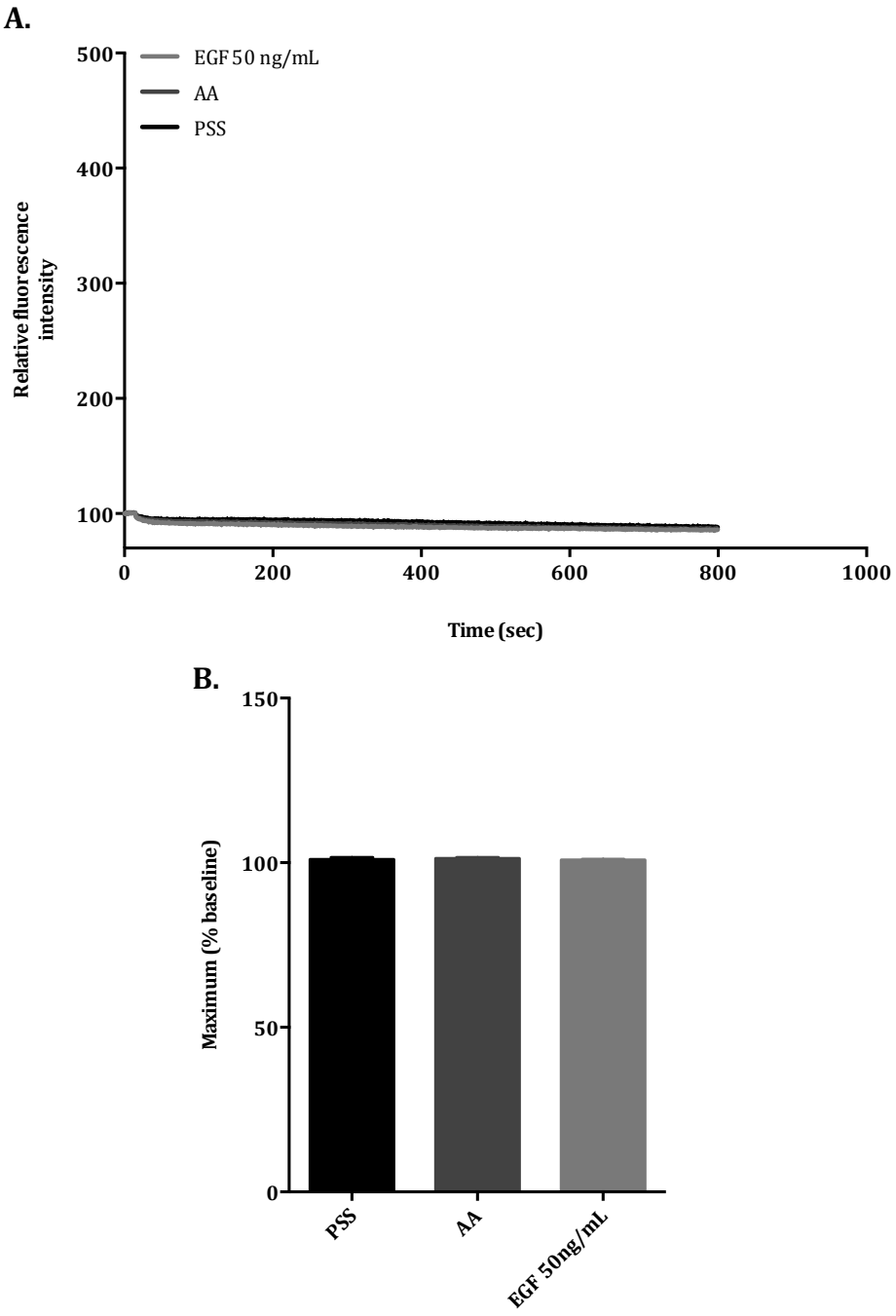

Figure 2.5 Assessment of $[Ca^{2+}]_i$ in SKBR3 cells following stimulation with 50ng/mL EGF

A. Example of a Ca^{2+} trace upon EGF treatment. Acetic acid (AA) was used as the vehicle. **B**. The graph represents the measurement of maximum $[Ca^{2+}]_i$ assessed using 50 ng/mL of EGF (n=3, ± S.D.).

SOCE influx is caused by the emptying of internal stores, mostly the ER store; this causes STIM1 Ca^{2+} sensors, present on the ER membrane, to dimerize and activate Orai channels present on the plasma membrane to induce Ca^{2+} influx to replenish the empty Ca^{2+} stores (62). To evaluate store operated Ca^{2+} entry, SKBR3 cells were pretreated with 500 μM BAPTA (to chelate all extracellular Ca^{2+}), followed by the addition of 10 μM CPA that causes the release of calcium from the ER. Upon re-addition of extracellular Ca^{2+} (2 mM), a calcium influx was produced increasing the cytosolic Ca^{2+} concentration (Fig. 2.6).

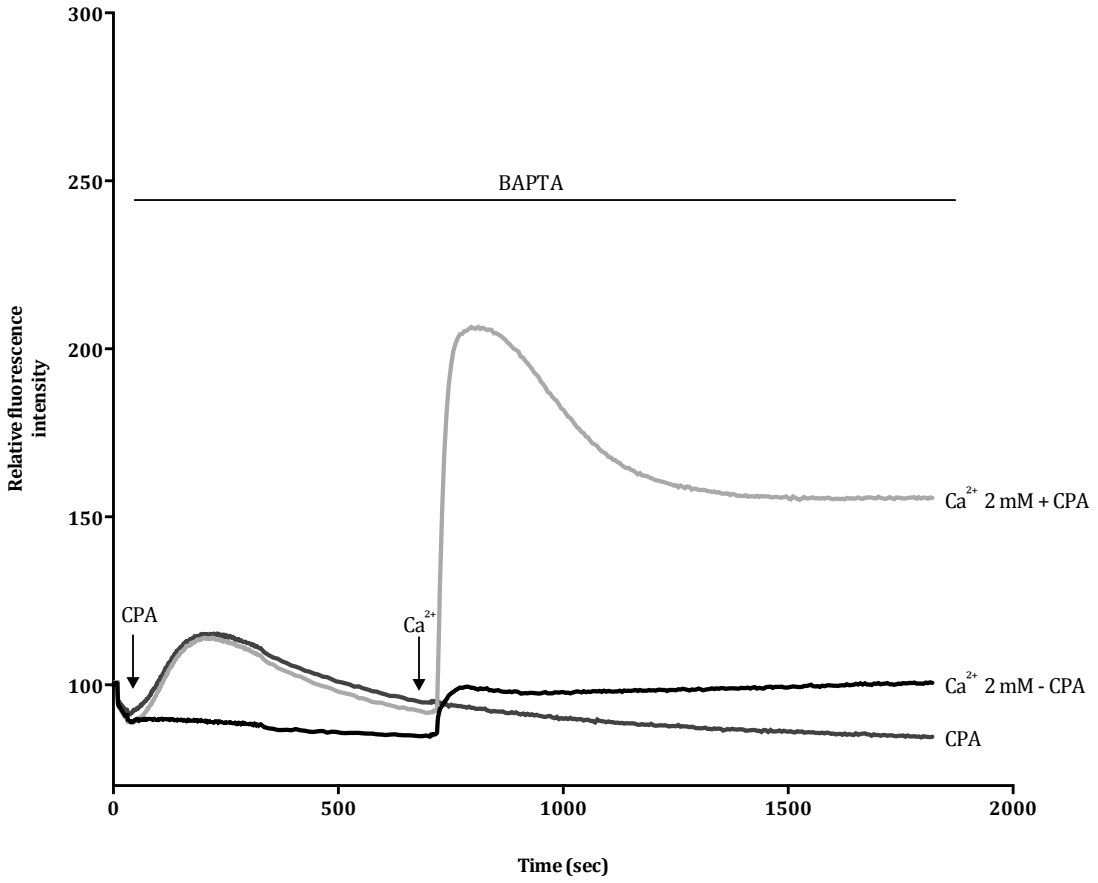

Figure 2.6 Assessment of $[Ca^{2+}]_i$ in SKBR3 cells following SOCE stimulation

Average of Ca^{2+} traces from three different experiments showing the SOCE in SKBR3 cell line. In the presence of external BAPTA (500 μM), CPA (10 μM) was added to empty the calcium store (first peak), then Ca^{2+} (2 mM) was added to assess store-depletion mediated Ca^{2+} influx (second peak).

The transient increase in $[Ca^{2+}]_i$ due to store depletion (first peak) was not affected by the removal of extracellular Ca^{2+}. The addition of CPA clearly promoted SOCE as evidenced by the greater Ca^{2+} influx (peak 2) in the presence of CPA-mediated Ca^{2+} store depletion (Fig. 2.6). A small Ca^{2+} influx (Ca^{2+} leak) was observed in the absence of CPA, this Ca^{2+} leak was similar in magnitude to that reported in MCF-7 and MDA-MB-231 breast cancer cells (72), but less than that recently reported in MDA-MB-468 breast cancer cells (238).

2.4.3 Effect of Ca^{2+} pumps, channels and channel modulators silencing on the proliferation of SKBR3 cells

In order to evaluate the effect of silencing specific Ca^{2+} pumps, channels and channel modulators on the proliferation of SKBR3 cells siRNA was used. The screen included 19 Ca^{2+} related targets chosen from the siRNA library present in the Calcium Signaling in Cancer Research Laboratory at the time these experiments were performed. The siRNA treatment was optimized as described in the methods section of this chapter.

From the siRNA screen, three targets, STIM1, TPC2 and TRPV1 that potentially decrease SKBR3 cell proliferation were selected as they reduced the percentage of cells in S phase (Fig. 2.7). Orai2 and STIM2 siRNA appeared to also inhibit proliferation although to a lesser extent using this assay (Fig. 2.7).

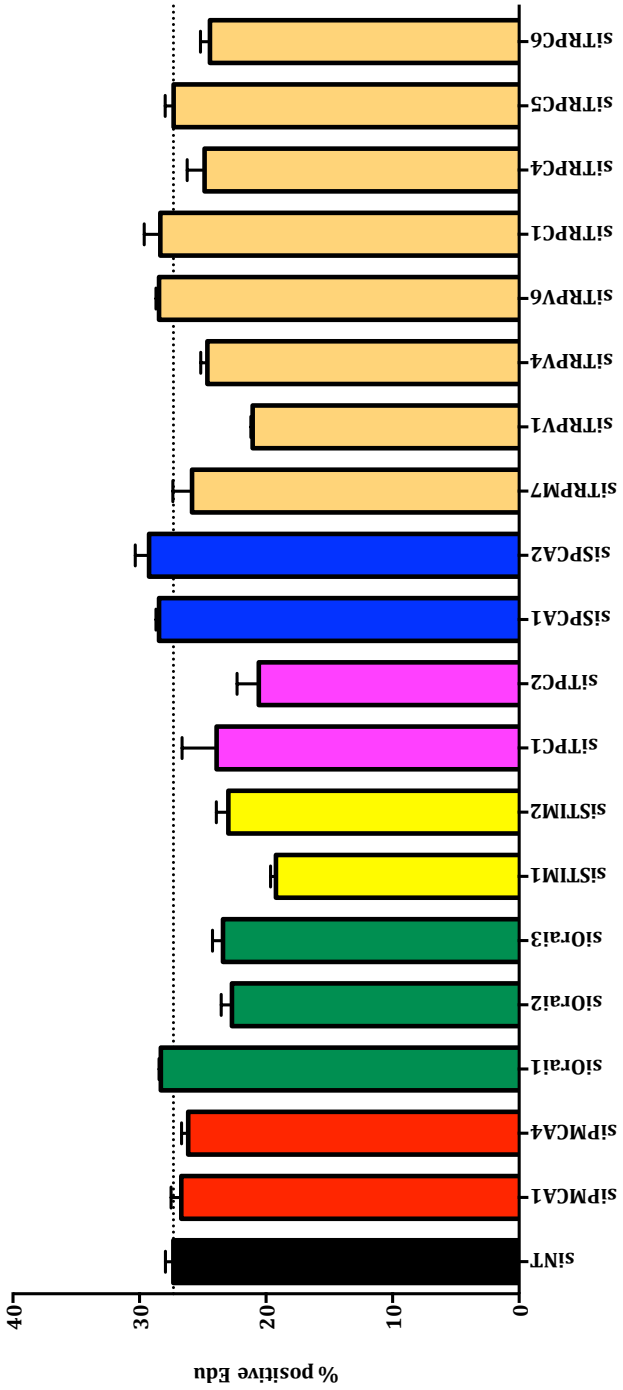

Figure 2.7 Effect of silencing of specific Ca^{2+} pumps, channels and modulators on the proliferation of SKBR3 cells

An siRNA screen of 19 targets evaluated possible anti-proliferative effects in SKBR3 cells through changes in the % of cells in S phase (produced from three separate wells from the same experiment, mean ± S.D.).

STIM1 is an important element of store-operated Ca^{2+} entry as it is the Ca^{2+} sensor present on the ER. It detects the depletion of Ca^{2+} from the store and, via self-association activates Orai channels present on the plasma membrane and produces Ca^{2+} influx to replenish internal Ca^{2+} stores (62).

STIM1 has been linked to cancer through its role in cell proliferation and migration (207, 254). Recently it has been shown that STIM1 is involved in cell proliferation in human epidermoid carcinoma A431 cells, where the silencing of STIM1 reduced cell proliferation *in vitro* and *in vivo* (xenografts) (254).

The TPC2 channel, as discussion in section 1.1.2.1, is a recently discovered voltage-gated ion channel made up of 12 putative transmembrane segments (82). It is activated by NAADP and is mainly located on the lysosomal membranes (82). It is believed to function as a dual sensor for luminal pH and Ca^{2+} (83). Few studies have been carried out on the role of TPC2 in cancer, however, it appears that TPC2 may be involved in autophagy in astrocytes (255). TPC2 appears to be often overexpressed in primary human oral cancers even without gene amplification, and has been proposed as a potential contributor to the progression of some cancer cells (256).

The transient receptor potential vanilloid 1 (TRPV1) channel is involved in nociception and coordination of painful stimuli (257). TRPV1 channels have been reported to increase expression in some prostate, colon, pancreatic and bladder cancers (258-261). TRPV1 overexpression can increase the migration and invasion in human hepatoblastoma cells (262).

2.4.4 Effect of silenced Ca^{2+} pumps, channels and channel modulators on the proliferation of SKBR3 cell treated with trastuzumab

The SKBR3 cell line was also used to evaluate trastuzumab activity and the role of Ca^{2+} pumps, channels and channel modulators in potentially modulating trastuzumab activity.

Following the protocol described in section 2.3.4, different concentrations of trastuzumab (0.1 μg/mL, 0.3 μg/mL, 1 μg/mL, 3 μg/mL, 10 μg/mL, 30 μg/mL, 100 μg/mL) were added 4 days after seeding, after 72 h of trastuzumab treatment, the percentage of cells in S phase was assessed using the Click-iT® Edu assay.

Trastuzumab induces cell-cycle arrest, in particular G_1 to S phase (263) and thus has an anti-proliferative effect in HER2-positive cells (264). The Click-iT® Edu assay clearly showed S phase decrease due to the anti-proliferative activity of trastuzumab (Fig. 2.8).

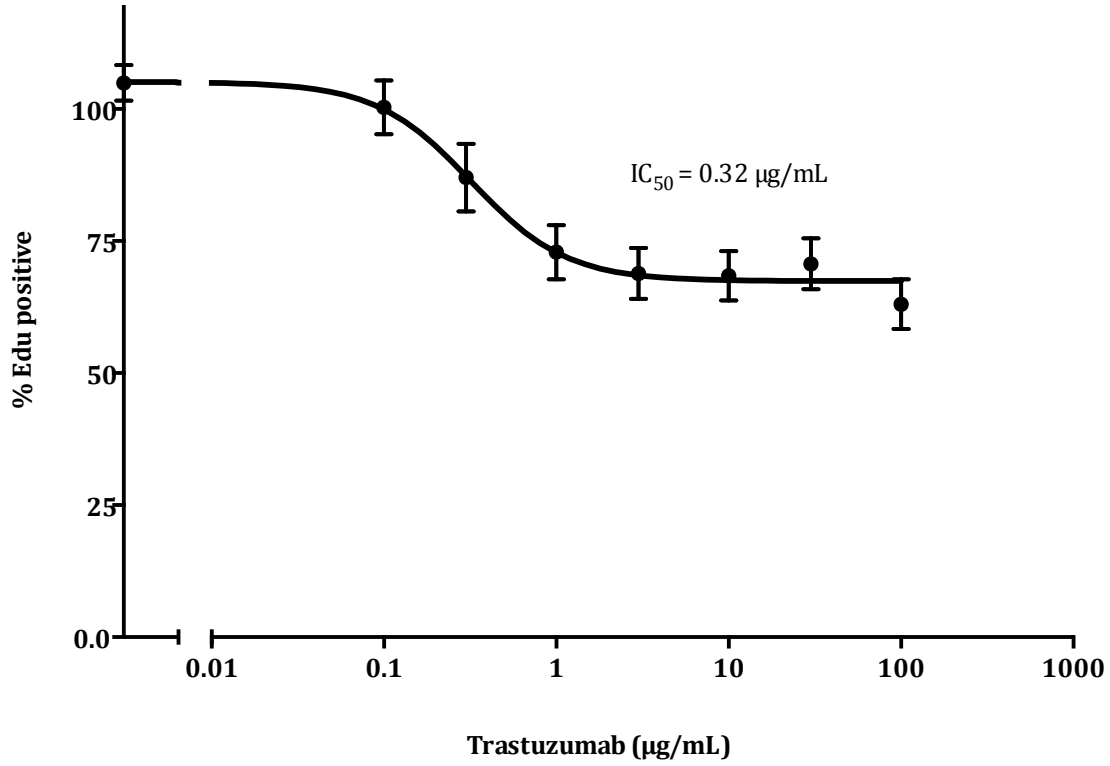

Figure 2.8 Dose response curve for trastuzumab inhibitory effect on the proliferation of SKBR3 cells

In SKBR3 cells 72 h treatment with trastuzumab produced concentration dependent effects on the % of cells in S Phase. The IC_{50} for trastuzumab effects was 0.32 µg/mL (n= 3, ± S.D.).

The assesment of proliferation produced a concentration response curve which showed that trastuzumab inhibits the proliferation of SKBR3 cells with an IC_{50} of 0.32 μg/mL (Fig. 2.8).

After assessing the effect of trastuzumab in SKBR3 cells, the next step was to evaluate how silencing selected Ca^{2+} pumps, channels and channel modulators could affect the trastuzumab response. Each siRNA sample was tested using two different concentrations of trastuzumab, 30 μg/mL (maximal dose) and 0.3 μg/mL (submaximal dose), and water as a control. Non-Targeting siRNA (siNT) siRNA was transfected into SKBR3 cells treated with the same concentrations of trastuzumab and water as a control. Cells treated with only trastuzumab 30 μg/mL or 0.3 μg/mL were also included as additional controls. Results for each target were normalized to the cells treated with the respective siRNA and vehicle in order to evaluate the effect of silencing on the activity of trastuzumab and discount targets which simply affected proliferation. Figure 2.9 shows the combined effect of the silencing of each target and the activity of trastuzumab on cell proliferation using the Click-iT® Edu assay in comparison with cells treated with siNT and trastuzumab.

At a submaximal dose of 0.3 μg/mL trastuzumab SPCA1, STIM1 and TRPM7 siRNA decreased the proliferation of SKBR3 cells, while TPC1 and TPC2 siRNA appeared to increase it (Fig. 2.9a). From this screen, these 3 targets, SPCA1, TRPM7 and STIM1, were selected for further assessment based on their more pronounced effects on the trastuzumab response (Fig. 2.9a). At a maximal dose of 30 μg/mL trastuzumab it appeared that TPC1 and TPC2 may have increased the effect of trastuzumab on SKBR3 (Fig. 2.9b).

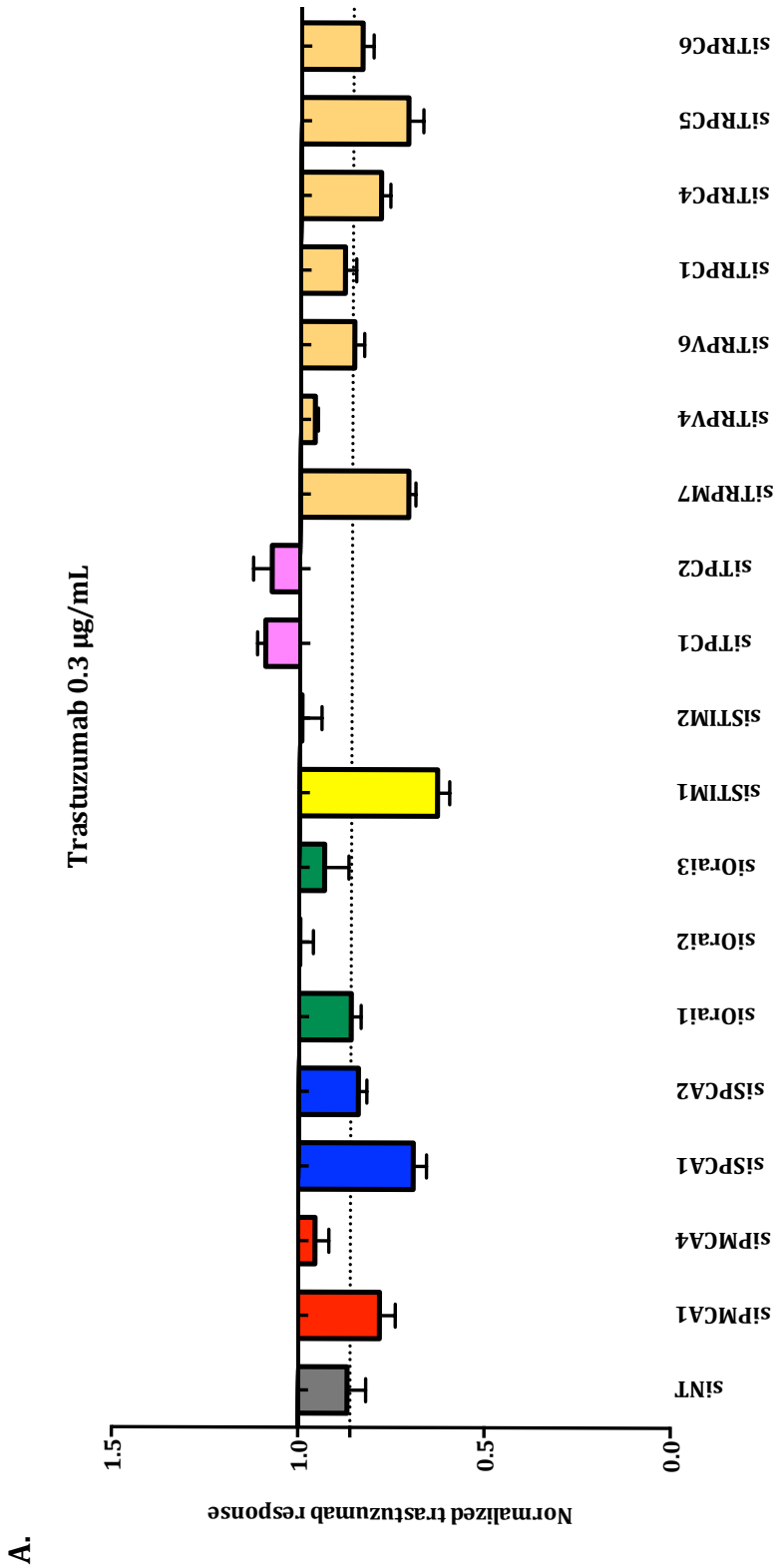
A.
Trastuzumab 0.3 µg/mL
Normalized trastuzumab response
1.5
1.0
0.5
0.0
siNT
siPMCA1
siPMCA4
siSPCA1
siSPCA2
siOrai1
siOrai2
siOrai3
siSTIM1
siSTIM2
siTPC1
siTPC2
siTRPM7
siTRPV4
siTRPV6
siTRPC1
siTRPC4
siTRPC5
siTRPC6

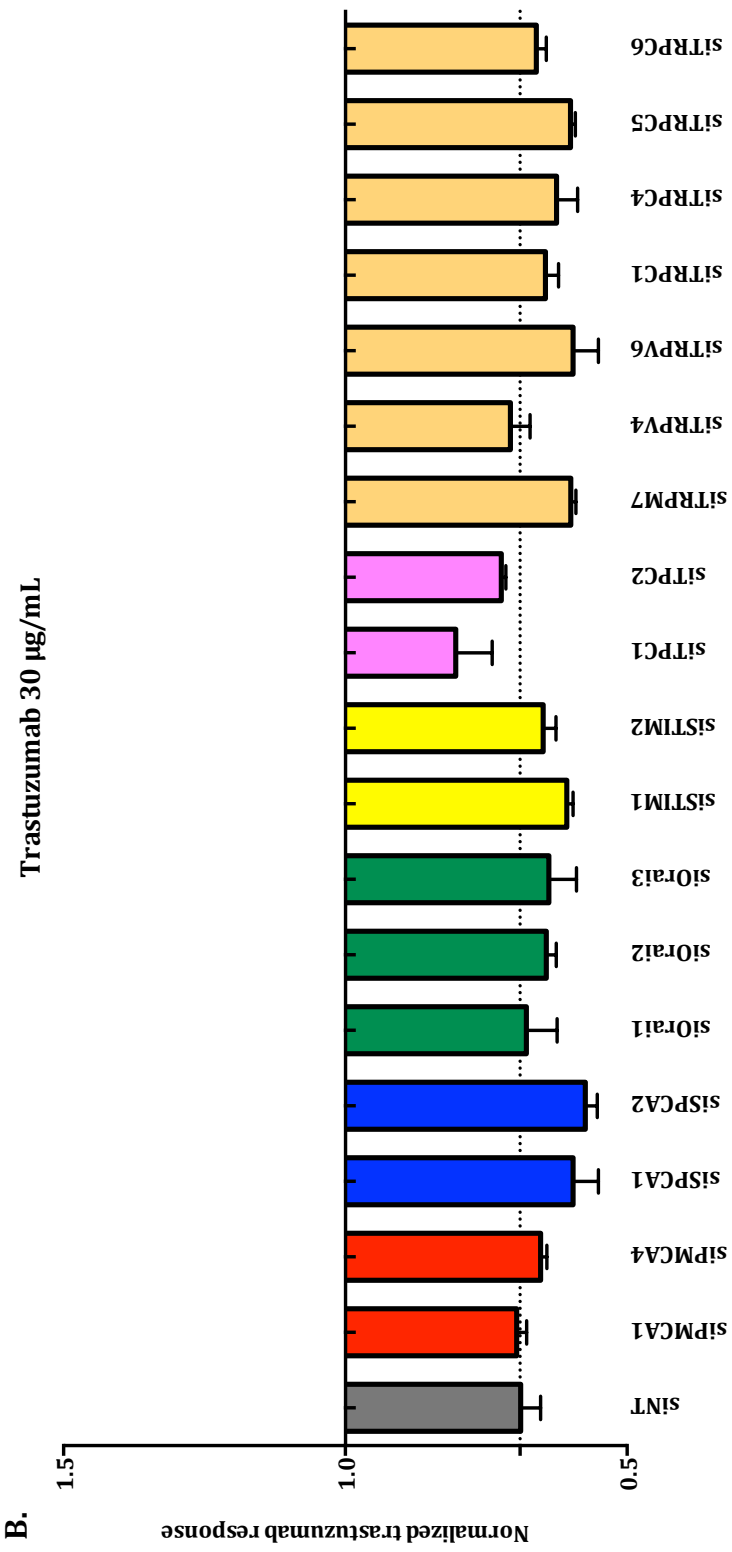
B.
Trastuzumab 30 µg/mL
Normalized trastuzumab response
1.5
1.0
0.5
siNT
siPMCA1
siPMCA4
siSPCA1
siSPCA2
siOrai1
siOrai2
siOrai3
siSTIM1
siSTIM2
siTPC1
siTPC2
siTRPM7
siTRPV4
siTRPV6
siTRPC1
siTRPC4
siTRPC5
siTRPC6

Figure 2.9 siRNA screen of 19 Ca^{2+} pumps, channels and channel modulators in SKBR3 cells treated with trastuzumab

The graph shows the normalized trastuzumab response. **A.** Effect of silencing 19 Ca^{2+} pumps, channels and channel modulators in SKBR3 using trastuzumab at submaximal concentration (0.3 μg/mL), (n=1, S.D. produced from three separate wells from the same experiment). **B.** Effect of silencing 19 Ca^{2+} transporters in SKBR3 using trastuzumab at maximal concentration (30 μg/mL), (produced from three separate wells from the same experiment ± S.D.).

For each of the selected targets confirmation assays using the Click-iT® Edu assay to measure S phase were performed using three to four independent experiments. TRPM7 silencing at 7 days after siRNA treatment was confirmed using quantitative RT-PCR (Fig. 2.10a). TRPM7 siRNA treatment increased the anti-proliferative effect of 0.3 μg/mL trastuzumab as assessed by a reduction in the number of cells in S phase (Fig. 2.10b).

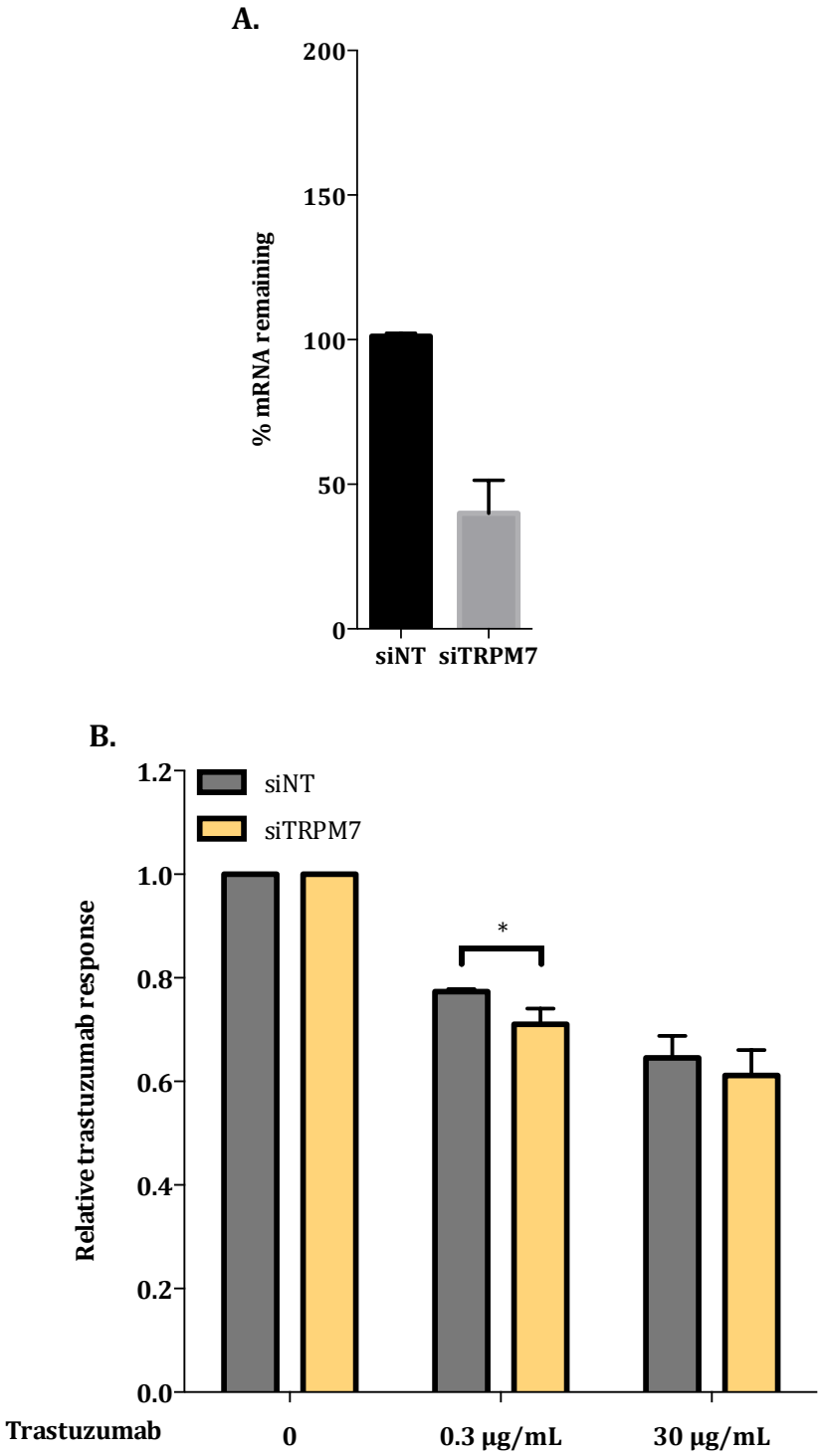

Figure 2.10 Effect of TRPM7 silencing on trastuzumab activity

A. Quantitative RT-PCR at 7 days after siRNA treatment confirmed TRPM7 silencing in SKBR3 cells (n=3, ± S.D.). 18s rRNA was used as internal control. **B**. TRPM7 silencing significantly enhanced the reduction in the percentage of cells in S phase induced by trastuzumab at submaximal but not at maximal concentrations (n=4, ± S.D.). Statistical analysis was performed using two-way ANOVA with Bonferroni post-test (* $p \leq 0.05$).

The silencing of STIM1 7 days after siRNA treatment was confirmed using quantitative RT-PCR (Fig. 2.11a). The silencing of STIM1 enhanced trastuzumab activity at both 0.3 μg/mL and 30 μg/mL trastuzumab (Fig. 2.11b).

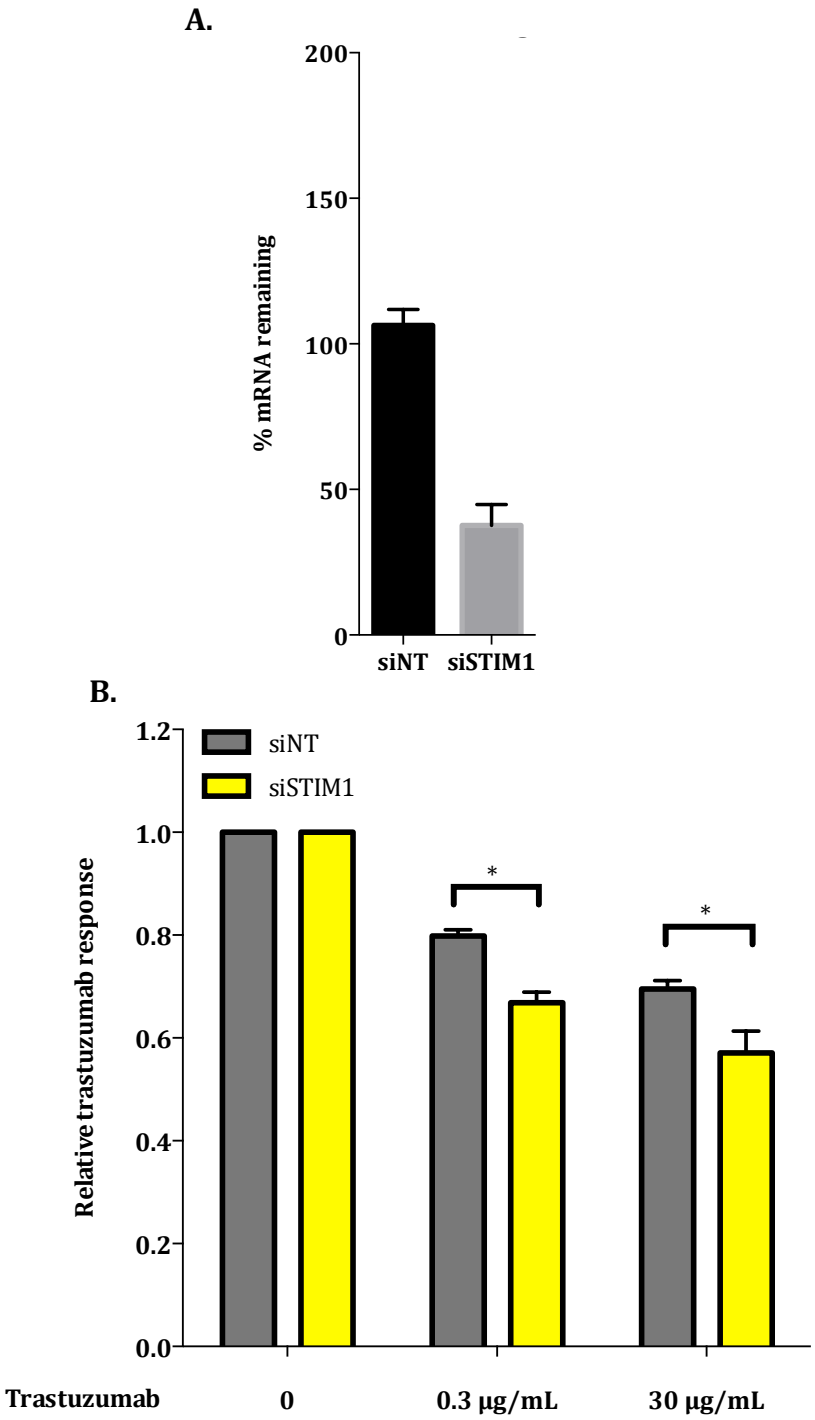

Figure 2.11 Effect of STIM1 silencing on trastuzumab activity

A. Quantitative RT-PCR at 7 days after siRNA treatment confirmed STIM1 silencing in SKBR3 cell (n=3, ± S.D.). 18s rRNA was used as internal control. **B**. STIM1 silencing significantly enhanced trastuzumab effects on the % of cells in S phase at both concentrations tested (n=4, ± S.D.). Statistical analysis was performed using two-way ANOVA with Bonferroni post-test (* $p \leq 0.05$).

The silencing of SPCA1 was confirmed at day 7 after siRNA treatment using quantitative RT-PCR (Fig. 2.12a). The silencing of SPCA1 appeared to enhance the anti-proliferative activity of trastuzumab at the submaximal concentration tested (Fig. 2.12b). Because SPCA1 has been shown to be a key regulator of IGFR (106) a protein linked to trastuzumab resistance (265), this potential mechanism was further assessed.

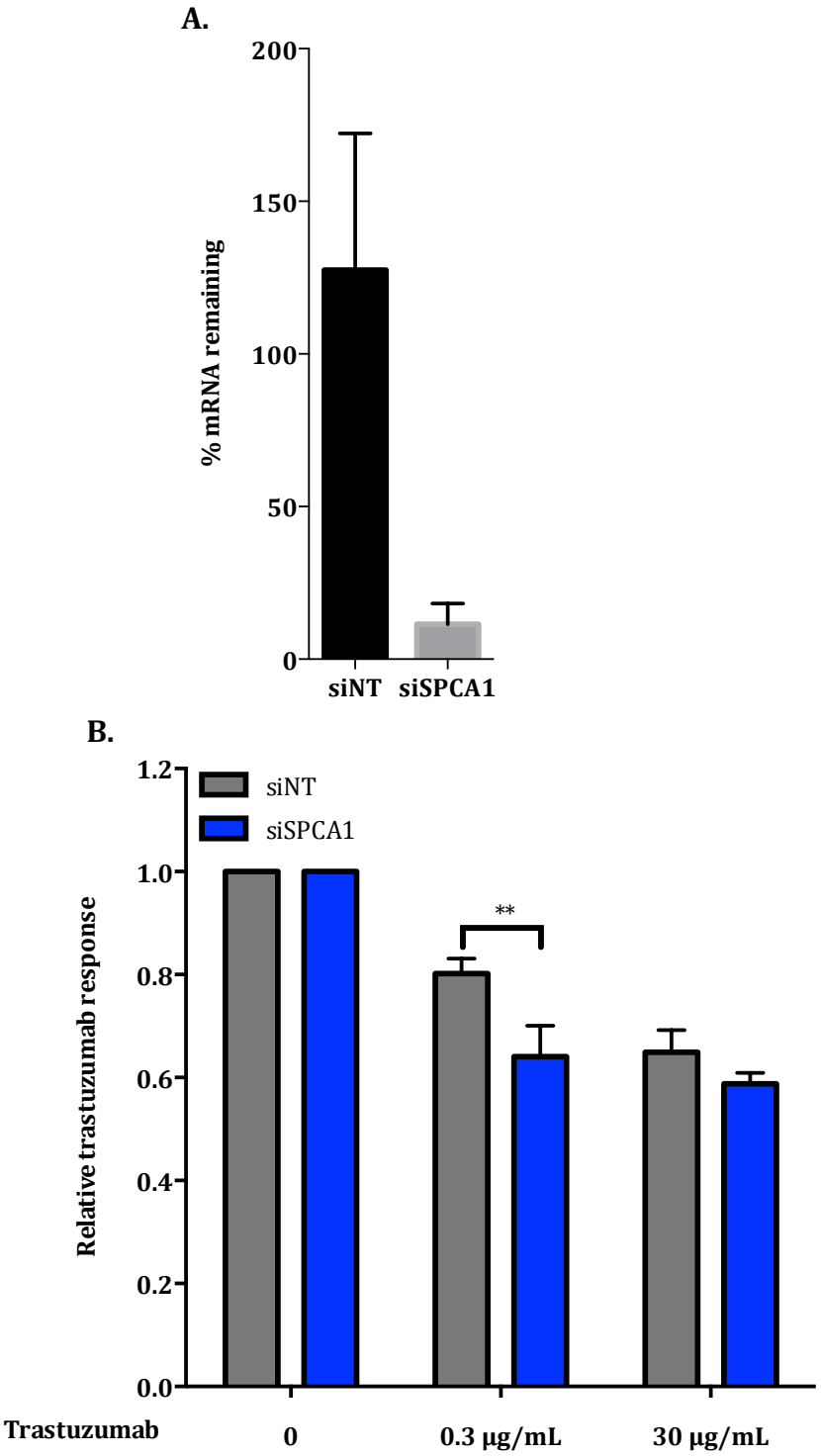

Figure 2.12 Effect of SPCA1 silencing on trastuzumab activity

A. Quantitative RT-PCR at 7 days after siRNA treatment confirmed SPCA1 silencing in SKBR3 cell (n=3, ± S.D.). 18s rRNA was used as internal control. **B.** SPCA1 silencing significantly enhanced trastuzumab anti-proliferative effect at the submaximal concentration but not the maximal concentration (n=4, ± S.D.). Statistical analysis was performed using two-way ANOVA with Bonferroni post-test *(* $p \leq 0.01$).

2.4.4.1 Effect of SPCA1 silencing on the proliferation of SKBR3 cell line treated with trastuzumab

SPCA1 has been shown to be involved in the processing of IGF1R from its pro-form to the mature form in MDA-MD-231 cells (106). In this study, the expression of IGF1R forms in SKBR3 cells were evaluated and compared to expression of IGF1R in MDA-MB-231 cells. It appeared that the SKBR3 cell line did not showed very little expression of either the pro-form or mature IGF1R-β form, whereas these were observed in MDA-MB-231 cells, where the SPCA1 silencing phenotype was reproduced (Fig. 2.13). In SKBR3 cells the antibody (IGF1R-β rabbit polyclonal sc-713 (C-20) from SantaCruz Technologies), detected a band of approximately 130 kDa, which may be the IGF1R-α subunit (Fig. 2.13). This 130 kDa band may be slightly lighter in the SPCA1 siRNA treated sample. Further studies are required to assess other IGF1R–dependent and independent mechanisms for the promotion of the trastuzumab response with SPCA1 silencing.

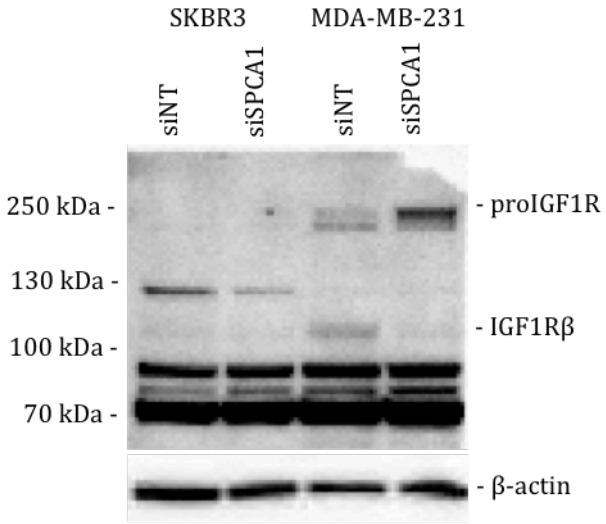

Figure 2.13 Effect of siRNA silencing on the protein expression of IGF1R in SKBR3 and MDA-MB-231 cells

An immunoblot showing IGF1R protein 48 h after SPCA1 silencing using siRNA in SKBR3 and MDA-MD-231 cells. An upper band around 250 kDa shows the pro-form of IGF1R and a band around 100 kDa shows the mature form of IGF1Rβ in MDA-MB-231.

Since the previous antibody used was a polyclonal antibody, another antibody for IGF1R, a monoclonal antibody selective for IGF1R-β receptor (IGF1R monoclonal XP® rabbit #9750 (IGF-I Receptor β, D23H3) from Cell Signaling), was used on untreated cell lines. The expected pro-form and the mature form of the IGF1R-β receptor in both SKBR3 and MDA-MB-231 cells was observed (Fig. 2.14). Silencing IGF1R using siRNA confirmed that the two bands were IGF1R (Fig. 2.14b). However, the expression of IGF1R-β in SKBR3 cells appeared to be much smaller compared to MDA-MB-231 (Fig. 2.14a). Moreover, SPCA1 silencing clearly did not increase levels of the pro form in SKBR3 cells as it did in MDA-MB-231 cells (Fig. 2.14b).

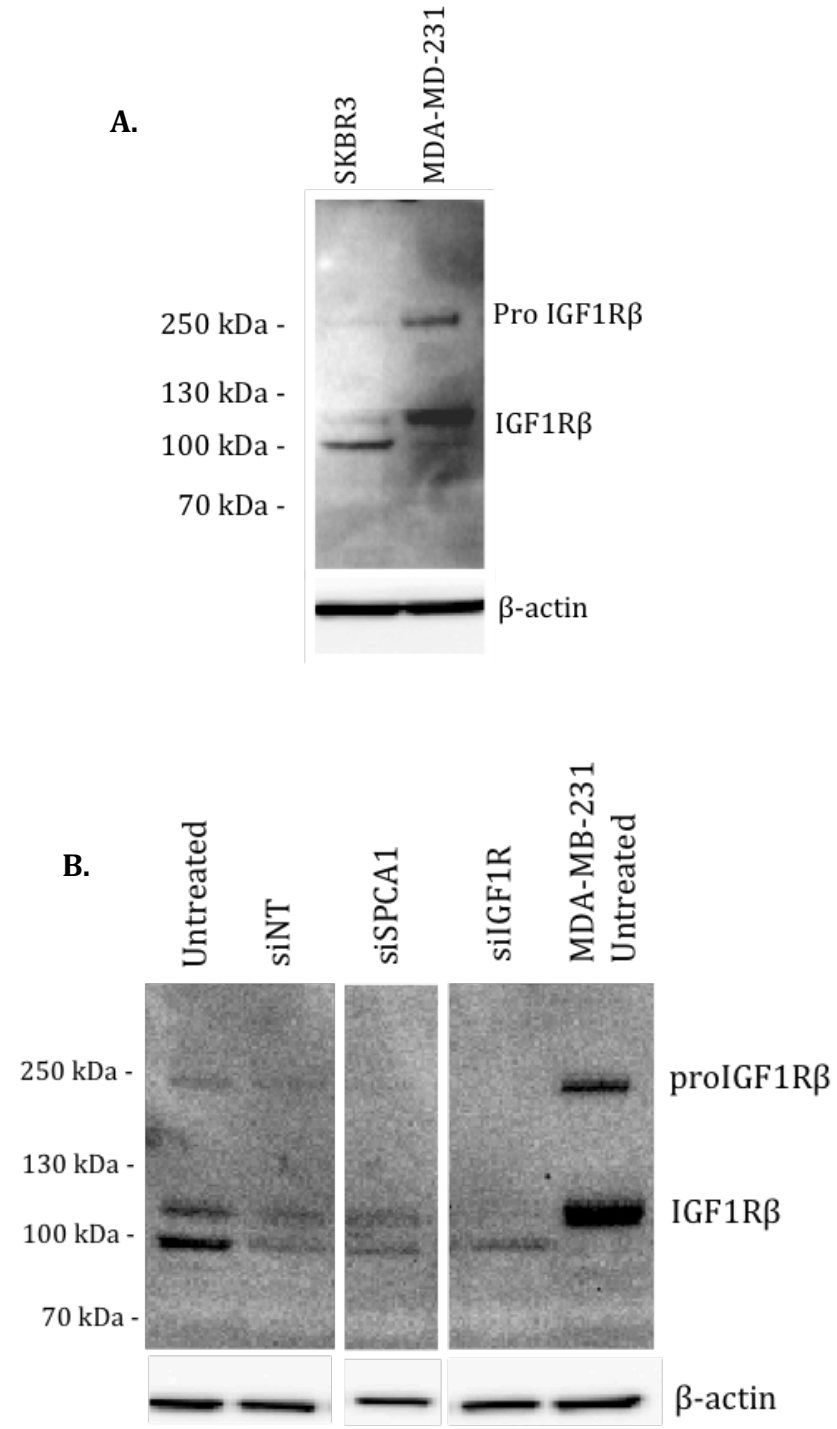

Figure 2.14 Effect of siRNA silencing on the protein expression of IGF1R in SKBR3 and MDA-MB-231 cells

A. Immunoblot showing IGF1R protein in SKBR3 and MDA-MD-231 using a monoclonal antibody for the IGF1R-β. **B.** Immunoblot showing IGF1R protein level in SKBR3 after silencing of IGF1R and SPCA1 in SKBR3. MDA-MB-231 cells were used as control.

2.5 Discussion

In this chapter I have evaluated the expression and the effect of silencing of Ca^{2+} channel, pumps and channel modulators on the HER2-positive SKBR3 breast cancer cell line.

Assessment of mRNA levels in SKBR3 cells showed that the expression of several Ca^{2+} transporters and modulators in some cases differed from other breast cancer cell lines. For example, SKBR3 cells had similar levels of SPCA1 and SPCA2, which is in contrast to MDA-MB-231 cells, which are characterized by lower levels of SPCA2 compared to SPCA1 (107). Moreover, SKBR3 cells do not express PMCA2, which is in contrast to another luminal cell line, ZR-75-1 cells (228).

Assessment of Ca^{2+} signaling in SKBR3 cells, demonstrated responsiveness to the purinergic receptor activator ATP. In contrast, EGF did not increase $[Ca^{2+}]_i$ in this cell line. This was despite reports that 50 ng/mL of EGF can activate the EGFR receptor and downstream signaling such as ERK and Akt in this cell line (253). It might be that the EGF concentration required to activate the ERK and Akt pathways is less than the concentration required to show a cytosolic Ca^{2+} increase in SKBR3 cells. Indeed, in other cancer cell lines, such as gliomas and hepatoma cells, the concentration of EGF used to measure Ca^{2+} mobilization was higher (200-300 ng/mL) (252, 266). SOCE was also present in SKBR3 cells, consistent with studies in other breast cancer cell lines such as MCF-7 and MDA-MB-231 cells (72, 238).

A screen of a variety of siRNAs to calcium pumps, channels and channel modulators identified that STIM1, TPC2 and TRPV1 silencing potentially have anti-proliferative effects in SKBR3 cells. TPC2 and TRPV1 have not been extensively studied in breast cancer cells, and this study suggests that these proteins should be further studied in SKBR3 cells, since TRPV1 is up-regulated in some breast cancer cell lines (267) and TPC2 has not been extensively studied in the context of breast cancer. However, studying TPC channels may be challenging since it is currently debated if these are Ca^{2+} channels or Na^{2+} channels (268).

STIM1 silencing decreased SKBR3 proliferation and also enhanced the effects of trastuzumab. As described in section 1.5.3, STIM1 is associated with altered cell migration mediated by calpain activity, and STIM1 knockdown inhibits EGF-induced calpain activation (207). Moreover, the STIM1/STIM2 mRNA ratio appears to be higher in SKBR3 cells compared to other breast cancer cell lines (72), suggesting that STIM1 may be particularly important in this HER2-positive cell line.

Recently, STIM1, as part of SOCE, has been shown to be involved in the progression towards advanced androgen-independent prostate cancer, which is characterized by resistance to apoptotic cell death (161). It appears that a cytoskeleton reorganization occurs during neuroendocrine differentiation, which is a feature of advanced androgen-independent prostate cancer. This may contribute to SOCE down-regulation and progression of some cancers (269). As trastuzumab resistance is usually associated with progression to metastasis (128), it could be possible that STIM1 may play an important role in the acquisition of resistance and progression of the tumor to a more aggressive stage.

Results in this chapter also identified that SPCA1 and TRPM7 silencing appear to increase trastuzumab effects in SKBR3 cells. SPCA1 has been linked to breast cancer (see section 1.1.2.2). SPCA1 silencing in MDA-MB-231 breast cancer cells alters the processing of IGF1R (106). Several studies have associated IGF1R with proliferation in cancer and trastuzumab resistance (108-110). Increased IGF1R signaling and expression have been shown only in trastuzumab resistant cells (189), and it has been reported that heterodimerization and/or heterotrimerization with IGF1R occurs only in trastuzumab resistant cell lines (158, 190). However, the results presented in this chapter do not support the hypothesis that SPCA1 silencing promotes trastuzumab sensitivity through alterations in IGFR1 processing and further studies are required.

TRPM7 is a regulator of the proliferation of MCF-7 and MDA-MB-231 breast cancer cells (245, 270). TRPM7 also regulates cell adhesion through calpain by mediating the local influx of Ca^{2+} into peripheral adhesion complexes (271). TRPM7 is also reported to modulate NF-κB to regulate HIF-1α activity, which plays a key role in tumor progression by regulating genes involved in cancer cell survival, proliferation and metastasis (199). The results in this chapter suggesting the involvement of TRPM7 in trastuzumab responsiveness are further investigated in chapter 5 of this thesis, in the context of trastuzumab resistance.

The results presented in this chapter suggest a potential role for some calcium pumps, channels and channel modulators in trastuzumab responsiveness in SKBR3 cells. The rest of the work presented in this thesis will seek to determine the potential for some calcium pumps, channels and channel modulators to contribute to trastuzumab resistance and/or the reversal of trastuzumab resistance in SKBR3 cells.

3 Characterization of trastuzumab resistant HER2-positive SKBR3 cell lines

3.1 Introduction

Trastuzumab, as discussed in section 1.2.2, is a monoclonal antibody used for the treatment of HER2-positive breast tumors (132). Trastuzumab is used either in combination with chemotherapy or alone, and is one of the few treatments specifically approved for HER2-positive breast cancers. However, 25-30% of patients do not respond initially to this therapeutic agent (intrinsic or *de novo* resistance) (148) and it has been reported that most patients that are treated with trastuzumab acquire resistance within one year of the commencement of therapy (146).

Trastuzumab resistance has been the subject of several studies (272), however the mechanisms involved in resistance remain unclear. Different approaches have been adopted to study mechanisms of trastuzumab resistance. The most common approach has been to use breast cancer cell lines that have been induced to become resistant to trastuzumab. This is achieved through maintained culturing of trastuzumab sensitive breast cancer cell lines in the presence of this agent (273, 274) or via cell lines established from mouse xenografts that have become resistant to trastuzumab treatment *in vivo* (275).

This chapter describes the establishment of trastuzumab resistant and age-matched control cell lines from HER2-positive SKBR3 cells. These cell lines were developed to evaluate the possible alterations in calcium signaling associated with the acquisition of trastuzumab resistance in SKBR3 cells.

3.2 Chapter Hypothesis

The acquisition of trastuzumab resistance is associated with alterations in the expression of specific calcium channels, channel regulators and pumps.

3.2.1 Aims

a. To develop and characterize trastuzumab resistant cell lines using SKBR3 trastuzumab sensitive cells.
b. To compare calcium signaling in SKBR3 trastuzumab sensitive and resistant cells.
c. To compare mRNA and protein levels of specific calcium channels, channel regulators and pumps in SKBR3 trastuzumab sensitive and resistant cells using quantitative RT-PCR and immunoblot analysis.

3.3 Methods

3.3.1 Materials and Cell Culture

Trastuzumab was purchased from Roche Products, aliquoted and dissolved in sterile water to obtain a 10 mg/mL stock solution. The solution was stored at 4°C and was used within 1 month of preparation.

The HER2-positive human breast cancer cell line SKBR3 and the other cell lines derived from SKBR3 were cultured in McCoy's A5 media (Invitrogen) supplemented with 10% FBS and 5% Penicillin-Streptomycin mixture (Invitrogen) as recommended by ATCC (210). Cells were maintained at 37°C in a humidified atmosphere containing 95% O_2 and 5% CO_2, and passaged twice a week. A detailed passaging protocol is described in section 2.3.1.

The culture conditions used to establish the resistant cell lines are discussed in detail in this chapter as part of the description of the development of methods to establish trastuzumab resistant SKBR3 cell lines.

SKBR3 cells were periodically tested for mycoplasma using MycoAlert™ Mycoplasma Detection Kit (Lonza) and they were genotyped to authenticate the cell line using the STR Promega StemElite™ ID Profiling Kit. The detail of the STR protocol is described in section 2.3.1.

3.3.2 Approximation of viable cell number using an MTS assay

Viable cells were measured using a CellTiter 96® AQueous Non-Radioactive Cell Proliferation Assay kit (Promega). MTS assays were used to evaluate the anti-proliferative activity of trastuzumab in parental SKBR3 cells and control and resistant cell lines. The MTS assay protocol for SKBR3 cells is described in section 2.3.5 of this thesis.

3.3.3 Quantitative RT-PCR

RNA was isolated using the protocol described in section 2.3.2. RNA was reverse transcribed as described in section 2.3.2. Protocol details for quantitative RT-PCR are described in section 2.3.2. RT-PCR was used in this chapter to evaluate the expression of selected calcium channels, pumps and channels modulators in the SKBR3 resistant cell lines produced.

3.3.4 siRNA-mediated silencing

Small interfering RNA (siRNA) technology was used to silence selected calcium channels, pumps and channels modulators in this chapter. The siRNA used in these studies were ON-TARGET*plus* siRNAs (SMARTpool, Dharmacon). A detailed protocol of siRNA treatment is described in section 2.3.3.

3.3.5 Ca^{2+} measurement assays

Calcium measurement assays were performed using a fluorometric imaging plate reader (FLIPR^{TETRA}, Molecular Biosciences). $[Ca^{2+}]_i$ was assessed to evaluate the nature of ATP or EGF induced Ca^{2+} transients and SOCE in trastuzumab resistant and age-matched control cell lines that were established as discussed in section 3.4.1 of this chapter. Protocol details for Ca^{2+} measurement assays using FLIPR are described in section 2.3.6 of this thesis.

3.3.6 Immunoblotting

Immunoblotting was used in this chapter to evaluate the expression levels of some growth factor receptor proteins in trastuzumab resistant and age-matched control cell lines that were established as discussed in section 3.4.1 of this chapter. Immunoblotting uses antibodies to quantify expression levels of specific proteins. The primary antibodies used were: HER2 polyclonal rabbit (Tyr1222), EGFR polyclonal rabbit (Tyr992), IGF1R monoclonal XP® rabbit (IGF-I Receptor β, D23H3) (Cell Signaling) (Table 3.1). Each antibody was used at a dilution of 1:1000. Horseradish peroxidase (HRP) conjugated goat anti-rabbit IgG (H&L) (Bio-Rad) at 1:10,000 dilution was used as the secondary antibody (Table 3.1). Anti-mouse β-actin monoclonal antibody (Sigma Aldrich) was used at 1:10,000 dilution to detect β-actin as an internal loading control (Table 3.1). Horseradish peroxidase (HRP) conjugated goat anti-mouse IgG (Bio-Rad) at 1:10,000 was used as a secondary antibody (Table 3.1). Full protocol details for immunoblotting are presented in section 2.3.7 of this thesis.

Table 3.1 Antibodies used in this chapter for immunoblotting

Primary antibody				Secondary Antibody				Solution
Name	**type**	**Catalog number, Company**	**dilution**	**name**	**type**	**Catalog number, Company**	**dilution**	
HER2	rabbit polyclonal	Tyr1222 #2242 Cell Signaling	1:1000	Horseradish peroxidase (HRP) conjugated	goat anti-rabbit IgG (H&L)	#172-1019, Bio-Rad	1:10,000	PBS-T + BSA 5%
EGFR	monoclonal XP® rabbit	Tyr992 #2232 Cell Signaling	1:1000	Horseradish peroxidase (HRP) conjugated	goat anti-rabbit IgG (H&L)	#172-1019, Bio-Rad	1:10,000	PBS-T + BSA 5%
IGF1R	monoclonal XP® rabbit	#9750 β D23H3, Cell Signaling	1:1000	Horseradish peroxidase (HRP) conjugated	goat anti-rabbit IgG (H&L	#172-1019, Bio-Rad	1:10,000	PBS-T + BSA 5%
β-actin	Monoclonal anti-mouse	AC-15, Sigma Aldrich	1:10,000	Horseradish peroxidase (HRP) conjugated	goat anti-mouse IgG	170-6516, Bio-Rad	1:10,000	PBS-T + Milk 5%

3.4 Results

3.4.1 Establishment of trastuzumab resistant SKBR3 cell lines

The HER2-positive human breast cancer cell line SKBR3 was a gift from a collaborator at the Garven Institute, Sydney. The general protocol for the establishment of trastuzumab resistance cells is illustrated in figure 3.1.

SKBR3 cells were seeded into 8 individual wells of two 96-well plates (4 for each plate). For the establishment of acquired resistance cell lines, media was replaced with media containing trastuzumab (10 μg/mL) 24 h after plating. Each plate was maintained in a different incubator and cultured separately. During passaging, one of the 8 trastuzumab-treated cell lines was lost, due to loss of the cell pellet after centrifugation. In order to produce age-matched control cell lines, SKBR3 cells were cultured over a similar period, using the protocol described above, but in the absence of trastuzumab (media containing 1% cell culture grade water) (Fig. 3.1). Media was replaced every three days and cells were passaged at 80% confluence. After 4 passages in a 96 well plate, each cell line was scaled up to a 24-well plate, and consequently to a T25 flask after a further 4 passages. Cell lines were then maintained in a T25 flask for continuous culturing in the presence of trastuzumab 10 μg/mL or control media for the duration of experiments (Fig. 3.1).

For both groups, cells were detached with trypsin as described in section 2.3.1. Cells were cultured in 96-well plates, 24-well plates or T25 flasks with 150 μL, 1.5 mL and 5 mL of media, respectively. For passaging, the monolayers were washed with 50 μL, 600 μL or 2 mL PBS/EDTA followed by 30 μL, 300 μL or 1 mL of trypsin (depending on the cell culture surface area). Media (300 μL, 600 μL or 3 mL, respectively for 96-well plates, 24-well plates or T25 flasks) was used to stop the trypsin reaction. After centrifugation at 400 g for 2 min the cell pellet was re-suspended in 150 μL, 1.5 mL or 3 mL of media and re-plated in a ratio of 1:6, 1:6 or 1:4 depending on well or flask size used.

At every second passage, RNA was isolated from each cell line as described in section 2.3.2.1 of this thesis. This RNA was isolated to allow future studies for the assessment of temporal aspect changes in mRNA levels of targets during the development of trastuzumab resistance.

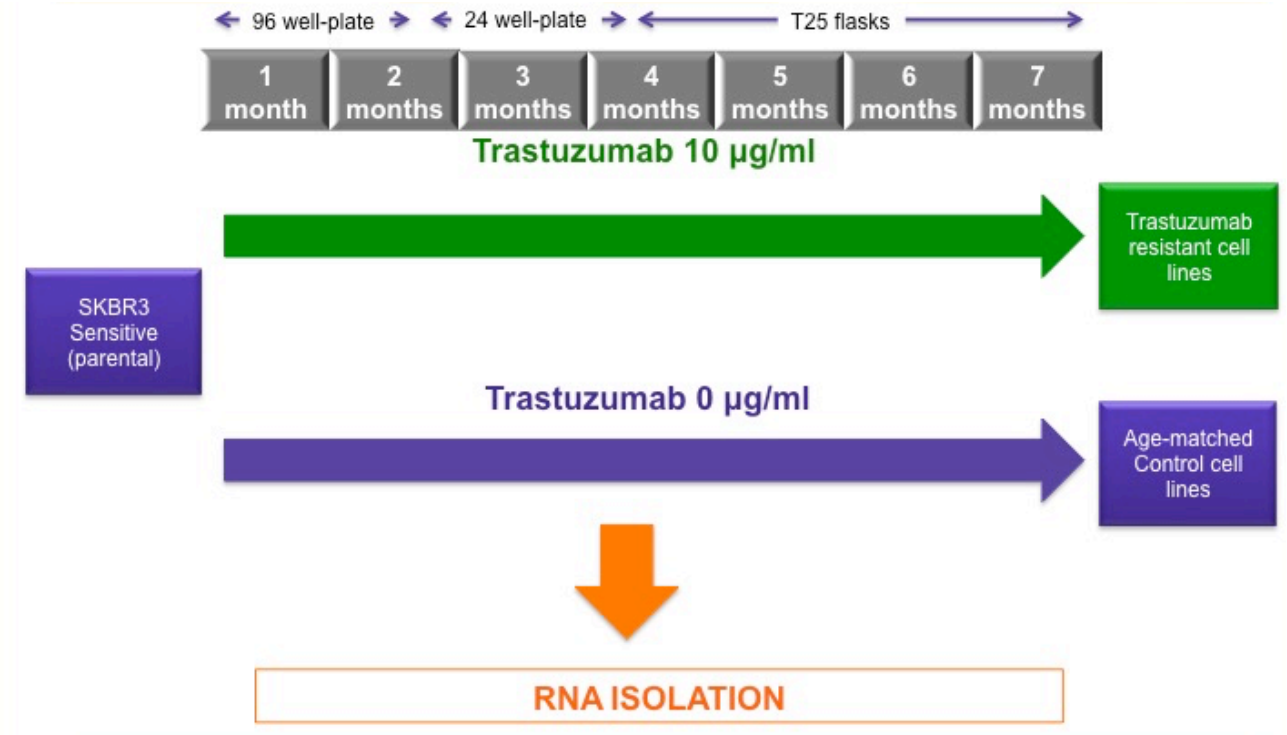

Figure 3.1 Timeline for the development of trastuzumab resistant cell lines

Parental SKBR3 cells were incubated for 7 months in the presence or absence of trastuzumab (10 µg/mL) to produce trastuzumab resistant and age-matched control cell lines. At every second passage, RNA was isolated from each cell line to evaluate the process of resistance acquisition.

After 4 months of continuous cell culture, the sensitivity of the cell lines to trastuzumab was assessed. The 8 control and 7 trastuzumab-treated cell lines were tested with 0.3 μg/mL of trastuzumab or with vehicle control. Each cell line was seeded into a 96-well plate in trastuzumab-free media. Cells were then treated with 0.3 μg/mL of trastuzumab or vehicle for 24 h after plating. After 7 days an MTS assay was performed. As shown in figure 3.2 some of the trastuzumab-treated cell lines such as T3 and T6 were less sensitive to trastuzumab. However, these experiments showed that at this time point most of the cell lines did not display pronounced resistance to trastuzumab. Hence, cell lines were cultured with trastuzumab for an additional 3 more months before trastuzumab sensitivity was again assessed.

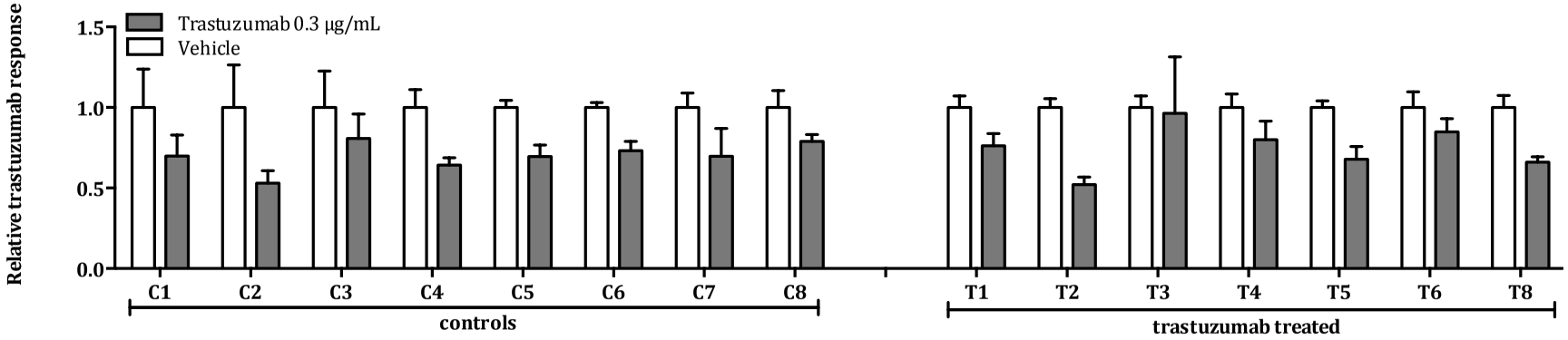

Figure 3.2 Assessment of resistance in SKBR3 trastuzumab-treated cells

Cell lines were assessed for sensitivity to trastuzumab after 4 months of continuous culture (C = age-matched control cell line, T = trastuzumab-treated cell line). MTS assays showed that the T3 and T6 cell lines were less sensitive to the effects of trastuzumab (n=1, ± S.D from 3 technical replicates.).

At the end of the 7 months period, growth curves for each cell line were produced using an MTS assay to evaluate the proliferation of all the cell lines in the presence and absence of trastuzumab (10 μg/mL) over a 9 day protocol (Fig. 3.3 and Fig. 3.4). Six of the age-matched control cell lines (cultured with vehicle) retained their sensitivity to trastuzumab (Fig. 3.3). However, two of the cell lines from the age-matched control group (C5 and C6) did not respond to trastuzumab and hence demonstrated *de novo* resistance (Fig. 3.3e and Fig. 3.3f).

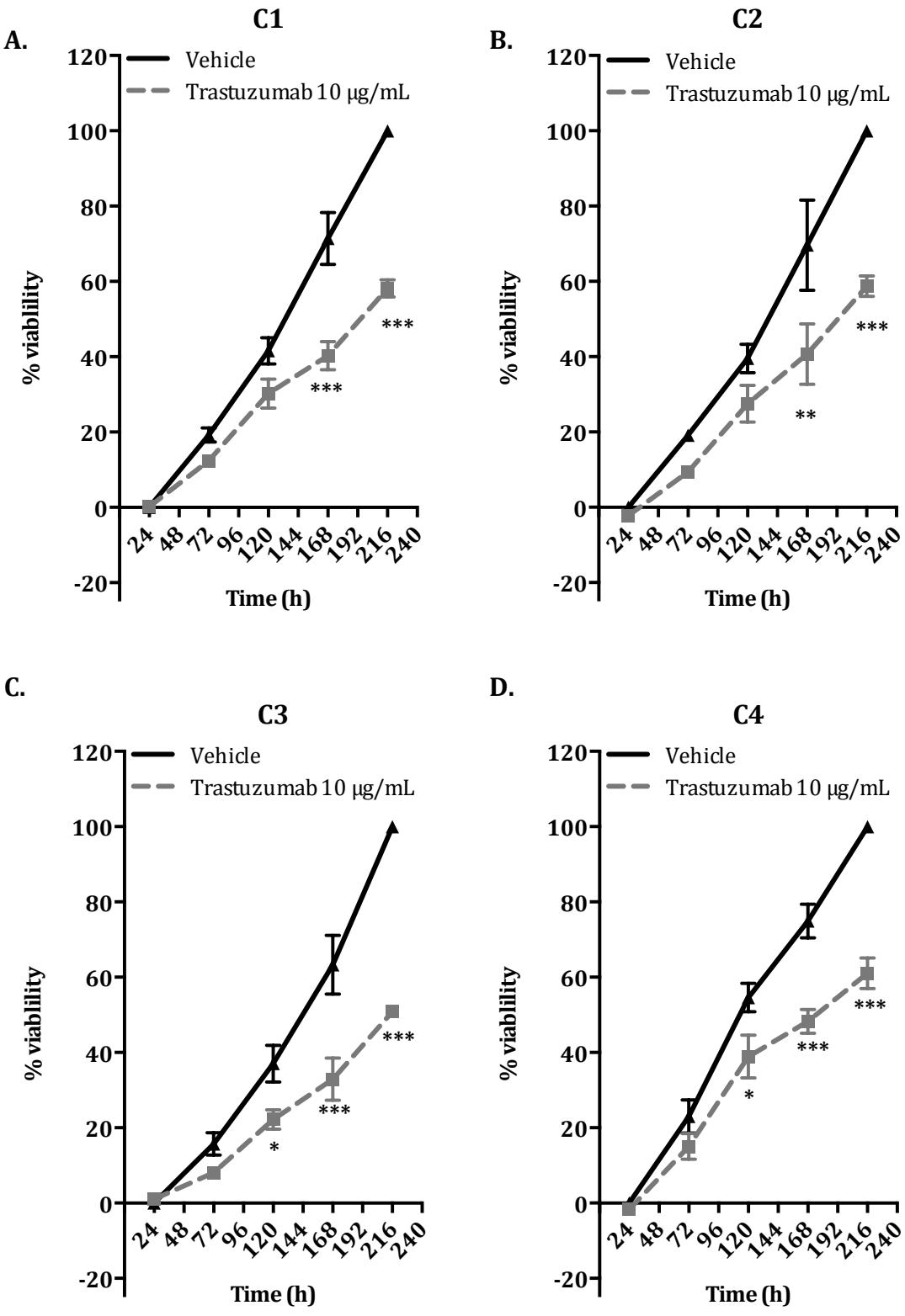
A.
C1
Vehicle
Trastuzumab 10 µg/mL
% viablility
Time (h)
B.
C2
Vehicle
Trastuzumab 10 µg/mL
% viablility
Time (h)
C.
C3
Vehicle
Trastuzumab 10 µg/mL
% viablility
Time (h)
D.
C4
Vehicle
Trastuzumab 10 µg/mL
% viablility
Time (h)

E.

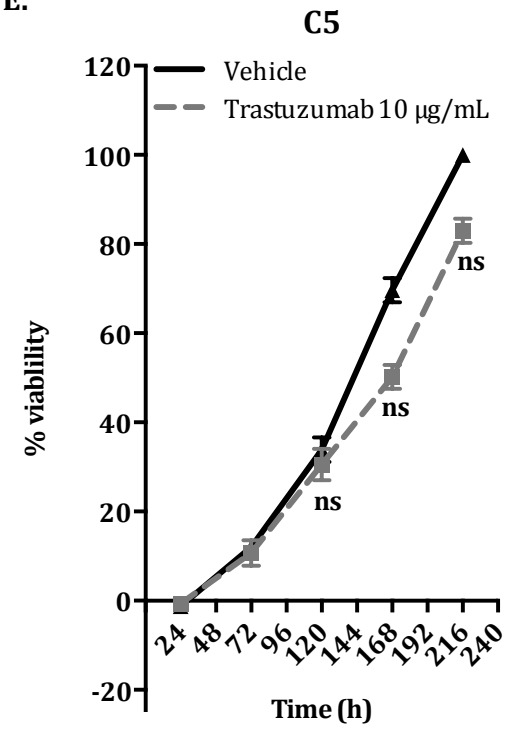
C5
Vehicle
Trastuzumab 10 µg/mL
% viablility
Time (h)
ns
ns
ns

F.

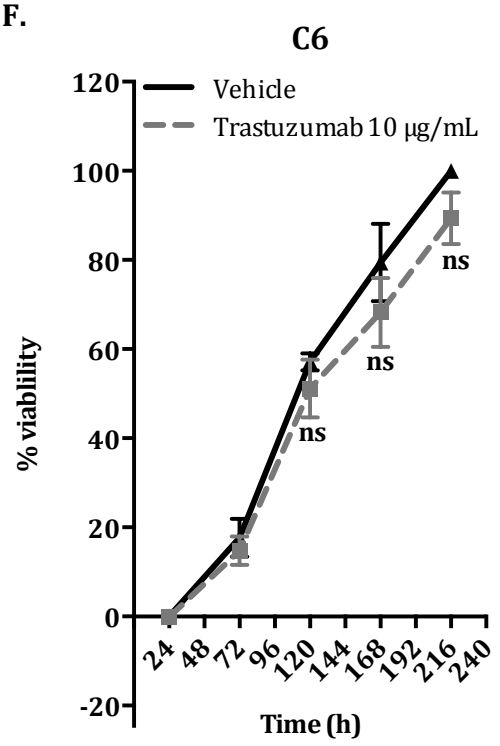
C6
Vehicle
Trastuzumab 10 µg/mL
% viablility
Time (h)
ns
ns
ns

G.

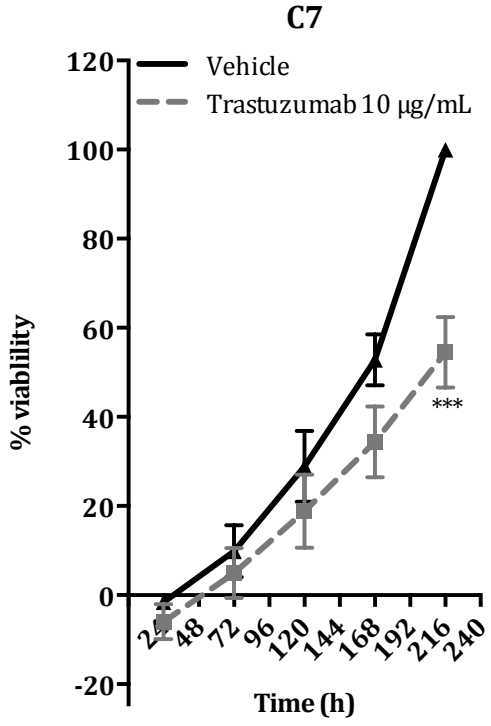
C7
Vehicle
Trastuzumab 10 µg/mL
% viablility
Time (h)
***

H.

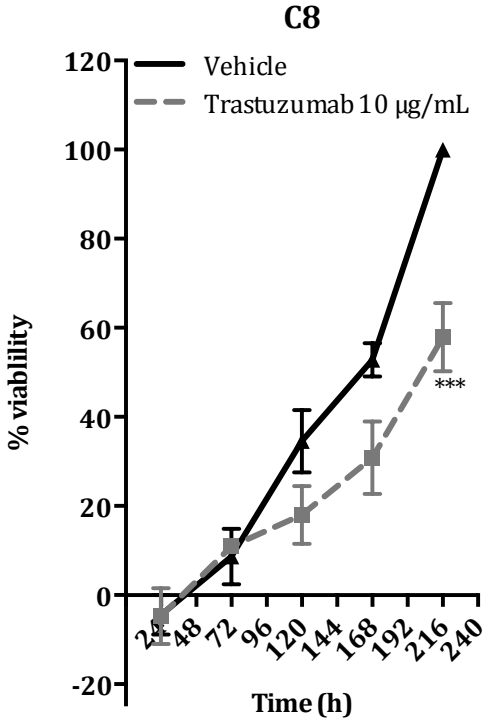
C8
Vehicle
Trastuzumab 10 µg/mL
% viablility
Time (h)
***

Figure 3.3 Assessment of trastuzumab response in age-matched control cells

Cell lines were tested at 5 different time points for their response to trastuzumab using an MTS assay (n=3, ± S.D.). The cell lines C1, C2, C3, C4, C7 and C8 retained trastuzumab sensitivity, whereas C5 and C6 (**E.** and **F.**) exhibited *de novo* resistance. Statistical analysis was performed using two-way ANOVA with Bonferroni post-tests (ns = not significant, * $p \leq 0.05$, ** $p \leq 0.01$, *** $p \leq 0.001$).

From the growth curves of the trastuzumab-treated cell lines it was observed that two cell lines (T3 and T8) exhibited acquired resistance to this therapeutic agent (Fig. 3.4c and Fig. 3.4e).

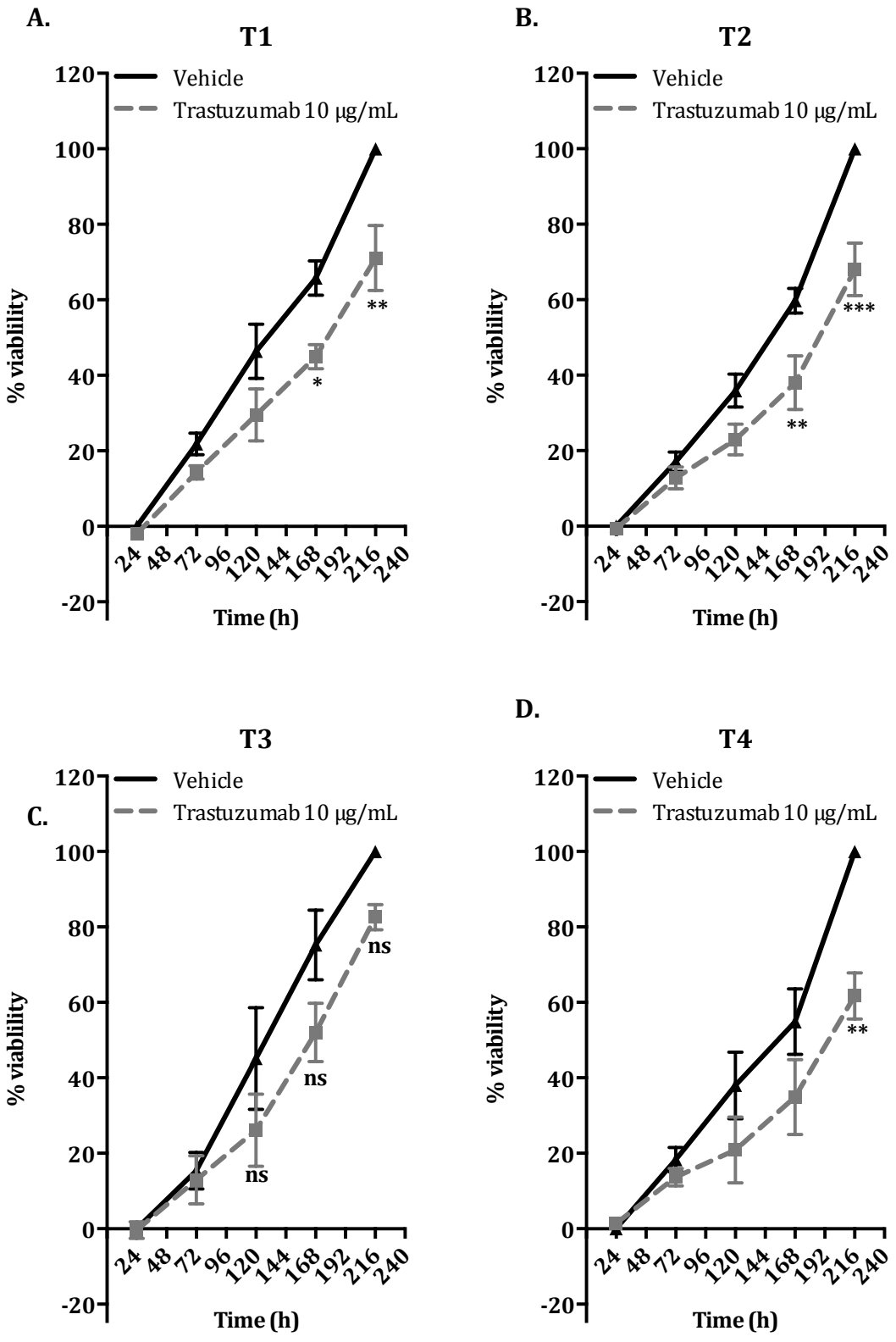
A.
T1
Vehicle
Trastuzumab 10 µg/mL
% viability
Time (h)
*
**
B.
T2
Vehicle
Trastuzumab 10 µg/mL
% viability
Time (h)
**
***
C.
T3
Vehicle
Trastuzumab 10 µg/mL
% viability
Time (h)
ns
ns
ns
D.
T4
Vehicle
Trastuzumab 10 µg/mL
% viability
Time (h)
**

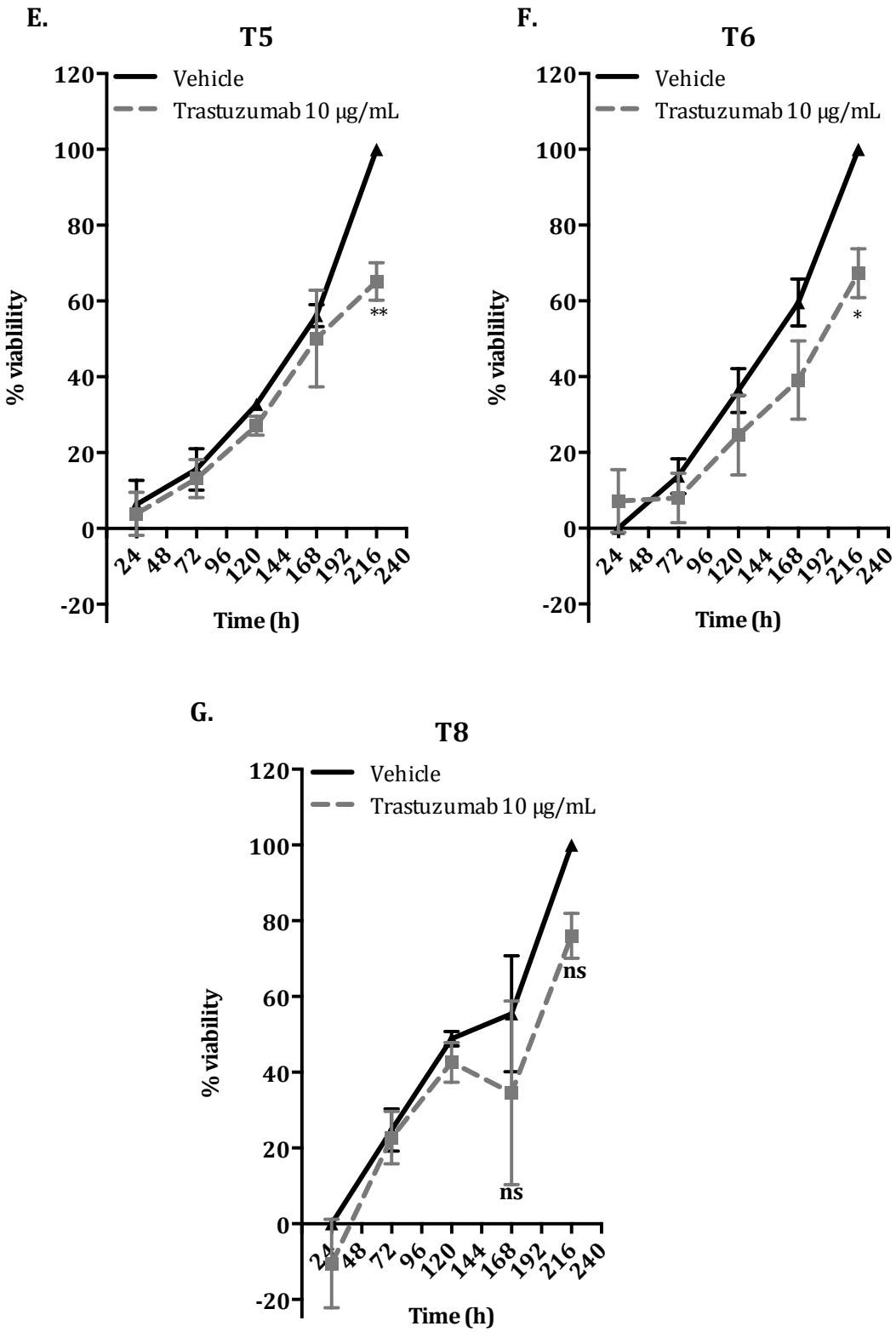
E.
T5
Vehicle
Trastuzumab 10 µg/mL
% viability
Time (h)
**
F.
T6
Vehicle
Trastuzumab 10 µg/mL
% viability
Time (h)
*
G.
T8
Vehicle
Trastuzumab 10 µg/mL
% viability
Time (h)
ns
ns

Figure 3.4 Assessment of trastuzumab response in trastuzumab-treated cells

Cell lines were tested at 5 different time points for their response to trastuzumab using an MTS assay (n=3, ± S.D.). The cell lines T3 and T8 (**C.** and **D.**) displayed acquired resistance to trastuzumab. Statistical analysis was performed using two-way ANOVA with Bonferroni post-tests (ns = not significant, * $p \leq 0.05$, ** $p \leq 0.01$, *** $p \leq 0.001$).

Two age-matched control cell lines were chosen (C1 and C7) and were renamed sensitive vehicle 1 and 2 (SV1 and SV2), respectively (Table 3.2, Fig. 3.5 and Fig. 3.6). The two acquired resistant cell lines, T3 and T8, were renamed resistant trastuzumab 1 and 2 (RT1 and RT2), respectively and the two *de novo* resistant cell lines, C5 and C6, were renamed resistant vehicle 1 and 2 (RV1 and RV2), respectively (Table 3.2, Fig. 3.5 and Fig. 3.6).

Table 3.2 Colonies and names of the selected age-matched and resistant cell lines

Colonies	Type of cell lines	Name
C1	Age-matched control	SV1
C7	Age-matched control	SV2
T3	Acquired resistant	RT1
T8	Acquired resistant	RT2
C5	*de novo* resistant	RV1
C6	*de novo* resistant	RV2

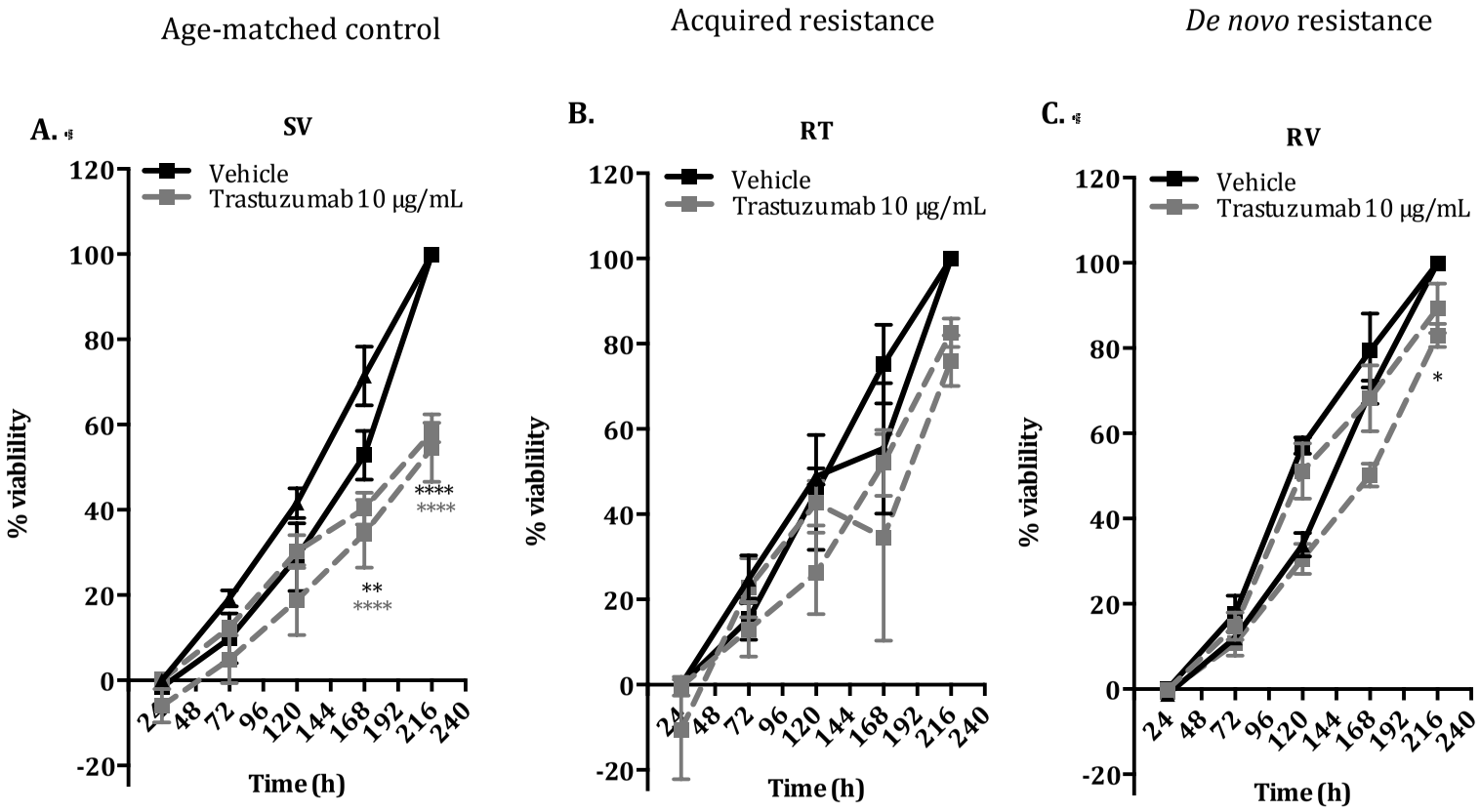

Figure 3.5 Growth curves of the selected age-matched control and resistant cell lines

A. C1 and C7 age-matched control cells growth curves (SV) (n=3, ± S.D.). **B**. T3 and T8 acquired resistant cells growth curves (RT) (n=3, ± S.D.). **C**. C5 and C6 *de novo* resistant cells growth curves (RV) (n=3, ± S.D.).

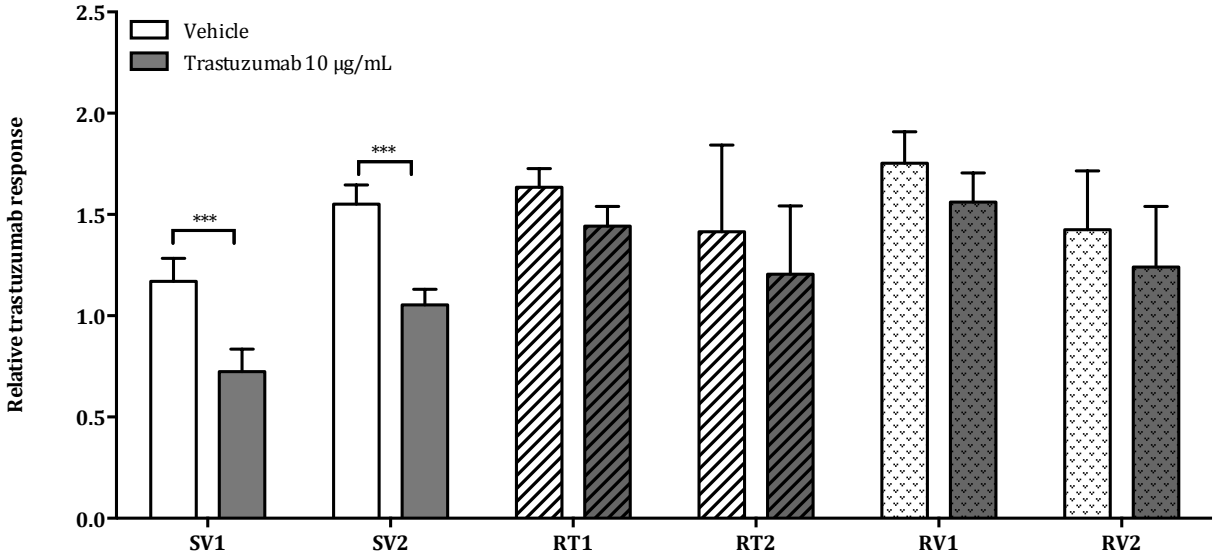

Figure 3.6 Response to trastuzumab at 216 h in the age-matched control and resistant SKBR3 cell lines

The bar graph shows the response to trastuzumab at the final time point (t=216 h) (n=3, ± S.D.). Statistical analysis was performed using two-way ANOVA with Bonferroni post-tests (*** $p \leq 0.001$).

One of the possible causes of trastuzumab resistance that has been evaluated is a possible N-terminally truncated form of HER2 receptor, which is approximately 95 kDa (140). For all six cell lines the HER2 status at both the mRNA and protein level was assessed using quantitative RT-PCR and immunoblot assays, respectively. All the cell lines maintained HER2 overexpression at the mRNA (Fig. 3.7) and protein level (Fig. 3.8).

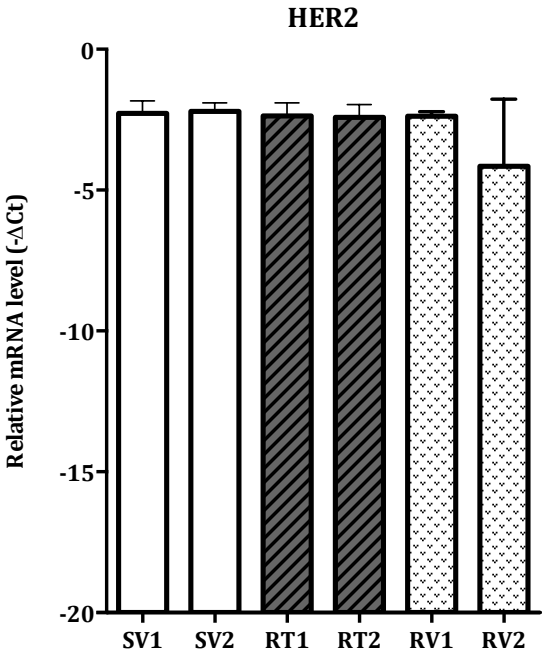

Figure 3.7 Characterization of HER2 mRNA in the SKBR3 derived cell lines

Normalized mRNA levels of HER2 in the age-matched control and resistance cell lines produced (n=3, ± S.D.). 18s rRNA was used as an internal control and the results are shown as –ΔCt.

The antibody used to detect HER2 proteins recognizes the Tyr1222 located at the intracellular C-terminal. The antibody used is able to detect the truncated form of HER2, but since a band was not observed at the expected size of the truncated HER2 (95 kDa), the trastuzumab resistance in these cell lines is not due to the presence of a truncated form of HER2. It appears that the level of HER2 protein expression in the age-matched control and resistant cell lines was similar and comparable to the expression level in SKBR3 parental cells (Fig. 3.8).

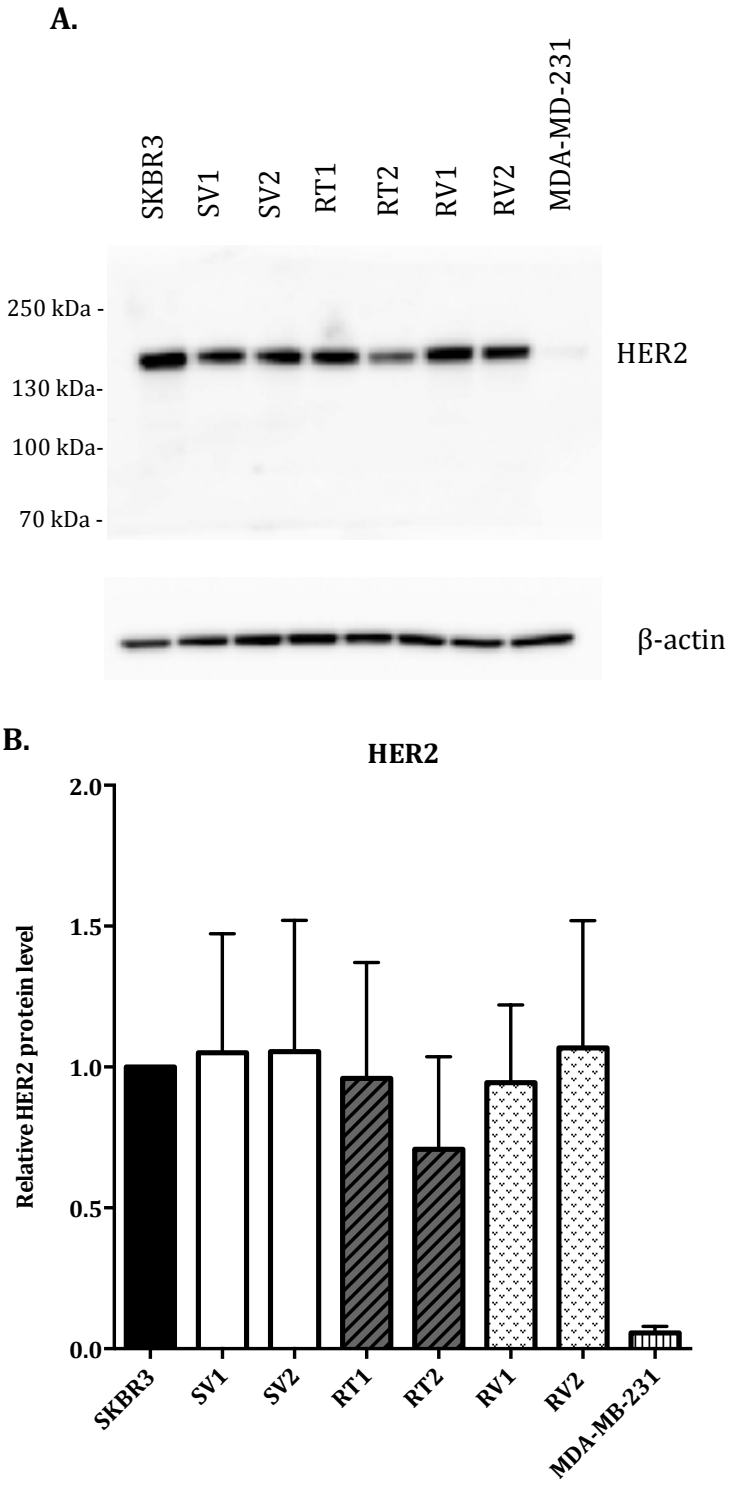

Figure 3.8 Characterization of HER2 protein in the SKBR3 derived cell lines

A. Representative immunoblot showing HER2 protein levels in the different cell lines, β-actin was used as a loading control, while MDA-MB-231 cell line was used as a negative control for HER2 protein expression. **B**. Quantification of HER2 protein levels (n=3, ± S.D.). Statistical analysis was performed using one-way ANOVA with Bonferroni post-tests.

Some studies have shown that overexpression of EGFR may contribute to trastuzumab resistance in HER2-positive breast cancer (276, 277). Therefore, EGFR expression was assessed at the mRNA (Fig. 3.9) and protein level (Fig. 3.10) in the cell lines produced in this chapter. Neither EGFR mRNA or protein differed amongst the cell lines assessed (Fig. 3.9 and Fig. 3.10).

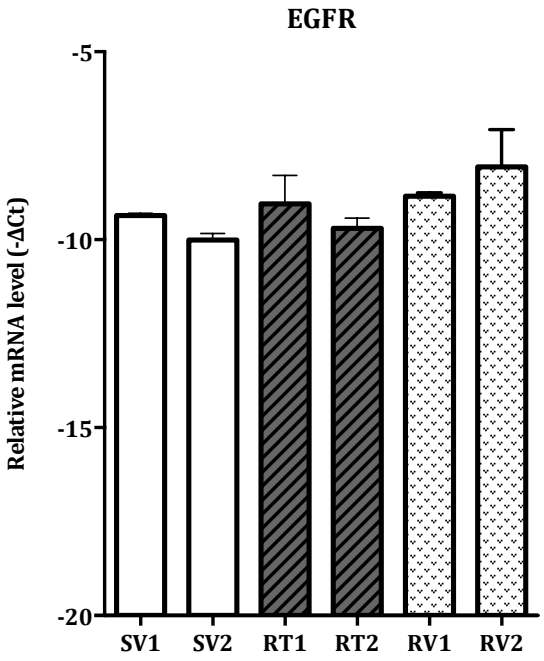

Figure 3.9 Characterization of EGFR mRNA in the SKBR3 derived cell lines

Normalized mRNA levels of EGFR in the age-matched control and resistant cell lines (n=3, ± S.D.). 18s rRNA was used as an internal control and the results are showed as -ΔCt.

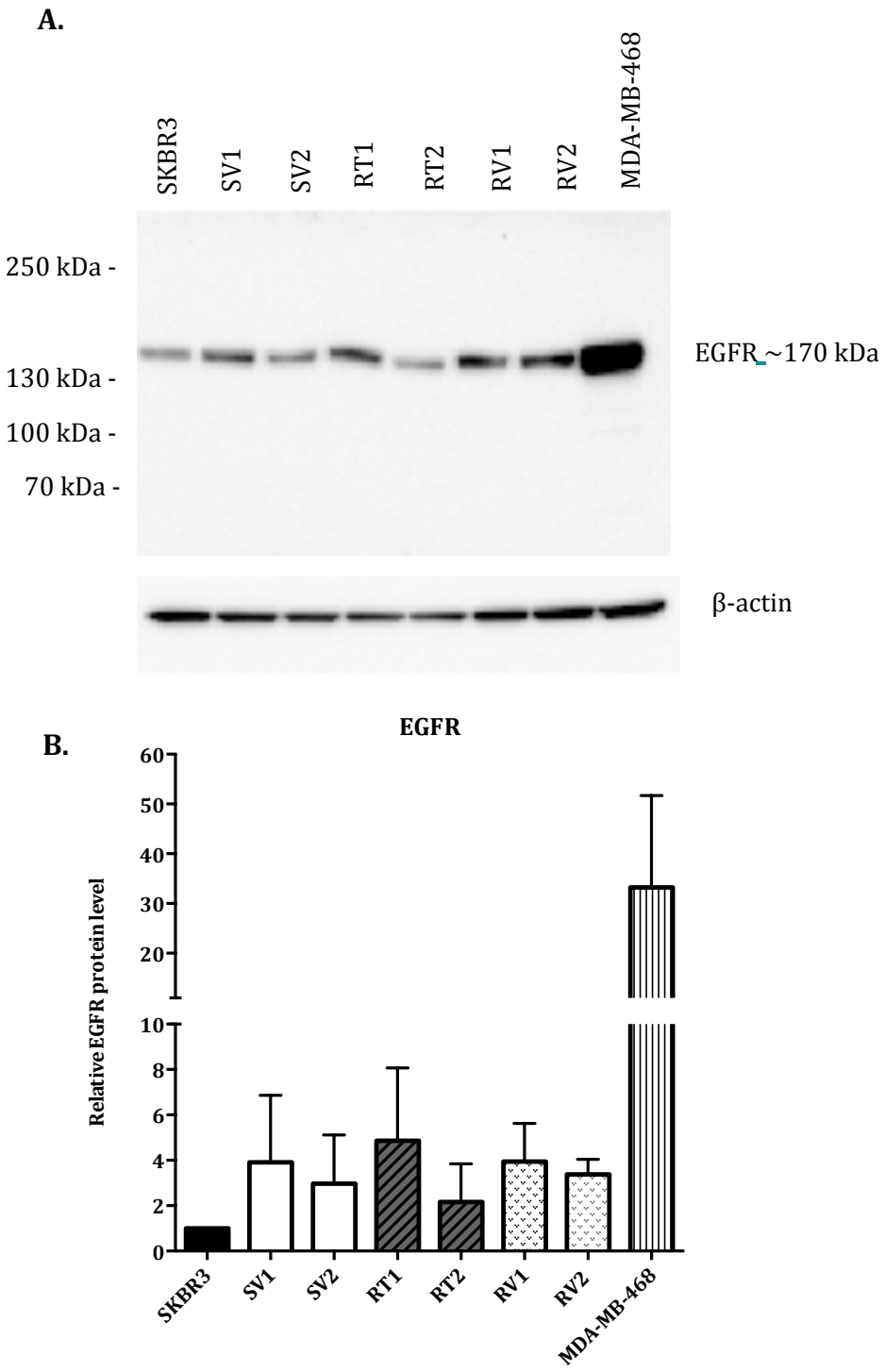

Figure 3.10 Characterization of EGFR protein in the SKBR3 derived cell lines

A. Representative immunoblot showing EGFR protein levels in the different cell lines. β-actin was used as loading control, while MDA-MB-468 cells were used as a positive control for high levels of EGFR expression (278). **B**. Quantification of EGFR protein levels (n=3, ± S.D.). Statistical analysis was performed using one-way ANOVA with Bonferroni post-tests, no significant difference ($p > 0.05$) was observed between the SV1, SV2, RT1, RT2, RV1 and RV2.

One of the most studied potential causes of the acquisition of trastuzumab resistance (as discussed in section 1.5.1) is the up-regulation of IGF1R protein (155, 158, 190, 279). The level of IGF1R protein was therefore compared in the age-matched control and resistant cell lines. No significant differences were observed in the protein expression of the mature IGF1R-β in the resistant cell lines compared to the age-matched control cells (Fig. 3.11).

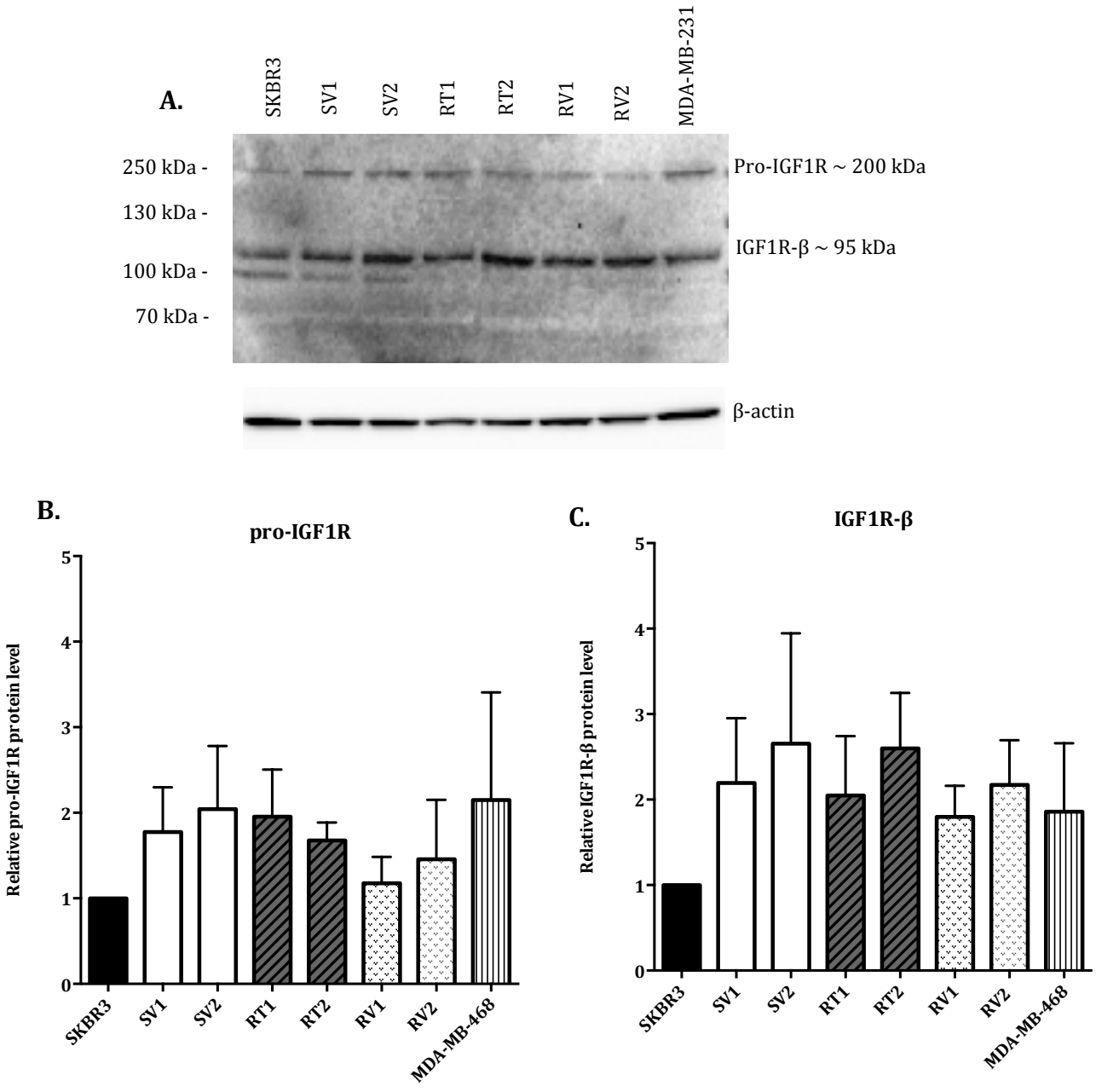

Figure 3.11 IGF1R expression in the age-matched control and resistant cell lines

A. Representative immunoblot of IGF1R in different cell lines. The antibody recognized the pro-form of IGF1R and the mature form IGF1R-β (280). β-actin was used as a loading control, while MDA-MB-231 cells were used as positive control for IGF1R expression (281). **B**. Densitometry performed for the pro-IGF1R isoform (n=3, ± S.D.). **C**. Densitometry performed for the IGF1R-β isoform. (n=3, ± S.D.). Statistical analysis was performed using one-way ANOVA with Bonferroni post-tests, no significant difference ($p > 0.05$) was observed between the SV1, SV2, RT1, RT2, RV1 and RV2.

Comparison of the expression of the pro-IGF1R and the mature IGF1R-β showed that the resistant RT2 cell line had a significant difference in the relative level of the two forms (Fig. 3.12) and thus, RT2 may have a higher post-translational modification of IGF1R.

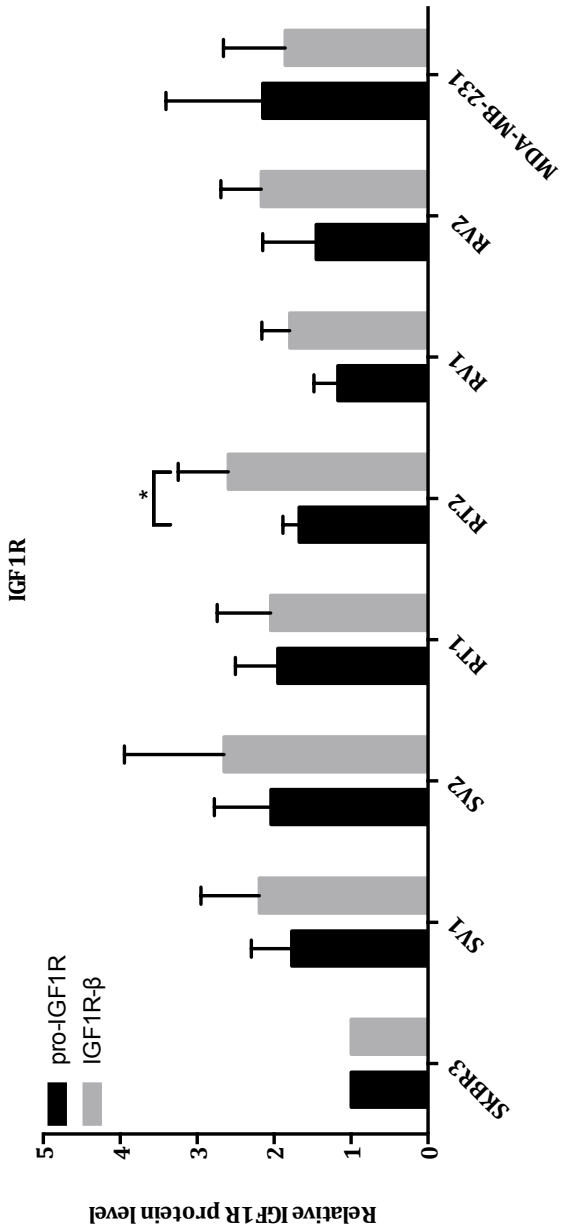

Figure 3.12 Comparison of the expression of pro-IGF1R and IGF1R-β in the age-matched control and resistant cell lines

The bar graph shows the expression level of the two IGF1R isoforms in the age-matched control and resistant cell lines. The RT2 cell line showed a significant difference between the pro-form and the mature form of IGF1R (n=3, ± S.D.). Statistical analysis was performed using two-way ANOVA with Bonferroni post-tests (* $p \leq 0.05$).

3.4.2 Characterization of acquired trastuzumab resistant HER2-positive SKBR3 cell lines

After the characterization of growth factor receptors, the mRNA levels and consequences of silencing of different calcium transporters and modulators were evaluated in the two acquired trastuzumab resistant cell lines. Calcium signaling was assessed through evaluation of ATP and EGF responses and also SOCE.

3.4.2.1 Assessment of Ca^{2+} channels, pumps and modulators in acquired trastuzumab resistant SKBR3 cells

In order to evaluate the mRNA levels of calcium-related proteins, the mRNA levels of 45 targets were assessed, which included different types of calcium channels, pumps and also calcium channel modulators (Fig. 3.13).

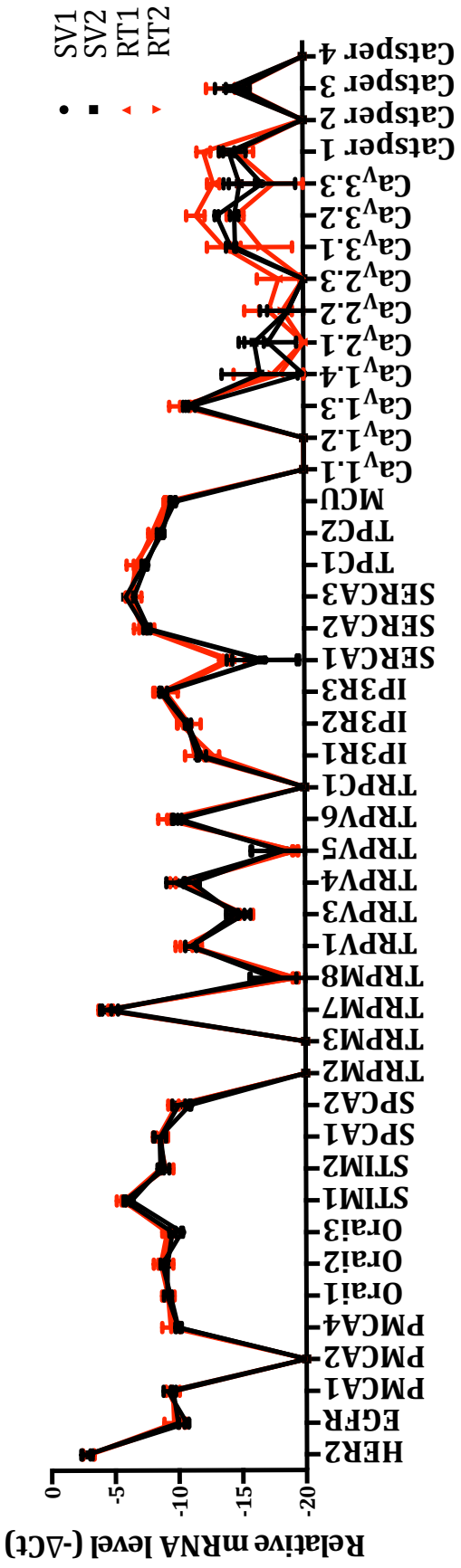

Figure 3.13 Assessment of mRNA levels of 45 calcium channels, pumps and channel modulators in the acquired resistant cell lines, RT1 and RT2

Normalized expression levels of 45 calcium channels, pumps and modulators. 18s rRNA was used as an internal control and the results are showed as mean −ΔCt (n=3, ± S.D.). Targets with dot points on the X axis showed no detection of mRNA levels.

From the assessment of these 45 targets, it was observed that most of the targets showed similar expression levels between the two age-matched control cell lines and the acquired resistant cell lines. Single graph columns for each target can be found in appendix 2 and mean $-\Delta Ct$ values for each target can be found in appendix 3.

Voltage-gated calcium channels appeared to be the only class of target that showed a difference between the mRNA levels of the age-matched control cell lines and the acquired resistant cell lines. Evaluation of the voltage-gated Ca^{2+} channels across 3 independent cultures is shown in figure 3.13. $Ca_V3.2$ showed a significant difference in mRNA in the two acquired resistant cell lines (RT1 and RT2) compared to the control cell lines SV1 and SV2 (Fig. 3.14).

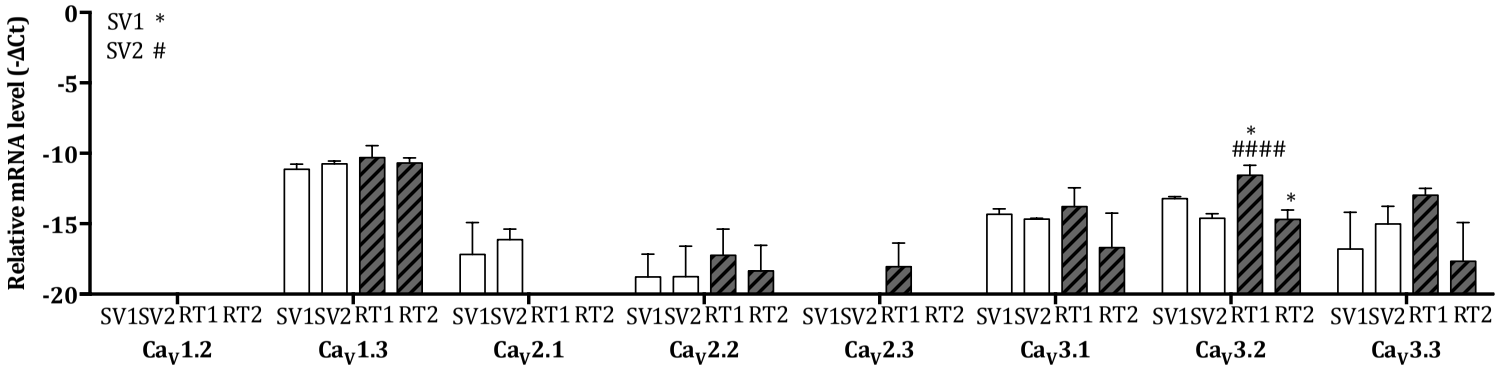

Figure 3.14 mRNA level of voltage-gated calcium channels in the age-matched control and acquired resistant cell lines

Normalized mRNA expression levels of the voltage-gated calcium channels in the age-matched control (SV) and acquired-resistant (RT) cell lines produced (n=3, ± S.D.). 18s rRNA was used as an internal control and the results are showed as –ΔCt. Statistical analysis was performed using two-way ANOVA with Bonferroni post-tests, the * refer to a statistic significance compared to SV1, while the # refers to SV2 (* $p \leq 0.05$, #### $p \leq 0.0001$).

Fourteen Ca^{2+} signaling related targets were selected to evaluate the effect of their silencing on responses to trastuzumab in the acquired resistant cell line RT1. These targets were selected based on 1) mRNA changes associated with resistance (e.g. $Ca_V3.2$), 2) their ability to increase trastuzumab response in SKBR3 cells in experiments conducted in chapter 2 (e.g. SPCA1, TRPM7 and STIM1) or 3) the availability of siRNA at the time these experiments were completed (SPCA2, STIM2, PMCA1, Orai1, Orai2, Orai3, TRPV1, TRPV4, TRPC1 and TRPC5).

In order to confirm the resistance of the cell lines produced and validate each experiment performed on these cell lines, from the growth curves shown in figure 3.5, a threshold for trastuzumab response was set. The inhibition of cell growth by trastuzumab was no more than 25% in the resistant cell lines. Thus, for the siRNA screen a silenced target was considered as reversing trastuzumab resistance if it was able to produce a trastuzumab response higher than 25% (a dash line was drawn at 75% on the Y axis). Trastuzumab was added 24 h after siRNA treatment and repeated every two days. MTS assay was performed to evaluate cells viability after 196 h after siRNA treatment. None of the 14 targets tested reversed the resistance and sensitized the cells to the effect of trastuzumab (Fig. 3.15).

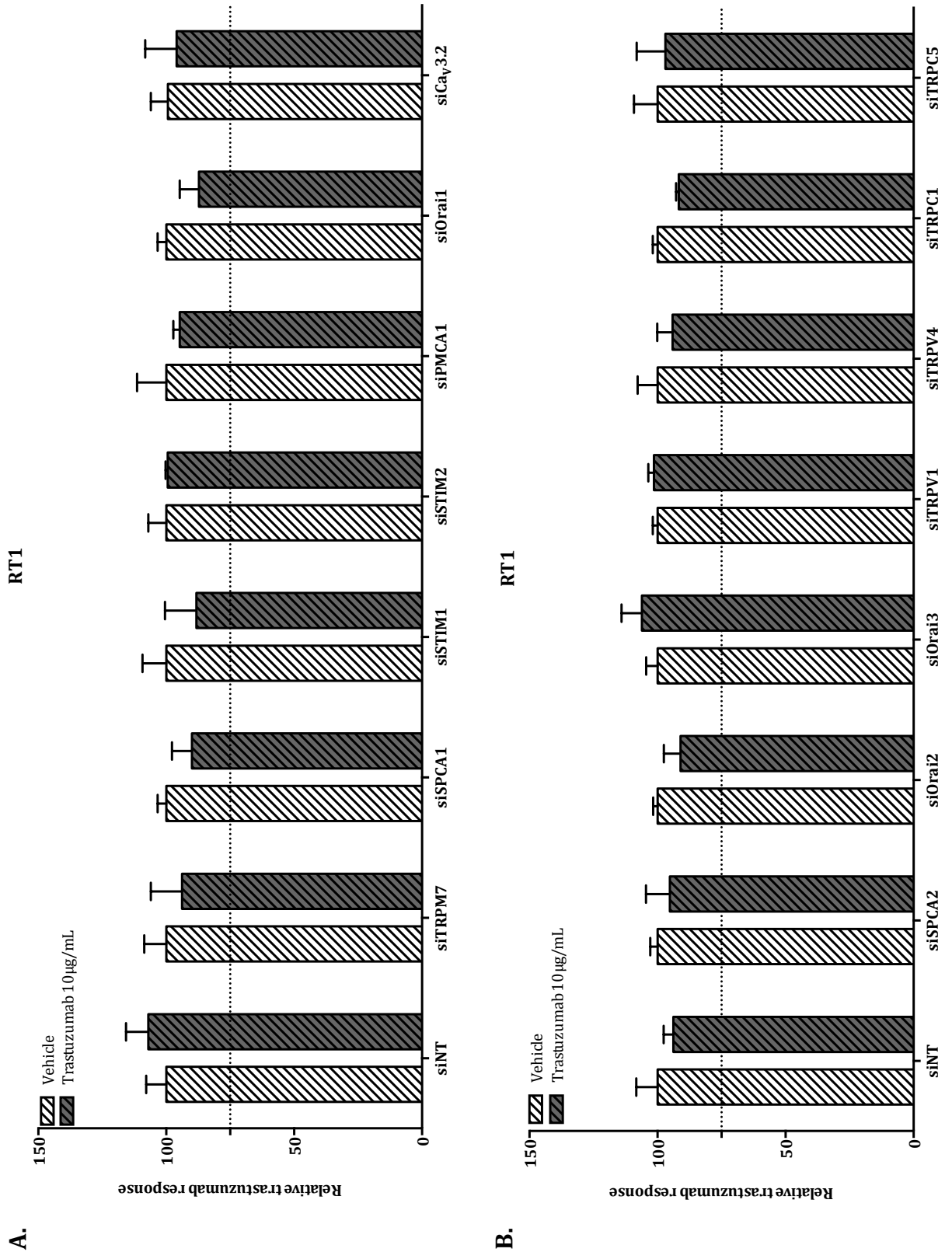
A.
RT1
Vehicle
Trastuzumab 10 µg/mL
Relative trastuzumab response
150
100
50
0
siNT
siTRPM7
siSPCA1
siSTIM1
siSTIM2
siPMCA1
siOrai1
siCaV3.2
B.
RT1
Vehicle
Trastuzumab 10 µg/mL
Relative trastuzumab response
150
100
50
0
siNT
siSPCA2
siOrai2
siOrai3
siTRPV1
siTRPV4
siTRPC1
siTRPC5

Figure 3.15 siRNA screen of 14 Ca^{2+} targets on the acquired resistant cell line RT1

An MTS assay performed on the acquired resistant cell line RT1 to evaluate the silencing effect of 14 calcium targets on the trastuzumab response (3 wells, ± S.D.). Targets that showed a response lower than the dashed line drawn at 75% would have indicated a potential reversal of trastuzumab resistance.

3.4.2.2 Ca^{2+} signaling profile of acquired trastuzumab resistant SKBR3 cells

In order to evaluate possible differences in global calcium homeostasis between the age-matched controls and acquired resistant cell lines, the nature of ATP or EGF induced Ca^{2+} transients and the SOCE profile in these cell lines was assessed using the Ca^{2+} indicator Fluo-4 AM as described in section 2.3.6.

A concentration-response curve of ATP was produced for each cell line to evaluate possible changes in intracellular Ca^{2+} signaling between the two types of cell lines (Fig. 3.16 and Fig. 3.17). The traces for each cell line showed a difference in responses to different concentrations of ATP. The SV2 cell line showed a higher response to ATP compared to the other age-matched control cell line SV1 (Fig. 3.16a and Fig. 3.16b). The acquired resistant cell line RT1 had an increased response to ATP at higher concentrations compared to SV1 (Fig. 3.16c). Moreover, some modest Ca^{2+} oscillation behavior (a second peak) was observed for the two acquired resistant cell line at a higher concentration of ATP (Fig. 3.16c and Fig. 3.16d).

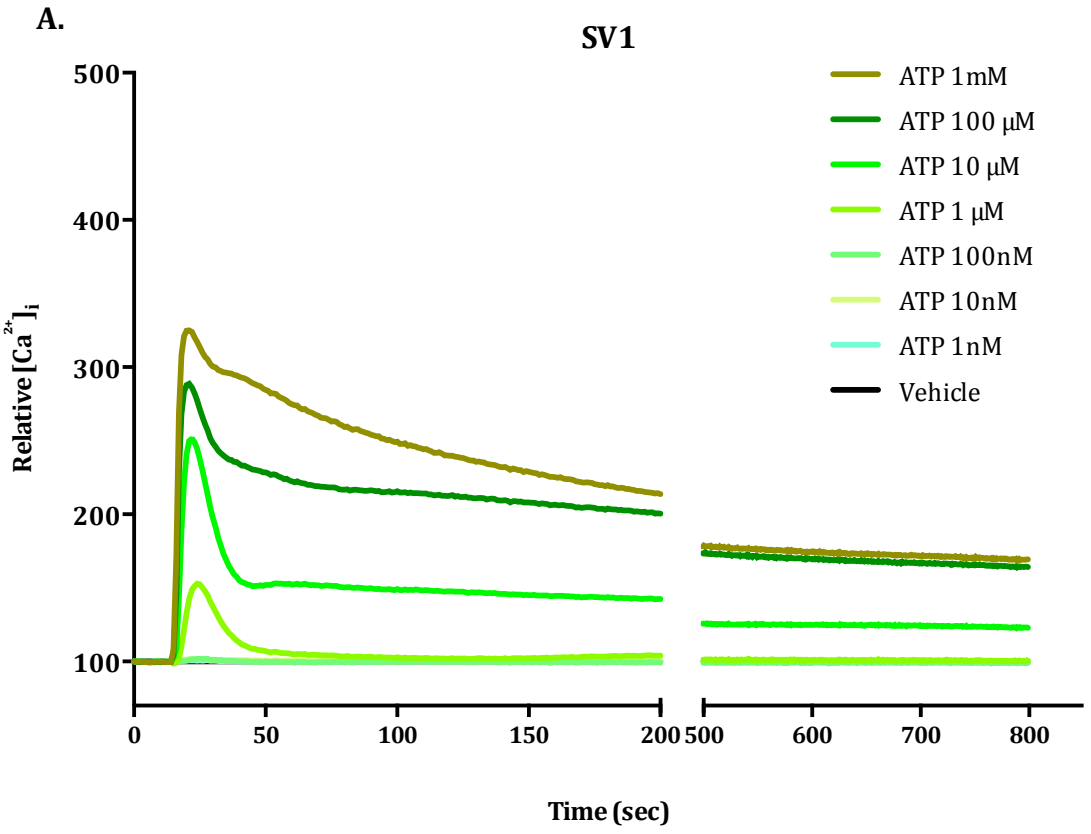
A.
SV1
ATP 1mM
ATP 100 µM
ATP 10 µM
ATP 1 µM
ATP 100nM
ATP 10nM
ATP 1nM
Vehicle
Relative [Ca2+]i
500
400
300
200
100
0
50
100
150
200
500
600
700
800
Time (sec)

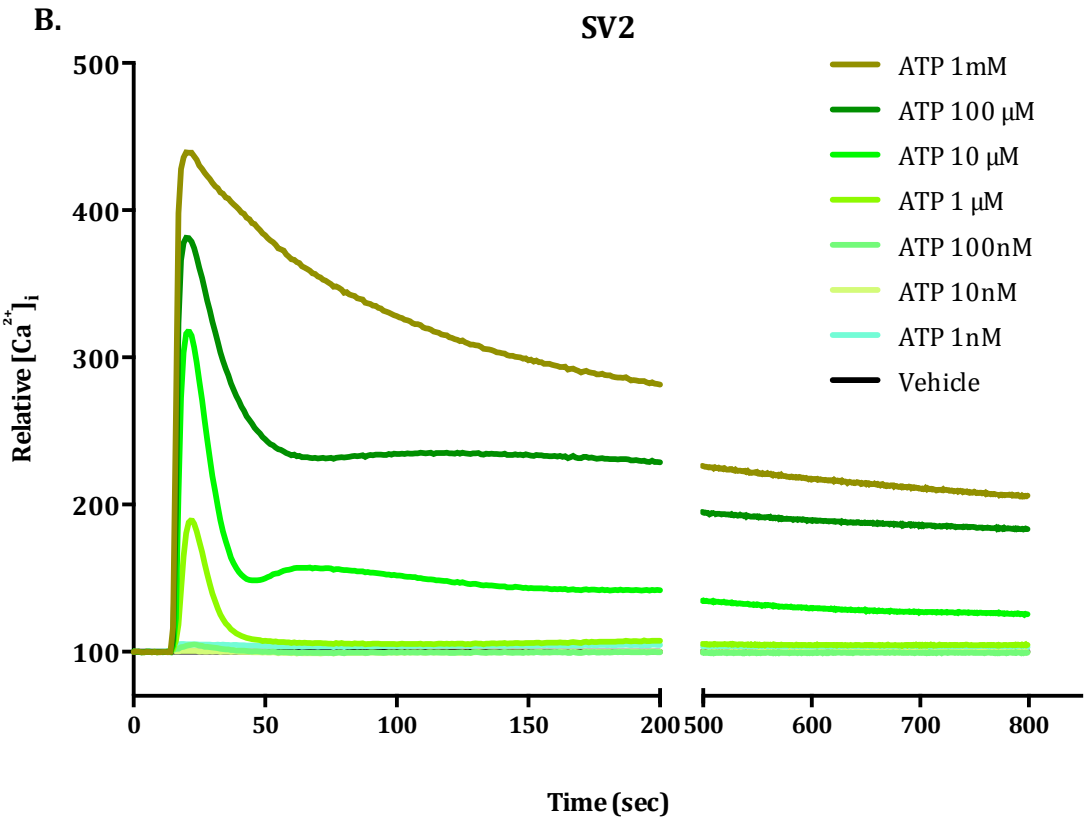
B.
SV2
ATP 1mM
ATP 100 µM
ATP 10 µM
ATP 1 µM
ATP 100nM
ATP 10nM
ATP 1nM
Vehicle
Relative [Ca2+]i
500
400
300
200
100
0
50
100
150
200
500
600
700
800
Time (sec)

C.

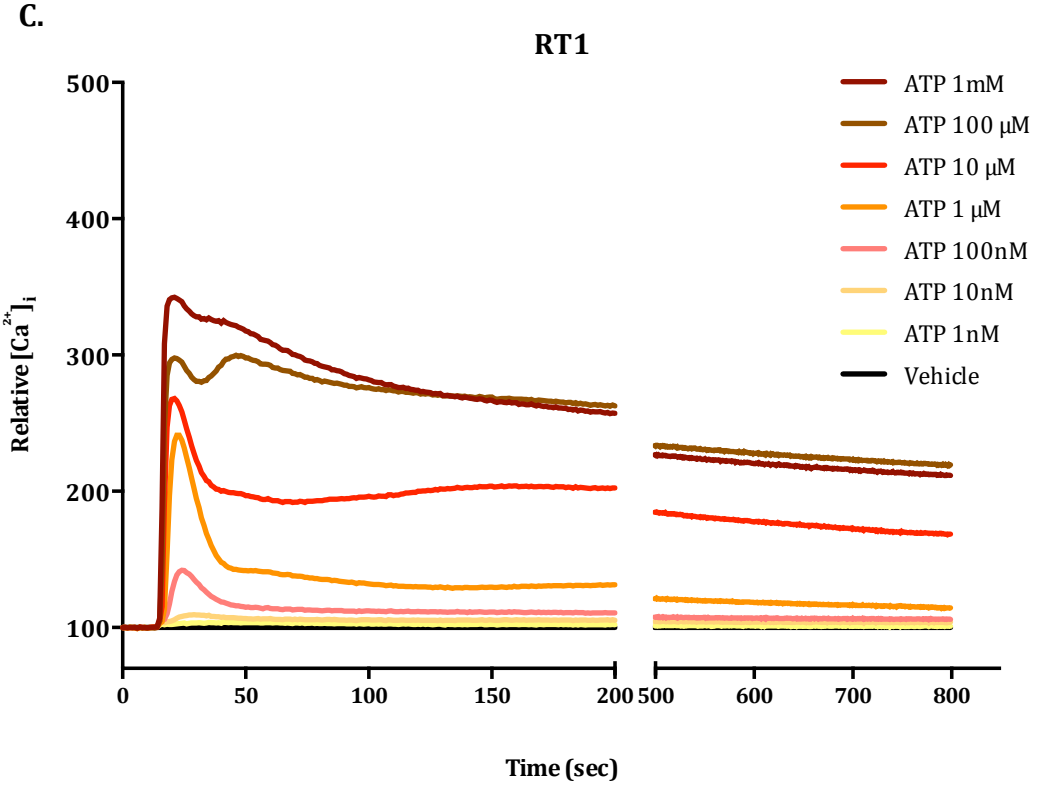
RT1
ATP 1mM
ATP 100 µM
ATP 10 µM
ATP 1 µM
ATP 100nM
ATP 10nM
ATP 1nM
Vehicle
Relative [Ca2+]i
500
400
300
200
100
0
50
100
150
200
500
600
700
800
Time (sec)

D.

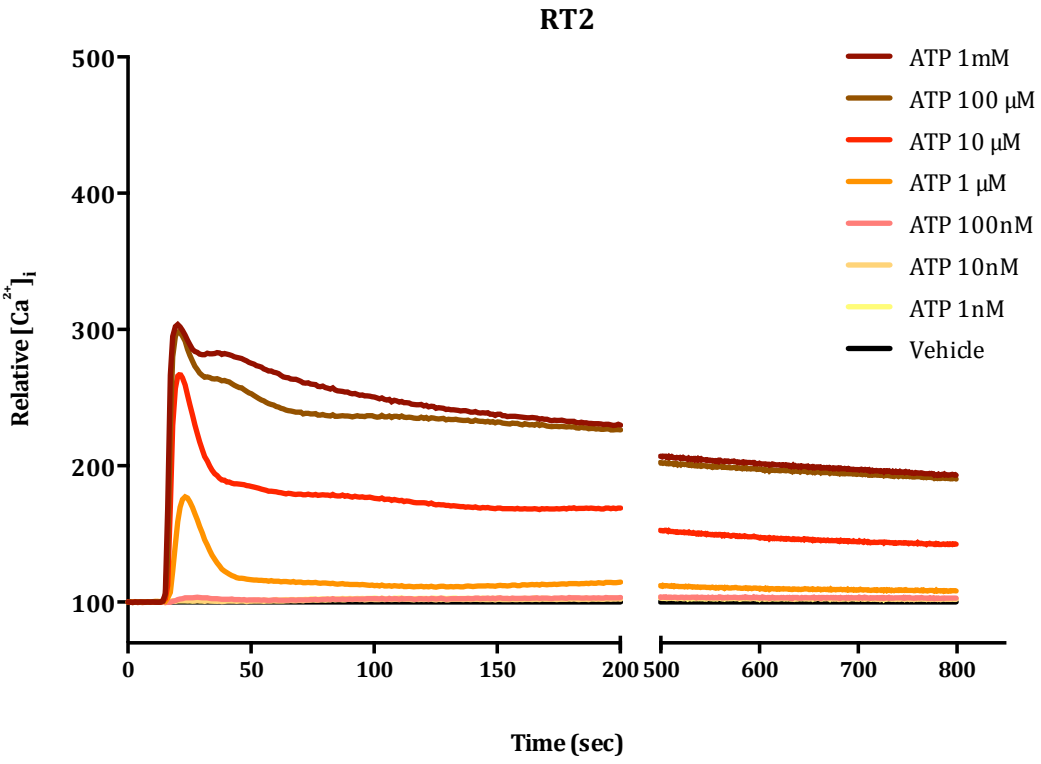
RT2
ATP 1mM
ATP 100 µM
ATP 10 µM
ATP 1 µM
ATP 100nM
ATP 10nM
ATP 1nM
Vehicle
Relative [Ca2+]i
500
400
300
200
100
0
50
100
150
200
500
600
700
800
Time (sec)

Figure 3.16 Ca^{2+} traces of intracellular calcium in the age-matched control and acquired resistant cells upon ATP stimulation

Average Ca^{2+} traces from three independent experiments measured using FLIPR showing the relative $[Ca^{2+}]_i$ in response to increased concentrations of ATP (1mM, 100 μM, 10 μM, 1 μM, 100 nM, 10 nM, 1nM) in the age-matched control (**A.** and **B.**) and acquired resistant cell lines (**C.** and **D.**) (n=3).

The maximum Ca^{2+} response to ATP in the age-matched control cell lines and acquired resistant cells differed; the EC_{50} of the age-matched control cell lines SV1 and SV2 were 3.4 μM and 2.9 μM, respectively, while the EC_{50} for the two acquired resistant cell lines were 0.9 μM (RT1) and 1.6 μM (RT2), respectively (Fig. 3.17). Statistical analysis was performed comparing each acquired resistant cell line to the age-matched control cell line SV1. The acquired resistant cell lines RT1 showed a statistically significant higher response to ATP at concentrations of 10 μM, 100 μM and 1 mM (Fig. 3.17), however, significance was not achieved if compared to the age-matched control cell line SV2.

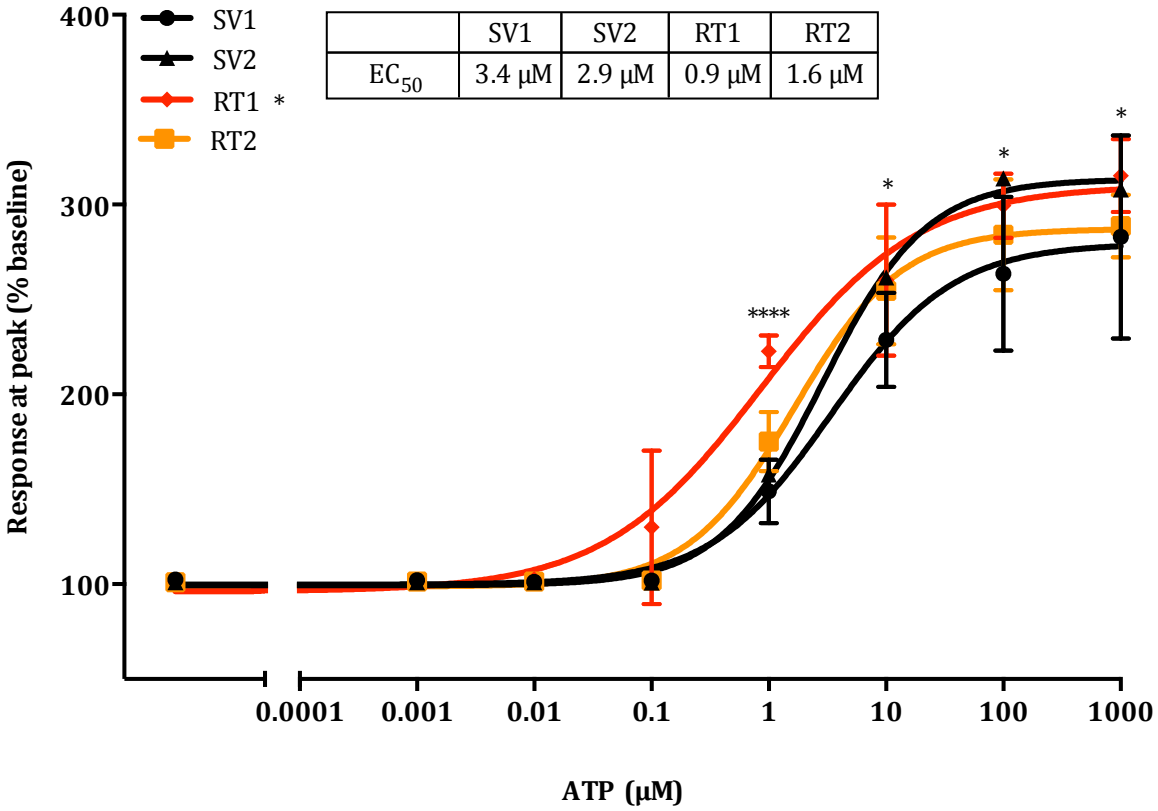

	SV1	SV2	RT1	RT2
EC_{50}	3.4 µM	2.9 µM	0.9 µM	1.6 µM

Figure 3.17 ATP concentration-response curve of the acquired resistant and age-matched control cell lines

The concentration response curves for maximum $[Ca^{2+}]_i$ was assessed using 0.001 µM, 0.01 µM 0.1 µM, 1 µM, 10 µM, 100 µM and 1 mM of ATP in the age-matched control and acquired resistant cell lines (n=3, ± S.D.). Statistical analysis was performed using two-way ANOVA with Bonferroni post-tests. Statistical analysis refers to SV1, the * indicates statistical significance between SV1 and RT1, while the # between SV1 and RT2 (* $p \leq 0.05$ **** $p \leq 0.0001$).

Furthermore, it was observed that the acquired resistant cell lines showed a slower recovery after ATP addition (Fig. 3.18) with a significantly higher relative $[Ca^{2+}]_i$ level at 800 s (Fig. 3.18). It could be speculated that Ca^{2+} was either sequestered or extruded at a slower rate in the resistant cell lines.

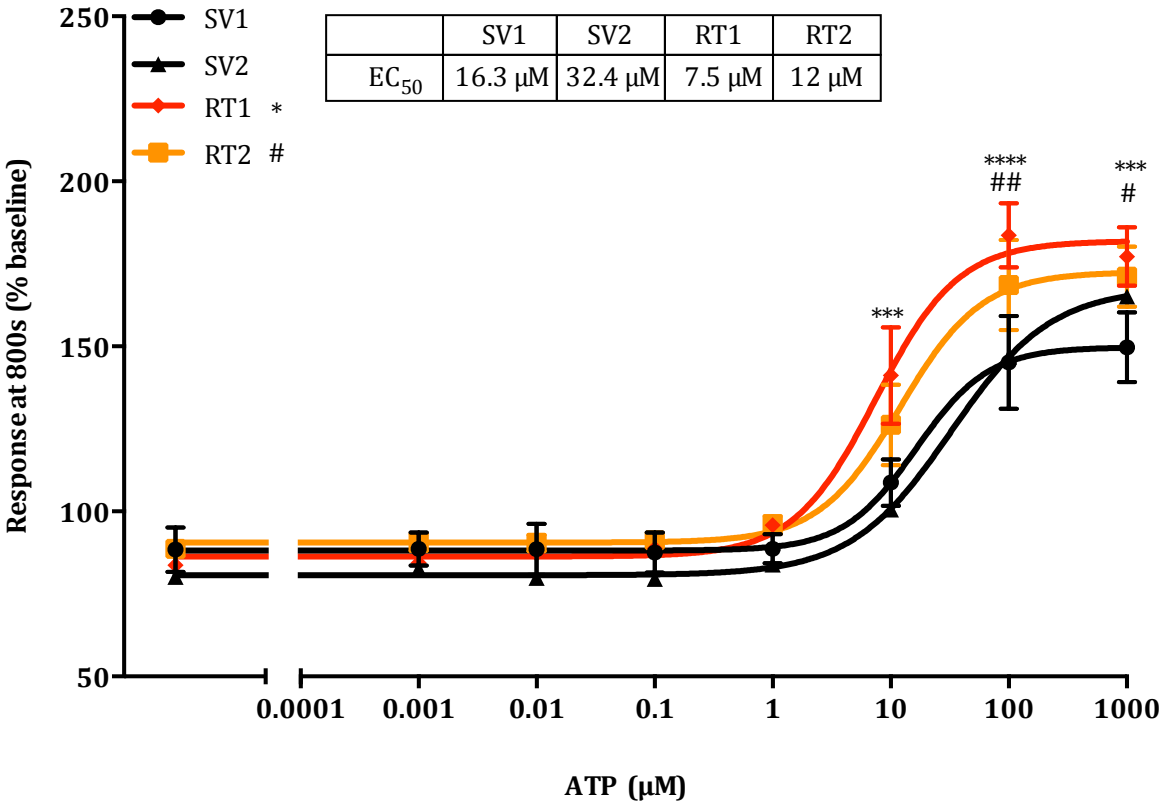

	SV1	SV2	RT1	RT2
EC_{50}	16.3 µM	32.4 µM	7.5 µM	12 µM

Figure 3.18 ATP concentration-response curve of the acquired resistant and age-matched control cell lines at 800 s

Concentration response curves for measurements of $[Ca^{2+}]_i$ after 800 s after addition of ATP (0.001 µM, 0.01 µM 0.1 µM, 1 µM, 10 µM, 100 µM and 1 mM) in age-matched control and acquired resistant cell lines (n=3, ± S.D.). Statistical analysis was performed using two-way ANOVA with Bonferroni post-tests. Statistical analysis refers to SV1, the * is associated with statistically significant between SV1 and RT1, while the # is between SV1 and RT2 (# $p \leq 0.05$, ** or ## $p \leq 0.01$, *** $p \leq 0.001$, **** $p \leq 0.0001$).

The response to 50 ng/mL EGF was also assessed in the acquired resistant cells. Similar to the results obtained from the SKBR3 parental cell line (section 2.4), EGF treatment did not produce any detectable $[Ca^{2+}]_i$ increase in the two acquired resistant and age-matched control cell lines (Fig. 3.19 and Fig. 3.20).

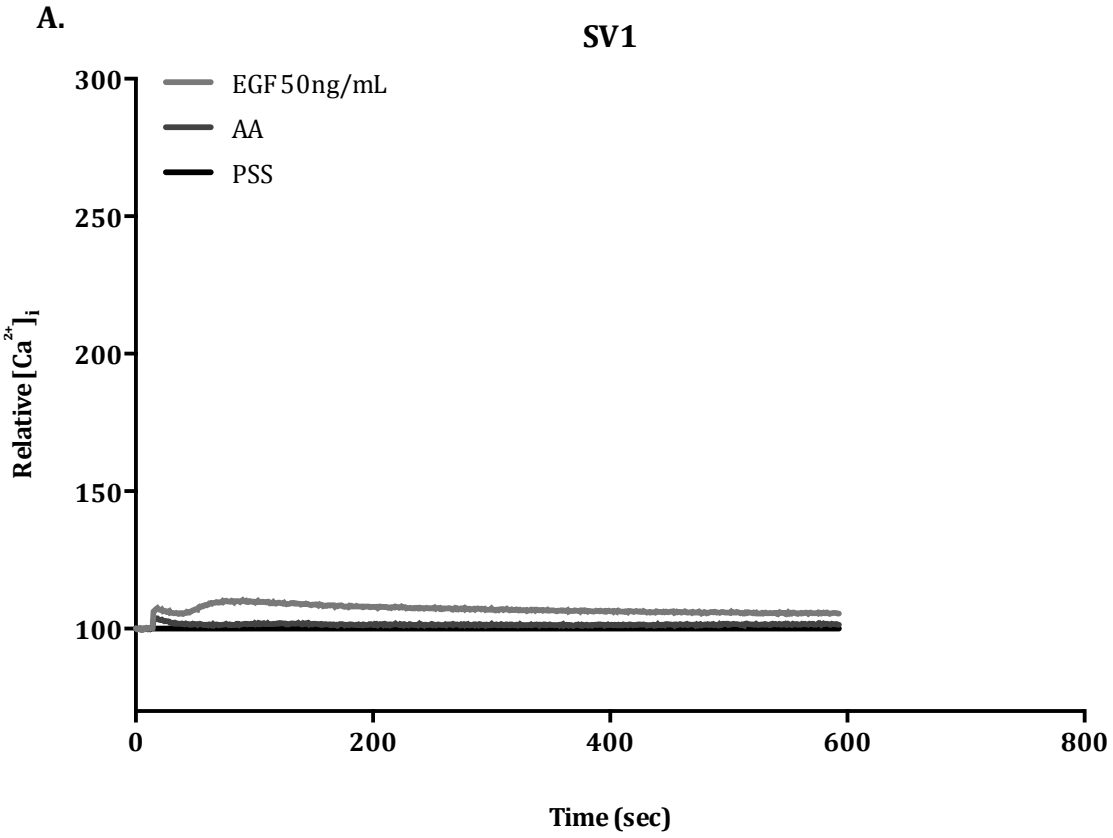
A.
SV1
EGF 50ng/mL
AA
PSS
300
250
200
150
100
Relative [Ca2+]i
0
200
400
600
800
Time (sec)

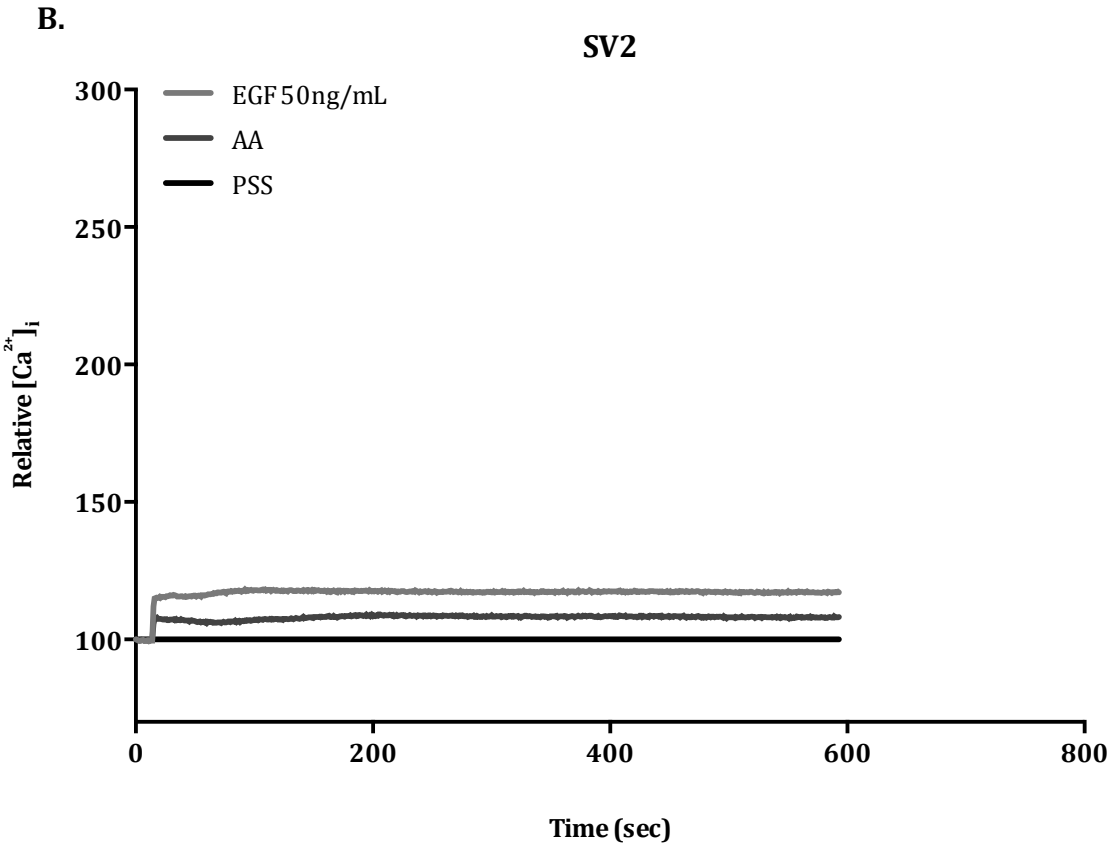
B.
SV2
EGF 50ng/mL
AA
PSS
300
250
200
150
100
Relative [Ca2+]i
0
200
400
600
800
Time (sec)

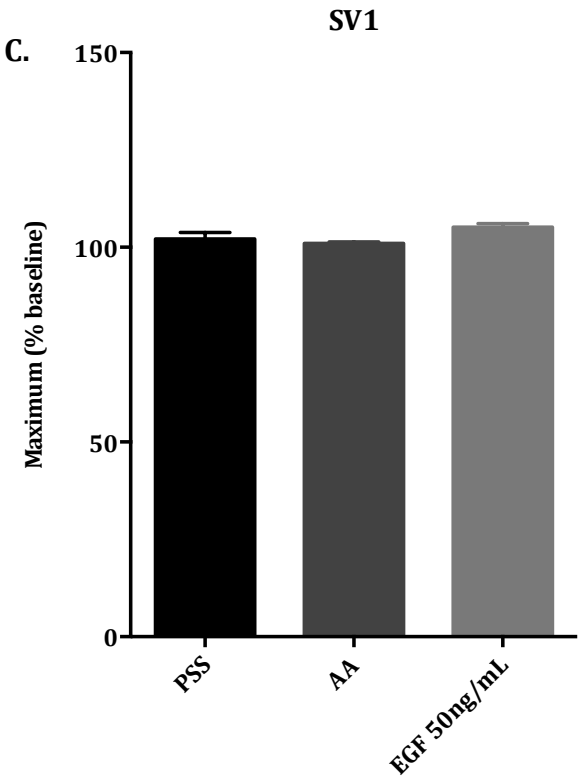
C.
SV1
150
100
50
0
Maximum (% baseline)
PSS
AA
EGF 50ng/mL

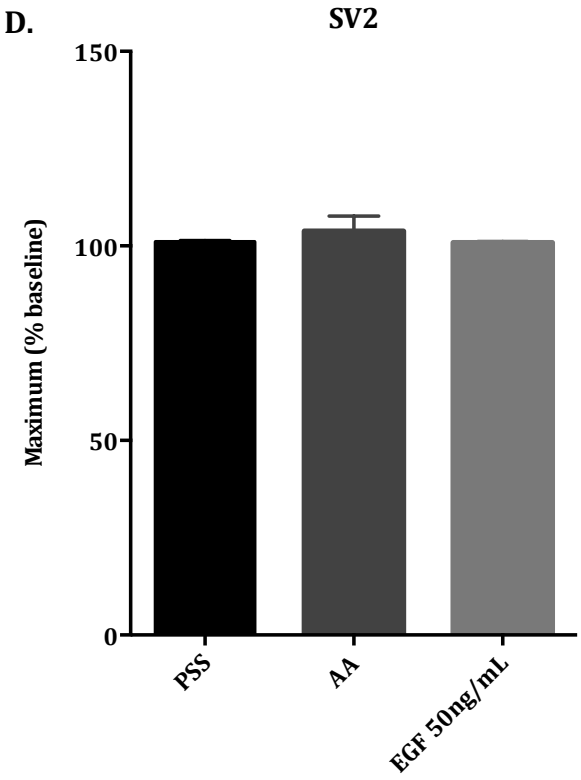
D.
SV2
150
100
50
0
Maximum (% baseline)
PSS
AA
EGF 50ng/mL

Figure 3.19 Assessment of $[Ca^{2+}]_i$ in the age-matched control cell lines following stimulation with 50ng/mL EGF

A. and **B**. Ca^{2+} traces upon EGF treatment from three independent experiments, acetic acid (AA) was a control for EGF. **C**. and **D**. The graphs represent the measurement of maximum $[Ca^{2+}]_i$ assessed using 50 ng/mL of EGF (n=3, ± S.D.). Statistical analysis was performed using one-way ANOVA with Bonferroni post-tests.

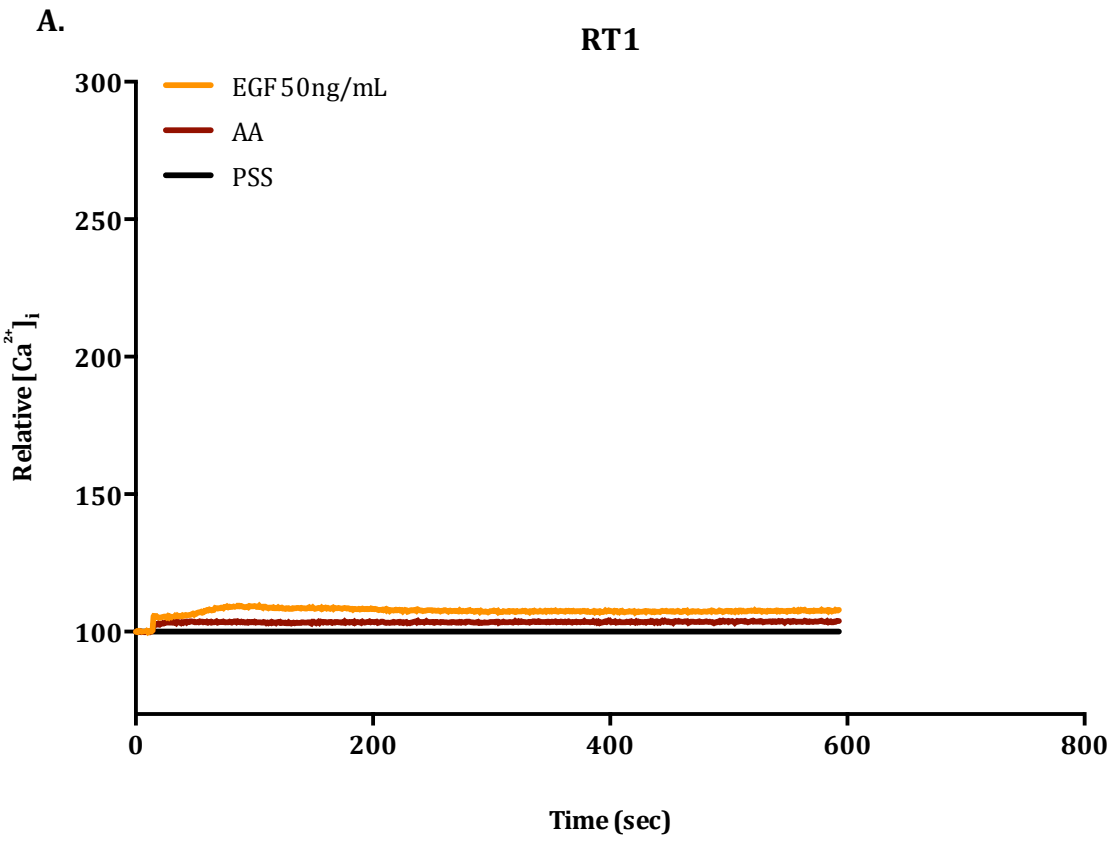
A.
RT1
EGF 50ng/mL
AA
PSS
300
250
200
150
100
Relative [Ca2+]i
0
200
400
600
800
Time (sec)

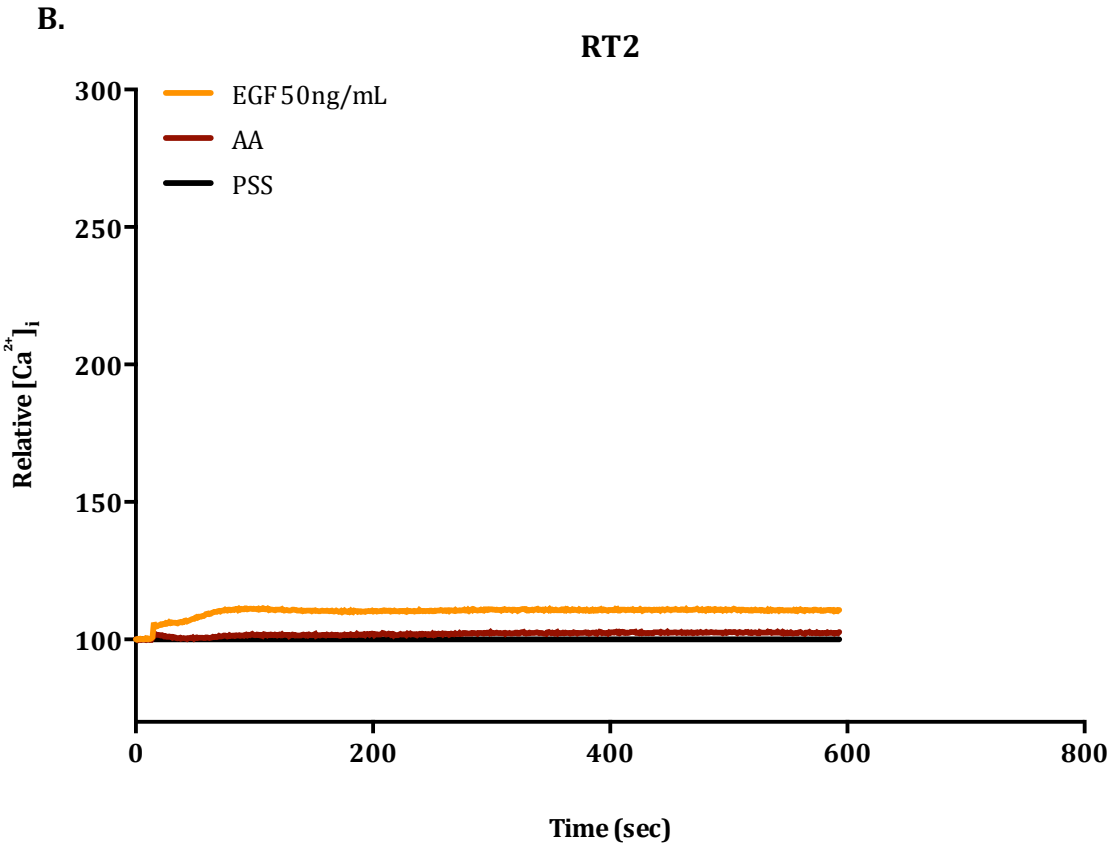
B.
RT2
EGF 50ng/mL
AA
PSS
300
250
200
150
100
Relative [Ca2+]i
0
200
400
600
800
Time (sec)

C.

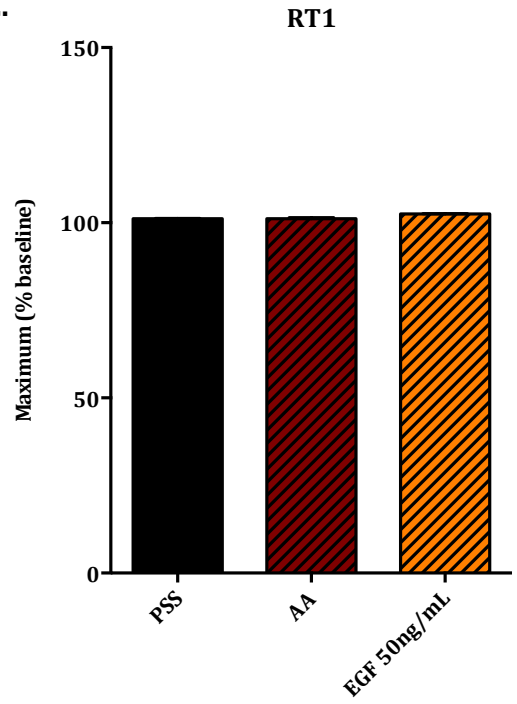
RT1
150
100
50
0
Maximum (% baseline)
PSS
AA
EGF 50ng/mL

D.

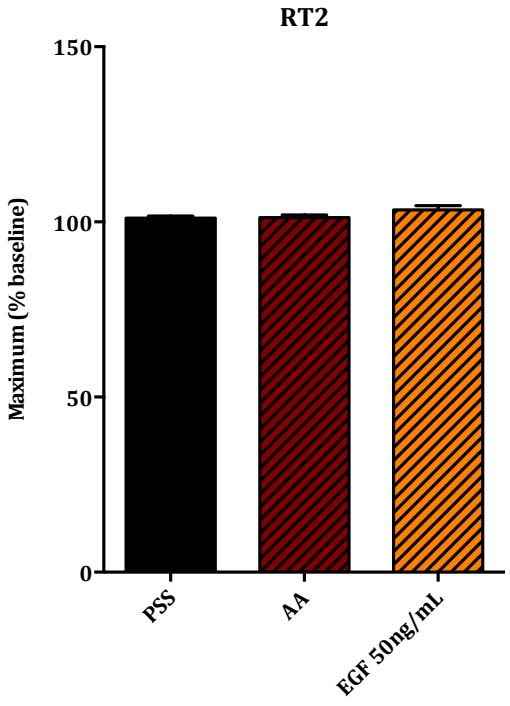
RT2
150
100
50
0
Maximum (% baseline)
PSS
AA
EGF 50ng/mL

Figure 3.20 Assessment of $[Ca^{2+}]_i$ in the acquired resistant cell lines following stimulation with 50ng/mL EGF

A. and **B**. Ca^{2+} traces upon EGF treatment from three independent experiments. **C.** and **D**. The graph represents the measurement of maximum $[Ca^{2+}]_i$ assessed using 50 ng/mL of EGF (n=3, ± S.D.). Statistical analysis was performed using one-way ANOVA with Bonferroni post-tests.

SOCE was assessed in the acquired resistant and age-matched control cell lines, using the same protocol used to evaluate SOCE in SKBR3 parental cells (section 2.3.2). Responses to the SERCA inhibitor CPA were similar in resistant and control cell lines as assessed by peak 1 (Fig. 3.21). These differences were quantified across 3 independent experiments (Fig. 3.22).

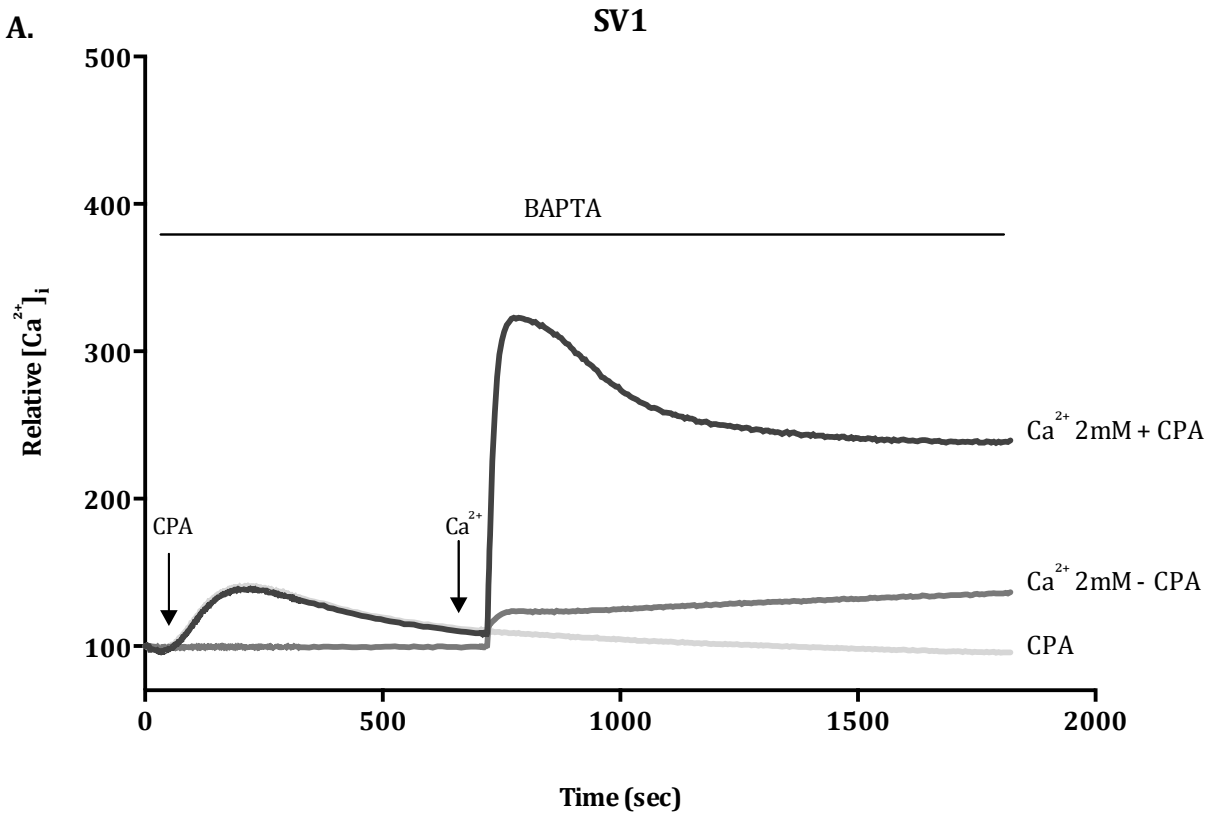
A.
SV1
500
400
300
200
100
BAPTA
Relative [Ca 2+]i
CPA
Ca2+
Ca2+ 2mM + CPA
Ca2+ 2mM - CPA
CPA
0
500
1000
1500
2000
Time (sec)

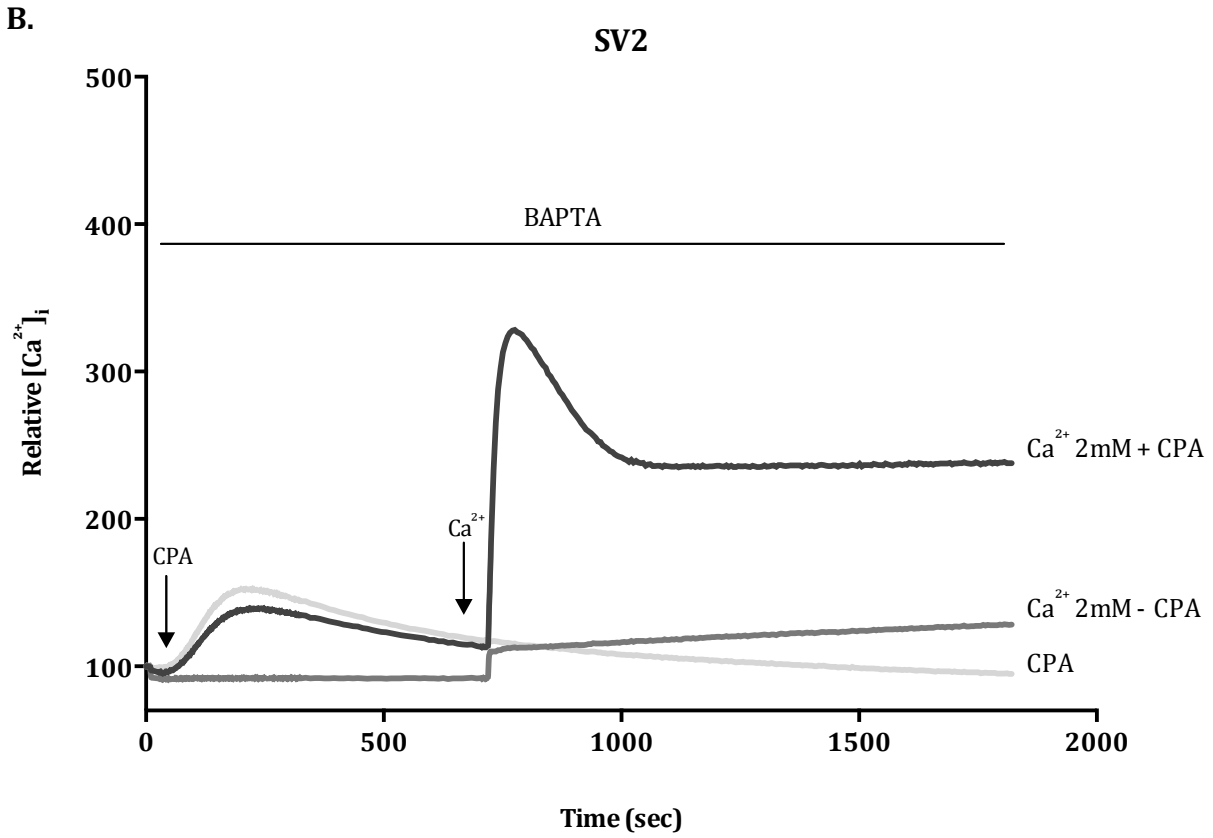
B.
SV2
500
400
300
200
100
BAPTA
Relative [Ca 2+]i
CPA
Ca2+
Ca2+ 2mM + CPA
Ca2+ 2mM - CPA
CPA
0
500
1000
1500
2000
Time (sec)

C.

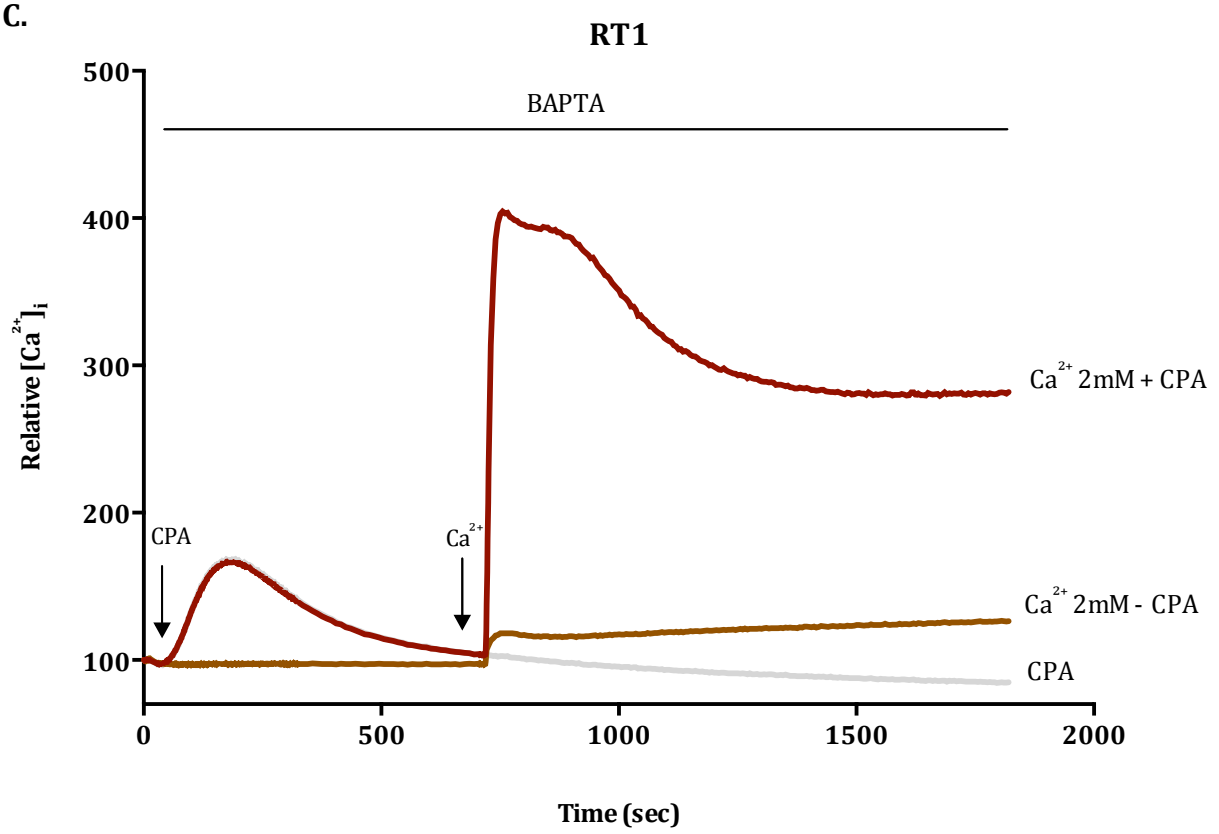
RT1
BAPTA
500
400
300
200
100
Relative [Ca2+]i
CPA
Ca2+
Ca2+ 2mM + CPA
Ca2+ 2mM - CPA
CPA
0
500
1000
1500
2000
Time (sec)

D.

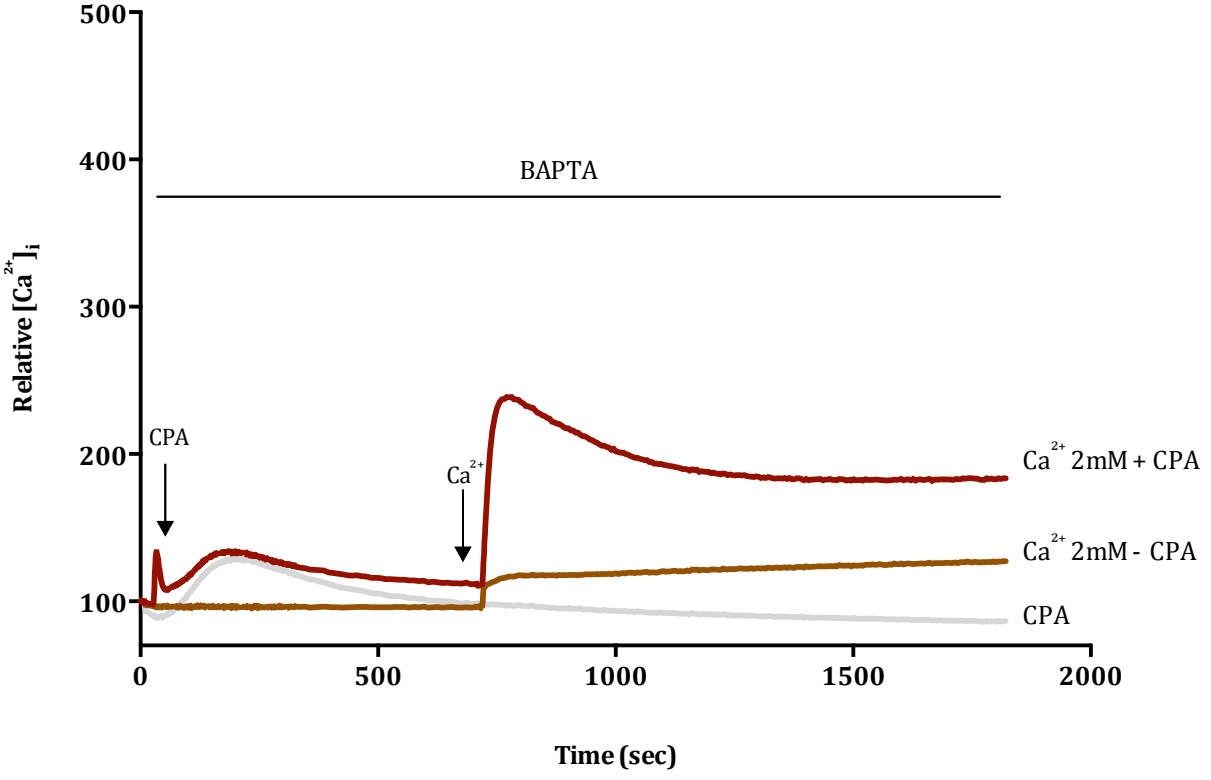
RT2
BAPTA
500
400
300
200
100
Relative [Ca2+]i
CPA
Ca2+
Ca2+ 2mM + CPA
Ca2+ 2mM - CPA
CPA
0
500
1000
1500
2000
Time (sec)

Figure 3.21 Assessment of SOCE in the age-matched control and acquired resistant cell lines

Average of $[Ca^{2+}]_i$ traces from three different experiments assessing SOCE in age-matched control and acquired resistant cell lines (n=3). In the presence of extracellular BAPTA (500 μM), CPA (10 μM) was added to empty the calcium store (first peak), then Ca^{2+} (2 mM) was added to assess SOCE (second peak).

The two age-matched control cell lines showed similar maximum responses to CPA response (peak 1), while the acquired resistant cell line RT1 had a modestly higher release of calcium from the stores upon CPA treatment (Fig. 3.22a). The second peak associated with 2 mM Ca^{2+} showed a higher response for the acquired resistant cell line RT1 cell line compared to SV1 (Fig. 3.22b).

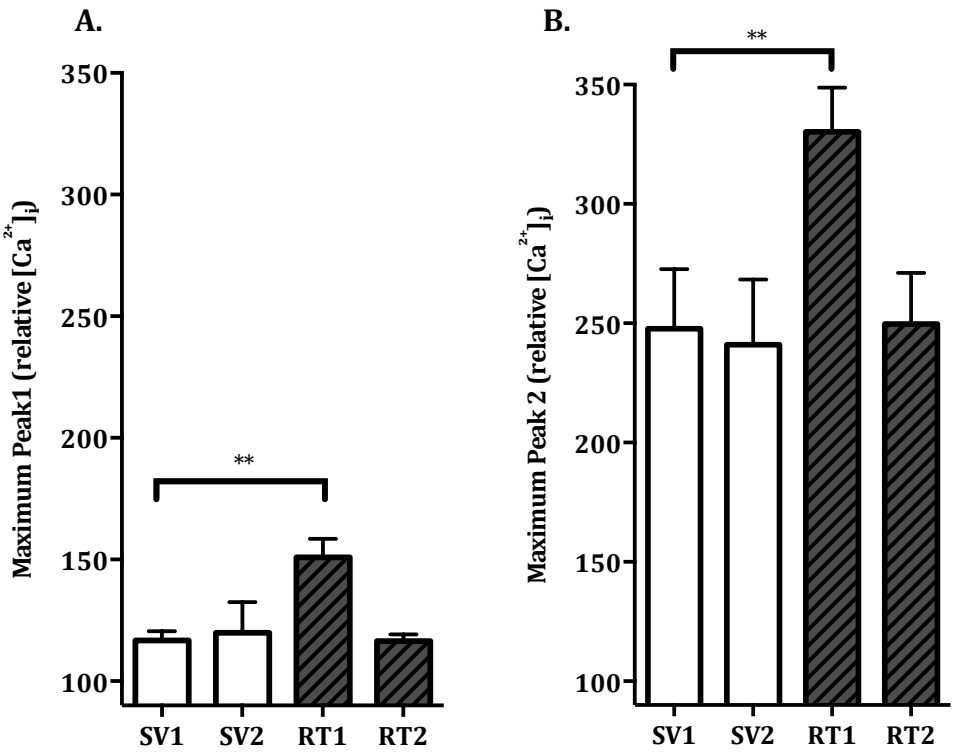

Figure 3.22 Assessment of SOCE in the age-matched control and acquired resistant cell lines

A. Maximum $[Ca^{2+}]_i$ after addition of CPA (first peak) (n=3, ± S.D.). **B**. Maximum $[Ca^{2+}]_i$ recorded after addition of CPA followed by re-addition of 2 mM Ca^{2+} (second peak) (n=3, ± S.D.). Statistical analysis was performed using two-way ANOVA with Bonferroni post-tests (** $p \leq 0.01$).

The ratio between the second and first peaks (a common assessment for store operated calcium entry to discount effects on calcium influx due to differences in the degree of calcium store release (238, 282, 283) did not show a significant difference at 2 mM Ca^{2+} (Fig. 3.23).

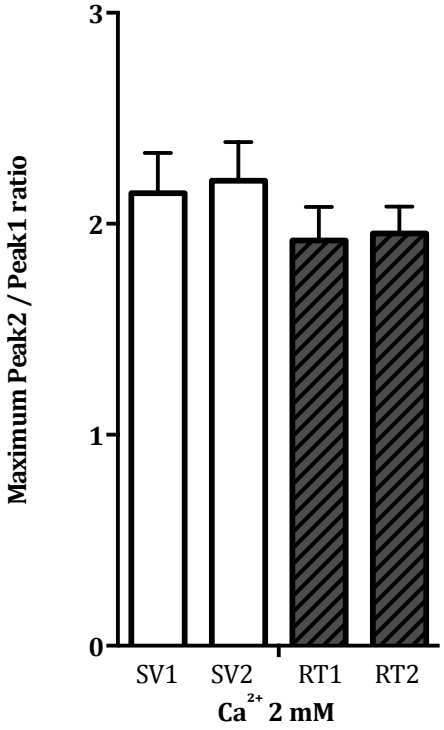

Figure 3.23 Assessment of SOCE in the age-matched control and acquired resistant cell lines

The bar graph represents the measurement of maximum $[Ca^{2+}]_i$ assessed in the presence of external BAPTA using CPA to empty the stores (peak 1) in relation to the increase in $[Ca^{2+}]_i$ associated with the re-addition of Ca^{2+} (n=3, ± S.D.). Statistical analysis was performed using one-way ANOVA with Bonferroni post-tests no significant difference ($p > 0.05$) was observed.

3.4.3 Characterization of *de novo* trastuzumab resistant HER2-positive SKBR3 cell lines

As for the acquired resistant cell lines, the mRNA expression and function of calcium transporters and modulators were also assessed for the *de novo* trastuzumab resistant cell lines. The Ca^{2+} response to ATP and EGF and SOCE profile were likewise assessed in these cells.

3.4.3.1 Assessment of Ca^{2+} channels, pumps and modulators in *de novo* trastuzumab resistant SKBR3 cells

The mRNA level of the 45 targets that were assessed for the acquired resistant cell lines RT1 and RT2 were also evaluated for the *de novo* resistant cell line RV1 and RV2 (Fig. 3.24).

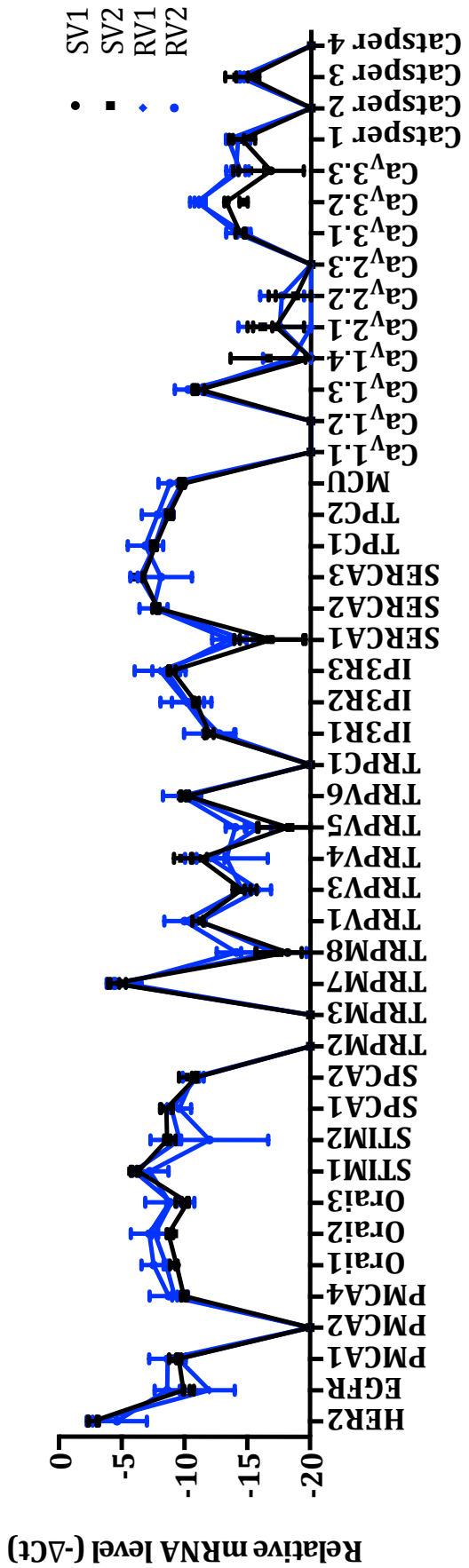

Figure 3.24 Assessment of mRNA of 45 calcium channels, pumps and channel modulators in the *de novo* resistant cell lines, RV1 and RV2

The graph shows the normalized expression level of the 45 calcium channels, pumps and channel modulators. 18s rRNA was used as internal control and the results are shown as –ΔCt (n=3, ± S.D.).

As for the acquired resistant cell lines, the 45 targets that were assessed showed a similar expression levels between the two age-matched control cell lines and the *de novo* resistant cell lines (Fig. 3.24). Individual graphs for each target can be found in appendix 2 and mean $-\Delta Ct$ values for each target can be found in appendix 3. The Orai1, Orai2 and Orai3 channels and the Ca^{2+} sensors STIM1 and STIM2 as well as the voltage-gated calcium channels appeared to show altered mRNA levels in *de novo* resistant cell lines compared to age-matched control cell lines (Fig. 3.24).

It was observed from the bar graphs that the Orai channels and the Ca^{2+} sensors STIM1 and STIM2 did not show a significant difference in mRNA levels between the age-matched control cells and the *de novo* group. Only STIM2 showed a significant difference in mRNA expression and this was only compared to SV1 cell line (Fig. 3.25a).

The expression of some voltage-gated calcium channels was significantly different in the two *de novo* resistant cell line compared to the age-matched of cell lines (Fig. 3.25b). The $Ca_V3.2$ channel showed significantly higher mRNA levels in both *de novo* cell lines. $Ca_V2.1$ channel showed significant lower expression in the *de novo* RV1 cell line compared to the age-matched control cell lines, however its mRNA levels were low in all the cell lines ($\Delta Ct < -20$). $Ca_V3.3$ showed a significant lower mRNA expression in both *de novo* cell lines RV1 and RV2 compared to one of the two age-matched control cell lines, SV1.

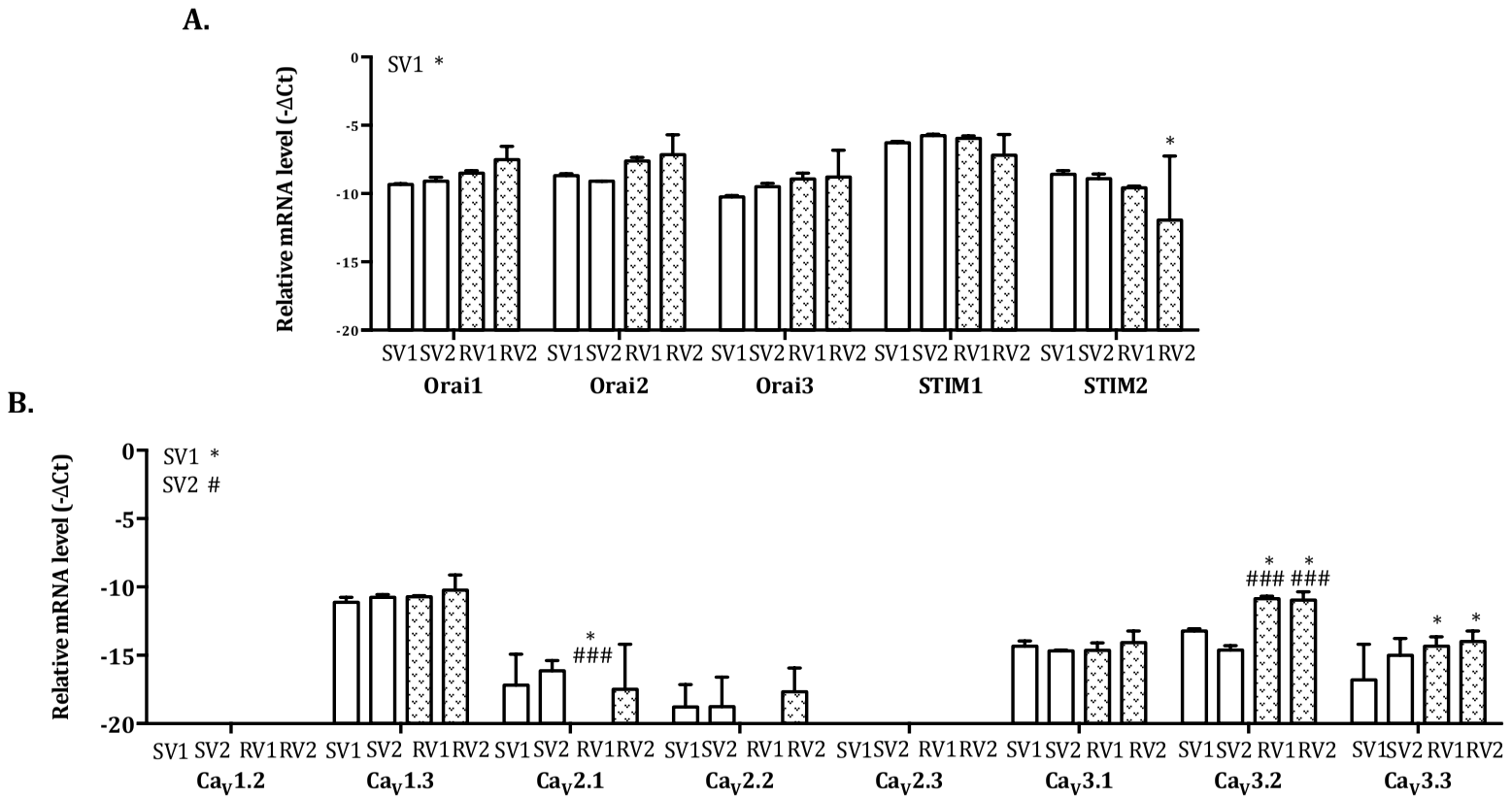

Figure 3.25 mRNA levels of Orai channels, STIM1 and STIM2 and voltage-gated calcium channels in the age-matched control and *de novo* resistant cell lines

A. and **B.** Normalized mRNA expression of the different Orai channels, STIM1 and STIM2 and voltage-gated calcium channels in the age-matched control and *de novo* resistant cell lines produced (n=3, ± S.D.). 18s rRNA was used as internal control and the results are shown as –ΔCt. Statistical analysis was performed using two-way ANOVA with Bonferroni post-tests, the * refers to a statistical significance compared to SV1, while # refers to SV2 (* $p \leq 0.05$, ** $p \leq 0.01$, ### $p \leq 0.001$).

The 14 targets tested for the acquired resistant cell line RT1 were assessed to evaluate the effect of their silencing on trastuzumab sensitivity. Trastuzumab was added 24 h after siRNA treatment and repeated every two days. MTS assay was performed to evaluate cells viability after 196 h after siRNA treatment.

From this screen, it was observed that TRPM7 and SPCA1, which were found to affect trastuzumab response in SKBR3 parental in section 2.6, as well as SPCA2, Orai1 and Orai2 may have also sensitized *de novo* resistant cells to trastuzumab (Fig. 3.26a and Fig. 3.26b).

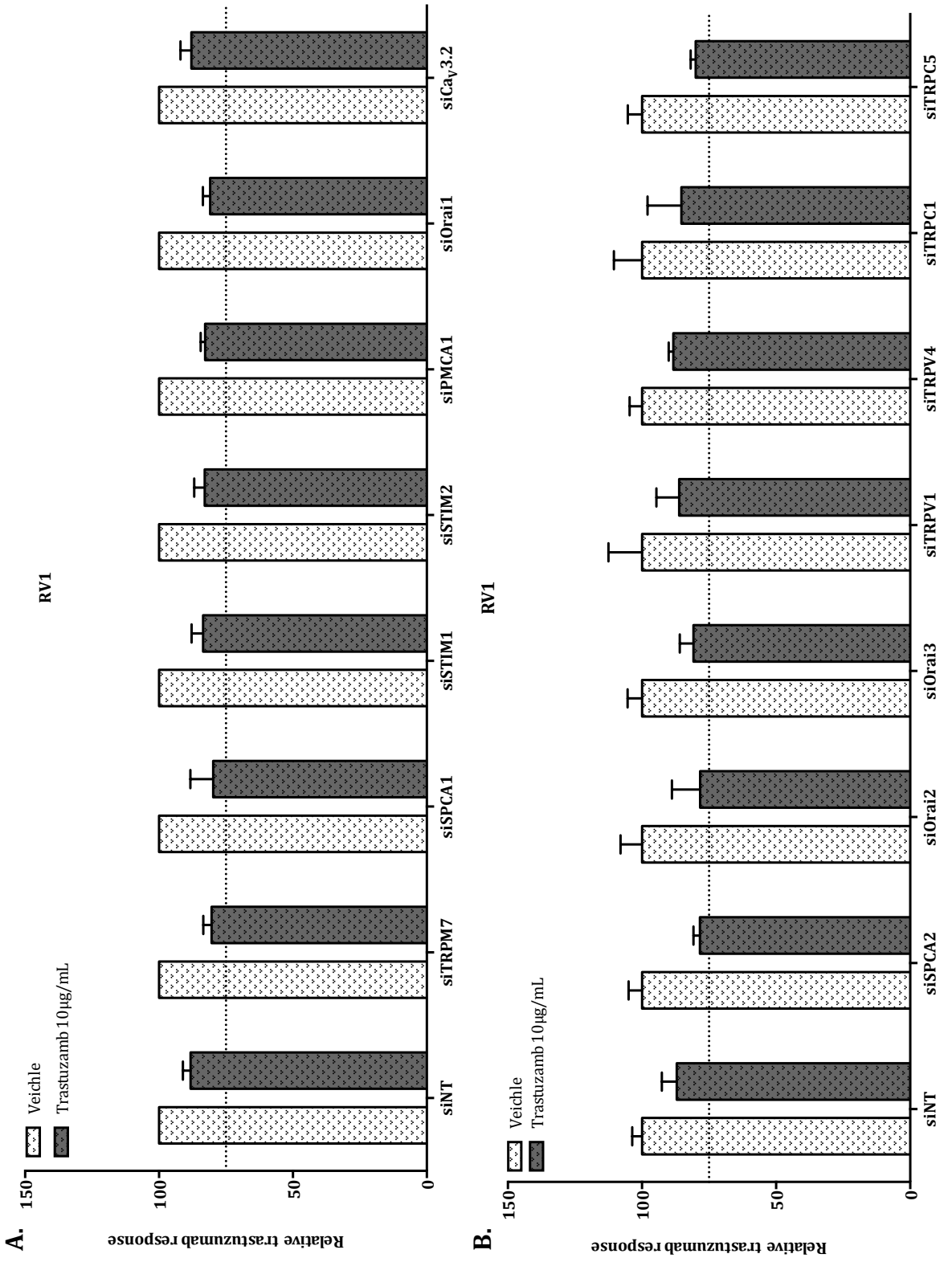
A.
RV1
Veichle
Trastuzamb 10µg/mL
Relative trastuzumab response
150
100
50
0
siNT
siTRPM7
siSPCA1
siSTIM1
siSTIM2
siPMCA1
siOrai1
siCaV3.2
B.
RV1
Veichle
Trastuzamb 10µg/mL
Relative trastuzumab response
150
100
50
0
siNT
siSPCA2
siOrai2
siOrai3
siTRPV1
siTRPV4
siTRPC1
siTRPC5

Figure 3.26 siRNA screen of 14 Ca^{2+} targets on the *de novo* resistant cell line RV1 cell line

An MTS assay was performed on the *de novo* resistant cell line RV1 to evaluate the effect of silencing 14 calcium targets on the response to trastuzumab (3 wells, ± S.D). Targets that showed a response lower than the dashed line drawn at 75% indicated a potential reversal of trastuzumab resistance.

Confirmation analyses were performed on SPCA1, SPCA2, Orai1, Orai2 and TRPM7. However, results from three independent experiments showed that the response to trastuzumab was not significantly restored when these target were silenced compared to the non-targeting control (siNT) (Fig. 3.27).

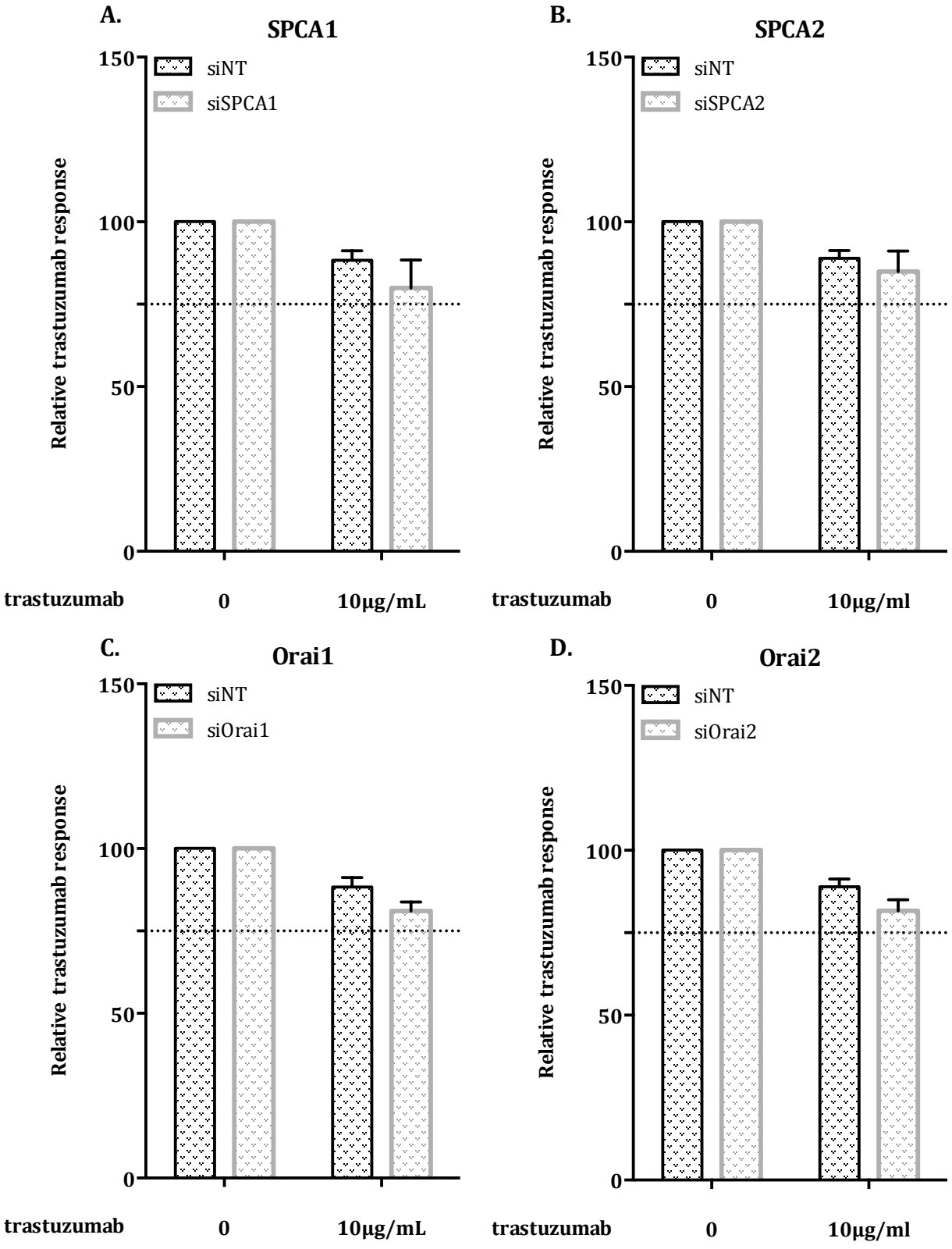
A.
SPCA1
siNT
siSPCA1
Relative trastuzumab response
150
100
50
0
trastuzumab
0
10µg/mL
B.
SPCA2
siNT
siSPCA2
Relative trastuzumab response
150
100
50
0
trastuzumab
0
10µg/ml
C.
Orai1
siNT
siOrai1
Relative trastuzumab response
150
100
50
0
trastuzumab
0
10µg/mL
D.
Orai2
siNT
siOrai2
Relative trastuzumab response
150
100
50
0
trastuzumab
0
10µg/ml

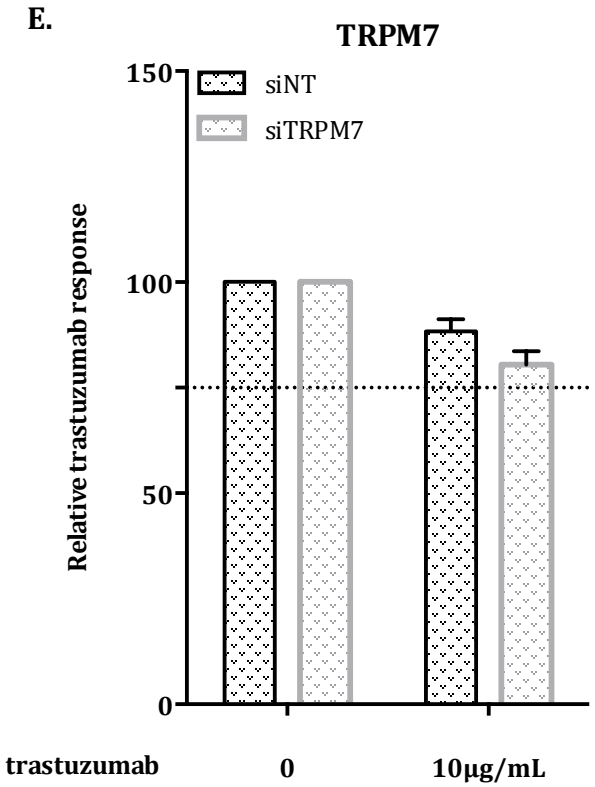

Figure 3.27 Confirmation analysis for targets that showed possible reversal of trastuzumab resistance in the *de novo* resistance RV1 cell line

Results from three independent experiments for SPCA1, SPCA2, Orai1, Orai2 and TRPM7 using MTS assay (n=3, ± S.D.). Statistical analysis was performed using two-way ANOVA with Bonferroni post-tests. No significant difference ($p > 0.05$) was observed.

3.4.3.2 Ca^{2+} signaling profile of *de novo* trastuzumab resistant SKBR3 cells

The nature of the ATP, EGF induced Ca^{2+} transient and the SOCE profile were also assessed for the *de novo* resistant cells using the Ca^{2+} indicator Fluo-4 AM in a Ca^{2+} measurement assay using FLIPR to evaluate possible differences in global calcium.

A concentration-response curve of ATP was produced for each cell line. The traces for the *de novo* cell lines showed similar response to ATP (Fig. 3.28). Age-matched control traces were discussed in section 3.4.2. In regards to the two *de novo* resistant cell lines, RV1 and RV2, these showed similar increases in intracellular calcium upon ATP stimulation (Fig. 3.28c and Fig. 3.28d).

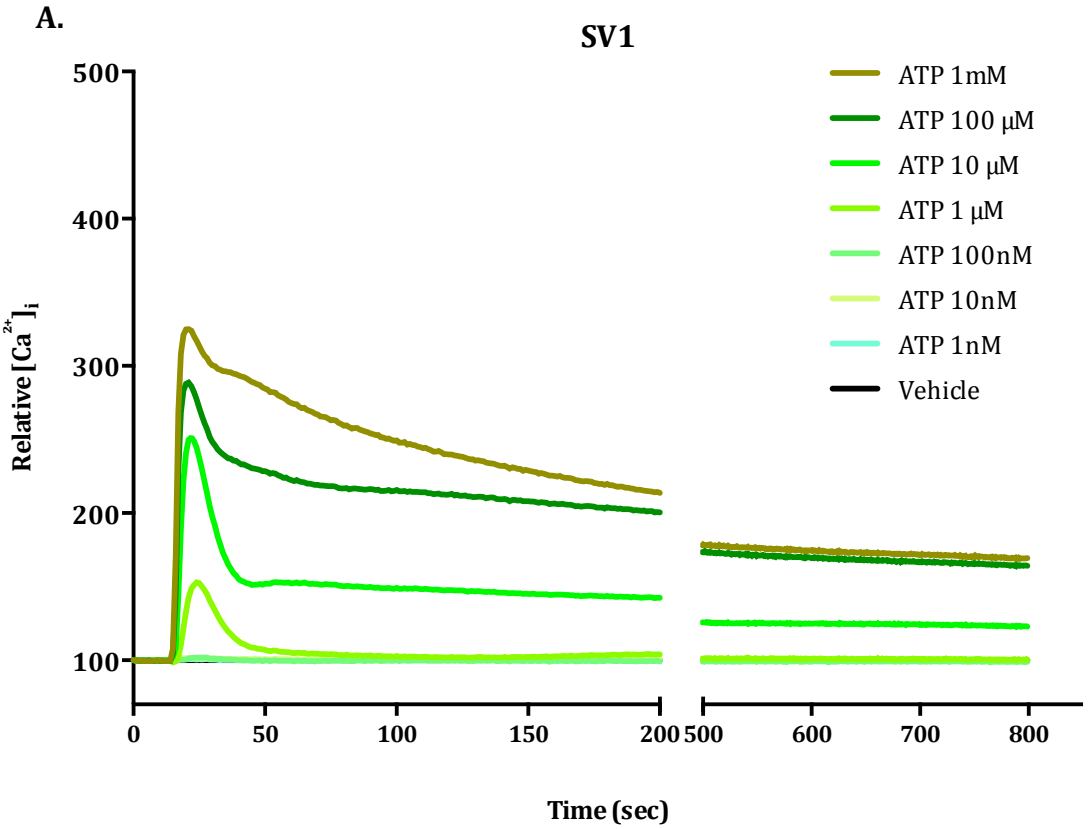
A.
SV1
ATP 1mM
ATP 100 µM
ATP 10 µM
ATP 1 µM
ATP 100nM
ATP 10nM
ATP 1nM
Vehicle
Relative [Ca2+]i
500
400
300
200
100
0
50
100
150
200
500
600
700
800
Time (sec)

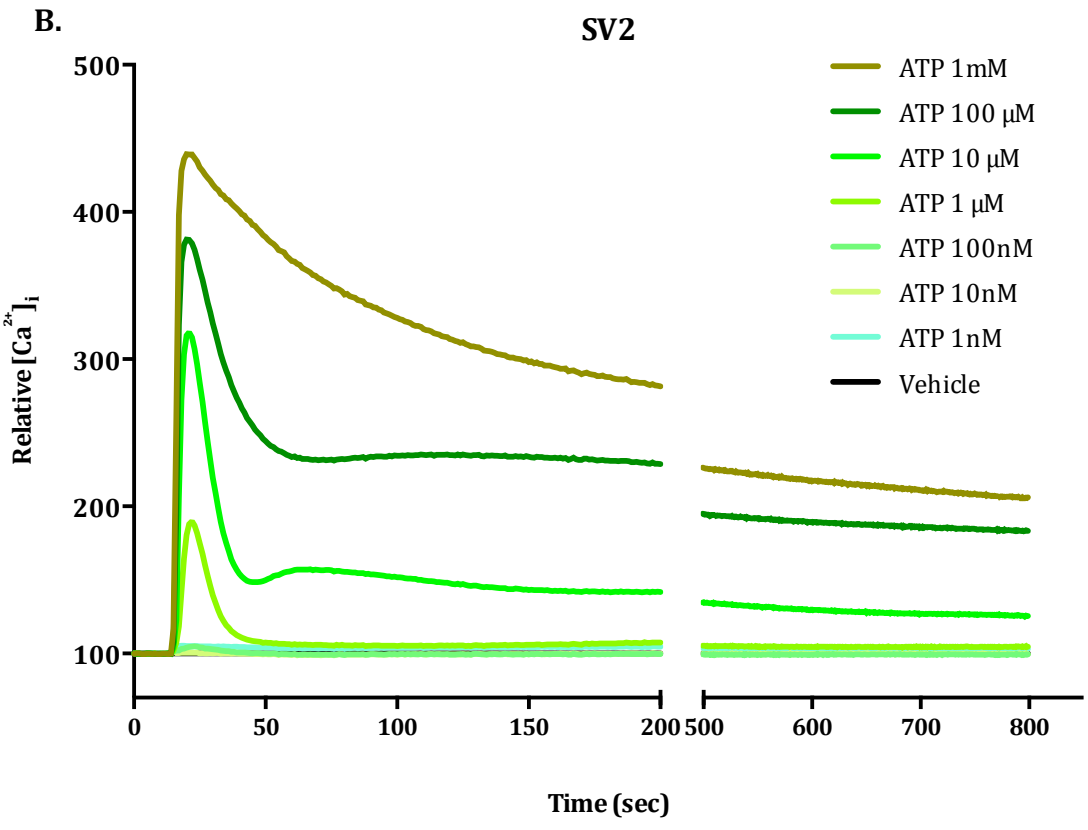
B.
SV2
ATP 1mM
ATP 100 µM
ATP 10 µM
ATP 1 µM
ATP 100nM
ATP 10nM
ATP 1nM
Vehicle
Relative [Ca2+]i
500
400
300
200
100
0
50
100
150
200
500
600
700
800
Time (sec)

C.

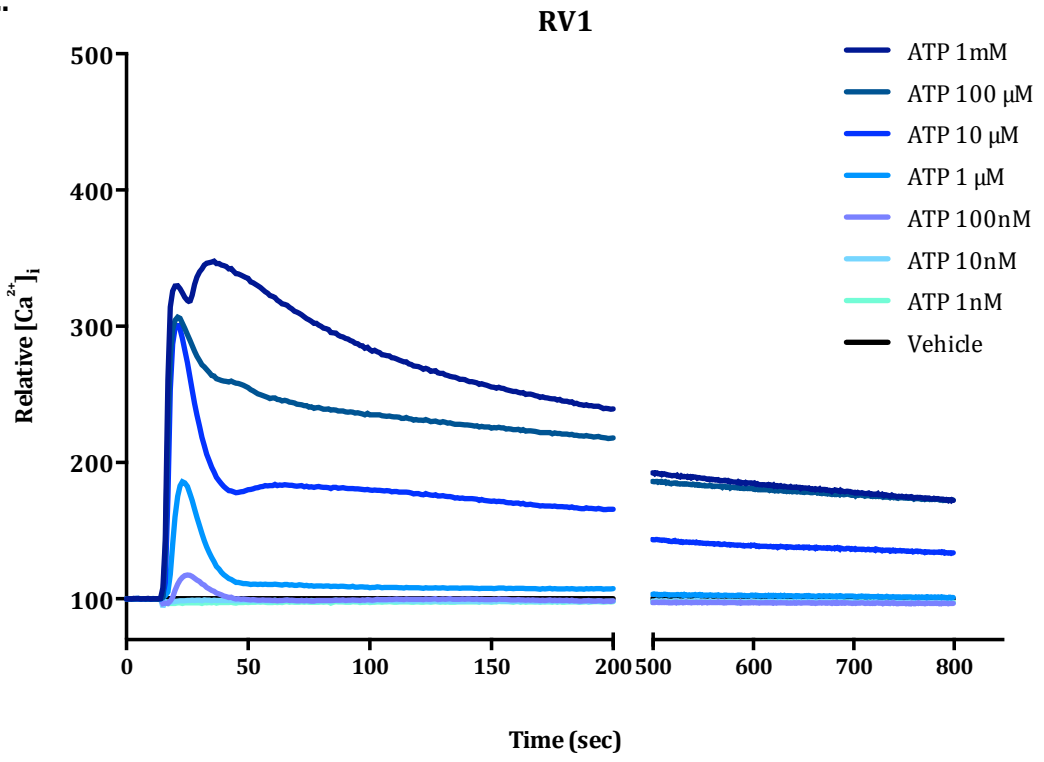
RV1
ATP 1mM
ATP 100 µM
ATP 10 µM
ATP 1 µM
ATP 100nM
ATP 10nM
ATP 1nM
Vehicle
Relative [Ca2+]i
500
400
300
200
100
0
50
100
150
200
500
600
700
800
Time (sec)

D.

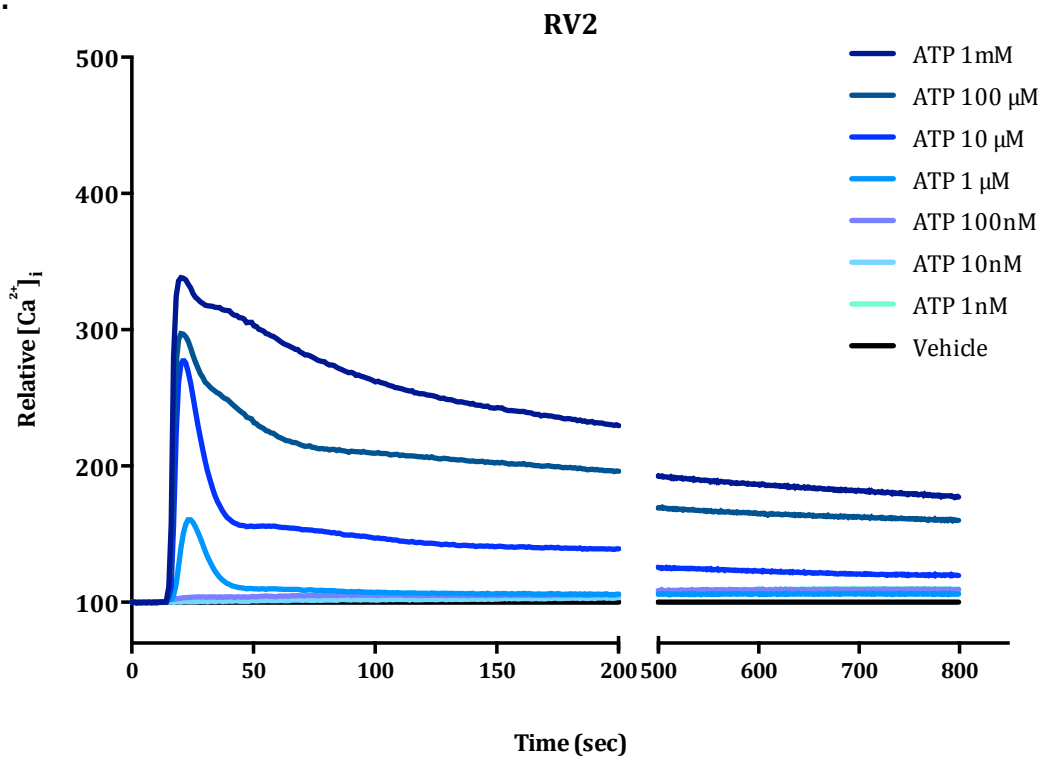
RV2
ATP 1mM
ATP 100 µM
ATP 10 µM
ATP 1 µM
ATP 100nM
ATP 10nM
ATP 1nM
Vehicle
Relative [Ca2+]i
500
400
300
200
100
0
50
100
150
200
500
600
700
800
Time (sec)

Figure 3.28 $[Ca^{2+}]_i$ traces in the age-matched control and *de novo* resistant cells upon ATP stimulation

Average $[Ca^{2+}]_i$ traces from three independent experiments measured using FLIPR showing the relative $[Ca^{2+}]_i$ in response to different concentration of ATP (1mM, 100 μM, 10 μM, 1 μM, 100 nM, 10 nM, 1nM) in the age-matched control and *de novo* resistant cell lines.

Ca^{2+} response from the concentration-response curves for the *de novo* resistant cells RV1 and RV2 showed an EC_{50} of 2.5 μM and 2.9 μM, respectively, which were similar to the EC_{50} of the age-matched control cells (3.4 μM and 2.9 μM) (Fig 3.29). Thus, it appeared that, in contrast to the acquired resistant cells, the *de novo* resistant cell lines respond to ATP similarly to the age-matched control cell lines.

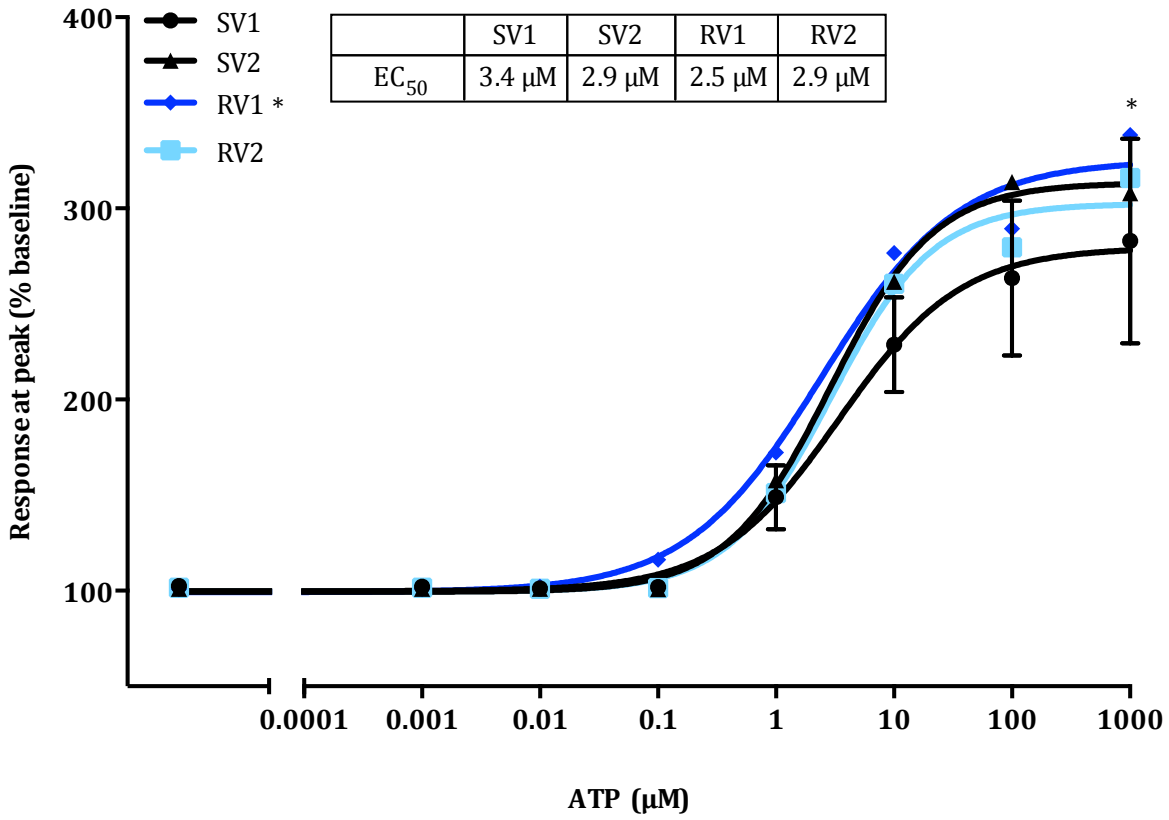

	SV1	SV2	RV1	RV2
EC_{50}	3.4 µM	2.9 µM	2.5 µM	2.9 µM

Figure 3.29 ATP concentration-response curve of the *de novo* resistant cell lines

The graph represents the concentration-response curves for measurement of the maximum $[Ca^{2+}]_i$ assessed using 0.001 µM, 0.01 µM 0.1 µM, 1 µM, 10 µM, 100 µM and 1 mM of ATP in the age-matched control and *de novo* resistant cell lines (n=3, ± S.D.). Statistical analysis was performed using two-way ANOVA with Bonferroni post-tests. Statistics refers to SV1, the * is associated with statistical significance between SV1 and RT1, while the # is between SV1 and RT2 (* $p \leq 0.05$).

The acquired resistant cell lines, as discussed in section 3.4.2, showed a delayed recovery compared to the age-matched control cell lines. In contrast, the *de novo* resistant cell lines did not show a slower recovery in comparison with the age-matched control cells (Fig. 3.30).

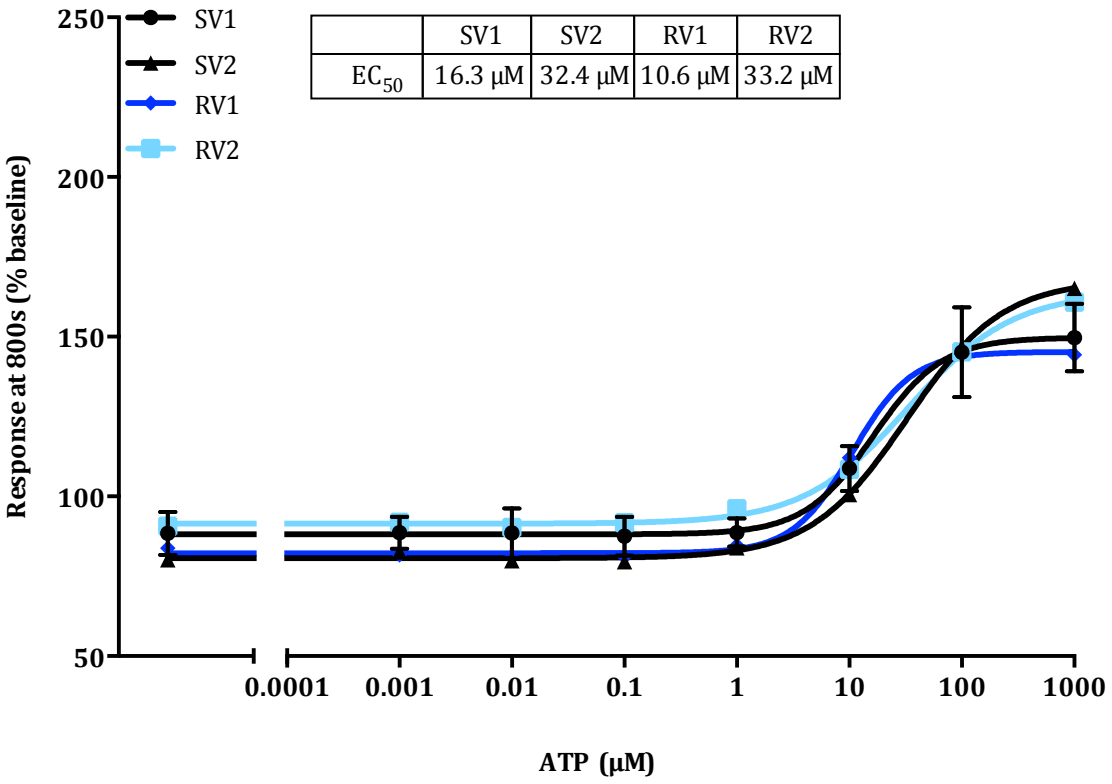

	SV1	SV2	RV1	RV2
EC_{50}	16.3 µM	32.4 µM	10.6 µM	33.2 µM

Figure 3.30 ATP concentration-response curve of the *de novo* resistant cell lines at 800 s

The graph represents the concentration-response curves for measurements of $[Ca^{2+}]_i$ at 800 seconds after the addition of ATP, assessed using 0.001 µM, 0.01 µM 0.1 µM, 1 µM, 10 µM, 100 µM and 1 mM of ATP in the age-matched control and *de novo* resistant cell lines (n=3, ± S.D.). Statistical analysis was performed using two-way ANOVA with Bonferroni post-tests. No significant difference ($p > 0.05$) was observed.

The *de novo* resistant cells were also assessed for their Ca^{2+} response to 50 ng/mL EGF. As for the SKBR3 parental cell line showed in section 2.4, the age-matched and acquired resistant cell lines discussed in section 3.4.2, the *de novo* resistant cells EGF treatment did not produce increases in $[Ca^{2+}]_i$ (Fig. 3.31).

A.

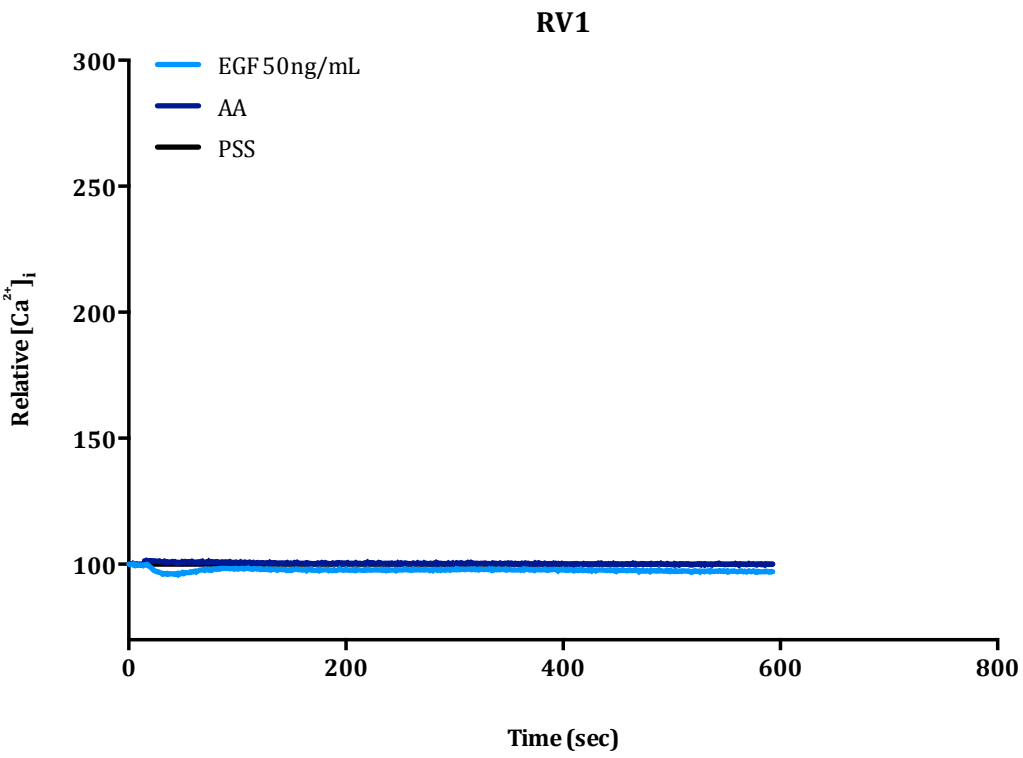
RV1
EGF 50ng/mL
AA
PSS
300
250
200
150
100
0
200
400
600
800
Relative [Ca2+]i
Time (sec)

B.

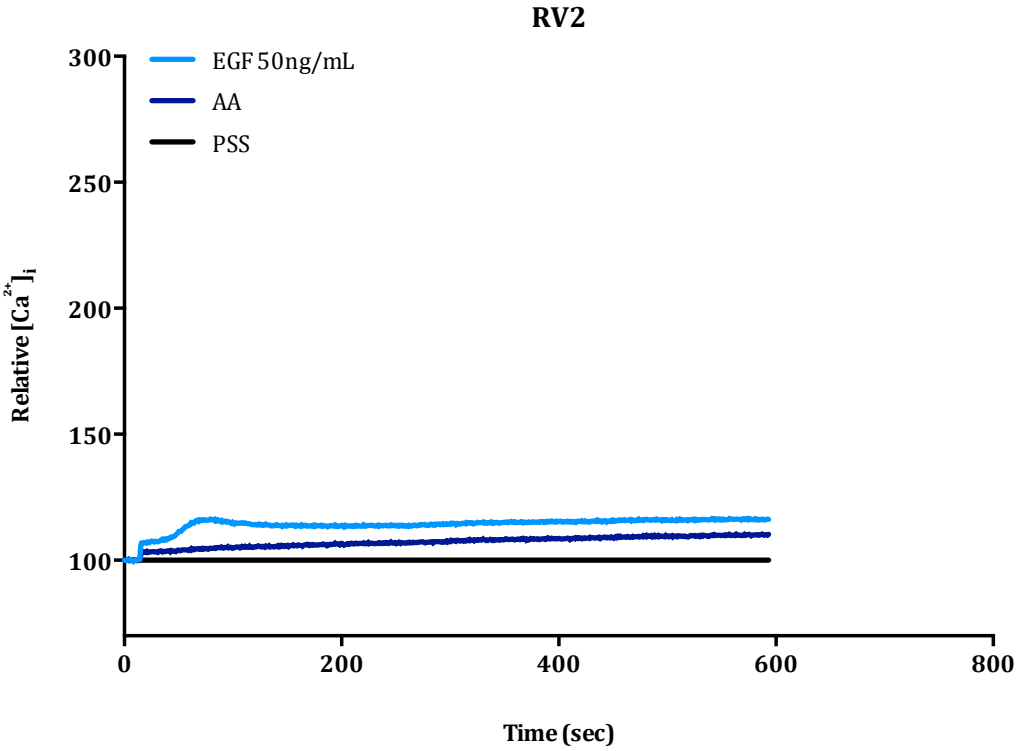
RV2
EGF 50ng/mL
AA
PSS
300
250
200
150
100
0
200
400
600
800
Relative [Ca2+]i
Time (sec)

C.

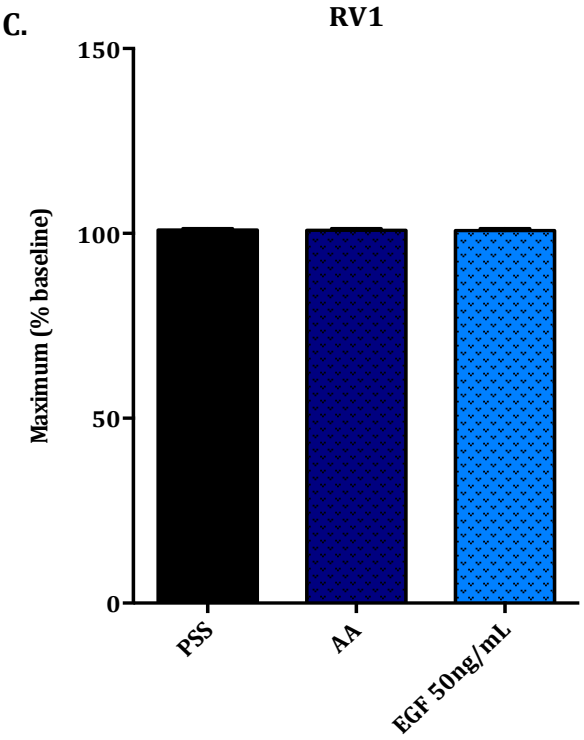
RV1
150
100
50
0
Maximum (% baseline)
PSS
AA
EGF 50ng/mL

D.

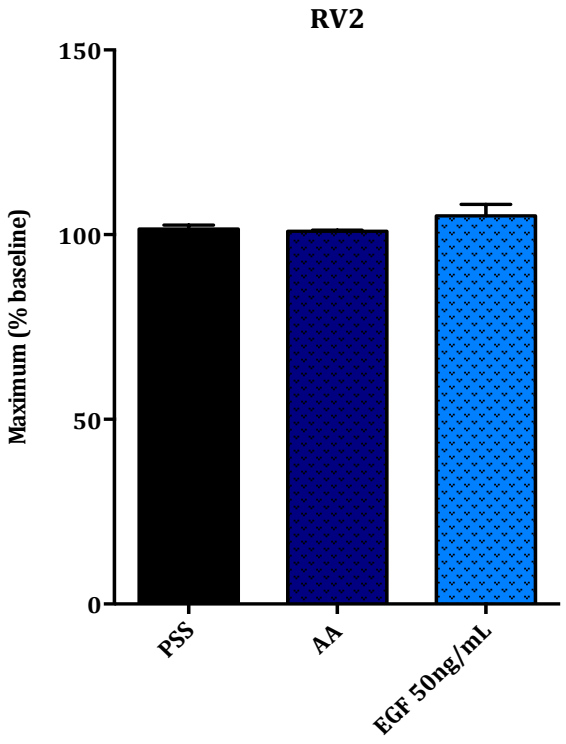
RV2
150
100
50
0
Maximum (% baseline)
PSS
AA
EGF 50ng/mL

Figure 3.31 Assessment of $[Ca^{2+}]_i$ in the age-matched control and *de novo* resistant cells following stimulation with 50 ng/mL EGF

A. and **B**. $[Ca^{2+}]_i$ traces upon EGF treatment from three independent experiments, acetic acid (AA) was a control for EGF. **C**. and **D**. The graph represents the measurement of maximum $[Ca^{2+}]_i$ assessed using 50 ng/mL of EGF (n=3, ± S.D.). Statistical analysis was performed using two-way ANOVA with Bonferroni post-tests.

The SOCE profile was also assessed for these cell lines (Fig. 3.32). The calcium traces for the age-matched cell lines were discussed in section 3.4.2.

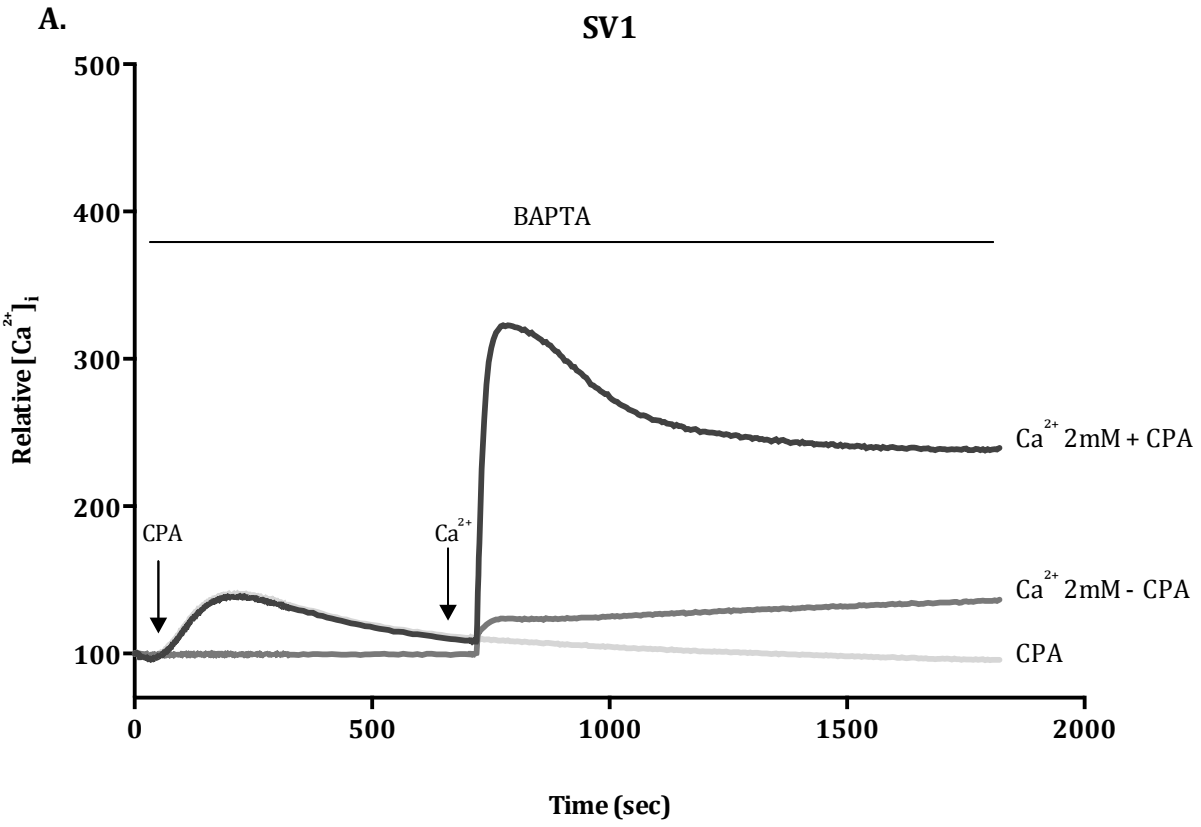
A.
SV1
500
400
300
200
100
BAPTA
Relative [Ca2+]i
CPA
Ca2+
Ca2+ 2mM + CPA
Ca2+ 2mM - CPA
CPA
0
500
1000
1500
2000
Time (sec)

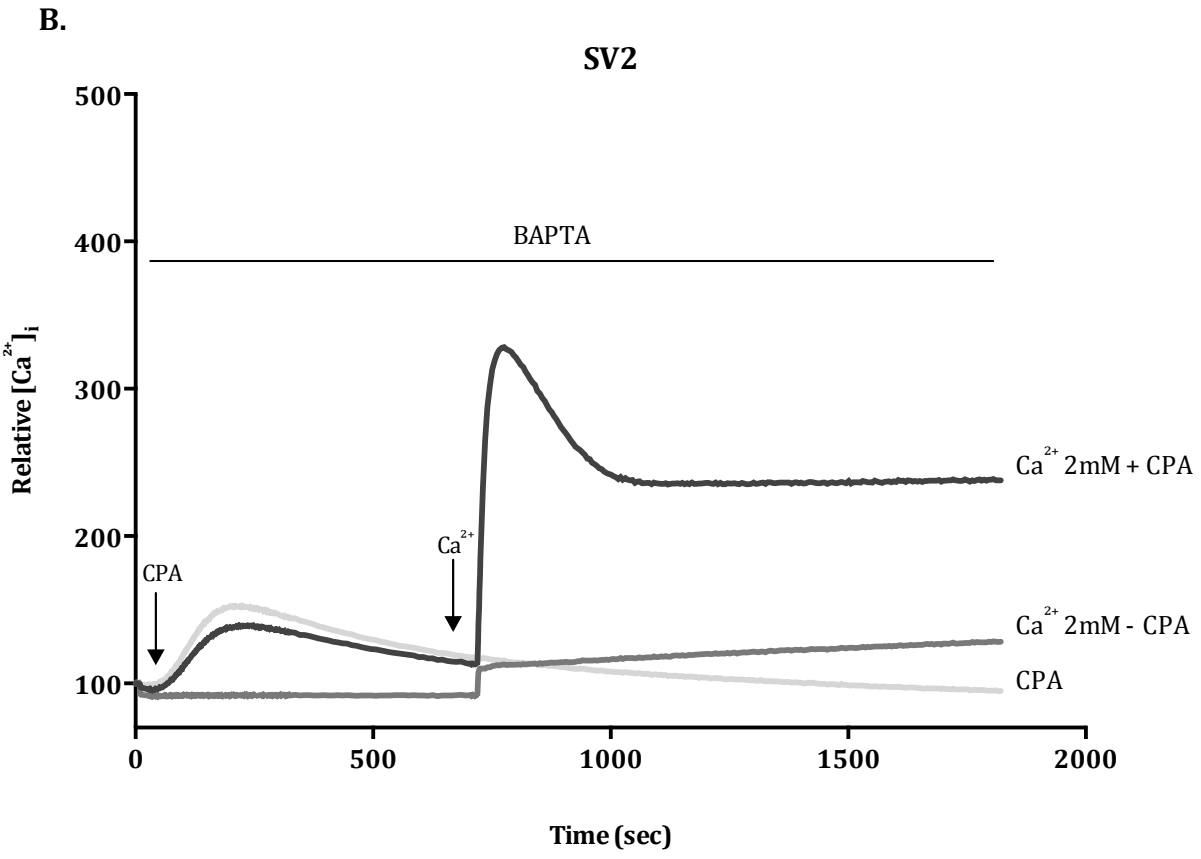
B.
SV2
500
400
300
200
100
BAPTA
Relative [Ca2+]i
CPA
Ca2+
Ca2+ 2mM + CPA
Ca2+ 2mM - CPA
CPA
0
500
1000
1500
2000
Time (sec)

C.

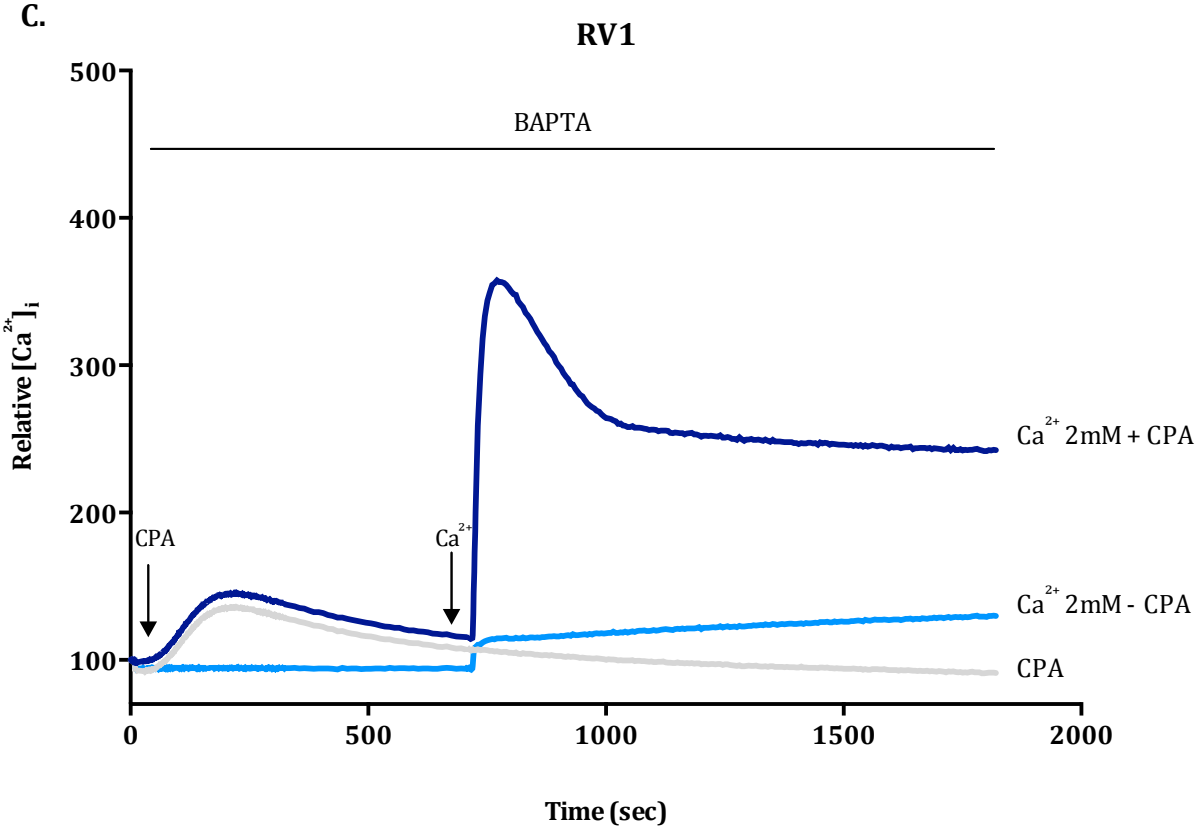
RV1
BAPTA
500
400
300
200
100
Relative [Ca2+]i
CPA
Ca2+
Ca2+ 2mM + CPA
Ca2+ 2mM - CPA
CPA
0
500
1000
1500
2000
Time (sec)

D.

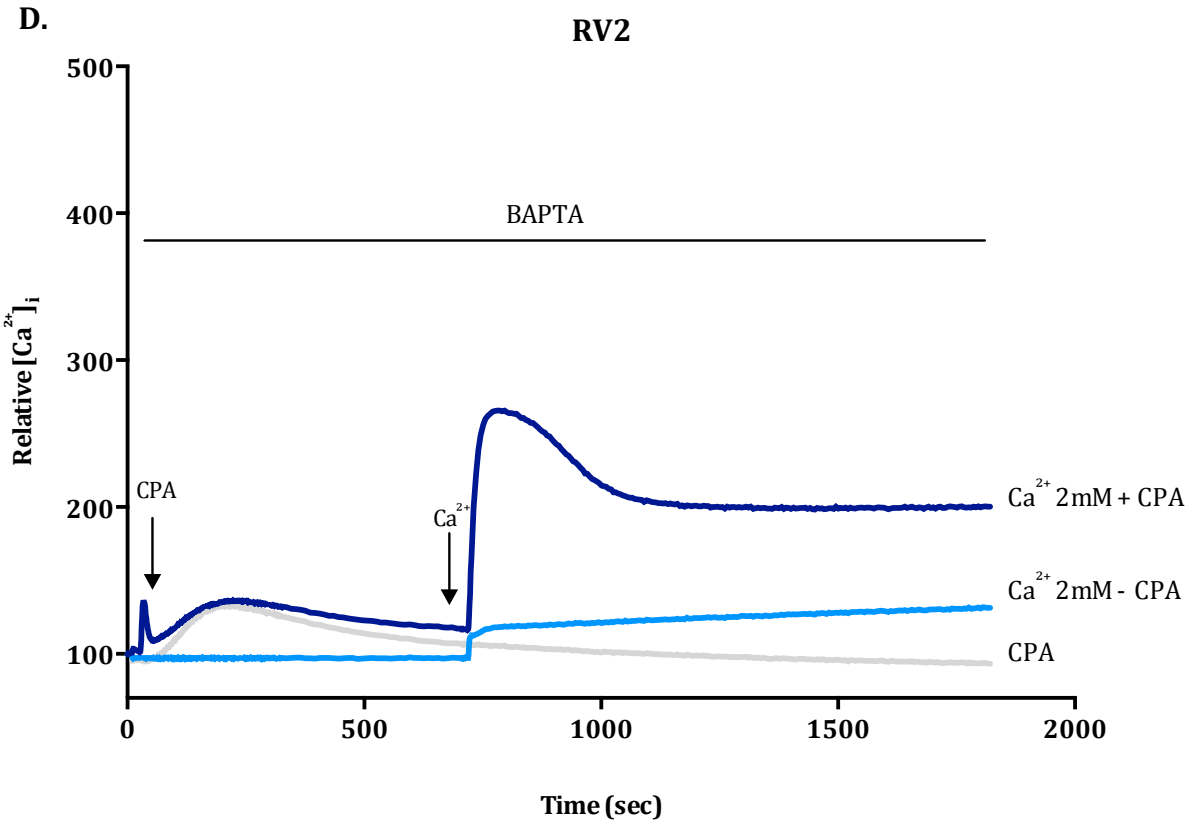
RV2
BAPTA
500
400
300
200
100
Relative [Ca2+]i
CPA
Ca2+
Ca2+ 2mM + CPA
Ca2+ 2mM - CPA
CPA
0
500
1000
1500
2000
Time (sec)

Figure 3.32 Assessment of SOCE in the age-matched control and *de novo* resistant cell lines

Average of $[Ca^{2+}]i$ traces from three different experiments assessing SOCE in the age-matched control and acquired resistant cell lines. In the presence of extracellular BAPTA (500 μM), CPA (10 μM) was added to empty the calcium store (first peak), then Ca^{2+} (2mM) was added to assess SOCE (second peak).

The release of calcium from internal stores upon CPA treatment and re-addition of 2 mM Ca^{2+} was similar between the *de novo* and the age-matched control groups (Fig. 3.33a and 3.33b).

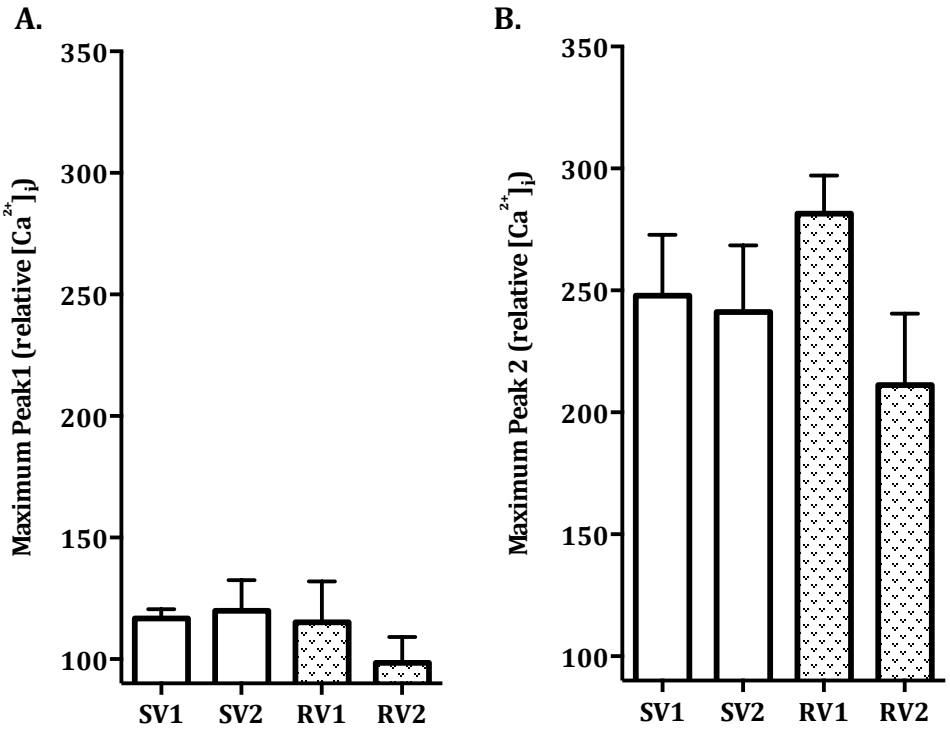

Figure 3.33 Assessment of SOCE in the age-matched control and *de novo* resistant cell lines

A. Maximum $[Ca^{2+}]_i$ recorded after addition of CPA (first peak) (n=3, ± S.D.). **B.** Maximum $[Ca^{2+}]_i$ recorded after addition of 2 mM Ca^{2+} (second peak) (n=3, ± S.D.). Statistical analysis was performed using two-way ANOVA with Bonferroni post-tests. No significant difference ($p > 0.05$) was observed.

Furthermore, the ratio between second and first peak showed no significant difference between the two *de novo* cell lines and the age-matched control cell lines (Fig. 3.34).

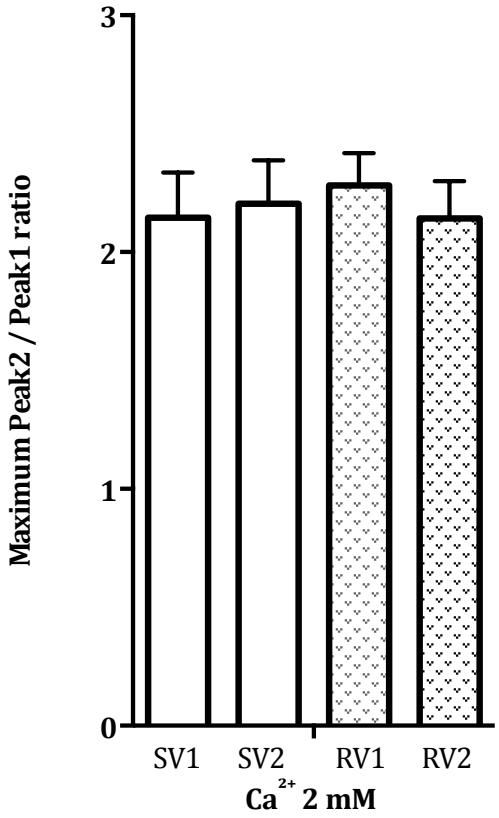

Figure 3.34 Assessment of SOCE in the age-matched control and *de novo* resistant cell lines

The bar graphs represent the relative measurement of maximum $[Ca^{2+}]_i$ assessed in the presence of external BAPTA using CPA to empty the stores (peak 1) in relation to the peak associated with 2 mM Ca^{2+} addition (peak 2) (n=3, ± S.D.). Statistical analysis was performed using one-way ANOVA with Bonferroni post-tests. No significant difference ($p > 0.05$) was observed.

3.5 Discussion

The establishment of SKBR3 trastuzumab resistant cell lines produced age-matched control cell lines, two acquired resistant cell lines (RT1 and RT2) and two *de novo* resistant cell lines (RV1 and RV2). The time taken to establish the resistant cell lines was 7 months, which was within the time range used in other studies to establish trastuzumab resistance (273, 274). Natha and Esteva developed trastuzumab resistant cell lines by continuously exposing SKBR3 parental cell lines to trastuzumab (4 μg/mL and 8 μg/mL) for 3 months (273), while Vazquez-Martin and colleagues developed them by exposing SKBR3 cells to increased concentration of trastuzumab for a minimum of 10 months (274). Their protocol consisted of 4 weekly treatments of trastuzumab 20 μg/mL for 3 months, followed by two treatments weekly of 185 μg/mL for 2 months, then resistant cell lines were continuously cultured with trastuzumab 200 μg/mL for 5 months (274). However, in both studies, age-matched control cell lines were not produced during the development and the SKBR3 parental cell lines were used as control. Continuous culture of cell lines for a long period of time may change the phenotype of the cell lines (284, 285). An example could be the two *de novo* resistant cell lines derived from the age-matched control cell lines that were developed during this thesis project. In recent studies where lapatin-resistant cell lines were established, age-matched control cell lines were also developed (286, 287). However, so far no studies using age-matched control cell lines have shown development of *de novo* resistant cell lines.

The level of HER2 receptor was evaluated at both the mRNA and protein levels to confirm that trastuzumab resistance was not simply due to a loss of HER2 expression. It has been shown that the HER2 receptor may undergo a proteolytical cleavage of the extracellular domain and/or form alternative splice variants lacking the transmembrane and cytoplasmic domain (288). This produces a truncated HER2 receptor of about 95 kDa, which confers resistance to trastuzumab (288). A truncated HER2 receptor was not detected in any of the cell lines produced in this chapter.

EGFR and IGF1R were also assessed in the produced cell lines, as it has been reported that they may also be involved in trastuzumab resistance, since EGFR and IGF1R proteins were found to be overexpressed in patients treated with trastuzumab (265). However, neither of these receptors showed an altered expression in the resistant cell lines compared to the age-matched control cells and EGF treatment did not produce a change in global cytosolic calcium in all of the cell lines tested, suggesting that EGFR may not play a role in trastuzumab resistance in this model.

Assessing mRNA levels in the cell lines produced identified that the $Ca_V3.2$ channel had a higher expression in three out of four resistant cell lines compared to the age-matched controls. The $Ca_V3.2$ channel has been studied previously in prostate cancer and it was shown that up-regulation of this channel may be involved in the progression towards an androgen independent prostate cancer (289).

In cancer cells, resistance to conventional treatment can often be due to a presence of residual cancer stem cells that cannot be targeted by the drug and these cells can then reproduce the tumor, which is often resistant to therapy (290). During cell development there is a switch between $Ca_V3.2$ and $Ca_V3.1$ channel expression in cardiomyocytes (291, 292). In embryonic stem cells, $Ca_V3.2$ channel expression is higher than $Ca_V3.1$, once the embryonic cells mature to a differentiated state, this ratio is switched with higher levels of $Ca_V3.1$ compared to $Ca_V3.2$ (291). Further work assessing $Ca_V3.2$ channel in resistant cell lines are described in chapter 4, where the properties of $Ca_V3.2$ are discussed in detail.

Fourteen targets were also selected and silenced using siRNA to evaluate their potential effects on trastuzumab response in the acquired resistant cell line RT1 and the *de novo* resistance cell line RV1. The targets were chosen because they showed an altered mRNA expression (such as $Ca_V3.2$) or showed an enhancement of trastuzumab activity when silenced in SKBR3 parental cells (such as SPCA1, TRPM7 and STIM1) or because there was sufficient siRNA available in the laboratory at the time these experiments were conducted. While none of the selected targets reversed trastuzumab resistance in the RT1 cell line, assessing the same targets in the *de novo* resistant RV1 cell line showed that TRPM7, SPCA1, SPCA2, Orai1 and Orai2 silencing appeared to increase sensitivity to trastuzumab. TRPM7 and SPCA1 were particularly interesting as they also enhanced trastuzumab activity in the SKBR3 parental cell line. However, confirmation assays (3 independent experiments) showed that there was no significant differences in the trastuzumab response when these targets were silenced compared to the age-matched control cell lines. Thus, the transient silencing of these targets do not reverse trastuzumab resistance in the *de novo* resistant cell line RV1 and this highlights the importance of validation assays of siRNA screens in resistance studies.

Despite TRPM7 silencing did not re-establish sensitivity to trastuzumab in the *de novo* resistant cell line RV1, TRPM7 promoted trastuzumab response in parental SKBR3 cells (section 2.4.4). Thus, it may be an interesting target as it has also been linked to epithelial–mesenchymal transition (EMT)

in breast cancer cells (221). For these reasons, further experiments were carried out to evaluate the role of TRPM7 on trastuzumab resistance and these are presented in chapter 5.

Calcium signaling was assessed in each of the cell lines established. The response to ATP produced an EC_{50} of 3.4 μM and 2.9 μM for SV1 and SV2, respectively, and an EC_{50} of 2.5 μM and 2.9 μM for RV1 and RV2, respectively. The EC_{50} for the two acquired resistant cell lines was 0.9 μM (RT1) and 1.6 μM (RT2). The response to ATP for the SKBR3 parental cell lines was 0.51 μM (showed in section 2.3.2), about 6-7 fold lower EC_{50} than the age-matched control cells. This suggests a remodeling of calcium handling due to long-term culturing and emphasizes the importance of using age-matched control cell lines. The differences in EC_{50} between the age-matched control cells and the resistant cell lines were only significant for the acquired resistant cell lines, which showed a 2-3.5 fold lower ATP EC_{50} response compared to the age-matched control cell lines. The acquired resistant cell lines also had a prolonged recovery rate after stimulation with ATP compared with age-matched controls. Since the *de novo* resistant cell lines did not show differences compared to the age-matched control cell lines in Ca^{2+} handling upon ATP stimulation, this suggests that the mechanism of resistance may differ between the acquired and the *de novo* cells.

Prolonged plateau after ATP stimulation has also been observed in taxol-resistant cell lines, which had lower ryanodine and IP_3 receptor sensitive Ca^{2+} stores than sensitive cell lines (293). The delayed recovery after ATP stimulation may be due to an altered activity and/or expression of purinergic receptors or a slower reuptake of intracellular Ca^{2+} by the ER due to altered expression or activity of SERCA pumps, ryanodine receptor or IP_3 receptors. Moreover, another reason could be a decreased efflux of Ca^{2+} through PMCA pumps or Ca^{2+} exchangers. IP_3 receptors and PMCA pumps did not show altered mRNA expression in the resistant cell lines produced in the current study. It has been reported that in taxol-resistant adenocarcinomas cell lines the calcium profile of IP_3 receptors, which showed similar expression in taxol-resistant and taxol-sensitive cell lines, was still significantly different in response to IP_3 receptor agonists (293). Thus, further experiments investigating the expression, activity and role of purinergic, ryanodine and IP_3 receptors are needed to assess the mechanism of delayed recovery in these resistant cell lines.

Another reason for the delayed recovery after ATP stimulation in the acquired resistant cell line could be due to altered SOCE. This was also evaluated and although the acquired resistant cell line RT1 showed a higher CPA and calcium addition response, the ratio between the two peaks did not

appear to be changed. This suggests that SOCE is not altered in the resistant cell lines compared to age-matched control cell lines. SOCE has not previously been assessed in trastuzumab resistance. However, in other type of cancers, such as androgen independent prostate cancer PCa cells, apoptosis resistance is associated with decreased Orai1 expression and SOCE (161). Moreover, in the glutamate-mediated cell death resistant HT-22 cell lines SOCE is significantly reduced (294).

In summary, the profiling of the age-matched control and trastuzumab resistant cell lines have underlined the importance of having an age-matched control group since the cells may undergo signal remodeling independent of the mechanism of resistance. Additionally, the ATP response appeared to be altered in the acquired resistant cell lines RT1 and RT2, but not in the *de novo* resistant cell lines RV1 and RV2. Finally, from the assessment of the mRNA expression of 45 targets, $Ca_V3.2$ channel showed a higher expression in three out of four resistant cell lines and appears to be an interesting target to further evaluate in the context of trastuzumab resistance.

4 The role of $Ca_V3.2$ channel in trastuzumab resistance in trastuzumab resistant SKBR3R cells

4.1 Introduction

The $Ca_V3.2$ channel is a T-type voltage-gated calcium channel (295). T-type channels are activated by low voltage and they mediate the influx of calcium into cells. T-type voltage-gated calcium channels are formed by an α1 subunit, that consists of four repeats each of six transmembrane domains; these repeats form the pore of the channel, which is highly conserved (295). Other auxiliary subunits associate with the α1 subunit, such as the β subunit (296). Three isoforms of T-type channels are known, and they differ due to their α1 subunit ($Ca_V3.1$, $Ca_V3.2$ and $Ca_V3.3$) encoded by *CACNA1G*, *CACNA1H* and *CACNA1I*, respectively (297).

T-type channels are found in neurons, heart, kidneys, smooth and skeletal muscles, endocrine tissues and sperm, but compared to L-type channels they are more limited in their tissue distribution (297). $Ca_V3.2$ channel is manly found in the kidney and liver, but is also expressed in the heart, brain, pancreas, placenta, testis, lung, skeletal muscle and adrenal cortex (297). $Ca_V3.2$ channels are also involved in smooth muscle contraction, proliferation of some cell types and aldosterone and cortisol secretion from adrenal zona fasciculate cells (295, 298).

Mutations of this channel are involved in childhood absence epilepsy (299). The $Ca_V3.2$ channel is also implicated in painful diabetic neuropathy where aberrant up-regulation of the channel activity was reported in response to glucose elevation (300). Moreover, inhibition of post-translational modification (glycosylation) of $Ca_V3.2$ channel or channel activity reverse mechanical and thermal hyperalgesia in diabetic animals *in vivo* (301, 302).

In cancer, $Ca_V3.2$ channels are expressed in T-cell Jurkat cell line, neuroblastoma (303, 304), glioma (304), retinoblastoma cell lines (305), but not in the HL-60 leukemia cell line. Indeed, HL-60 cells are insensitive to $Ca_V3.2$ channel inhibitors (306). $Ca_V3.2$ channels are also expressed in the prostate cancer cell lines PC3, DU-145 (306) and LNCaP (303). In the latter cell line, $Ca_V3.2$ channel mRNA increases with neuroendocrine-mediated differentiation, which is associated with a more aggressive tumor and invasiveness (303). $Ca_V3.2$ channels are also expressed in the basal breast cancer cell lines MDA-MB-435, MDA-MB-231 (306) but not in the basal BT-20 cell line (307). $Ca_V3.2$ is also expressed in luminal MCF-7 and T-47D breast cancer cell lines (307) and in

the luminal HER2-positive breast cancer cell line MDA-MB-361 (306). However, no expression of $Ca_V3.2$ channels was reported by Asaga et al, in SKBR3 cells, the HER2-positive cell line used in my study (307). A splice variant (δ25B) of $Ca_V3.2$ channel has been reported to be a function channel able to facilitate Ca^{2+} entry (306). In some breast cancer cell lines (SK-N-SH, MDA-MB-231 and MDA-MB-361) only one splice variant form (δ25B) of $Ca_V3.2$ channel was reported to be expressed, while in other cell lines both, the $Ca_V3.2$ isoform and splice variant, were expressed (PC3 and MDA-MB-435) (306).

Despite a study showing that $Ca_V3.1$, but not $Ca_V3.2$ channels are involved in the regulation of cellular proliferation and apoptosis in MCF-7 breast cancer cells (308), an *in vivo* study performed on athymic nude mice injected with MCF-7 breast cancer cells showed a reduction of cell proliferation with $Ca_V3.2$ channel inhibition (309). $Ca_V3.2$ channel expression has also been reported to be elevated in malignant mesothelioma (a rare and highly aggressive tumor) patient samples compared to normal mesothelium (310).

Basal-like and HER2-positive breast cancers are known to have poorer prognosis than other molecular subtypes (121, 311). HER2-positive breast cancer subtypes are usually enriched with the luminal gene cluster (312). However, it appears that when the HER2 receptor is amplified in basal breast cancers this results in a novel breast cancer sub-entity that exhibits *de novo* trastuzumab resistance (313, 314). Indeed, the HER2-positive JIMT-1 cell line, derived from a patient who did not respond to trastuzumab, expresses basal and mesenchymal markers such as SLUG, TWIST1, ZEB1 and vimentin (312, 313). Thus, it appears that the heterogeneity of HER2-positive breast tumor produces variability in clinical outcome. For this reason, Staaf and colleagues (315), developed the HER2-derived prognostic predictor (HDPP), a 158 genes signature, which includes genes involved in tumor invasion and metastasis such as *CXCR4*, *PLAU*, *CX3CR1*, *TGFBR3*, and *STAT5A*. The HDPP signature is a prognostic factor in HER2-positive and also in basal subtype and is an effective predictor of patient outcome (315).

T-type Ca^{2+} channels are known to increase motility and invasion in HT1080 fibrosarcoma cells (316). Moreover, as described earlier, the $Ca_V3.2$ channel is found to have an increased expression during neuroendocrine differentiation in prostate cancer and induces progression towards the more aggressive androgen-independent stage (289). Thus, it could be speculated that the $Ca_V3.2$ channel levels may be a useful diagnostic tool to predict a more aggressive and metastatic HER2-positive tumor that is unresponsive to trastuzumab.

As presented in chapter 3, $Ca_V3.2$ channel showed a significantly higher expression in the two *de novo* resistant cell lines RV1 and RV2 compared to the age-matched control cell lines SV1 and SV2. Hence in this chapter the following hypotheses and aims were addressed.

4.2 Chapter Hypotheses

Alterations of $Ca_V3.2$ are a characterizing feature of some breast cancer cells lines and breast cancer subtypes and is an early event in the development of trastuzumab resistance.

4.2.1 Aims

a. To assess $Ca_V3.2$ mRNA levels in basal-like and luminal breast cancer cell lines and clinical breast cancer subtypes.
b. To characterize the temporal changes in $Ca_V3.2$ mRNA associated with the acquisition of trastuzumab resistance in SKBR3 cells.
c. To assess the ability of siRNA-mediated silencing of $Ca_V3.2$ channels, to reverse trastuzumab resistance in trastuzumab resistant SKBR3 cells.
d. To assess the ability of pharmacological inhibitors of $Ca_V3.2$ channels, to reverse trastuzumab resistance in trastuzumab resistant SKBR3 cells.

4.3 Methods

4.3.1 Materials

Trastuzumab was purchased from Roche Products, aliquoted and dissolved in sterile water to obtain a 10 mg/mL stock solution. The solution was stored at 4°C and was used within 1 month of preparation. Mibefradil (Sigma Aldrich) was dissolved in water to obtain a 100 mM stock solution, which was aliquoted and maintained at -20 °C prior to use. ML218 (Sigma Aldrich) was dissolved in DMSO to obtain a stock solution of 10 mM and aliquoted and maintained at 4°C.

4.3.2 Cell Culture

The HER2-positive human breast cancer cell line SKBR3, the age-matched control and resistant SKBR3 cell lines were cultured in McCoy's A5 media (Invitrogen) supplemented with 10% FBS and 5% Penicillin-Streptomycin mixture (Invitrogen) as recommended by ATCC (210). Media used to culture the acquired resistant cell lines was supplemented with trastuzumab (10 μg/mL). Cells were maintained at 37°C in a humidified atmosphere containing 95% O_2 and 5% CO_2, and passaged twice a week. A detailed passaging protocol is described in section 2.3.1.

SKBR3 cells and the established cell lines were periodically tested for mycoplasma using MycoAlert™ Mycoplasma Detection Kit (Lonza) and were genotyped to authenticate the cell line using the STR Promega StemElite™ ID Profiling Kit. The STR protocol is described in section 2.3.1.

4.3.3 MTS assay

Viable cell numbers were approximated using a CellTiter 96® AQueous Non-Radioactive Cell Proliferation Assay kit (Promega). MTS assays were used to evaluate the anti-proliferative activity of trastuzumab in parental SKBR3 cells, control and resistant cell lines. The protocol for MTS assays in SKBR3 cells is described in section 2.3.5 of this thesis.

4.3.4 Quantitative RT-PCR

RNA was isolated using the protocol described in section 2.3.2. RNA was reverse transcribed as described in section 2.3.2. Protocol details for quantitative RT-PCR are described in section 2.3.2.

In this chapter, a plate study was performed using StepOne Plus v2.3 software (Applied Biosystems) (317) to compare mRNA levels of $Ca_V3.2$ channels in a panel of different breast cancer cell lines and normal breast cancer cells, with those of the SKBR3 cell lines developed in chapter 3.

4.3.5 siRNA-mediated silencing

Small interfering RNA (siRNA) technology was used to silence $Ca_V3.2$ channels in this chapter. The siRNA used in these studies was ON-TARGET*plus* siRNA (SMARTpool, Dharmacon). A detailed protocol of siRNA treatment is described in section 2.3.3.

4.3.6 Gene expression profile in human breast tumors

Microarray is used to evaluate the expression of a large number of genes simultaneously (318). It hybridizes a target DNA strand to a large set of oligonucleotide probes attached to a solid support, which can be detected by fluorescence since the target sample and the reference sample are labeled with Cy3 or Cy5 probes, respectively (318). Data from a single experiment is viewed as a normalized ratio (Cy3/Cy5), where deviation from 1 is indicative of increased or decreased levels of gene expression in relation to the reference sample (318).

Analysis of the microarray profiles of 547 human breast tumors from an Agilent mRNA expression microarray platform (319) is freely available online. Tumors were grouped by molecular subtypes (103 basal-like, 58 HER2-amplified, 241 luminal A and 145 luminal B) and analyzed for $Ca_V3.2$ channel expression using Partek Genomics Suite (Partek Inc.).

4.4 Results

4.4.1 Assessment of $Ca_V3.2$ channel mRNA expression in different breast cancer cell lines

The mRNA of $Ca_V3.2$ channel was found to be up-regulated in two *de novo* resistant cell lines compared to the age-matched control cell lines as described in section 3.4.3.1. Further experiments were performed to evaluate the mRNA expression in a panel of breast cancer cell lines including HER2-positive and HER2-negative cell lines, basal and luminal cell lines and four cell lines derived from non-cancer breast tissue. These results were compared, using a plate study (317), to the $Ca_V3.2$ channel mRNA levels in the six cell lines produced in chapter 3.

$Ca_V3.2$ channels were not present in any of the non-cancer derived breast cell lines, however $Ca_V3.2$ mRNA levels were high in MCF-7 and T-47D which are two luminal estrogen receptor and/or progesterone receptor positive and HER2-negative breast cancer cell lines (Fig. 4.1). While $Ca_V3.2$ mRNA levels were lower in the ZR-75-1 cell line (estrogen receptor positive and HER2-negative) and in the SKBR3 cell line (Fig. 4.1) compared to the luminal cell lines. Among the three basal cell lines tested, only HCC1569, a HER2-positive breast cancer cell line had detectable levels of $Ca_V3.2$ mRNA (Fig. 4.1).

Comparing these results with the mRNA expression observed for the cell lines produced in chapter 3, it can be noted that the two age-matched control cell lines have similar $Ca_V3.2$ mRNA levels to SKBR3 cells, while RT1, RV1 and RV2 showed similar $Ca_V3.2$ levels to the basal-like HCC1569 cell line (Fig. 4.1), which is known to have an intrinsic resistance to trastuzumab (156).

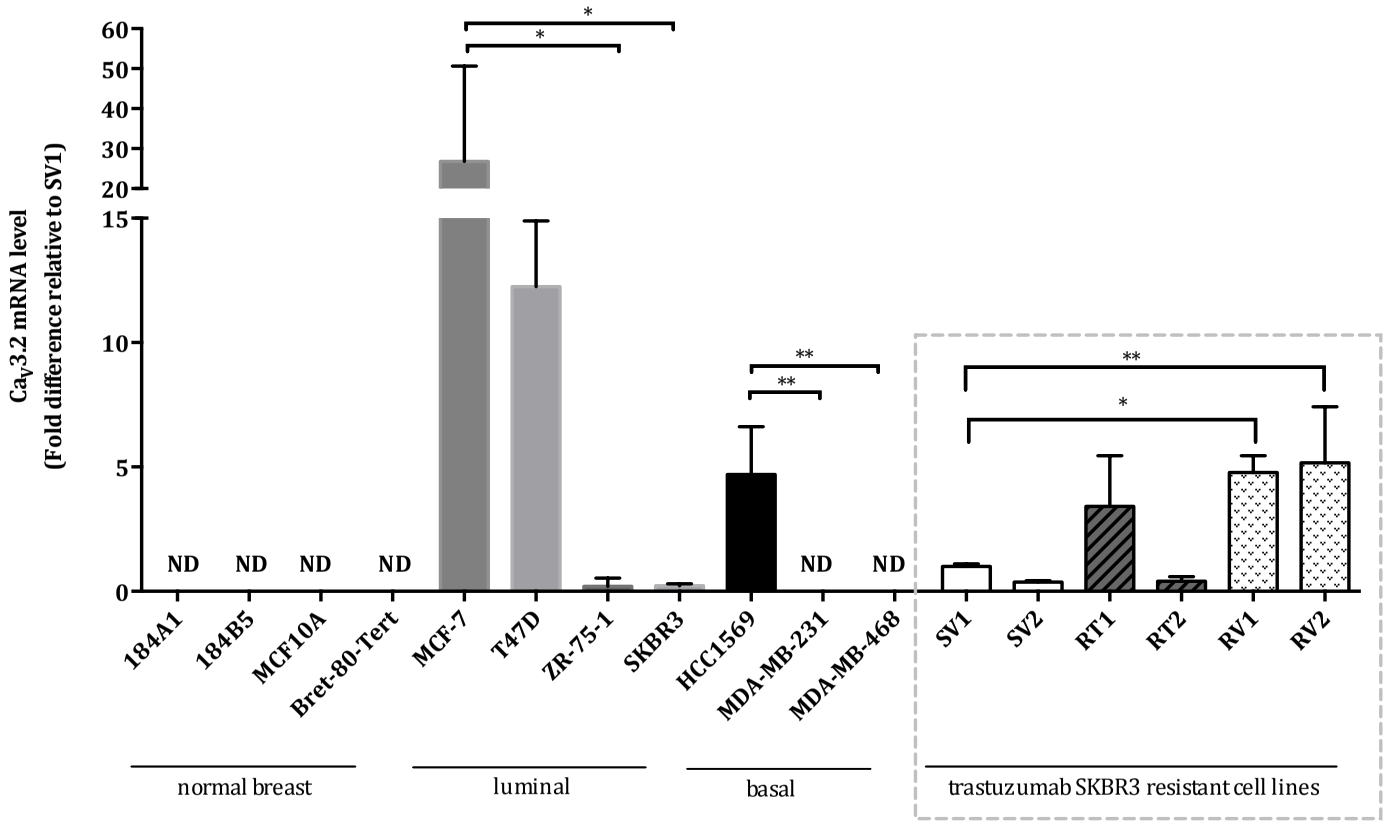

Figure 4.1 The mRNA level of $Ca_V3.2$ channel in different breast cancer cell lines and normal breast cell lines

$Ca_V3.2$ channel was not detected (ND) in normal breast cell lines and also in the basal breast cancer cell lines MDA-MD-231 and MDA-MB-468. The luminal breast cancer cell lines MCF-7 and T-47D showed the highest expression of $Ca_V3.2$ channel. The results were normalized to the SV1 cell line. Statistical analysis was performed for each subtype: for the luminal subtype results were compared to MCF-7, for the basal subtype results were compared to HCC1569 and for the resistant cell lines were compared to SV1 cells. Statistical analysis was performed using one-way ANOVA with Bonferroni post-tests (* $p \leq 0.05$, ** $p \leq 0.01$, *** $p \leq 0.001$).

$Ca_V3.2$ channel mRNA was also evaluated during the development of the age-matched control and resistant cell lines (Fig. 4.2). During the 7 months of development of these cell lines, RNA was isolated regularly to evaluate changes in mRNA expression of targets during the acquisition of trastuzumab resistance as described in section 3.4.1.

Five time points of 1, 3, 4, 6 and 6+ months after the start of the protocol were selected to evaluate $Ca_V3.2$ channel mRNA levels, for the last time point cells were assessed after defrosting from liquid nitrogen. From figure 4.2 it can be observed that $Ca_V3.2$ channel mRNA levels were increased by 3-5 fold in RV1, RV2 and RT1 cells compared to the SV1 cell line after 6 months and that this elevation was maintained in RT1 and RV1 (2-7 fold) compared to the age-matched control SV1 cell line even after defrosting from liquid nitrogen (Fig. 4.2).

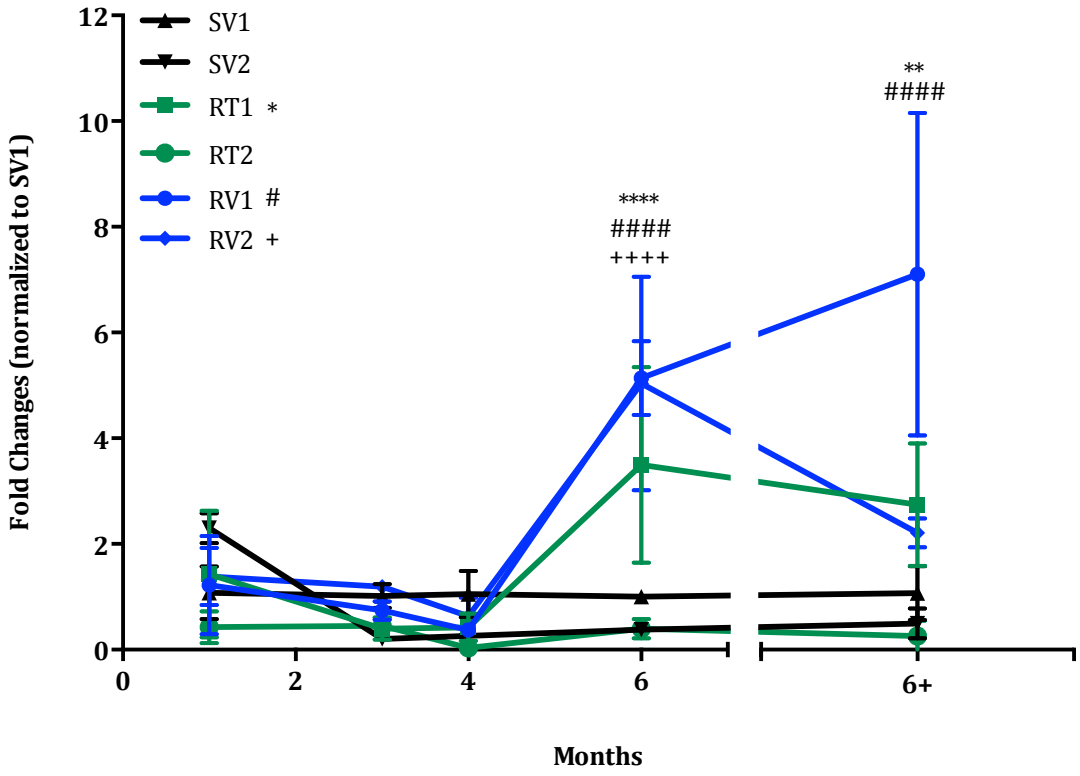

Figure 4.2 $Ca_V3.2$ channel mRNA levels during the development of the age-matched control and resistant cell lines

The mRNA expression of $Ca_V3.2$ channel was 3-5 fold higher than SV1 in three out of four resistant cell lines (RT1, RV1 and RV2) after 6 months from the beginning of the protocol and this elevation (3-7 fold) was maintained compared to the age-matched control SV1 cell line after defrosting from liquid nitrogen (6+ months) for RT1 and RV1. Statistical analysis was performed using two-way ANOVA with Bonferroni post-tests, the * indicates statistical significance between SV1 and RT1, # between SV1 and RV1, and + between SV1 and RV2 (** $p \leq 0.01$, **** or #### or ++++ $p \leq 0.001$).

4.4.2 Assessment of $Ca_V3.2$ channel in a gene expression database of human breast cancer tumors

$Ca_V3.2$ channel expression was also evaluated in a database of human breast tumors. Since mRNA assessment of $Ca_V3.2$ in the panel of different breast cancer cell line suggested a correlation between luminal and basal HER2-positive breast cancer cells, this was assessed in clinical samples (section 4.4.1).

This assessment was kindly performed with A/Prof. Paraic Kenny at the Albert Einstein College of Medicine, Bronx NY (USA). The mRNA expression of $Ca_V3.2$ channel was evaluated among different breast cancer subtypes (Fig. 4.3). In accordance with the mRNA level assessment of $Ca_V3.2$ in a panel of breast cell lines (section 4.4.1) the luminal breast cancer subtype showed a higher expression of this channel while the basal-like subtype tumors showed the lowest expression (Fig. 4.3). HER2-positive breast cancer tumors presented an intermediate expression between the luminal and the basal (Fig. 4.3).

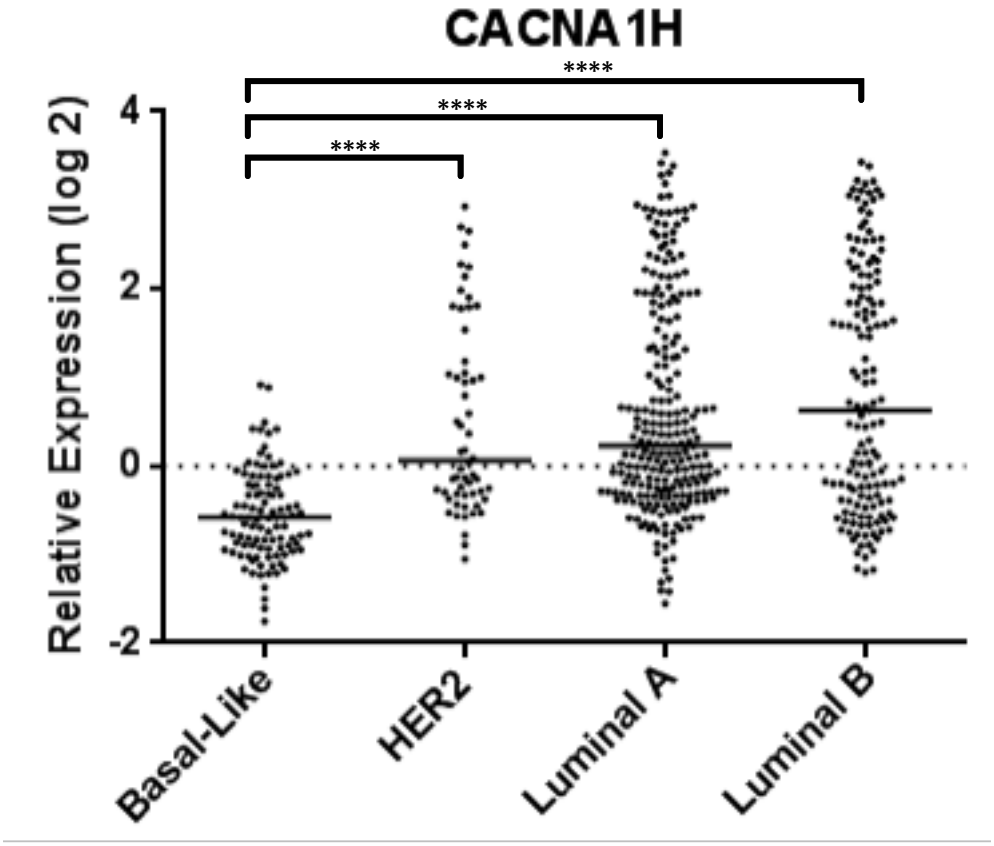

Figure 4.3 Assessment of the expression of $Ca_V3.2$ channels in a gene expression database of human breast tumors

The graph shows the relative expression of $Ca_V3.2$ channel (*CACNA1H*) in different molecular subtypes of human breast tumors. 103 basal-like, 58 HER2-amplified, 241 Luminal A and 145 Luminal B cases were included in the analysis (319). $Ca_V3.2$ channel had a higher level in the luminal subtypes and lower levels in the basal-like subtype. This analysis was kindly performed by A/Prof. Paraic Kenny from the Albert Einstein College of Medicine, Bronx NY (USA). Statistical analysis was assessed by comparing medians using the Kruskall-Wallis test followed by Dunn's Multiple Comparison Test (*** $p \leq 0.001$).

Basal HER2-positive breast cancer cell lines are known to be resistant to trastuzumab and thus they show an intrinsic resistance to this therapeutic agent (156). Indeed, basal markers are associated with resistance to trastuzumab (313). The basal HER2-positive breast cancer cell line HCC1569 had a significantly higher expression of $Ca_V3.2$ channels compared to the luminal SKBR3 cell line and this also correlates with the expression of this channel in the two *de novo* resistant cell lines RV1 and RV2 as described in section 4.4.1. Thus, I evaluated if the elevated expression of $Ca_V3.2$ correlates with HER2 status in basal tumors. Among the 103 clinical samples that belonged to the basal subtype, two tumors showed very high expression levels of both the HER2 receptor and $Ca_V3.2$ channels (Fig. 4.4). The R-squared value for this analysis was 0.047, thus only a weak correlation is shared between the expressions of HER2 and $Ca_V3.2$ channel. Unfortunately, the clinical treatment (e.g. trastuzumab therapy) and outcomes of these patients are not available, so trastuzumab resistance could not be assessed.

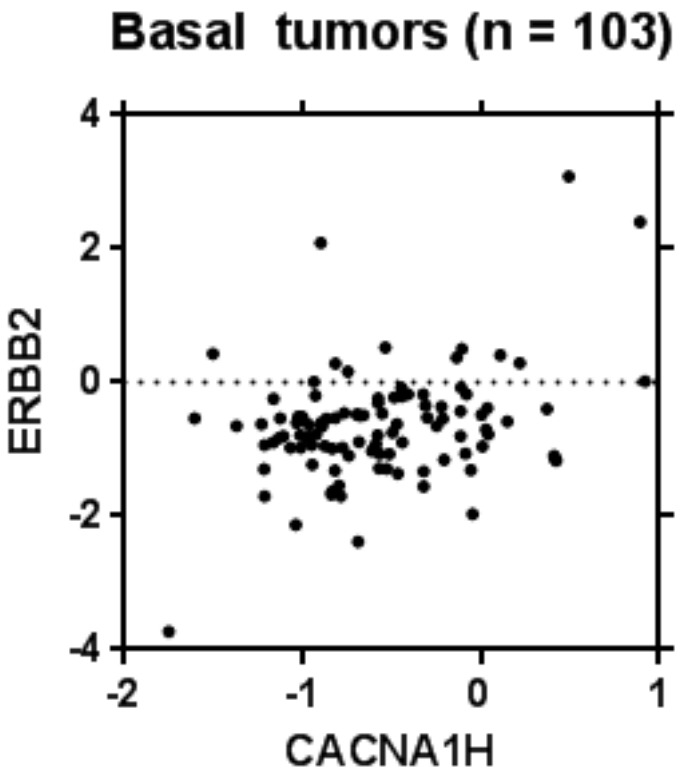

Figure 4.4 Assessment of the correlation of HER2 status with the $Ca_V3.2$ channel expression in basal tumors

The graph shows the correlation between $Ca_V3.2$ channel (*CACNA1H*) expression and HER2 status in the human basal breast tumors. This analysis was kindly performed with A/Prof. Paraic Kenny from the Albert Einstein College of Medicine, Bronx NY (USA). The R-squared for these results was 0.047.

4.4.3 Assessment of the consequences of $Ca_V3.2$ silencing on trastuzumab resistance in SKBR3 resistant cell lines

The $Ca_V3.2$ channel was part of the assessment of silencing of selected targets in RT1 and RV1 cell lines presented in sections 3.4.2.1 and 3.4.3.1. However, since elevated mRNA levels of $Ca_V3.2$ were a feature of the *de novo* resistant cell lines (RV1 and RV2), further experiments were performed to evaluate the effect of $Ca_V3.2$ channel silencing in all of the six cell lines produced. The efficacy of the siRNA to silence $Ca_V3.2$ channel was first assessed in RV1 cell line, mRNA levels were reduced of approximately 46% at the time that the MTS assay was performed (Fig. 4.5).

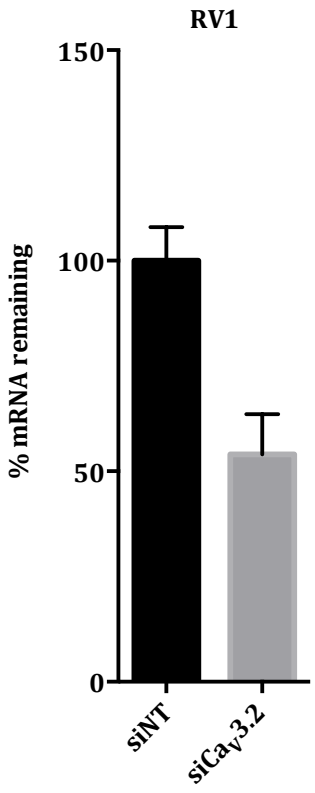

Figure 4.5 Assessment of $Ca_V3.2$ channel silencing efficacy

$Ca_V3.2$ mRNA remaining 192 h after silencing. The silencing of $Ca_V3.2$ channel was assessed in the RV1 cell line. At this time point, when the cell viability was assessed $Ca_V3.2$ channel was silenced by about 46% in RV1 cell line (3 wells ± S.D.).

As described in section 3.3.8.1, silencing of the $Ca_V3.2$ channel was defined as reversing trastuzumab resistance if it was able to produce a trastuzumab response higher than 25% (a dash line was drawn at 75% on the Y axis). From three independent experiments using an MTS assay, it was observed that the silencing of $Ca_V3.2$ in the age-matched control cell lines did not produce an enhancement of the trastuzumab response (Fig. 4.6), while for the resistant cell lines, the silencing of $Ca_V3.2$ channel did not reverse trastuzumab resistance (Fig. 4.6).

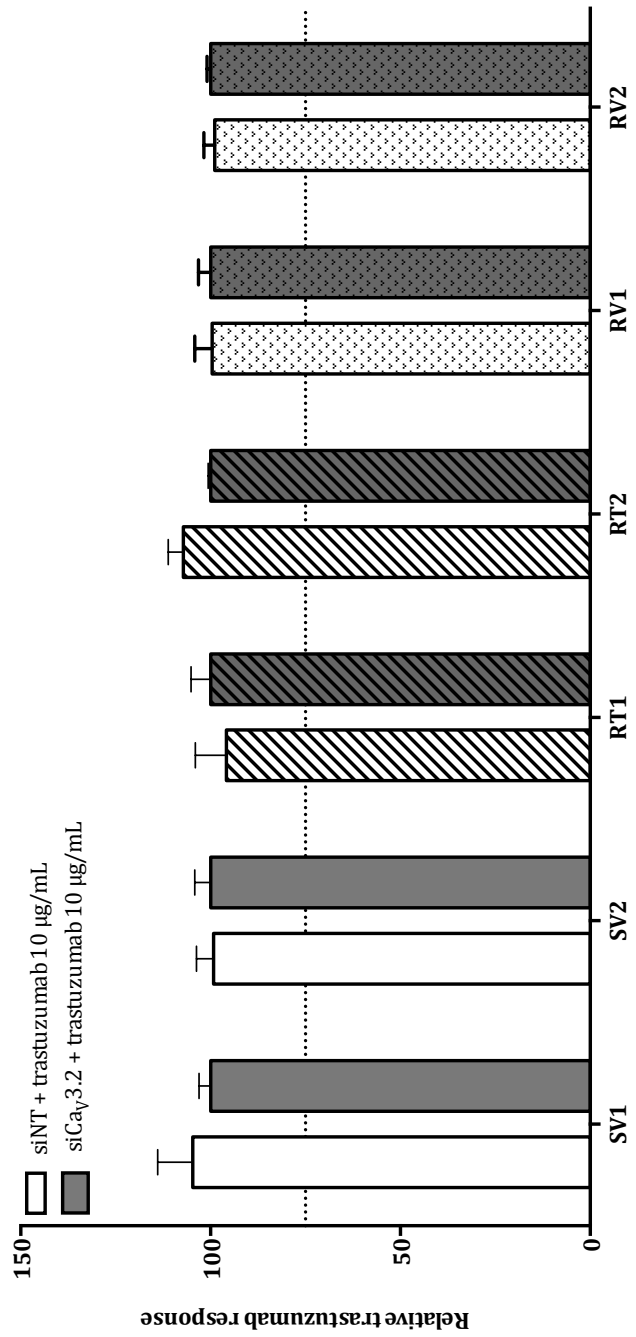

Figure 4.6 Assessment of trastuzumab response with $Ca_V3.2$ channel silencing in the age-matched control and resistant cell lines

Silencing of $Ca_V3.2$ channel in the age-matched control and resistant cell lines did not increase sensitivity to trastuzumab measured using MTS assay (10 µg/mL, 216 h post cell seeding) (n=3, ± S.D.) Statistical analysis was performed using two-way ANOVA with Bonferroni post-tests ($p > 0.05$).

4.4.4 Assessment of the effects of the $Ca_V3.2$ pharmacological inhibitors mibefradil and ML218 on trastuzumab resistance in RV1 resistant cell line

The lack of effect of $Ca_V3.2$ silencing on trastuzumab resistance could have been due to incomplete silencing of $Ca_V3.2$ with the long protocol. Therefore a pharmacological approach was carried out to evaluate the effect of $Ca_V3.2$ channel inhibitors on resistance to trastuzumab. These studies were conducted in the RV1 cell line since the cells has high levels of $Ca_V3.2$ channel.

Mibefradil was clinically used for the treatment of hypertension before being withdrawn from the market due to metabolic drug interactions (320). Mibefradil inhibits both T-type and L-type voltage-gated Ca^{2+} channels, but is more selective for the T-type subtype (321). It is known to inhibit the proliferation of various cell types that express T-type Ca^{2+} channels (322). Mibefradil was used in combination with trastuzumab (10 μg/mL) at three different concentrations (0.01 μM, 0.1 μM and 1 μM) on the *de novo* resistant cell line RV1 (Fig. 4.7). These concentrations were chosen based on concentrations used to inhibit T-type channels in several cancer cell lines including MCF-7 cells (321, 323). After seeding (24 h), cells were treated with mibefradil alone or in combination with trastuzumab and the treatment was repeated every two days. After 216 h an MTS assay was performed to evaluate cell viability. As described for siRNA treatment in section 4.4.3, similarly, pharmacological inhibition of $Ca_V3.2$ channel was considered as reversing trastuzumab resistance if it was able to produce a trastuzumab response higher than 25% (a dash line was drawn at 75% on the Y axis). Mibefradil alone did not have any effect on the proliferation of RV1 cell lines and in combination with trastuzumab, the inhibitor did not re-establish trastuzumab sensitivity at any of the concentrations assessed (Fig. 4.7).

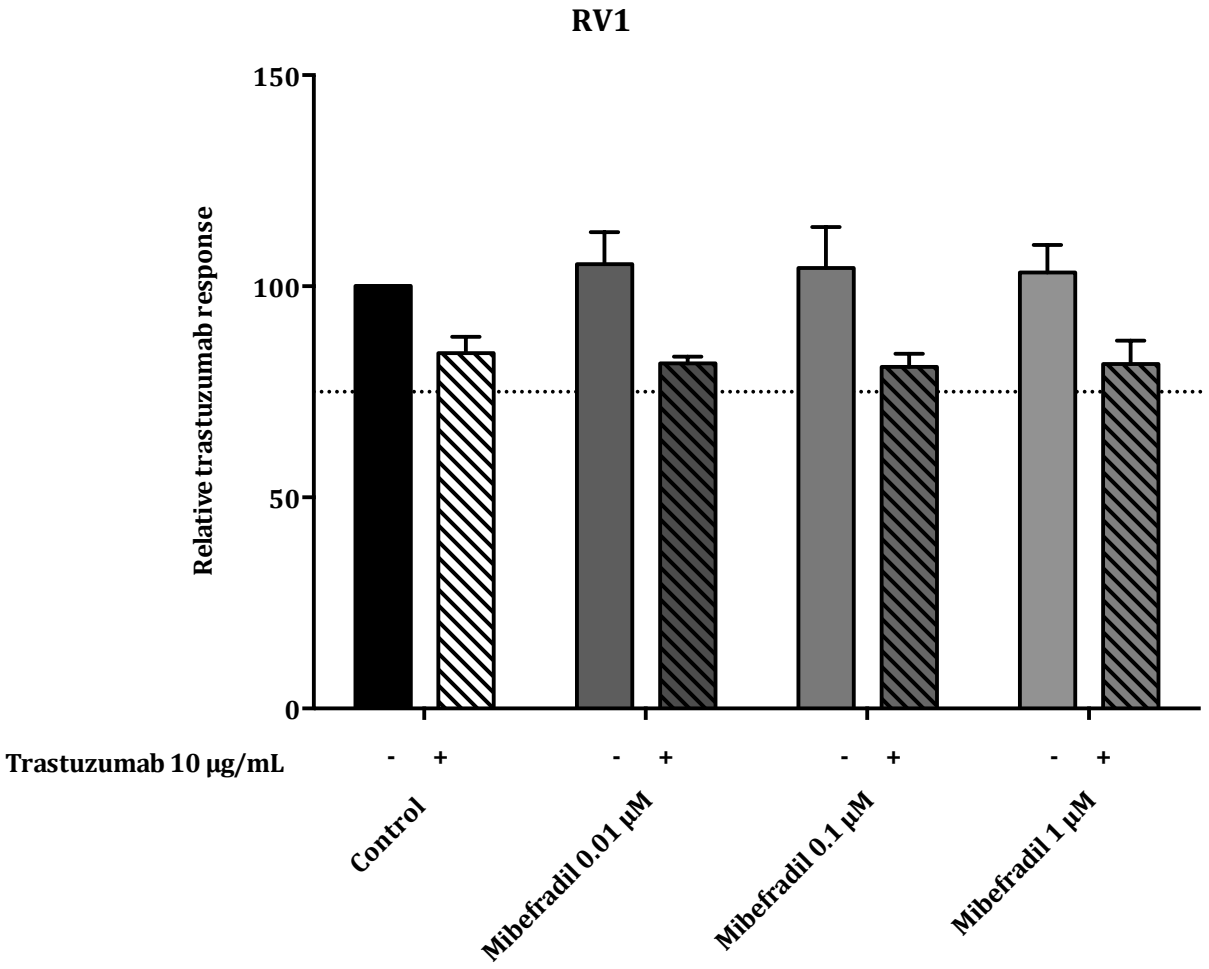

Figure 4.7 Effect of mibefradil on trastuzumab sensitivity in the RV1 *de novo* resistant cell line

An MTS assay after 216 h after seeding was performed on the RV1 cell line using mibefradil at three different concentrations (0.01 µM, 0.1 µM and 1 µM) alone and in combination with trastuzumab (10 µg/mL) to evaluate the pharmacological inhibition of $Ca_V3.2$ channel on the proliferation of RV1 and the effect on trastuzumab response. After seeding (24 h), cells were treated with mibefradil alone or in combination with trastuzumab and the treatment was repeated every two days (n=3, ± S.D.). Water was used as control. Statistical analysis was performed using two-way ANOVA with Bonferroni post-tests, Mibefradil alone was compared to vehicle, while the combination of mibefradil and trastuzumab was compared to trastzumab alone ($p > 0.05$).

ML218 appears to be more selective for $Ca_V3.2$ compared to the other T-type Ca^{2+} channels (324), but as yet has not been widely used (324, 325). ML218 was also used to evaluate the effect of pharmacological inhibition of $Ca_V3.2$ channel on trastuzumab responses.

Three different concentrations of ML218 were used (100 nM, 1 μM and 10 μM) alone and in combination with trastuzumab (10 μg/mL) (Fig. 4.8). These concentrations were chosen based on studies carried out in HEK293 cells (324). After seeding (24 h), cells were treated with ML218 alone or in combination with trastuzumab and the treatment was repeated every two days. After 216 h an MTS assay was performed to approximate viable cell number. As observed for mibefradil, ML218 alone did not have any effect on RV1 proliferation or responses to trastuzumab (Fig. 4.8).

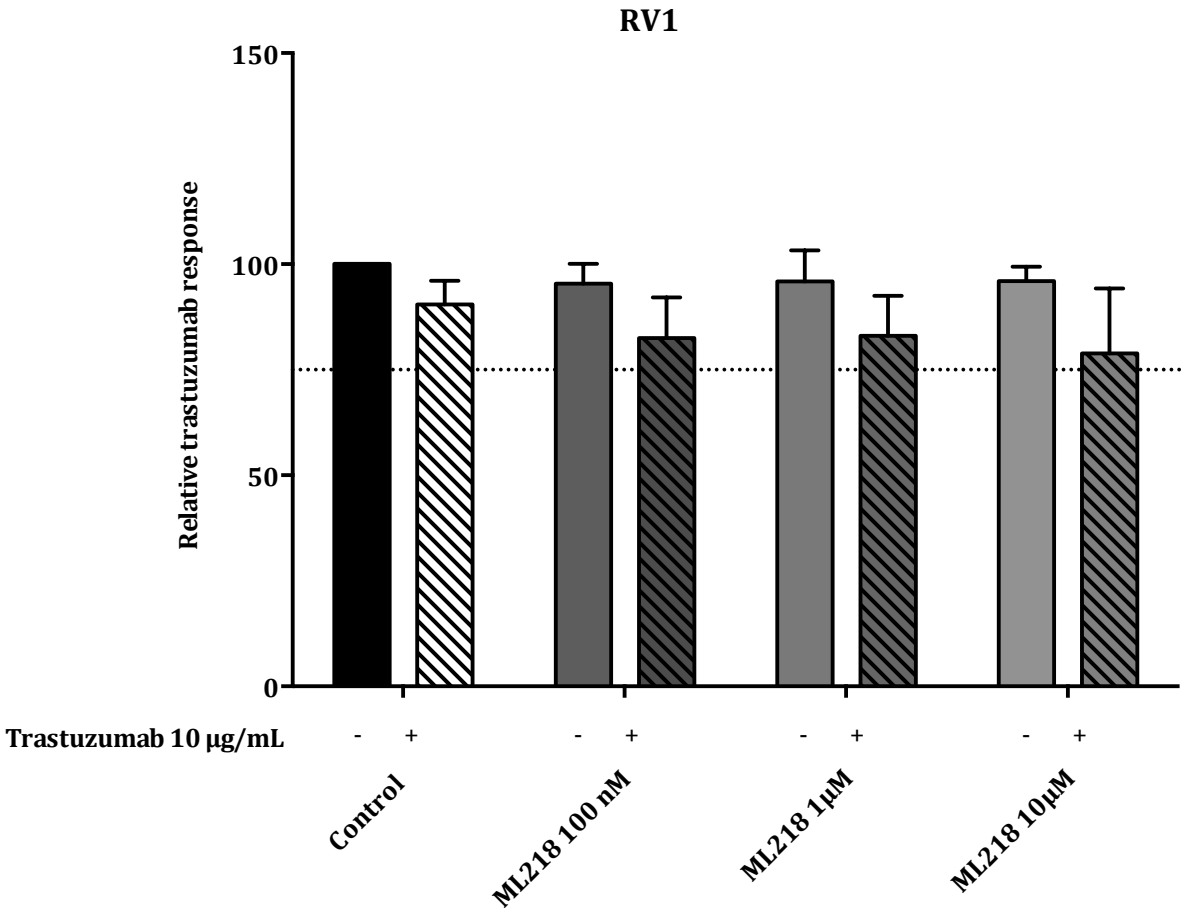

Figure 4.8 Effect of ML218 on the proliferation of RV1 *de novo* resistant cell line

MTS assay 216 h after seeding performed on RV1 cell line using ML218 at three different concentrations (100 nM, 1 µM and 10 µM) alone and in combination with trastuzumab (10 µg/mL) to evaluate the pharmacological inhibition of $Ca_V3.2$ channel on the proliferation of RV1 and the effect on trastuzumab resistance 24 h after seeding, cells were treated with ML218 alone or in combination with trastuzumab and the treatment was repeated every two days (n=3, ± S.D.). DMSO was used as control. Statistical analysis was performed using two-way ANOVA with Bonferroni post-tests, ML218 alone was compared to vehicle, while the combination of ML218 and trastuzumab was compared to trastzumab alone ($p > 0.05$).

4.5 Discussion

In this chapter the role of $Ca_V3.2$ channel in trastuzumab resistance was further evaluated. The expression of $Ca_V3.2$ channel was assessed in a panel of breast cell lines in order to evaluate any possible correlations between $Ca_V3.2$ expression and breast cancer characteristics. From this investigation, it was observed that the $Ca_V3.2$ channel was not expressed in cell lines derived from non-cancer breast tissue, while it was highly expressed in two luminal breast cancer cell lines (MCF-7 and T-47D). The luminal ZR-75-1 cell line and the HER2-positive SKBR3 cell lines showed a lower level of $Ca_V3.2$ mRNA. Among the basal subtypes, only the HER2-positive HCC1569 cell line had detectable levels of $Ca_V3.2$ mRNA. These levels were 4 fold higher than the luminal SKBR3 cell line. These results are consistent with a restriction landmark genomic scanning (RLGS) study that assessed the expression of $Ca_V3.2$ in breast cancer cell lines, where MCF-7 was reported to have high levels of $Ca_V3.2$ and the basal cell line MDA-MD-231 had little or no $Ca_V3.2$ (307).

The expression of $Ca_V3.2$ channel was also evaluated in a gene expression database of human breast tumors. The results from this analysis also correlate with the expression seen in the breast cancer cell lines. The luminal molecular subtype showed the highest levels of this channel while the basal subtype the lowest.

Interestingly, the only basal breast cancer cell line that had detectable levels of $Ca_V3.2$ mRNA was the HER2-positive HCC1569 cell line. HCC1569 cells are known to express HER2 and be resistant to trastuzumab, as appears to be the case for most HER2-positive breast cancer cell lines of the basal molecular subtype (156). Indeed, intrinsic resistance to trastuzumab is associated with the expression of basal markers such as cytokeratines 5 and 6 (313). The JIMT-1 cell line that was established from a patient that was resistant to trastuzumab from the beginning of the therapy also has several features of the basal subtype (149). Thus, it could be speculated that $Ca_V3.2$ channels up-regulation is a feature of HER2-positive breast cancers with basal characteristics. The correlation of $Ca_V3.2$ channel and HER2 receptor expression in the basal breast tumor subtype showed that only two samples out of the 103 basal tumors presented a high expression of both targets. The R-squared for this experiment was 0.047, thus only a weak correlation is shared between the expression of HER2 and $Ca_V3.2$ channel. One of the reasons of this low percentage could be due to a low number of HER2-positive tumors within the 103 basal samples tested.

$Ca_V3.2$ mRNA was also evaluated during the development of the trastuzumab resistant cell lines. It was observed that $Ca_V3.2$ mRNA levels were elevated in three out of the four resistant cell lines (RT1, RV1 and RV2) compared to the two age-matched control cell lines 6 months after the beginning of the protocol, and this elevation was maintained for RT1 and RV1 after defrosting from liquid nitrogen. Since resistance to trastuzumab developed at 7 months, it appears that increased $Ca_V3.2$ mRNA was associated with the development of trastuzumab resistance but was not an event that clearly preceded resistance.

$Ca_V3.2$ channel silencing was assessed as part of an siRNA screen in chapter 3. Further experiments were conducted in all the cell lines produced in this chapter. Firstly, siRNA efficacy in silencing $Ca_V3.2$ channel in the resistant cell line, RV1 was confirmed. At 196 h from the siRNA treatment (the same time point used to evaluate cell viability using MTS assay) $Ca_V3.2$ channel was silenced by 46%. However, from three independent experiments performed for each cell lines, $Ca_V3.2$ silencing did not re-establish trastuzumab sensitivity.

The cells that were treated with $Ca_V3.2$ siRNA still retained 54% of $Ca_V3.2$ mRNA and this incomplete silencing could have prevented the re-establishment of trastuzumab sensitivity. Thus, a pharmacological approach tested two T-type Ca^{2+} channel inhibitors, mibefradil and ML218. However, neither of these were able to re-establish trastuzumab sensitivity, suggesting that these agents do not represent a clinical approach to reverse trastuzumab resistance.

Altered glycosylation is a characteristic of many cancers (326) and may play an important role in breast cancer (327). HER2 may increase N-acetylglucosaminyl transferase activity (328) and Fc functions can be modulated by altering glycosylation status and binding affinity to Fc receptors, resulting in changes in antibody-dependent cellular cytotoxicity, serum half-life, anti-inflammatory properties, and complement activation (329). It has been proposed that trastuzumab may have altered activity in trastuzumab resistant breast cancer due to altered glycosylation status of HER2 (327). In this context, it is interesting to note that the surface expression and activity of $Ca_V3.2$ channel is controlled by N-linked glycosylation, which is essential for the sorting of proteins and their trafficking to the plasma membrane (300). It could be that altered N-glycosylation may lead to reductions in $Ca_V3.2$ surface expression and activity in the resistant cell lines. Thus, although $Ca_V3.2$ mRNA is up-regulated, the channel may not be functional. De-glycosylation of $Ca_V3.2$ channel using neuraminidase can reverse peripheral diabetic neuropathic pain where $Ca_V3.2$ channel is known to play a role (301). Moreover, glucose levels (which are reported to be higher in

trastuzumab resistant cell lines) (330), can regulate the glycosylation of $Ca_V3.2$ channels (300). Future studies could assess the glycosylation state of $Ca_V3.2$ channels in trastuzumab resistant breast cancer cells.

$Ca_V3.2$ channel is considered a candidate oncogene in T-cell leukemia (331) and in prostate cancer (289). From the results shown in this chapter, $Ca_V3.2$ channels showed higher expression levels in basal HER2-positive HCC1659 breast cancer cell line and in the two *de novo* resistant cell lines RV1 and RV2. Thus, $Ca_V3.2$ channel could be used as diagnostic marker to predict responses to trastuzumab. However, more studies are needed to be carried out on HER2-positive breast tumor samples from trastuzumab treated patients with survival data, to evaluate if $Ca_V3.2$ channel expression may predict responsiveness to this therapeutic.

5 Assessment of TRPM7 in trastuzumab resistant HER2-positive SKBR3R cell lines

5.1 Introduction

Transient receptor potential cation channel melastatin 7 (TRPM7) is a Ca^{2+} channel present on the plasma membrane that mediates the influx of Ca^{2+} and Mg^{2+} (Fig. 5.1). The *TRPM7* gene is also known by other names, such as *CHAK1*, *TRP-PLIK*, and *LTRPC7* (332-334). The TRPM7 channel is an ion channel linked to an atypical α-kinase (Fig. 5.1) and it was discovered by screening databases for homologs of human eukaryotic elongation factor 2 kinase (eEF2K) (335). Only one other TRP channel is known to be linked to a kinase, the TRPM6 channel (336, 337). TRPM7 channel activity is regulated by free magnesium and Mg-nucleotide complexes such as Mg-ATP, which inhibits the TRPM7 channel (338).

The atypical α-kinase does not seem to be essential for channel activity (339, 340), although the kinase can auto-phosphorylate at Ser^{1511} and Ser^{1567}, mutation of these two amino acids does not alter channel activity as measured by Ca^{2+} influx (341). However, complete deletion of the kinase produces an apparently inactive TRPM7 channel, possibly due to altered processing and trafficking of TRPM7 to the plasma membrane (341).

There are only a few substrates that are known for the TRPM7 α-kinase. The phosphorylation of myosin IIA, IIB and IIC by the TRPM7 kinase has been linked to the regulation of cell motility and adhesion (342-344). Another substrate of the kinase is annexin A1, an important regulator of membrane fusion (345). The phosphorylation of annexin A1 by the TRPM7 kinase has been linked to the regulation of cell growth and apoptosis (345, 346). Moreover, TRPM7 kinase is able to phosphorylate another atypical α-kinase, eEF2K, which is then associated with the inhibition of eukaryotic elongation factor 2 (eEF2) activity (347). The TRPM7 kinase can also phosphorylate myelin basic protein and the histone H3 (341). These phosphorylation events are Mg-dependent (348). Manganese like magnesium, zinc, and cobalt, can also inhibit the kinase activity of TRPM7, while Ca^{2+} does not appear to play a role (348).

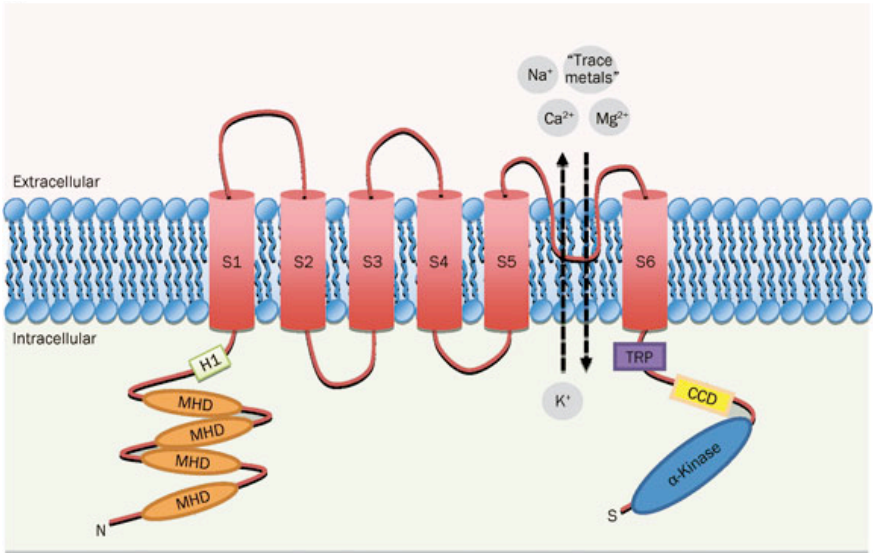

Figure 5.1 Structure of TRPM7 channel

The TRPM7 channel is an ion channel linked to an atypical α-kinase and it mediates the influx of both Ca^{2+} and Mg^{2+}. The few known substrates for this kinase are myosin IIA, IIB and IIC, annexin A1 and the eEF2K. (Taken from Bae CY and Sun H, 2011 (349))

TRPM7 channels are ubiquitously expressed, with TRPM7 expression reported in almost every tissue (340), and high expression in the heart, pituitary, bone, and adipose tissue (350). TRPM7 has been linked to a number of diseases or disease relevant processes including brain ischemia, cardiovascular disease and specific processes important in cancer progression (351). Inhibition of TRPM7 can produce cell cycle arrest in Jurkat T-cells (352), and apoptosis in differentiated mast cells (353) and hepatic stellate cells (354). In the rat, embryonic hepatocytes have a higher level of TRPM7 expression than adult hepatocytes, showing a possible involvement of TRPM7 in the differentiation process (355). As discussed above, TRPM7 can also regulate cell adhesion. Indeed, overexpression of this channel produces cell rounding and detachment of cells by m-calpain in a Ca^{2+} dependent manner (271, 332).

Global disruption of TRPM7 expression in mice at early embryonic stages is lethal (356), while deletion at later embryonic stages produces viable mice or mice with cardiomyopathy at intermediate embryonic stages (357). Ablation of TRPM7 in a mouse model of global ischemia protects neurons from cell death (358). TRPM7 may also be involved in hypertension, as hypertensive rats show lower levels of TRPM7 mRNA compared to control rats and angiotensin II stimulation increases TRPM7 mRNA in control rats, but not in those with hypertension (359).

Since TRPM7 is involved in cell proliferation, differentiation and migration, this protein has also been studied in cancer (360). TRPM7 is up-regulated in pancreatic adenocarcinomas (361) and primary breast cancer tissues compared to normal tissue (245). Due to increased metastasis formation in breast cancers with high levels of TRPM7, this channel is considered a predictor of poor prognosis (245, 362). Support for the involvement of TRPM7 in cancer progression is also suggested by the ability of TRPM7 silencing to inhibit proliferation of different cancers such as gastric adenocarcinoma (363) and head and neck carcinomas (364), and to reduce cell migration and invasiveness in cancers of the lung (365), nasopharynx (366), pancreas (361), and the MDA-MB-435 breast cell line (362). Moreover, in pancreatic ductal adenocarcinomas, patient survival is inversely correlated with TRPM7 expression (361). TRPM7 silencing also reduces the ability of MDA-MB-468 breast cancer cells to undergo EGF-induced EMT (221). Collectively, the aforementioned studies highlight the potential importance of TRPM7 in various aspects of cancer progression; however, its role in the development of resistance to trastuzumab has not yet been explored.

Recently, two pharmacological TRPM7 inhibitors have been identified; NS8593 (367) and waixenicin A (352). NS8593 is a gating modulator potentiated by Mg^{2+} that produces a reversible blockage of the channel (367), while waixenicin A is a compound isolated from Hawaiian Soft Coral *Sarcothelia edmondsoni* that exhibits cytosolic activity potentiated by Mg^{2+} binding to the kinase (352). Indeed, mutation of the Mg^{2+} binding site on the kinase domain of TRPM7 reduces the potency of waixenicin A, while deletion of the kinase domain enhances its efficacy independently of Mg^{2+} (352). Recently, a TRPM7 kinase inhibitor has been identified - NH125 (368). However, this compound is not selective for TRPM7, as it inhibits another atypical α-kinase - eEF2K (368).

In chapter 2, TRPM7 silencing was found to enhance trastuzumab response in SKBR3 cells (section 2.4.4). Despite TRPM7 mRNA levels remaining constant in the acquisition of trastuzumab resistance (sections 3.4.2.1 and 3.4.3.1), TRPM7 activity may still be a critical regulator of trastuzumab responses in trastuzumab resistant cells. This chapter therefore sort to evaluate the ability of TRPM7 inhibition to reverse trastuzumab resistance in SKBR3 cells using siRNA-mediated silencing and TRPM7 pharmacological inhibitors.

5.2 Chapter Hypothesis

Inhibition of TRPM7 will reverse trastuzumab resistance in breast cancer cells.

5.2.1 Aims

a. To assess TRPM7 mRNA levels in normal breast cells, basal-like and luminal breast cancer cell lines.
b. To assess the ability of siRNA-mediated silencing of TRPM7 channels to reverse trastuzumab resistance in trastuzumab resistant SKBR3 cells.
c. To assess the ability of pharmacological inhibitors of TRPM7 channels to reverse trastuzumab resistance in trastuzumab resistant SKBR3 cells.

5.3 Methods

5.3.1 Materials

Trastuzumab, purchased from Roche Products, was aliquoted and dissolved in sterile water to obtain a 10 mg/mL stock solution. The solution was stored at 4°C and was used within 1 month of preparation. The NS8593, purchased from Sigma Aldrich, was dissolved in DMSO to obtain a 30 mM stock solution, and aliquoted and maintained at 4°C. The NH125 was purchased from Tocris Bioscience, dissolved in DMSO to obtain a stock solution of 100 mM and maintained aliquoted at -20 °C.

5.3.2 Cell Culture

The HER2-positive human breast cancer cell line SKBR3, age-matched control and resistant SKBR3 cell lines were cultured in McCoy's A5 media (Invitrogen) supplemented with 10% FBS and 5% Penicillin-Streptomycin mixture (Invitrogen), as recommended by ATCC (210). Media used to culture acquired resistant cell lines was supplemented with trastuzumab (10 μg/mL). Cells were maintained at 37°C in a humidified atmosphere containing 95% O_2 and 5% CO_2, and passaged twice a week. A detailed passaging protocol is described in section 2.3.1.

SKBR3 cells and the established cell lines were periodically tested for mycoplasma using MycoAlert™ Mycoplasma Detection Kit (Lonza) and were genotyped to authenticate the cell line using the STR Promega StemElite™ ID Profiling Kit. The STR protocol is described in section 2.3.1.

5.3.3 MTS assay

Viable cell numbers were approximated using a CellTiter 96® AQueous Non-Radioactive Cell Proliferation Assay kit (Promega). MTS assays were used to evaluate the anti-proliferative activity of trastuzumab in the age-matched control and resistant cell lines. The protocol for MTS assays used for SKBR3 cells was also applied to age-matched and resistant cell lines and is described in section 2.3.5 of this thesis.

5.3.4 Quantitative RT-PCR

RNA was isolated using the protocol described in section 2.3.2. RNA was reverse transcribed as described in section 2.3.2. Protocol details for quantitative RT-PCR are described in section 2.3.2. In this chapter, a plate study was performed using StepOne Plus v2.3 software (Applied Biosystems) (317) to compare the mRNA levels of TRPM7 channels in different breast cancer cell lines and normal breast cancer cells with those of the SKBR3 cell lines developed in chapter 3.

5.3.5 siRNA-mediated silencing

Small interfering RNA (siRNA) technology was used to silence TRPM7 channels in this chapter. The siRNA used in these studies was ON-TARGET*plus* siRNA (SMARTpool, Dharmacon). A detailed protocol of siRNA treatment is described in section 2.3.3.

5.4 Results

5.4.1 Assessment of TRPM7 channel mRNA expression in different breast cancer cell lines

TRPM7 mRNA levels were not significantly different between the resistant cell lines compared to the age-matched control cell lines, as described in sections 3.4.2.1 and 3.4.3.1. However, to evaluate a possible correlation between different subtypes of breast cancer and non-malignant breast tissue, TRPM7 mRNA expression was assessed in a panel of breast cell lines including HER2-positive and HER2-negative cell lines, basal and luminal cell lines, and four cell lines derived from non-cancer breast tissue. These results were compared using a plate study (317) to allow comparison with the TRPM7 mRNA levels of the six cell lines produced in chapter 3.

TRPM7 mRNA was present in all the breast cancer cell lines tested (Fig. 5.2), and in contrast with the $Ca_V3.2$ channel mRNA expression shown in figure 4.1 of chapter 4, TRPM7 was also present in the non-cancer derived breast cell lines examined. TRPM7 mRNA did not show any expression trends (e.g. relation to estrogen receptor status, luminal or basal subtype) for any of the breast cancer subtypes, however its mRNA levels were higher in the MCF-7 cancer cell line (Fig. 5.2). Interestingly, TRPM7 mRNA was elevated in the resistant and the age-matched control cell lines compared to the SKBR3 parental cell line, and their levels of mRNA expression were similar to the TRPM7 expression seen in MCF-7 cells (Fig. 5.2). This suggests that continual passaging may have increased levels on TRPM7 mRNA levels in SKBR3 cells to levels equivalent to MCF-7 cells.

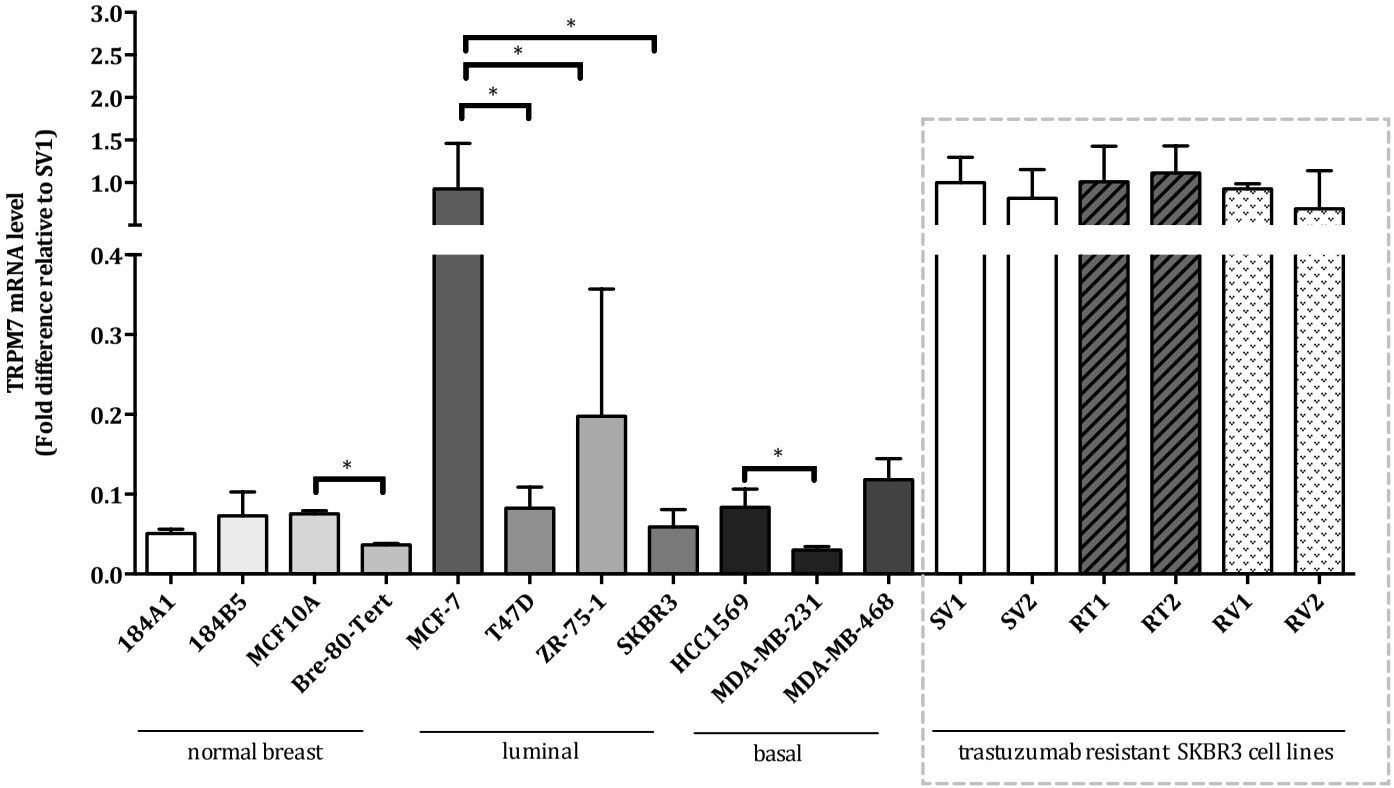

Figure 5.2 mRNA levels of TRPM7 in different breast cancer cell lines and normal breast cell lines

TRPM7 was detected in both normal breast and breast cancer cell lines. The luminal breast cancer cell line MCF-7 showed the highest expression of TRPM7. The results were normalized to the SV1 cell line. Statistical analysis was performed for each subtype: for normal breast cell lines, results were compared to MCF10A, for the luminal subtype, results were compared to MCF-7, for the basal subtype, results were compared to HCC1569, and for the resistant cell lines, results were compared to SV1 cells. Statistical analysis was performed using one-way ANOVA with Bonferroni post-tests (n=3, ± S.D.) (* $p \leq 0.05$).

5.4.2 Silencing TRPM7 does not reverse trastuzumab resistance in SKBR3R cell lines

TRPM7 was part of the assessment of silencing of selected targets in RT1 and RV1 cell lines presented in sections 3.4.2.1 and 3.4.3.1. However, TRPM7 is a prognostic marker and a predictor of poor prognosis in breast cancer (245, 360, 362), and I found in this project that silencing of TRPM7 enhanced trastuzumab activity in the SKBR3 parental cell line (section 2.4.4). Thus, further experiments were performed to evaluate the effect of TRPM7 silencing in all the six cell lines produced in this thesis. The efficacy of the siRNA to silence TRPM7 was assessed in the RV1 cell line. TRPM7 mRNA levels were reduced by approximately 56% under these transfection conditions at the equivalent time point used for MTS assays (Fig. 5.3).

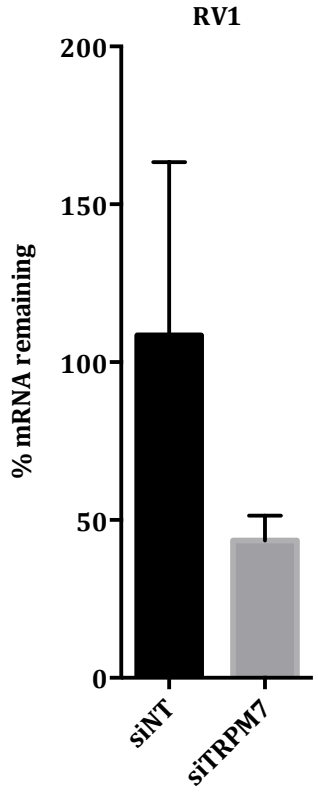

Figure 5.3 Assessment of the efficacy of TRPM7 silencing

TRPM7 mRNA remaining 192 h after silencing. The silencing efficacy of TRPM7 was assessed in the RV1 cell line. At this time point, when cell viability was assessed, TRPM7 was silenced by approximately 56% (3 wells ± S.D.).

As described earlier in section 3.3.8.1, silencing of the TRPM7 channel was defined as reversing trastuzumab resistance if it was able to produce a trastuzumab response higher than 25% (a dash line was drawn at 75% on the Y axis). From three independent experiments, it was observed that silencing of TRPM7 in the age-matched control cell lines did not enhance the trastuzumab response (Fig. 5.4), in resistant cell lines, the silencing of TRPM7 also did not reverse trastuzumab resistance (Fig. 5.4).

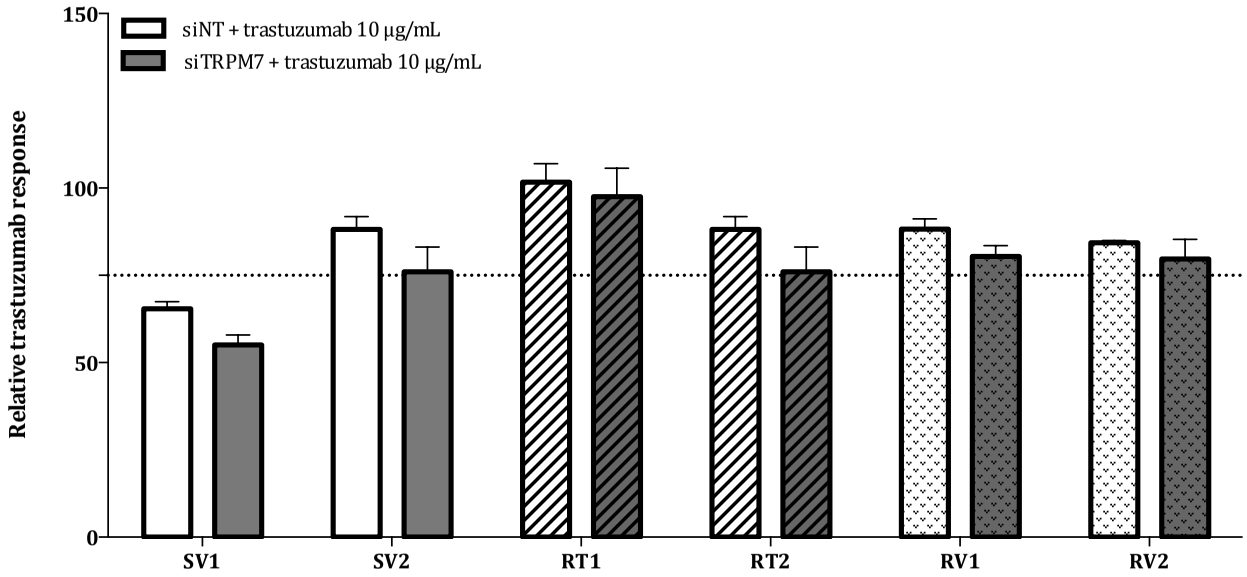

Figure 5.4 Assessment of trastuzumab response with TRPM7 silencing in the age-matched control and resistant cell lines

Silencing of TRPM7 in age-matched control and resistant cell lines did not increase sensitivity to trastuzumab using MTS assay (10 µg/mL, 216 h post cell seeding) (n=3, ± S.D.) Statistical analysis was performed using two-way ANOVA with Bonferroni post-tests ($p > 0.05$).

5.4.3 Pharmacological inhibitor

Similar to studies assessing the $Ca_V3.2$ Ca^{2+} channel (section 4.4.10), a pharmacological approach was taken to evaluate the effect of TRPM7 inhibition on resistance to trastuzumab. These studies were conducted in the RV1 cell line.

A recently discovered selective TRPM7 inhibitor NS8593 (367) is commercially available and was used in these studies. As described earlier, NS8593 is a gating modulator of the TRPM7 channel that is potentiated by Mg^{2+}, and it produces a reversible blockage of the channel (367). This compound is also known to inhibit Ca^{2+}-activated K^+ channels (369, 370). The earlier mentioned waixenicin A is another selective TRPM7 inhibitor (352) and it has a cytosolic activity potentiated by Mg^{2+} binding to the kinase (352). However, it appears that its binding site is not directly on the kinase, as deletion of the kinase domain does not suppress waixenicin A activity (352). Since waixenicin A is not currently commercially available, only NS8593 could be used to evaluate the effects of TRPM7 pharmacological inhibition on trastuzumab activity in these studies. NS8593 was used in combination with trastuzumab (10 μg/mL) at three different concentrations (100 nM, 1 μM and 10 μM) on the *de novo* resistant cell line RV1 (Fig. 5.5). These concentrations were chosen based on previous studies carried out in HEK293 cells (367) and MDA-MB-468 cells (221). After seeding (24 h), cells were treated with NS8593 alone or in combination with trastuzumab and the treatment was repeated every two days. After 216 h, an MTS assay was performed to evaluate cell viability. As described for siRNA treatment in section 5.4.2, pharmacological inhibition of TRPM7 channel was defined as reversing trastuzumab resistance if it was able to produce a trastuzumab response higher than 25% (a dash line was drawn at 75% on the Y axis). NS8593 alone did not have any effect on the proliferation of RV1 cell line, and in combination with trastuzumab, the inhibitor did not re-establish trastuzumab sensitivity at any of the concentrations assessed (Fig. 5.5).

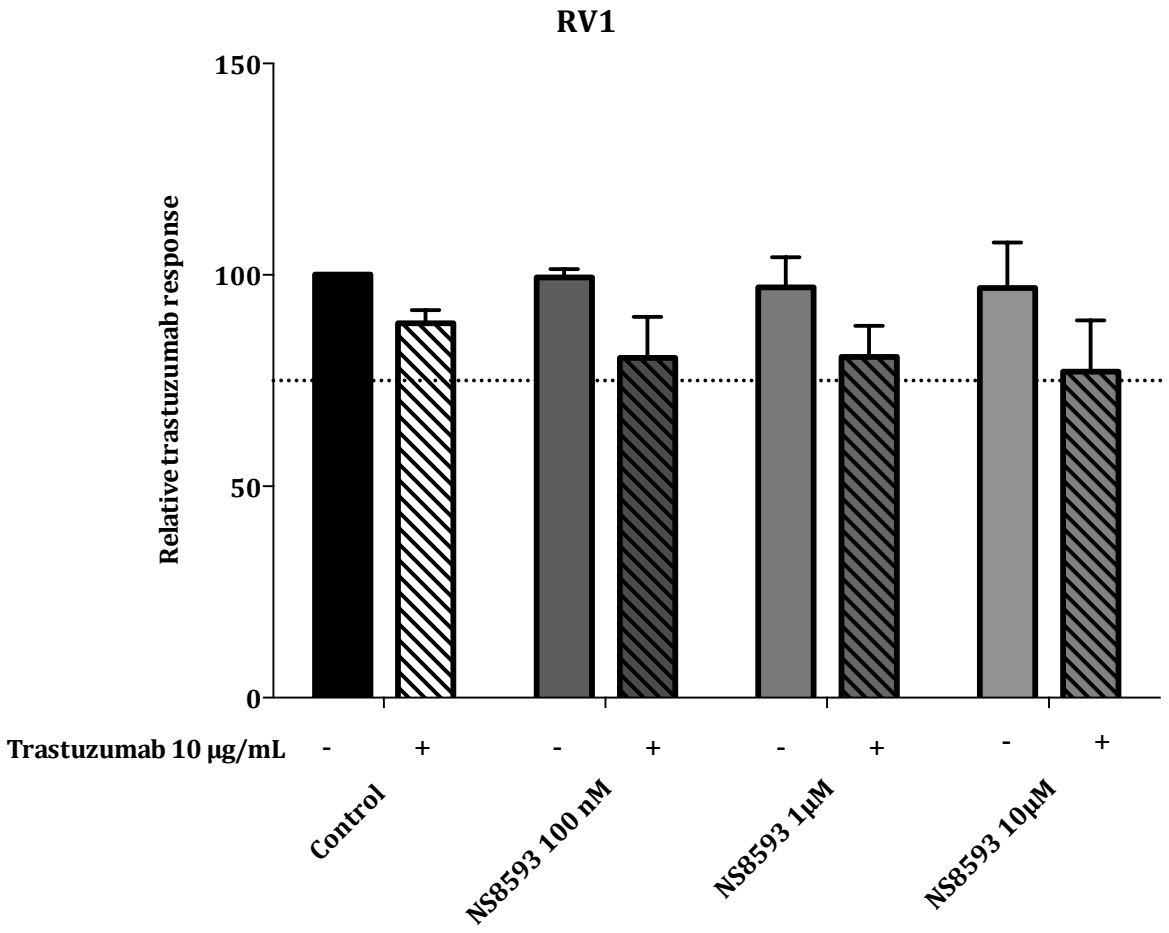

Figure 5.5 Effect of NS8593 on trastuzumab sensitivity in the RV1 *de novo* resistant cell line

An MTS assay 216 h after seeding was performed on the RV1 cell line using NS8593 at three different concentrations (100 nM, 1 µM and 10 µM) alone and in combination with trastuzumab (10 µg/mL) to evaluate pharmacological inhibition of TRPM7 channel on the proliferation of RV1 and the effect on the trastuzumab response. Cells were treated with NS8593 alone or in combination with trastuzumab (24 h after plating) and the treatment was repeated every two days (n=3, ± S.D.). DMSO was used as control. Statistical analysis was performed using two-way ANOVA with Bonferroni post-tests, NS8593 alone was compared to vehicle, while the combination of NS8593 and trastuzumab was compared to trastuzumab alone ($p > 0.05$).

Due to the dual activity of TRPM7 as a channel and kinase, and the inefficacy of the gating inhibitor NS8593, I evaluated if the kinase activity of TRPM7 could have a role in reversing trastuzumab resistance. Since a specific TRPM7 kinase inhibitor has not yet been developed, the most selective atypical α-kinase inhibitor commercially available was used - NH125. This compound inhibits eEF2K (371) with an IC_{50} of 18 μM in an *in vitro* kinase assay (368) and is able to inhibit the TRPM7 kinase with an IC_{50} of 55 μM. NH125 also inhibits ERK2 with an IC_{50} of 70 μM (368). NH125 decreases cell viability of several cancer cell lines with a reported IC_{50} of 1–5 μM, and an IC_{50} of 3.6 μM for MCF-7 breast cancer cells (372).

NH125 was used to evaluate the possible role of the TRPM7 atypical α-kinase in trastuzumab sensitivity in a resistant cell line. NH125 was used in combination with trastuzumab (10 μg/mL) at two different concentrations (10 μM and 30 μM) on the *de novo* resistant cell line RV1 (Fig. 5.6). These concentrations were chosen based on a previous kinase assay study (368). Similar to the NS8593 protocol, 24 h after seeding, cells were treated with NH125 alone or in combination with trastuzumab with treatments repeated every two days. After 216 h, an MTS assay was performed to evaluate cell viability. NH125 at 30 μM alone significantly decreased cell viability of RV1 cells, and this effect was greater when given in combination with trastuzumab, suggesting that some sensitivity to trastuzumab was restored (Fig. 5.6).

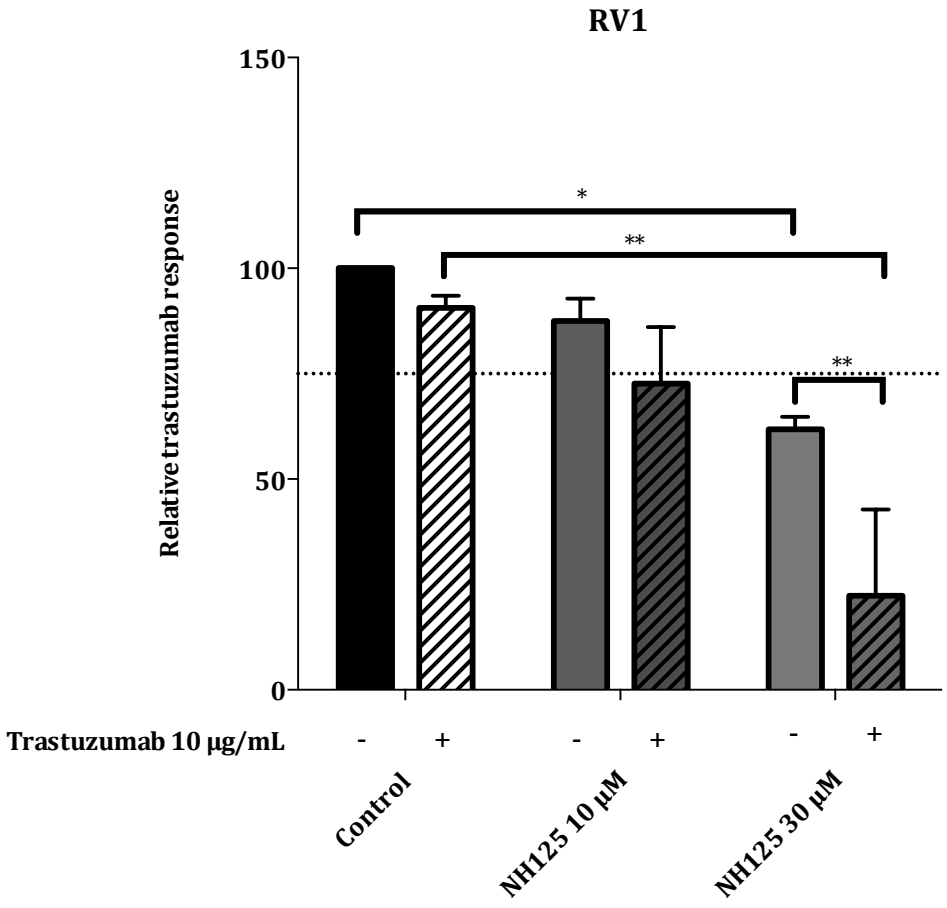

Figure 5.6 Effect of NH125 on the proliferation of the RV1 *de novo* resistant cell line

MTS assay performed 216 h after seeding on the RV1 cell line with NH125 at two different concentrations (10 µM and 30 µM) alone and in combination with trastuzumab (10 µg/mL) to evaluate the effect of pharmacological inhibition of TRPM7 kinase on the proliferation of RV1 and the effect on trastuzumab resistance. After plating (24 h), cells were treated with NH125 alone or in combination with trastuzumab and the treatment was repeated every two days (n=3, ± S.D.). DMSO was used as control. Statistical analysis was performed using two-way ANOVA with Bonferroni post-tests (* $p \leq 0.05$, ** $p \leq 0.01$).

5.5 Discussion

In this chapter the role of TRPM7 in trastuzumab resistance was further evaluated. As for the $Ca_V3.2$ channel studies in section 4.4.1, the expression of TRPM7 was evaluated in a panel of different breast cell lines in order to evaluate any possible correlations between TRPM7 expression and breast cancer characteristics. From this experiment it was shown that TRPM7 was expressed in all of the cell lines tested, including cell lines derived from non-cancer breast tissue. MCF-7 cells were associated with the highest levels of TRPM7 mRNA. In contrast to $Ca_V3.2$ mRNA levels (section 4.4.1), TRPM7 did not show any differences in mRNA levels between luminal (SKBR3) and basal (HCC1569) HER2-positive cell lines. Several studies of TRPM7 have been carried out in MCF-7 (245, 270, 373), MDA-MB-468 (221) and MDA-MB-435 breast cancer cell lines (362), however, only one study has compared the expression of TRPM7 in a panel of breast cancer cell lines. This current study compared TRPM7 mRNA levels in MCF-7, MDA-MB-231 and MDA-MB-435 cell lines. The data presented in this chapter showed a similar profile of mRNA levels in the cell lines evaluated (373), with higher TRPM7 levels in MCF-7 cells compared to MDA-MB-231 cells.

TRPM7 mRNA levels were increased in both age-matched control and resistant SKBR3 cell lines compared to the parental SKBR3 cell line. Thus, the continuous culture of the SKBR3 cell line produced an increase in TRPM7 mRNA, underlining the importance of age-matched control cell lines as appropriate controls for resistant cell line development. Indeed, as previously discussed in chapter 3, the continuous culture of cell lines for a long period may change many aspects of the phenotype of some cell lines (284, 285), the increase of TRPM7 mRNA in all the cell lines produced in this thesis may represent another example of such changes.

TRPM7 silencing was assessed as part of an siRNA screen described in chapter 3. Further experiments were conducted in all the cell lines produced in this chapter. Studies in this chapter confirmed the efficacy of siRNA-mediated silencing of TRPM7 in the resistant cell line, RV1. At 196 h from the siRNA treatment (the same time point used to evaluate cell viability), TRPM7 was silenced by 56%. However, this amount of TRPM7 silencing did not re-establish trastuzumab sensitivity.

Resistant and sensitive cell lines treated with TRPM7 siRNA likely still retained significant amounts of TRPM7 mRNA (~44% for RV1 cells). This incomplete silencing could have prevented the re-establishment of trastuzumab sensitivity. As described in section 2.4.4, in the SKBR3

parental cell line, where TRPM7 silencing produced an enhancement of the trastuzumab response, cells retained approximately 60% of TRPM7 mRNA expression at the equivalent time point used for the Click-iT® EdU proliferation assay. Thus, the larger amount of TRPM7 mRNA in the age-matched control and resistant cell lines compared to parental SKBR3 cells could have prevented the re-acquisition of trastuzumab sensitivity. Moreover, in the SKBR3 parental cell line, a different proliferation assay (Click-iT® EdU assay) was used to evaluate the effect of TRPM7 silencing on trastuzumab activity. Due to the large amount of experiments carried out in the 6 cell lines produced, a less expensive but less powerful assay, the MTS assay, was used, this could also be another reason for the lack of effect and should be addressed in future studies.

A pharmacological approach was also used in this chapter. Inhibition of TRPM7 gating with NS8593 did not decrease cell viability and it did not reverse trastuzumab resistance. This suggests that TRPM7 gating may not be involved in trastuzumab activity. This compound was previously used in another breast cancer cell line (MDA-MB-468), where inhibition of TRPM7 using NS8593 produced a decrease in EGF-induced vimentin expression (221). In SKBR3 resistant cell lines the inhibitor did not produce changes in cell viability, however, its role in EMT induction was not tested in this cell line.

The inhibitor of the TRPM7 atypical α-kinases, NH125, was also used to evaluate the possible involvement of TRPM7 kinase in trastuzumab resistance. NH125 at 30 μM alone significantly decreased cell viability in the RV1 cell line. This response was augmented when used in combination with trastuzumab. This suggests that the TRPM7 kinase may be involved in trastuzumab resistance. However, as previously stated, TRPM7 silencing was not able to replicate the effect observed with NH125. This could be due to an incomplete silencing of TRPM7 and the larger amount of mRNA present in this cell line, which may allow sufficient TRPM7 kinase activity to contribute to trastuzumab resistance. However, since NH125 is also able to inhibit eEF2K (371), the effect observed with this compound could also be due to its inhibition of eEF2K.

TRPM7 directly phosphorylates eEF2K and this kinase can phosphorylate eEF2 inhibiting its activity (347). Since eEF2 participates in protein synthesis (347), TRPM7 may indirectly regulate the elongation state of some proteins. Thus, even if the effect observed with NH125 was due solely to the inhibition of eEF2K activity, modulation of TRPM7 kinase, through its activity on eEF2K, could indirectly regulate eEF2 and represent a novel approach to reverse trastuzumab resistance. The atypical α-kinase eEF2K has also been shown to be involved in trastuzumab activity in MCF-7

and MDA-MB-468 cells, where the silencing of eEF2K in these cell lines enhanced the cytotoxicity effect of trastuzumab (374).

Recently, Chen and colleagues demonstrated that the ability of NH125 to inhibit the growth of PC3 prostate cancer cells via inhibition of eEF2 protein activity was not only due to the inhibition of eEF2K activity, but also via the inhibition of multiple pathways that included 5' AMP-activated protein kinase (AMPK) and protein phosphatase 2A (PP2A) (371). Chen and colleagues used nanomolar concentrations of NH125 based on an early study, which used different kinase assay conditions and showed that the IC_{50} of NH125 for eEF2K was 60 nM (372). However, a more recent study showed that NH125 inhibits TRPM7 and eEF2K in the micromolar range (368). Hence, the observations of Chen et al may be a consequence of NH125 preferentially inhibiting different kinases.

The role of eEF2K in trastuzumab resistance has not been previously evaluated, however, it has recently been assessed in a lapatinib resistant SKBR3 cell line (375). In this cell line, eEF2K had a higher expression and phosphorylation status and eEF2 was highly activated (dephosphorylated) (375). Since lapatinib induces the inhibition of eEF2 in SKBR3 parental cells, it was speculated that altered activity of eEF2K may have prevented the ability of lapatinib to induce the phosphorylation of eEF2 in lapatinib resistant cell lines (375). Indeed, the inhibition of eEF2K by NH125 in the SKBR3 parental cell line significantly decreased eEF2 phosphorylation. However, the combination of NH125 and lapatinib in SKBR3 parental cells did not reduce lapatinib sensitivity. It was therefore concluded that eEF2K is not a major mediator of lapatinib resistance (375). Since trastuzumab resistant cells maintain their sensitivity to lapatinib (154), the resistance mechanisms and the role of atypical α-kinases may be different between these two mechanisms of resistance.

Hence, the results presented in this chapter and the work of others suggests that atypical α-kinase eEF2K and/or the atypical α-kinase of TRPM7 may be involved in trastuzumab resistance in some HER2-positive breast cancer cell lines. However, further experiments are required to fully understand the relative roles of eEF2K and TRPM7 atypical α-kinases in potentially reversing trastuzumab resistance.

In order to further evaluate the role of TRPM7 kinase in trastuzumab resistance, a different TRPM7 inhibitor could be used, such as rottlerin, which was previously used to inhibit TRPM7 kinase (348). However, rottlerin inhibits several proteins such as different protein kinases C (376-378),

eEF2K (379), human ether-a-go-go hERG potassium channel (380) and Ca^{2+}-activated K^{+} channels (381). NH125 could also be used in association with TRPM7 and/or eEF2K silencing to further define the mechanism of the effect of NH125 in RV1 cells. The effect of NH125 should also be assessed in the other cell lines described in this thesis and other trastuzumab resistant cell lines.

6 Analysis of calcium-related protein expression from microarrays and clinical samples for the identification of possible therapeutic targets important in trastuzumab resistance

6.1 Introduction

The work described in chapters 3, 4 and 5 involved the assessment of a relatively small number of targets (9 calcium pumps, 31 calcium permeable channels and 2 calcium channel regulators) in the trastuzumab resistant SKBR3 cell lines developed during the current studies. $Ca_V3.2$ and TRPM7 mRNA expression was also assessed in a number of different cell lines developed from malignant and non-malignant breast tissue. $Ca_V3.2$ channel mRNA expression was also evaluated in a microarray data of primary human breast tumors (319) stratified by molecular subtypes (103 basal-like, 58 HER2-amplified, 241 Luminal A and 145 Luminal B).

The use of high-throughput large-scale gene expression microarray and proteomic analysis is now widely used in cancer research (382, 383). Microarray analysis has allowed the identification of breast cancer heterogeneity at the molecular level and can predict prognosis (118, 119). Microarray analysis can be also used with breast cancer tissues to predict response to chemotherapy (384, 385). Molecular signatures can also predict distant metastasis (386), invasiveness (387), survival (388) and chromosomal instability (389).

Stable isotope labeling by amino acids in cell culture (SILAC) assay is a powerful form of quantitative proteomic analysis. The technique uses a mass spectrometry method based on stable isotope quantitation (390, 391). In breast cancer, SILAC has been used to evaluate responses to chemotherapy in T47D (392) and MDA-MB-231 cells (393) and to evaluate new prognostic markers for estrogen receptor negative tumors (394). This assay has also been used to produce a proteomic profile of HER2-positive breast cancer cell line from the Her2 transgenic mouse model (395).

In this chapter, publically available cDNA microarray data and SILAC assay results from studies performed in SKBR3 cells and/or clinical samples have been used to identify proteins involved in calcium signaling that may be important in trastuzumab resistance.

6.2 Chapter Hypothesis

Alteration of specific calcium related proteins is a characteristic of trastuzumab resistance in HER2-positive trastuzumab sensitive breast cancer cell lines and in HER2-positive clinical breast cancers.

6.2.1 Aims

a. To assess changes in mRNA levels of calcium related proteins in SKBR3 sensitive and resistant cell lines using microarray data.
b. To assess changes in protein levels of calcium related proteins in SKBR3 sensitive and resistant cell line using SILAC data.
c. To assess changes in mRNA level of calcium related proteins in clinical breast cancers resistant to trastuzumab using microarray data.

6.3 Methods

6.3.1 Cell Culture

The HER2-positive human breast cancer cell line SKBR3, the age-matched control and resistant SKBR3 cell lines were cultured in McCoy's A5 media (Invitrogen) supplemented with 10% FBS and 5% Penicillin-Streptomycin mixture (Invitrogen) as recommended by ATCC (210). Media used to culture the acquired resistant cell lines was enriched with trastuzumab (10 μg/mL). Cells were maintained at 37°C in a humidified atmosphere containing 95% O_2 and 5% CO_2, and passaged twice a week. A detailed passaging protocol is described in section 2.3.1.

SKBR3 cells and the established cell lines were periodically tested for mycoplasma using MycoAlert™ Mycoplasma Detection Kit (Lonza) and were genotyped to authenticate the cell line using the STR Promega StemElite™ ID Profiling Kit. The STR protocol is described in section 2.3.1.

6.3.2 Quantitative RT-PCR

RNA was isolated using the protocol described in section 2.3.2. RNA was reverse transcribed as described in section 2.3.2. Protocol details for quantitative RT-PCR are described in section 2.3.2. In this chapter, a plate study was performed using StepOne Plus v2.3 software (Applied Biosystems) (317) to compare the mRNA levels in parental SKBR3 breast cancer cell lines with those of the SKBR3 cell lines developed in chapter 3.

6.3.3 Gene expression profile in human breast tumors

Microarray is used to evaluate the expression of a large number of genes simultaneously (318). It hybridizes between a target DNA strand with a large set of oligonucleotides probes attached to a solid support. Hybridization is detected by fluorescence since the target sample and the reference sample are labeled with different fluorescent probes (318). Data from a single experiment is viewed as a normalized ratio between the two probes, where deviation from 1 is indicative of increased or decreased levels of gene expression in relation to the reference sample (318). Microarray data from two different studies on a trastuzumab resistant SKBR3 cell line produced by exposing SKBR3 parental cells to trastuzumab (100 μg/mL) for 12 months (396) and clinical samples from patients that were resistant to trastuzumab (397) were analyzed to evaluate possible changes in the mRNA levels of Ca^{2+}-related proteins in trastuzumab resistance.

6.3.4 Stable isotope labeling by amino acids in cell culture (SILAC) analysis

SILAC is a high-throughput approach for quantitative proteomics that uses mass spectrometry (398). It allows the accurate quantification of proteins through metabolic encoding of whole cell proteomes using stable isotope labeled amino acids. For this analysis two cell populations are cultured under the same conditions except for the type of amino acid that is added to the culture, which can be light (for example natural ^{12}C arginine) or heavy (for example ^{13}C arginine) (398). These amino acids are incorporated into newly synthesized proteins usually after at least five cell divisions, each of these amino acids is then replaced by its isotope analog (398). The two types of samples are then combined, digested with trypsin and analyzed by mass spectrometry. The tryptic cleavage produces pairs of peptides that differ only by molecular weight, the heavy sample is detected via the mass shift since the two types of amino acids have the same chemical and physical properties (398). Since trypsin cleaves carboxy-terminal to lysine and arginine residues, double labeling of both amino acids is often used. The heavy/light (H/L) signal pairs are analyzed to quantify protein expression between the two samples.

In this chapter, publically available online SILAC data from Boyer and colleagues (399) were used to evaluate possible changes in protein expression of calcium related proteins in a trastuzumab resistant SKBR3 cell line produced by exposing parental SKBR3 cells to trastuzumab 100 μg/mL for 9 months (400).

6.4 Results and Discussion

6.4.1 Assessment of calcium signaling related proteins in a cDNA microarray of a trastuzumab resistant SKBR3 cell line

Valabrega and colleagues (396) produced cDNA microarray data, where the levels of a large number of genes in a trastuzumab resistant SKBR3 cell line, produced by exposing a SKBR3 parental cell line to trastuzumab 100 μg/mL for 12 months, were compared with the parental SKBR3 cell line (396). They identified 865 genes that were significantly altered, they selected 8 representative genes and confirmed their altered mRNA levels using quantitative RT-PCR; among these were signal transducer and activator of transcription 3 (STAT3), EGFR, HER2 and TNFα, which were all down-regulated, and growth factor receptor-bound protein 2 (GRB2), ATP-binding cassette sub-family C member 2 (ABCC2), dual specificity phosphatase 6 (DUSP6) and interleukin 1 receptor type I (IL1R1) which were all up-regulated (396). This microarray data set is freely available online (Accession n. GSE17630: http://www.ncbi.nlm.nih.gov/geo/query/acc.cgi?acc=GSE17630) and I analyzed it in order to evaluate the levels of calcium-related proteins, which may be altered in the Valabrega et al. (396) trastuzumab resistant SKBR3 cell line compared to the SKBR3 parental cell line. The full data set is represented in a volcano plot (Fig. 6.1). The gene list was classified using the gene ontology PANTHER (Protein Analysis Through Evolutionary Relationships, version 9.0), a Ca^{2+}-related protein list of 75 genes was evaluated (Table 6.1). Each Ca^{2+}-related protein is reported in the volcano plot graph in red (Fig. 6.1).

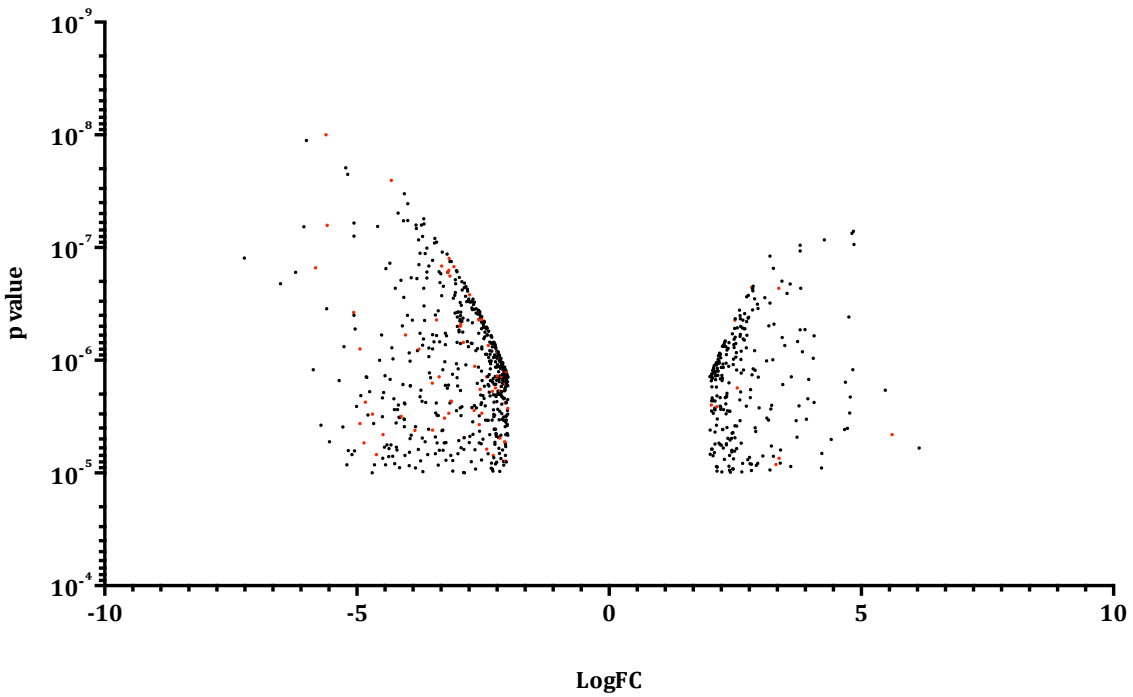

Figure 6.1 Global gene expression levels comparing the Valabrega et al. trastuzumab resistant SKBR3 cell line and the parental SKBR3 cell line

Volcano plot of 865 genes which are significantly ($p \leq 0.05$) alterated in the trastuzumab resistant SKBR3 cell line compared to the parental cell line with fold changes greater than 4 in the Valabrega et al. study (396). Data is graphed as logarithm fold change (LogFC) against p-value. Red dots represent the 75 calcium-related genes that were selected through the gene ontology program PHANTER.

From this analysis 65 calcium-related genes were down-regulated while 10 were up-regulated (Table 6.1). Among the 65 genes that showed a decrease in expression were several S100 calcium binding proteins (*S100A3*, *S100A4*, *S100A5*, *S100A7*, *S100A8*, *S100A9*, *S100A10* and *S100P*) (Table 6.1), members of a group of 22 proteins that are involved in several intracellular and extracellular functions (55). TUBB genes (*TUBB3*, *TUBB4*, *TUBB6*) encoding for β-tubulins were also down-regulated (Table 6.1). These are proteins that form with α-tubulins the microtubules (401). Coronin 1A (*CORO1A*), a microtubule interacting protein (402), and two ankyrin genes (*ANKS6* and *ANKRD58*), which are part of the cytoskeleton (403), also showed a decrease in mRNA levels (Table 6.1) with trastuzumab resistance. Genes involved in inflammation processes and/or immune responses such as chemokine ligands (*CCL2* and *CX3CL1*), bradykinin receptors (*BDKRB1* and *BDKRB2*), prostaglandin-endoperoxide synthase 1 (*PTGS1*) and TNF were down-regulated, while the chemokine (C-X-C motif) receptor 4 (*CXCR4*) was up-regulated (Table 6.1). Genes such as connective tissue growth factor (*CTGF*), *MMP9* and transforming growth factor 1 (*TGFBI*), which are all part of the extracellular matrix (404), showed decreased expression (Table 6.1). Similarly, glycoproteins such as wingless-type MMTV integration site family, member 5A (*WNT5A*), alpha-1 antiproteinase (*SERPINA3*) and zona pellucida glycoprotein 3 (ZP-3) were down-regulated (Table 6.1). Other important Ca^{2+}-related proteins such as the intermediate messenger calmodulin 1 (*CALM1*), calpain 1 and 2 (*CAPN1* and *CAPN2*) and calcium/calmodulin-dependent protein kinase II gamma (*CAMK2G*) showed decreased expression (Table 6.1). EGFR, which is involved in several cancers and is a target of some new anticancer agents (405), was down-regulated (Table 6.1) as previously reported and confirmed by Valabrega and colleagues (396). Two annexin proteins were also significantly altered: annexin A11 (*ANXA11*) was down-regulated, while annexin A2 (*ANXA2*) was up-regulated (Table 6.1).

Several Ca^{2+}-related transporters analyzed showed a decreased expression: SERCA3 (*ATP2A3*), the potassium intermediate/small conductance calcium-activated channel KCa3.1 (*KCNN4*), the calcium homeostasis modulator 2 (*FAM26B*), TRPM2 and TRPM4 channels, $Ca_V3.3$ channel (*CACNA1I*), the voltage-gated L-type calcium channel subunit β-1 (*CACNB1*) and the sodium/lithium/calcium exchanger NCKX6 (*SLC24A6*) (Table 6.1). In contrast, the potassium large conductance calcium-activated channel KCa1.1 (*KCNMA1*), the sodium/potassium/calcium exchanger NCKX3 (*SLC24A3*) and IP3R1 (*ITPR1*) were up-regulated (Table 6.1). The gene that showed the highest increase was galectin-3 (*LGALS3*) (Table 6.1), which has been previously

identified as playing important roles in cell adhesion, cell growth, differentiation and apoptosis (406).

Table 6.1 Changes in gene expression of calcium-related genes in the Valabrega et al. trastuzumab resistant SKBR3 cell line compared to the parental SKBR3 cell line

Calcium-related genes present in the Valabrega et al. microarray analysis (396) with significantly ($p \leq 0.05$) and greater than a 4 fold changes. Genes were selected through the gene ontology program PHANTER, 65 calcium-related genes were down-regulated (green) and 10 were up-regulated (red). The table reports the Logarithm Fold change and p-value for each gene. P-value ≤ 0.05 was considered significant.

Gene Name	Description	logFC	p-value
S100A4	S100 calcium binding protein A4	-5.819827636	1.51E-07
S100A8	S100 calcium binding protein A8	-5.613127666	9.98E-09
TUBB6	tubulin beta 6 class V	-5.58691565	6.36E-08
S100P	S100 calcium binding protein P	-5.063547579	3.76E-07
DHRS3	dehydrogenase/reductase (SDR family) member 3	-4.938890006	7.92E-07
DHRS2	dehydrogenase/reductase (SDR family) member 2	-4.938788317	3.64E-06
S100A9	S100 calcium binding protein A9	-4.861836544	5.40E-06
TGM1	transglutaminase 1	-4.830787517	2.35E-06
ATP2A3	ATPase, Ca^{2+} transporting (SERCA3)	-4.689038558	3.01E-06
KCNN4	potassium intermediate/small conductance calcium-activated channel subfamily N member 4 (KCa3.1)	-4.609674831	6.86E-06
ADA	adenosine deaminase	-4.479588372	4.57E-06
TRPM2	transient receptor potential cation channel melastatin 2	-4.366245053	6.06E-06
CORO1A	coronin actin binding protein 1A	-4.322808622	5.63E-06
CCL2	chemokine (C-C motif) ligand 2	-4.123764384	1.95E-07
PTGS1	prostaglandin-endoperoxide synthase 1 (prostaglandin G/H synthase and cyclooxygenase)	-4.118597865	3.14E-06
FAM26B	calcium homeostasis modulator 2	-4.037879457	5.97E-07
EGFR	epidermal growth factor receptor	-3.851552146	4.18E-06
TMC6	transmembrane channel-like 6	-3.772235815	7.98E-07

ADM	adrenomedullin	-3.732973327	1.84E-06
GAL	galanin/GMAP prepropeptide	-3.506804735	1.59E-06
AQP3	aquaporin 3	-3.50243339	4.16E-06
PACSIN1	protein kinase C and casein kinase substrate in neurons 1	-3.421906245	4.37E-07
S100A10	S100 calcium binding protein A10	-3.371730268	1.40E-06
CTGF	connective tissue growth factor	-3.319692778	1.46E-07
ADORA2A	adenosine A2a receptor	-3.26548744	3.26E-06
PRNP	prion protein	-3.196376297	1.66E-07
TMBIM1	transmembrane BAX inhibitor motif containing 1	-3.179250719	2.95E-06
ZP3	zona pellucida glycoprotein 3 (sperm receptor)	-3.176014814	1.59E-07
ANKS6	ankyrin repeat and sterile alpha motif domain containing 6	-3.172814483	1.25E-07
CDH24	cDNA FLJ25193 fis	-3.153883739	1.79E-07
TUBB4	tubulin, beta 4A class IVa	-3.127070651	2.32E-06
ANXA11	annexin A11	-3.077389225	1.48E-07
EDN2	endothelin 2	-2.948233038	4.98E-07
TRPM4	transient receptor potential cation channel melastatin 4	-2.939722594	4.78E-07
BDKRB1	bradykinin receptor B1	-2.891068931	6.94E-07
ASPHD1	aspartate beta-hydroxylase domain containing 1	-2.875269398	4.85E-06
TGFBI	transforming growth factor beta 1	-2.765385284	2.62E-07
CACNB1	calcium channel voltage-dependent beta 1 subunit	-2.676975593	2.79E-06
SLC24A6	solute carrier family 8 (sodium/lithium/calcium exchanger) member B1 (NCKX6)	-2.6656577	1.13E-06
ANKRD58	ankyrin repeat domain family member D	-2.580029928	4.38E-07
BDKRB2	bradykinin receptor B2	-2.576729588	3.73E-06
CX3CL1	chemokine (C-X3-C motif) ligand 1	-2.554766744	1.81E-06

WNT5A	wingless-type MMTV integration site family member 5A	-2.527245112	4.35E-07
JPH2	junctophilin 2	-2.523846551	2.96E-06
S100A5	S100 calcium binding protein A5	-2.470700329	4.59E-07
TUBB3	tubulin beta 3 class III	-2.427270499	1.40E-06
CD40	CD40 molecule, TNF receptor superfamily member 5	-2.42665339	6.14E-06
CACNA1I	calcium channel voltage-dependent T-type alpha 1I subunit ($Ca_V3.3$)	-2.394025191	7.41E-07
CAPN2	calpain 2	-2.314518696	1.89E-06
S100A7	S100 calcium binding protein A7	-2.294970552	6.98E-06
SRI	sorcin	-2.253750138	1.76E-06
SERPINA3	serpin peptidase inhibitor	-2.220675185	1.38E-06
CAPN1	calpain 1	-2.215508751	8.55E-07
VAMP5	vesicle-associated membrane protein 5	-2.180458476	1.00E-06
CAMK2G	calcium/calmodulin-dependent protein kinase II gamma	-2.163451898	4.91E-06
SCAMP5	secretory carrier membrane protein 5	-2.156457625	1.88E-06
CLIC4	chloride intracellular channel 4	-2.1274632	1.40E-06
SAA1	serum amyloid A1	-2.071115395	5.27E-06
DENND2D	cDNA DKFZp667I053	-2.06043246	2.40E-06
CALM1	calmodulin 1	-2.058147638	1.60E-06
PTPN21	protein tyrosine phosphatase non-receptor type 21	-2.057497049	1.27E-06
MMP9	matrix metalloproteinase 9	-2.056194708	5.38E-06
S100A3	S100 calcium binding protein A3	-2.053934471	7.83E-06
TNF	tumor necrosis factor	-2.03002356	1.29E-06
NMB	neuromedin B	-2.008299496	2.68E-06
CXCR4	chemokine (C-X-C motif) receptor 4	2.027921343	2.50E-06
ANXA2	annexin A2	2.136030312	2.58E-06
KCNMA1	potassium large conductance calcium-activated channel subfamily M alpha member 1 (KCa1.1)	2.492504484	4.40E-07

SLC25A4	solute carrier family 25 (mitochondrial carrier; adenine nucleotide translocator) member 4	2.537414689	1.76E-06
ASPH	aspartate beta-hydroxylase	2.825599379	2.26E-07
GNAS	GNAS complex locus	3.309578788	8.39E-06
SLC24A3	solute carrier family 24 (sodium/potassium/calcium exchanger) member 3 (NCKX3)	3.363325998	2.29E-07
CLCA2	chloride channel accessory 2	3.372484296	7.39E-06
ITPR1	inositol 1,4,5-trisphosphate receptor type 1	3.527589105	2.55E-07
LGALS3	galectin-3	5.61000007	4.58E-06

In their experiments, Valabrega and colleagues compared parental cell lines with trastuzumab resistant SKBR3 cell line that they established (396). However, it should be noted that some targets could change their expression levels during long-term continuous culturing as earlier described for TRPM7 in chapter 5 (section 5.4.1). In contrast, $Ca_V3.2$ did not show changes in mRNA expression between parental SKBR3 cells and age-matched control cell lines, but was significantly different between age-matched control and trastuzumab resistant cell lines (section 4.4.1). Other examples of alterations in mRNA levels with long-term culturing were also identified during the experiments conducted for this thesis. For example, Orai1 and Orai2 channels did not show significantly altered mRNA levels between age-matched control and resistant cell lines as described in sections 3.4.2.1 and 3.4.3.1. However, Orai1 mRNA levels were significantly increased in the age-matched control cell lines SV1 and SV2 cells and in the resistant cell lines RT1, RT2 and RV1 compared to the parental SKBR3 cell line (Fig. 6.2a). The mRNA levels of Orai2 were significantly increased between parental SKBR3 cells and the two *de novo* resistant cell lines RV1 and RV2 (Fig. 6.2b). Thus, in the absence of age-matched control cell lines, both Orai1 and Orai2 could have been identified as two possible targets due to their change in mRNA levels between parental and resistant SKBR3 cell lines.

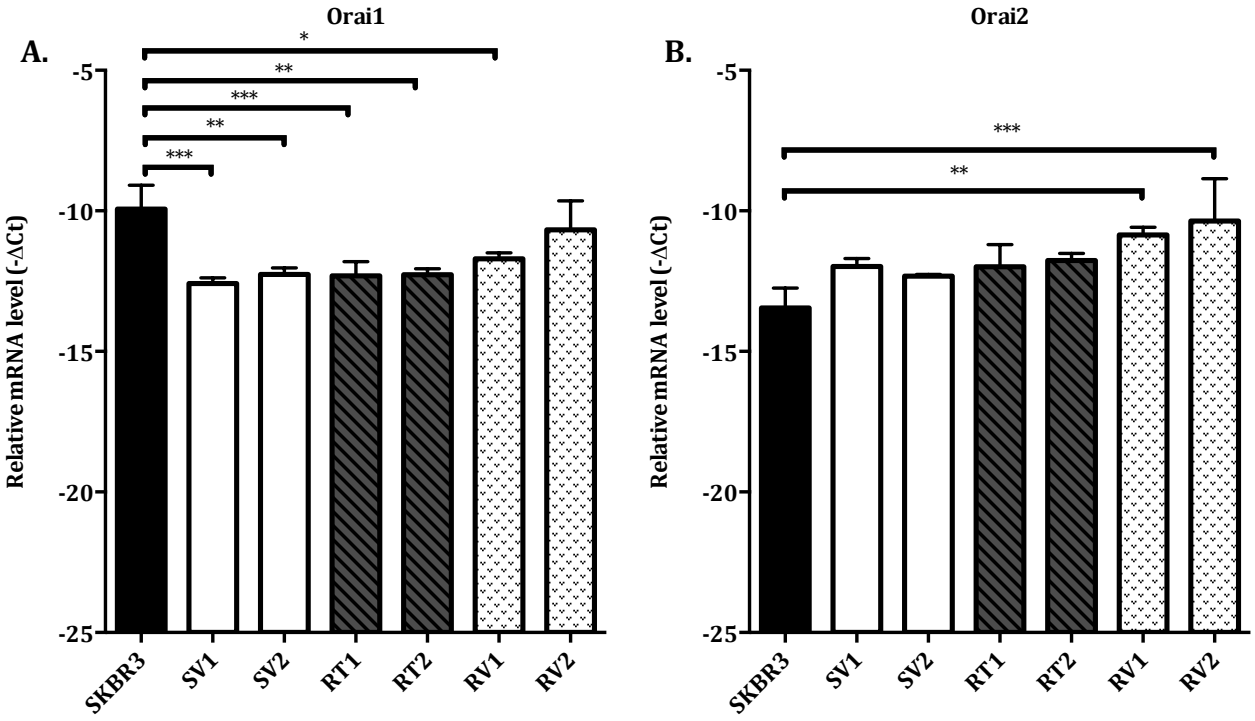

Figure 6.2 Levels of mRNA of Orai isoforms in the age-matched control (SV1 and SV2), resistant SKBR3 cell lines (RT1, RT2, RV1, RV2) and parental SKBR3 cells

A. Orai1 mRNA levels in parental SKBR3, age-matched control and resistant SKBR3 cell lines. Orai1 showed significantly lower mRNA levels in the SV1, SV2, RT1, RT2 and RV1 cell lines compared to parental SKBR3 cells. **B.** Orai2 mRNA levels in parental SKBR3, age-matched control and resistant SKBR3 cell lines. Orai2 showed significantly higher mRNA levels in the RV1 and RV2 cell lines compared to the parental SKBR3 cells. Statistical analysis was performed using one-way ANOVA with Bonferroni post-tests (* $p \leq 0.05$, ** $p \leq 0.01$, *** $p \leq 0.001$).

6.4.2 Assessment of calcium signaling related proteins in SILAC analysis of a trastuzumab resistant SKBR3 cell line

Similar to the gene expression microarray analysis, SILAC proteomics analysis has been used to evaluate changes in protein expression in a trastuzumab resistant SKBR3 cell line produced by exposing parental SKBR3 cells to trastuzumab 100 μg/mL for 9 months (400). Online, publically available SILAC data from the study by Boyer and colleagues (399) were analyzed. Boyer and colleagues (399) compared the expression of a set of proteins using SILAC in trastuzumab sensitive (light labeled) and trastuzumab resistant SKBR3 cell line (heavy labeled). They used two labeled amino acids (lysine and arginine) for each sample and in the second experiment they inverted these labels, in order to have the trastuzumab sensitive cells labeled with heavy amino acids and the trastuzumab resistant SKBR3 cell line labeled with the light amino acids (399). From their experiments they found that the CUB domain-containing protein 1 (*CDCP1*), paxillin (*PXN*) and MAPK1 had elevated protein expression in their trastuzumab resistant SKBR3 cell line compared to the parental cell line. They also identified that the silencing of these targets significantly increased trastuzumab sensitivity in trastuzumab resistant SKBR3 cells (399). Raw data from this SILAC experiment are shown in figure 6.3a and b. Lists of Ca^{2+}-related proteins from the SILAC data were generated by the gene ontology program PANTHER and those proteins with significant ($p \leq 0.05$) changes are shown in tables 6.2 and 6.3.

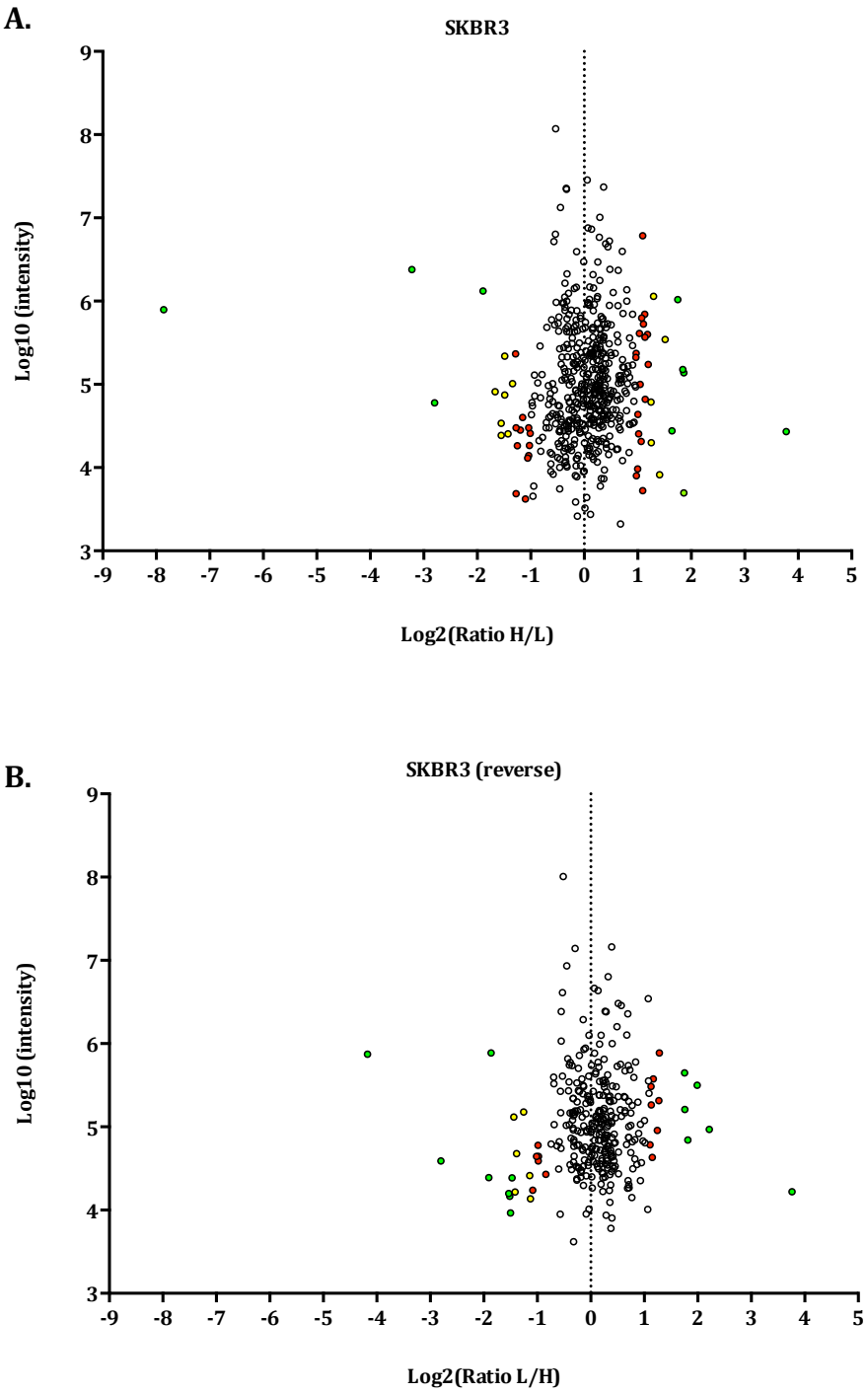

Figure 6.3 Protein expressions analyzed using SILAC analysis comparing the Boyer et al. trastuzumab resistant SKBR3 cell line and parental SKBR3 cells

A. Volcano plot showing differences in protein expression between Boyer et al. parental SKBR3 cell line (L) and trastuzumab resistant cell line (H) (399), the protein ratio is expressed as Log2. **B.** Volcano plot showing differences in protein expression between the parental SKBR3 cell line (H) and the trastuzumab resistant cell line (L), the protein ratio is expressed as Log2 where the labeling was inverted. Statistical significance was calculated using Perseus software. Targets with p-value between 0.01 and 0.05 are colored in red, between 0.01 and 0.001 are colored in yellow and <0.001 are colored in green.

Among the Ca^{2+}-related proteins only 7 appeared to be significantly altered; 4 down-regulated and 3 up-regulated. SERCA3 (*ATP2A3*), in accordance with the gene expression analysis shown in section 6.4.1 using a different trastuzumab resistant SKBR3 cell line, showed a decrease in protein levels in the trastuzumab resistant SKBR3 cell line (Table 6.2). The protein S100A6 was also down-regulated at protein level (Table 6.2), however this S100 protein isoform was not one of the isoforms identified as altered at the mRNA level in section 6.4.1. Another down-regulated protein was TMEM165 (Table 6.2), which is a transmembrane protein found in the Golgi that plays a role in terminal Golgi glycosylation (407). The sodium/potassium-transporting ATPase subunit beta-1 (*ATP1B1*) indirectly involved in intracellular Ca^{2+} homeostasis (408) also showed a lower protein expression in the Boyer et al. (399) trastuzumab resistant SKBR3 cell line (Table 6.2).

Three Ca^{2+}-related proteins (EGFR, IGF1R and galectin-3) were significantly up-regulated in the first replicate (Table 6.2). Interestingly, the data shown in section 6.4.1, also identified galectin-3 mRNA as higher in the Valabrega et al. (396) trastuzumab resistant SKBR3 cells. In contrast, EGFR showed down-regulation at mRNA levels but had higher protein levels (Table 6.2).

Table 6.2 Changes in protein expression of calcium-related proteins in the Boyer et al. trastuzumab resistant SKBR3 cell line compared to parental SKBR3 cell line

Calcium-related proteins from the first set of experiments from the Boyer et al. SILAC analysis (399), where sensitive SKBR3 cells were labeled with light isotopes and resistant SKBR3 cell line with heavy isotopes. The data were processed using the gene ontology program PHANTER and p-values were calculated with B significance using the Perseus software. The table shows the Log2 of the ratio between the values found for resistant (H) and sensitive (L) cell lines and the p-value for each protein. P-value ≤ 0.05 was considered significant.

Protein Name	Protein Descriptions	Log2 (Ratio H/L)	p-value
ATP2A3	Putative uncharacterized protein ATP2A3	-1.28514	0.01241
ATP1B1	Sodium/potassium-transporting ATPase subunit beta-1	-1.03913	0.03956
S100A6	S100 calcium binding protein A6	-1.03664	0.03999
TMEM165	Transmembrane protein 165	-1.01168	0.04454
EGFR	Epidermal growth factor receptor	1.09552	0.02389
LGALS3BP	Galectin-3-binding protein	1.63868	0.00047
IGF1R	Insulin-like growth factor 1 receptor	1.86084	0.00006

In the second replicate, where the labeled isotopes were inverted, two proteins were significantly down-regulated (Table 6.3): SERCA3 as reported in the first experiment (Table 6.2) and annexin A7 (*ANXA7*) (Table 6.3).

Table 6.3 Change in protein expression (reverse) of calcium-related proteins in the Boyer et al. trastuzumab resistant SKBR3 cell line compared to parental SKBR3 cell line

Calcium-related proteins from the second set of experiments from the Boyer et al. SILAC analysis (399), where the labeled isotopes were inverted. Thus sensitive SKBR3 cells were labeled with heavy isotopes and resistant SKBR3 cell line with light isotopes. The data were processed through gene ontology program PHANTER and p-value was calculated with B significance using Perseus software. The table also reports the Log2 of the ratio between the values found for resistant (L) and sensitive (H) cell lines and the p-value for each protein. P-value ≤ 0.05 was considered significant.

Protein Name	Protein Descriptions	Log2(Ratio L/H)	p-value
A8MYK9	Putative uncharacterized protein ATP2A3 (SERCA3)	-1.25401	0.00416
ANXA7	Annexin A7	-0.83874	0.04282

6.4.3 Assessment of calcium signaling related proteins in a cDNA microarray analysis of clinical breast cancers resistant to trastuzumab

In sections 6.4.1 and 6.4.2 of this chapter, cDNA microarray data and SILAC analysis were carried out *in vitro* comparing parental SKBR3 and trastuzumab resistant cell lines. In this section, Ca^{2+}-related genes were analyzed in samples derived from a study of 50 women with HER2-positive tumors treated with neoadjuvant chemotherapy plus trastuzumab and their responses to the therapeutic agent were evaluated (397). In their study Liu and colleagues produced a prognostic signature highly predictive for HER2-positive estrogen receptor negative breast cancer tumors (397). The signature was developed by evaluating the gene expression profile of tumor-initiating cells purified from a HER2-positive estrogen receptor negative mouse model (397). Tumor-initiating cells are the fraction of cancer cells that retain their tumorigenic potential (409). The prognostic signature consisted of 17 genes: 8 up-regulated (*Aurkb*, *Ccna2*, *Scrn1*, *Npy*, *Atp7b*, *Chaf1b*, *Ccnb1*, *Cldn8*) and 9 down-regulated (*Nrp1*, *Ccr2*, *C1qb*, *Cd74*, *Vcam1*, *Cd180*, *Itgb2*, *Cd72*, *St8sia4*) (397).

The prognostic signature obtained from the mouse model was then used to predict response to classic chemotherapy and/or trastuzumab in a cohort of 50 HER2-positive patients treated with chemotherapy plus trastuzumab (397). They concluded that the prognostic signature identified patients that could benefit from trastuzumab therapy (397).

The publically available microarray data (accession n. GSE37946: http://www.ncbi.nlm.nih.gov/geo/query/acc.cgi?acc=GSE37946) was kindly analyzed with A/Prof. Paraic Kenny at the Albert Einstein College of Medicine, Bronx NY (USA). Ca^{2+}-related genes (234) were selected by A/Prof. Paraic Kenny, and were assessed for their potential association with trastuzumab response (Fig. 6.4). Of the genes assessed 28 were significantly altered (21 down-regulated and 7 up-regulated) between the pathological complete trastuzumab response (pCR) group and the residual or recurrent disease (RD) group (Table 6.4).

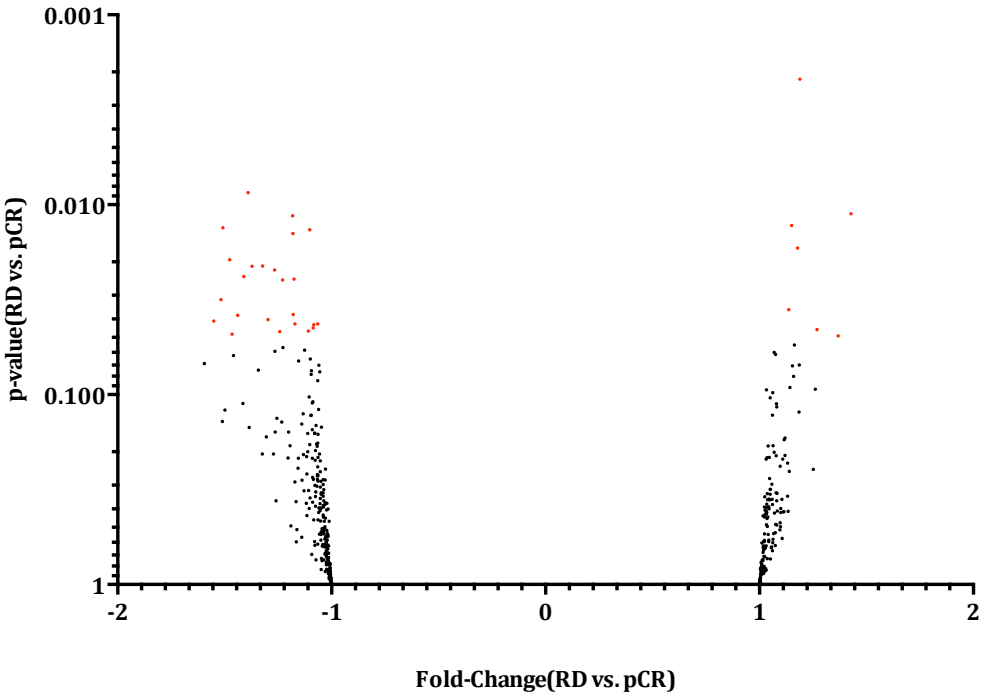

Figure 6.4 Gene expression profiles of 50 HER2-positive patients treated with neoadjuvant chemotherapy plus trastuzumab

Volcano Plot of the gene expression profile of the 234 Ca^{2+}-related genes performed on breast cancer tissues from 50 women treated with neoadjuvant chemotherapy plus trastuzumab. The gene expression profile of Ca^{2+}-related proteins between pathological complete response (pCR) to trastuzumab group and residual or recurrent disease (RD) group were compared. The Ca^{2+}-related genes that were significantly ($p \leq 0.05$) different are highlighted in red.

Among the 21 down-regulated genes, 11 are associated with immune response such as several chemokines like the chemokine (C-C motif) ligand 5 (*CCL5*) and 21 (*CCL21*), the chemokine (C-C motif) receptor 5 (*CCR5*) and the chemokine (C-X-C motif) receptor 3 (*CXCR3*) (Table 6.4). Tyrosine kinases and other proteins involved in the regulation of T- and B-cell antigen receptor signaling were down-regulated: coronin-1A (*CORO1A*), protein tyrosine phosphatase receptor type C (*PTPRC*), proto-oncogene tyrosine-protein kinase (*FYN*), lymphocyte-specific protein tyrosine kinase (*LCK*), protein kinase C β (*PRKCB*), transforming growth factor β 1 (*TGFBI*), leukocyte immunoglobulin-like receptor subfamily B member 1 (*LILRB1*), P2X purinergic receptor ligand-gated ion channel 5 (*P2XR5*) and GTPase IMAP family member 5 (*GIMAP5*) (Table 6.4) were also down-regulated. Proteins associated with mitochondria such as the glutathione S-transferase omega 1 (*GSTO1*) and the coiled-coil domain containing 109B (*CCDC109B*) also known as the calcium uniporter MCUb showed lower gene expression in the trastuzumab resistant samples, while the anti-apoptotic protein Blc-2 was up-regulated (Table 6.4). The calcium permeable ion channel TRPV2, the voltage-gated L-type calcium channel subunit β 2 (*CACNB2*) and the calcium store release regulator aspartate beta-hydroxylase (*ASPH*) were down-regulated (Table 6.4). Two proteins involved in transcriptional repression were up-regulated; the zinc finger protein RFP (*TRIM27*) and Myb proto-oncogene protein. Interestingly, galectin-3 was the most up-regulated gene in this data set of clinical samples and this was consistent with the *in vitro* microarray data set (section 6.4.1) and the first SILAC replicate (section 6.4.2).

Table 6.4 Changes in gene expression of calcium-related proteins in tumor samples resistant to trastuzumab

Calcium-related genes with significant ($p \leq 0.05$) alterations between trastuzumab resistant and sensitive HER2-positive breast cancers (397). The table shows the fold change of RD vs. pCR and p-value for each gene. P-value ≤ 0.05 was considered significant.

Gene Symbol	Gene Title	Fold-Change (RD vs. pCR)	p-value
CORO1A	coronin actin binding protein 1A	-1.55071	0.0409446
PTPRC	protein tyrosine phosphatase receptor type,C	-1.51766	0.0316064
FYN	FYN oncogene	-1.50765	0.0132336
CCL5	chemokine (C-C motif) ligand 5	-1.47577	0.0194717
LCK	lymphocyte-specific protein tyrosine kinase	-1.4651	0.0481232
PRKCB	protein kinase C beta	-1.43882	0.038215
CCL21	chemokine (C-C motif) ligand 21	-1.39039	0.00864041
TGFBI	transforming growth factor beta 1	-1.32253	0.0210382
CCDC109B	coiled-coil domain containing 109B (MCU)	-1.29713	0.0403331
P2RX5	purinergic receptor P2X ligand-gated ion channel 5	-1.26571	0.0220851
GIMAP5	GTPase IMAP family member 5	-1.24253	0.0465282
GSTO1	glutathione S-transferase omega 1	-1.22846	0.0248836
TRPV2	transient receptor potential cation channel vanilloid 2	-1.18225	0.0114534
CCR5	chemokine (C-C motif) receptor 5	-1.17992	0.0378762
LILRB1	leukocyte immunoglobulin-like receptor subfamily B member	-1.17499	0.0246245
ASPH	aspartate beta-hydroxylase	-1.17171	0.0424494
CXCR3	chemokine (C-X-C motif) receptor 3	-1.10822	0.0462544
CHRNA4	cholinergic receptor nicotinic alpha 4	-1.10212	0.0135477
RASA3	AS p21 protein activator 3	-1.08676	0.044573
RCVRN	recoverin	-1.08323	0.042936
CACNB2	voltage-dependent calcium channel beta 2	-1.06513	0.0423614

	subunit		
PKD1	polycystic kidney disease 1	1.13746	0.0356451
BCL2	B-cell lymphoma 2	1.15001	0.0128584
TRIM27	tripartite motif-containing 27	1.17819	0.0169138
SLC24A1	solute carrier family 24 (sodium/potassium/calcium exchanger) member 1 (NCKX1)	1.1892	0.0021799
PSEN1	presenilin 1	1.26903	0.0455082
MYB	myb oncogene	1.36808	0.0490876
LGALS3	galectin-3	1.42799	0.0111746

6.5 Conclusion

In this chapter, a different approach using large-scale high-throughput analyses was used to identify possible targets that may be associated with trastuzumab resistance. Different types of data sets were evaluated such as gene expression profile microarray data on trastuzumab sensitive and resistant SKBR3 cell lines and clinical samples and protein expression profiling by SILAC analysis from trastuzumab sensitive and resistant SKBR3 cell lines.

From the cDNA microarray data performed on Valabrega et al. (396) trastuzumab sensitive and resistant SKBR3 cell line, it was observed that several S100 proteins were down-regulated (*S100A3*, *S100A4*, *S100A5*, *S100A7*, *S100A8*, *S100A9*, *S100A10* and *S100P*) (Table 6.1 section 6.4.1) and the S100A6 protein was down-regulated in the first SILAC experiment (Table 6.2 section 6.4.2). Changes in the expression of S100 proteins has been reported in several cancers, they are important regulators of numerous intracellular and extracellular processes such as Ca^{2+} homeostasis, protein phosphorylation, enzyme activity, proliferation and cytoskeleton components such as microtubules (55). Rhee and colleagues showed that S100A4, S100A7, S100A8, and S100A9 were down-regulated in isogenic MCF10 breast cancer cell lines and they were involved in transformation and cancer progression (410). In contrast, in another study several S100 proteins (S100A1, S100A2, S100A4, S100A6, S100A8, S100A9, S100A10, S100A11, and S100A14) were found to have increased expression in basal breast tumor samples compared to non-basal subtype (411). S100A7 and S100P appear to have different roles depending on the estrogen receptor status of the breast cancer, and their up-regulation appears indicative of drug resistance, metastasis and a poor prognosis (55, 412). In the HER2-positive breast cancer tissues, S100A14 was found to be significantly up-regulated compared to normal adjacent tissue and able to modulate HER2 signaling in BT474 and SKBR3 cell lines (413), unfortunately S100A14 was not part of any data set tested in this project. Collectively these current studies and those of other investigators suggest that S100 proteins may have different roles depending on the breast cancer molecular subtype.

Several proteins involved in the organization of microtubules (*TUBB3*, *TUBB4*, *TUBB6*, *CORO1A*, *ANKS6* and *ANKRD58*) and of the extracellular matrix (*CTGF*, *MMP9*, *TGFBI*) were down-regulated in the gene expression profile shown in section 6.4.1. Coronin 1A and TGFBI also had reduced expression in the clinical microarray data set (Table 6.4 section 6.4.3). Different α- and β-tubulins including TUBB4 and TUBB6 were also tested in the two SILAC experiments, but none of these proteins appeared to be significantly altered at the protein level (Tables 6.2 and 6.3 section 6.4.2). Tubulins were not assessed in the clinical microarray data. From these analyses, it appears

that trastuzumab resistance may induce cells to undergo morphological remodeling. Indeed, microtubule formation is controlled by the extracellular matrix (414) and loss of TGFBI expression induces microtubules destabilization and resistance to paclitaxel in ovarian and breast cancer cell lines (415). β-tubulins are a drug target in several cancers (416, 417), but they are also associated with drug resistance in cancer (418, 419). Indeed, increased β-tubulin 3 mRNA levels are often associated with resistance to paclitaxel and vinorelbine in MCF-7 and MDA-MB-231 cells (420) and in breast cancer patients (421, 422). In contrast, overexpression of β-tubulin 3 in HER2-positive breast cancer patients is a predictor of good response to paclitaxel and trastuzumab (423). Since resistant SKBR3 cells were associated with potential alterations in β-tubulin 3 mRNA it would have been interesting to evaluate mRNA levels in the clinical samples analyzed in section 6.4.3, however tubulins were not part of this data set.

A number of genes involved in inflammation and immune response showed altered mRNA levels in the microarrays analyzed in section 6.4.1 and 6.4.3. Ca^{2+}-related proteins involved in these processes were present in the SILAC data set. Different chemokine ligands and receptors such as CCL2, CX3CL1 in the gene expression profile performed on the Valabrega et al. (396) SKBR3 cells (Table 6.1 section 6.4.1) and CCL5, CCL21, CCR5 and CXCR3 in the clinical samples microarray (Table 6.4 section 6.4.3) were down-regulated in the trastuzumab resistant group, while CXCR4 mRNA was up-regulated in the Valabrega et al. (396) trastuzumab resistant SKBR3 cell line (Table 6.1 section 6.4.1). Other genes linked to inflammation and immune response such as *BDKRB1*, *BDKRB2*, *TNF*, *TGFBI*, *CD40*, *PTGS1* and *PTPN21* in the microarray performed on the Valabrega et al. (396) resistant SKBR3 cells (Table 6.1 section 6.4.1) and *CORO1A*, *PTPRC*, *FYN*, *LCK*, *PRKCB*, *TGFBI*, *LILRB1* and also *P2XR5* and *GIMAP5* in the clinical samples (Table 6.4 section 6.4.3) were down-regulated. Galectin-3 was one of the genes that showed the highest change in trastuzumab resistant cell line at mRNA (396) (Table 6.1 section 6.4.1), protein level (399) (Table 6.2 section 6.4.2) and in trastuzumab non-responsive patients (Table 6.4 section 6.4.3). It should be noted that galectin-3 was not detected in the second replicate of the SILAC experiment possibly due low phosphopeptide abundances of this protein or biological noise in the second replicate (424). Galectin-3 is implicated in cell adhesion, cell growth and differentiation, apoptosis, inflammation in cancer (406) and tumor progression (425, 426). Galectin-3 has also been associated with metastasis in murine lung adenocarcinoma cell lines (427).

Trastuzumab response relies in part on the immune system since it induces an antibody cell mediated cytotoxicity and a subsequent antigen-specific immune activation (428). Indeed,

activation of immune pathways can predict trastuzumab response as reflected in the association between lymphocytes infiltration and trastuzumab efficacy and improved prognosis (428). Since several genes involved in inflammation and immune response showed altered levels in the data sets analyzed, the expression of some of these genes could perhaps restore normal immune signaling and thus reverse trastuzumab resistance.

Among the Ca^{2+} transporters assessed SERCA3, KCa3.1 channel, TRPM2 and TRPM4, NCKX6, $Ca_V3.3$ channel and CACNB1 in the microarray analysis of the Valabrega et al. (396) trastuzumab resistant SKBR3 cell line were down-regulated, while KCa1.1 channel, NCKX3 and IP3R1 were up-regulated (Table 6.1 section 6.4.1). From the SILAC experiments, SERCA3 in both replicates and the sodium/potassium-dependent ATPase subunit beta-1 in the first replicate showed significantly lower protein levels (Tables 6.2 and 6.3, section 6.4.2). In the clinical breast cancer samples TRPV2, MCUb and CACNB2 had decreased mRNA levels in trastuzumab non-responsive patients (Table 6.4 section 6.4.3), while the exchanger NCKX1 was up-regulated.

SERCA3 was one of the most down-regulated proteins in the Valabrega et al. (396) and Boyer et al. (399) trastuzumab resistant cell lines at the mRNA and protein levels, however, in HER2-positive trastuzumab non-responsive patients SERCA3 was not significantly altered. Down-regulation of SERCA3 is associated with tumorigenesis in HER2-negative and triple negative primary breast cancer tissue samples (429) and also with EGF-induced EMT in MDA-MB-468 cells (430). It should be noted that the down-regulation of SERCA3 mRNA observed in the trastuzumab resistant SKBR3 cell line with microarray (396) and SILAC (399) analysis, could be due to a possible change in SERCA3 expression with long-term culturing as was observed for TRPM7 in section 5.4.1 and as reported for two other Ca^{2+} channels Orai1 and Orai2 channels in section 6.4.1. Hence, assessment of SERCA3 in the cell lines produced in chapter 3 with age-matched controls would improve our understanding of changes in SERCA3 associated with trastuzumab resistance.

IGF1R has been widely studied in the context of trastuzumab resistance (155, 158, 190, 279). IGF1R showed higher protein levels in the first SILAC experiment (Table 6.2 section 6.4.2), while it was not detected in the second repeat. From the immunoblotting shown in chapter 3 section 3.4.1, IGF1R did not show changes at a protein level between the age-matched control and resistant SKBR3 cell lines. Thus, as discussed earlier for SERCA3 and TRPM7, the up-regulation observed in the SILAC experiment may be due to the use of a parental cell line rather than an age-matched control cell line. Indeed, a study, conducted using immunohistochemical analysis on clinical

samples from patients with metastatic HER2-positive tumors receiving trastuzumab therapy, concluded that IGF1R may not be relevant as a trastuzumab response predictor (191).

EGFR expression was down-regulated at the mRNA level, but up-regulated at the protein level in the two experiments performed comparing parental and trastuzumab resistant SKBR3 cell lines with publically available data (Table 6.1, section 6.4.1 and Tables 6.2 and 6.3, section 6.4.2). It should be noted that EGFR showed significantly higher expression levels only in the first SILAC experiment. From the screen I performed on the cell lines produced in chapter 3 it was observed that EGFR did not show a change in either mRNA or protein levels (section 3.4.1). A study that analyzed the expression of EGFR in HER2-positive patients treated with trastuzumab showed that EGFR expression was not correlated with trastuzumab response (431). Hence, changes in EGFR may not be uniform across experimental models or may not be clinically relevant.

In summary, from the analysis of three different data sets where the expression of Ca^{2+}-related proteins was evaluated in two different trastuzumab resistant SKBR3 cell lines and in patients that were not responsive to trastuzumab, it was observed that trastuzumab resistance may produce a reprogramming of signals between the cell and the extracellular matrix and a decrease in immune and inflammatory signaling. The only common result among the three data sets was the up-regulation of galectin-3 (Fig. 6.6), which is involved in tumor progression in breast cancer (425, 426). Thus, future studies should be conducted to further evaluate the functional role of galectin-3 in trastuzumab resistant cells. It should be noted that gene expression profiling and SILAC assays cannot identify changes in function and/or alterations in cellular localization; changes in calcium signaling in trastuzumab resistance could also be mediated by such changes.

A.

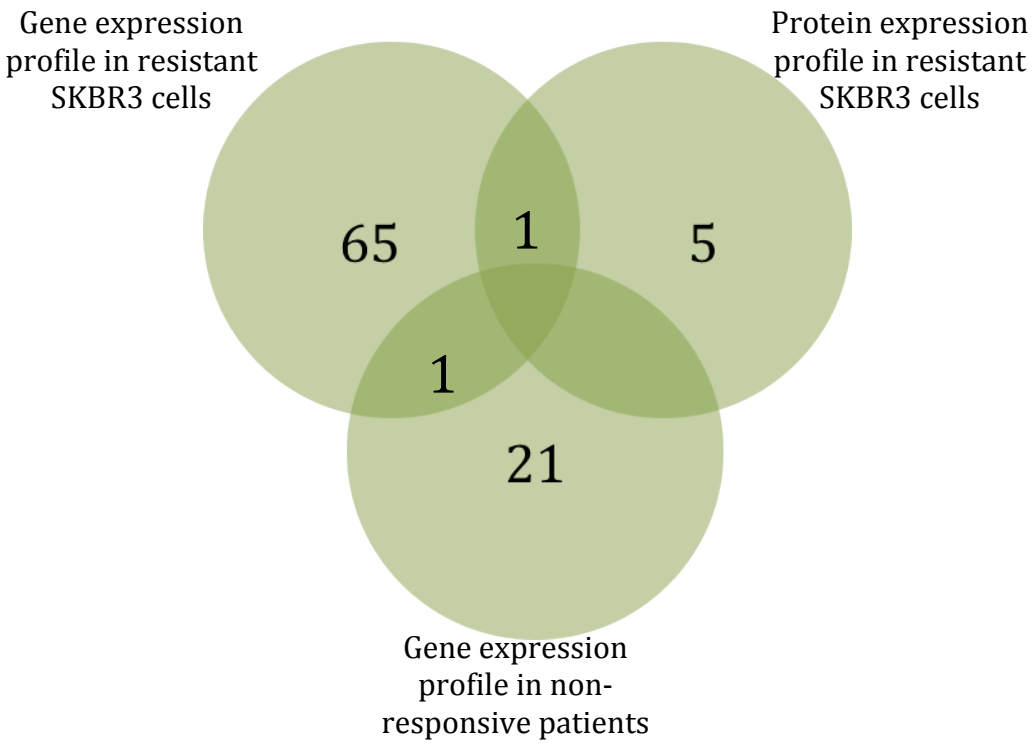

B.

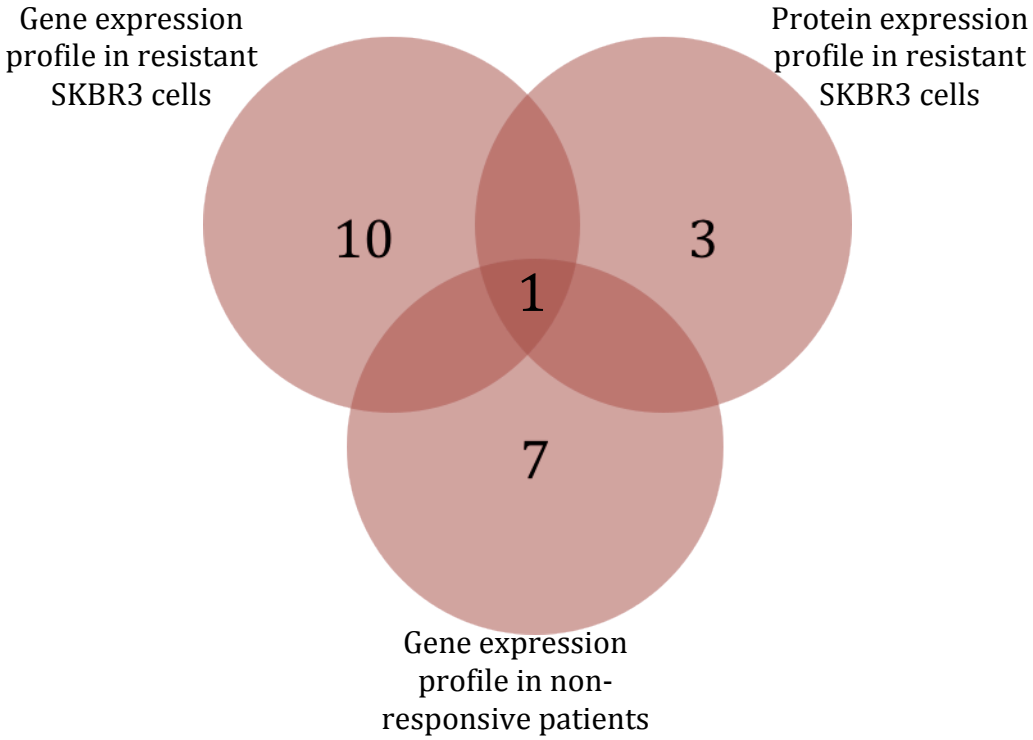

Figure 6.5 Comparison of all Ca^{2+}-related protein identified as significantly altered in the three data sets analyzed

A. Down-regulated Ca^{2+}-related proteins found in the three data sets analyzed (396, 397, 399), SERCA3 was common to the two data sets produced from SKBR3 cell lines, while coronin A1 was found in both gene profile microarrays. **B.** Up-regulated Ca^{2+}-related proteins found in the three data sets analyzed. Only galectin-3 was up-regulated in all of the three data sets (396, 397, 399).

7 Conclusions

Ca^{2+} is an essential element of the cell and it regulates several life and death processes (1-3, 74). Intracellular calcium concentrations are therefore highly regulated through a variety of calcium channels and pumps in order to maintain Ca^{2+} homeostasis and cell function (1, 3, 5, 74). Altered expression and/or function of Ca^{2+} channels and pumps are associated with several diseases including the progression of some cancers (7, 91, 432). Specific Ca^{2+} channels and pumps may represent novel therapeutic targets in some cancers, including those of the breast (4).

Breast cancer is the most commonly diagnosed cancer and the leading cause of cancer death in women worldwide (114). Breast cancer is a heterogenic disease, which is classified by tumor size, stage of the tumor, receptor status and cDNA microarray based on global gene expression to determine the molecular subtype of cancer (119). Among the different subtypes, HER2-positive breast cancers represent approximately 20-25% of all breast tumours (122-124). These breast cancers are associated with poor prognosis and a low overall survival rate (125, 126). The first and leading agent currently used for the treatment of HER2-positive breast cancers is the monoclonal antibody trastuzumab (132, 135, 136).

Despite the great improvement in HER2-positive patient outcome that trastuzumab has produced, 25-30% of eligible patients show an inherent resistance to trastuzumab (148) and a large number of patients who initially responded to the treatment acquire resistance within one year (140). Trastuzumab resistance has been widely studied (129, 146, 329, 433), however, the mechanisms of trastuzumab resistance are still not fully understood.

Since calcium signaling is involved in the development and progression of several types of cancer (4, 45, 99, 432) and chemoresistance (161-164, 166, 167), in this thesis I evaluated the role of calcium channels, pumps and channel modulators in the acquisition of trastuzumab resistance.

Characterization of HER2-positive, trastuzumab sensitive SKBR3 breast cancer cells showed that the inhibition of the Ca^{2+} channels TPC2 and TRPV1 and the Ca^{2+} channel modulator STIM1 decreased cell proliferation. The silencing of the calcium pump SPCA1, the calcium sensor STIM1 and the Ca^{2+} permeable ion channel TRPM7 enhanced the response to trastuzumab. This is the first study that has reported a link between regulators of Ca^{2+} signal and responses to trastuzumab. Studies should now be conducted in other HER2-positive cell lines (e.g. BT474) and in *in vivo* models to determine if these effects are not restricted to SKBR3 cells *in vitro*.

Despite promoting the sensitivity of SKBR3 cells to trastuzumab, the silencing of SPCA1, STIM1 and TRPM7 did not reverse trastuzumab resistance in the acquired or *de novo* trastuzumab resistant cell lines developed during these studies. This suggests that in trastuzumab resistance alternative signaling pathways may be activated and represents further evidence that approaches that increase trastuzumab responses in trastuzumab sensitive cells may not necessarily increase sensitivity to this therapeutic agent in resistant cells. The work presented in this thesis therefore provides further evidence for the importance of studies assessing trastuzumab resistant cell lines.

An extensive evaluation of several Ca^{2+} channels, pumps and channel modulators conducted in age-matched control and trastuzumab resistant SKBR3 cell lines identified $Ca_V3.2$ as the target among 45 tested targets to have altered mRNA levels between resistant and age-matched control cell lines. Although $Ca_V3.2$ channels showed higher mRNA in the two *de novo* resistant cell lines RV1 and RV2 and also in the basal HER2-positive HCC1569, it should be noted that $Ca_V3.2$ expression showed only a weak correlation with HER2 expression in clinical basal breast samples and it was not significantly altered in the clinical samples analyzed. This may indicate that $Ca_V3.2$ may not be a prognostic marker for trastuzumab resistance in basal HER2-positive breast tumors. However, since $Ca_V3.2$ channel mRNA was higher in the *de novo* resistant cell lines and in HCC1569 cells, additional studies to evaluate the role of $Ca_V3.2$ channel as a possible predictor of trastuzumab response in a clinical setting may be appropriate. $Ca_V3.2$ channel should also be further evaluated through overexpression of this protein in parental SKBR3 cell line to assess the consequences of elevated $Ca_V3.2$ levels on trastuzumab sensitivity. Although in these studies both siRNA and pharmacological inhibition of $Ca_V3.2$ did not restore trastuzumab sensitivity in a trastuzumab resistant SKBR3 cell line, siRNA and pharmacological inhibition of $Ca_V3.2$ could be conducted in the *de novo* trastuzumab resistant HER2-positive cell lines HCC1569 and JIMT-1.

Ca^{2+} signaling profiling was conducted in parental, age-matched control and trastuzumab resistant SKBR3 cell lines. These studies demonstrated that all of the cell lines tested showed responsiveness to the purinergic receptor activator ATP and had a functional SOCE pathway. The acquired resistant cell lines RT1 and RT2 showed lower sensitivity to ATP compared to the age-matched control cell lines (SV1 and SV2) suggesting that purinergic receptors and/or regulators of ATP-mediated Ca^{2+} signals may be associated with trastuzumab resistance. Further studies should be carried out to evaluate the role of purinergic receptors in trastuzumab resistance. The expression of

purinergic receptor isoforms should be assessed in trastuzumab resistant SKBR3 cells to help define the mechanism for this change in ATP-mediated Ca^{2+} signaling.

The SKBR3 parental cell line and age-matched controls showed a different sensitivity to ATP but similar SOCE. The different sensitivity to ATP may be due to a possible remodeling of Ca^{2+} signaling during continuous culturing. Indeed, long-term culture of cell lines have been reported to change the phenotype of many cell lines (284). Examples of such changes were also observed in this thesis. Results presented in this thesis showed that Orai channels and STIM sensors do not have altered mRNA levels in trastuzumab resistant cell lines compared to age-matched control cell lines. However, Orai1 and Orai2 channels showed significantly different mRNA levels between parental and age-matched control cell lines. This suggests that a remodelling of Orai mRNA levels may occur during long-term culturing. These findings support the use of age-matched cell lines in the assessment of changes associated with trastuzumab resistance.

TRPM7 also showed higher mRNA levels in the age-matched control and trastuzumab resistant cell lines compared to the parental SKBR3 cell line. Evaluation of TRPM7 in resistant cell lines showed that TRPM7 silencing and the TRPM7 gate inhibitor NS8593, did not reverse trastuzumab resistance. The inability of TRPM7 silencing to promote trastuzumab sensitivity in the trastuzumab resistant cell lines was in contrast to the inability of TRMP7 siRNA to completely silence the elevated TRPM7 mRNA levels, which occurred as a result of long-term culture. To improve the efficacy of TRPM7 silencing future studies could use an alternative method, such as shRNA. The TRPM7 α-kinase inhibitor NH125, was able to reverse trastuzumab resistance, however, since NH125 has also been reported to inhibit eEF2K, another α-kinases (368, 371), further experiments are needed to fully understand the mechanism by which NH125 reverses trastuzumab resistance. Such studies could involve eEF2K silencing and assessment of the effect of NH125 in eEF2K deficient cells. The phosphorylation of known substrates of TRPM7 kinase, such as annexin A1, myosin IIA, IIB and IIC could also be evaluated in samples treated with NH125 to further explore the association between NH125, TRPM7 kinase inhibition and trastuzumab resistance. In any case, these studies have identified NH125 as an agent capable of restoring trastuzumab sensitivity in trastuzumab resistant SKBR3 cells. This agent should now be evaluated in other trastuzumab resistance models.

Finally, the evaluation of the levels of several Ca^{2+}-related proteins in three different datasets suggests that SERCA3 may have reduced expression in trastuzumab resistant SKBR3 cell lines, but

not in clinical samples. This study also identified galectin-3, a protein involved in cell adhesion, cell growth and differentiation, apoptosis, inflammation in cancer (406) and tumor progression (425, 426), as up-regulated in both cell line and clinical sample datasets of trastuzumab resistance. Clinical samples demonstrated a potential remodelling of Ca^{2+}-related proteins involved in immune and inflammation response with trastuzumab resistance. Further experiments should now be performed to evaluate the functional role of SERCA3 and galectin-3 in trastuzumab resistant cells to confirm the results found from the gene expression datasets and SILAC experiments evaluated in this thesis.

In summary, it appears that some breast cells may undergo a reprogramming of cellular signaling with the acquisition of trastuzumab resistance. Future research on the targets identified in this thesis ($Ca_V3.2$, TRPM7, SERCA3 and galectin-3) may help identify new biomarkers for trastuzumab resistance and/or new ways to restore or induce trastuzumab sensitivity in HER2 breast cancers that are resistant to this important therapeutic.

8 References

1. Carafoli E, Santella L, Branca D, Brini M. Generation, control, and processing of cellular calcium signals. Crit Rev Biochem Mol Biol. 2001 Apr;36(2):107-260. PubMed PMID: 11370791.

2. De Smedt H, Verkhratsky A, Muallem S. Ca(2+) signaling mechanisms of cell survival and cell death: an introduction. Cell Calcium. 2011 Sep;50(3):207-10. PubMed PMID: 21741085.

3. Berridge MJ, Lipp P, Bootman MD. The versatility and universality of calcium signalling. Nat Rev Mol Cell Biol. 2000 Oct;1(1):11-21. PubMed PMID: 11413485.

4. Monteith GR, McAndrew D, Faddy HM, Roberts-Thomson SJ. Calcium and cancer: targeting Ca2+ transport. Nat Rev Cancer. 2007 Jul;7(7):519-30. PubMed PMID: 17585332.

5. Clapham DE. Calcium signaling. Cell. 2007 Dec;131(6):1047-58. PubMed PMID: 18083096.

6. Rizzuto R, Pozzan T. Microdomains of intracellular Ca2+: molecular determinants and functional consequences. Physiol Rev. 2006 Jan;86(1):369-408. PubMed PMID: 16371601.

7. Carafoli E, Brini M. Calcium signalling and disease: molecular pathology of calcium. New York: Springer; 2007. 592 p.

8. Murray AW, Hunt T. The cell cycle: an introduction. New York: Oxford University Press; 1993. 251 p.

9. Machaca K. Ca(2+) signaling, genes and the cell cycle. Cell Calcium. 2010 Nov;48(5):243-50. PubMed PMID: 21084120.

10. Kahl CR, Means AR. Regulation of cell cycle progression by calcium/calmodulin-dependent pathways. Endocr Rev. 2003 Dec;24(6):719-36. PubMed PMID: 14671000.

11. Skelding KA, Rostas JA, Verrills NM. Controlling the cell cycle: the role of calcium/calmodulin-stimulated protein kinases I and II. Cell Cycle. 2011 Feb;10(4):631-9. PubMed PMID: 21301225.

12. Chafouleas JG, Bolton WE, Hidaka H, Boyd AE, 3rd, Means AR. Calmodulin and the cell cycle: involvement in regulation of cell-cycle progression. Cell. 1982 Jan;28(1):41-50. PubMed PMID: 7066986.

13. Rasmussen CD, Means AR. Calmodulin is required for cell-cycle progression during G1 and mitosis. EMBO J. 1989 Jan;8(1):73-82. PubMed PMID: 2469574.

14. Planas-Silva MD, Means AR. Expression of a constitutive form of calcium/calmodulin dependent protein kinase II leads to arrest of the cell cycle in G2. EMBO J. 1992 Feb;11(2):507-17. PubMed PMID: 1371461.

15. Kahl CR, Means AR. Calcineurin regulates cyclin D1 accumulation in growth-stimulated fibroblasts. Mol Biol Cell. 2004 Apr;15(4):1833-42. PubMed PMID: 14767060.

16. Musgrove EA. Cyclins: roles in mitogenic signaling and oncogenic transformation. Growth Factors. 2006 Mar;24(1):13-9. PubMed PMID: 16393691.

17. Lewis RS. Calcium signaling mechanisms in T lymphocytes. Annu Rev Immunol. 2001 Apr;19:497-521. PubMed PMID: 11244045.

18. Graef IA, Mermelstein PG, Stankunas K, Neilson JR, Deisseroth K, Tsien RW, et al. L-type calcium channels and GSK-3 regulate the activity of NF-ATc4 in hippocampal neurons. Nature. 1999 Oct;401(6754):703-8. PubMed PMID: 10537109.

19. Van Rooij E, Sutherland LB, Liu N, Williams AH, McAnally J, Gerard RD, et al. A signature pattern of stress-responsive microRNAs that can evoke cardiac hypertrophy and

heart failure. Proc Natl Acad Sci U S A. 2006 Nov;103(48):18255-60. PubMed PMID: 17108080.

20. Buchholz M, Ellenrieder V. An emerging role for Ca2+/calcineurin/NFAT signaling in cancerogenesis. Cell Cycle. 2007 Jan;6(1):16-9. PubMed PMID: 17245111.

21. Zhivotovsky B, Orrenius S. Calcium and cell death mechanisms: a perspective from the cell death community. Cell Calcium. 2011 Sep;50(3):211-21. PubMed PMID: 21459443.

22. Cory S, Adams JM. The Bcl2 family: regulators of the cellular life-or-death switch. Nat Rev Cancer. 2002 Sep;2(9):647-56. PubMed PMID: 12209154.

23. Galluzzi L, Vitale I, Abrams JM, Alnemri ES, Baehrecke EH, Blagosklonny MV, et al. Molecular definitions of cell death subroutines: recommendations of the Nomenclature Committee on Cell Death 2012. Cell Death Differ. 2012 Jan;19(1):107-20. PubMed PMID: 21760595.

24. Pinton P, Rizzuto R. Bcl-2 and Ca2+ homeostasis in the endoplasmic reticulum. Cell Death Differ. 2006 Aug;13(8):1409-18. PubMed PMID: 16729032.

25. Pinton P, Giorgi C, Siviero R, Zecchini E, Rizzuto R. Calcium and apoptosis: ER-mitochondria Ca2+ transfer in the control of apoptosis. Oncogene. 2008 Oct;27(50):6407-18. PubMed PMID: 18955969.

26. Orrenius S, Zhivotovsky B, Nicotera P. Regulation of cell death: the calcium-apoptosis link. Nat Rev Mol Cell Biol. 2003 Jul;4(7):552-65. PubMed PMID: 12838338.

27. Pinton P, Ferrari D, Rapizzi E, Di Virgilio F, Pozzan T, Rizzuto R. The Ca2+ concentration of the endoplasmic reticulum is a key determinant of ceramide-induced apoptosis: significance for the molecular mechanism of Bcl-2 action. EMBO J. 2001 Jun;20(11):2690-701. PubMed PMID: 11387204.

28. Baffy G, Miyashita T, Williamson JR, Reed JC. Apoptosis induced by withdrawal of interleukin-3 (IL-3) from an IL-3-dependent hematopoietic cell line is associated with repartitioning of intracellular calcium and is blocked by enforced Bcl-2 oncoprotein production. J Biol Chem. 1993 Mar;268(9):6511-9. PubMed PMID: 8454620.

29. Distelhorst CW, Shore GC. Bcl-2 and calcium: controversy beneath the surface. Oncogene. 2004 Apr 23(16):2875-80. PubMed PMID: 15077150.

30. Scorrano L, Oakes SA, Opferman JT, Cheng EH, Sorcinelli MD, Pozzan T, et al. BAX and BAK regulation of endoplasmic reticulum Ca2+: a control point for apoptosis. Science. 2003 Apr;300(5616):135-9. PubMed PMID: 12624178.

31. Danial NN, Korsmeyer SJ. Cell death: critical control points. Cell. 2004 Jan;116(2):205-19. PubMed PMID: 14744432.

32. Mandic A, Viktorsson K, Strandberg L, Heiden T, Hansson J, Linder S, et al. Calpain-mediated Bid cleavage and calpain-independent Bak modulation: two separate pathways in cisplatin-induced apoptosis. Mol Cell Biol. 2002 May;22(9):3003-13. PubMed PMID: 11940658.

33. Nakagawa T, Yuan J. Cross-talk between two cysteine protease families. Activation of caspase-12 by calpain in apoptosis. J Cell Biol. 2000 Aug;150(4):887-94. PubMed PMID: 10953012.

34. Kobayashi S, Yamashita K, Takeoka T, Ohtsuki T, Suzuki Y, Takahashi R, et al. Calpain-mediated X-linked inhibitor of apoptosis degradation in neutrophil apoptosis and its impairment in chronic neutrophilic leukemia. J Biol Chem. 2002 Sep;277(37):33968-77. PubMed PMID: 12121983.

35. McCall K. Genetic control of necrosis - another type of programmed cell death. Curr Opin Cell Biol. 2010 Dec;22(6):882-8. PubMed PMID: 20889324.

36. Halestrap AP, Doran E, Gillespie JP, O'Toole A. Mitochondria and cell death. Biochem Soc Trans. 2000 Feb;28(2):170-7. PubMed PMID: 10816121.

37. Ermak G, Davies KJ. Calcium and oxidative stress: from cell signaling to cell death. Mol Immunol. 2002 Feb;38(10):713-21. PubMed PMID: 11841831.

38. Fazi B, Bursch W, Fimia GM, Nardacci R, Piacentini M, Di Sano F, et al. Fenretinide induces autophagic cell death in caspase-defective breast cancer cells. Autophagy. 2008 May;4(4):435-41. PubMed PMID: 18259116.

39. Shimizu S, Kanaseki T, Mizushima N, Mizuta T, Arakawa-Kobayashi S, Thompson CB, et al. Role of Bcl-2 family proteins in a non-apoptotic programmed cell death dependent on autophagy genes. Nat Cell Biol. 2004 Dec;6(12):1221-8. PubMed PMID: 15558033.

40. Decuypere JP, Bultynck G, Parys JB. A dual role for Ca(2+) in autophagy regulation. Cell Calcium. 2011 Sep;50(3):242-50. PubMed PMID: 21571367.

41. Li AE, Ito H, Rovira, II, Kim KS, Takeda K, Yu ZY, et al. A role for reactive oxygen species in endothelial cell anoikis. Circulation research. 1999 Aug;85(4):304-10. PubMed PMID: 10455058.

42. Touyz RM. Reactive oxygen species as mediators of calcium signaling by angiotensin II: implications in vascular physiology and pathophysiology. Antioxidants & redox signaling. 2005 Sep-Oct;7(9-10):1302-14. PubMed PMID: 16115036.

43. Elble RC, Pauli BU. Tumor suppression by a proapoptotic calcium-activated chloride channel in mammary epithelium. J Biol Chem. 2001 Nov 276(44):40510-7. PubMed PMID: 11483609.

44. Kumar V, Abbas AK, Fausto N, Robbins SL, Cotran RS. Robbins and Cotran pathologic basis of disease. 7th ed. Philadelphia: Elsevier Saunders; 2005. 1525 p.

45. Prevarskaya N, Skryma R, Shuba Y. Calcium in tumour metastasis: new roles for known actors. Nat Rev Cancer. 2011 Aug;11(8):609-18. PubMed PMID: 21779011.

46. Hanahan D, Weinberg RA. Hallmarks of cancer: the next generation. Cell. 2011 Mar 144(5):646-74. PubMed PMID: 21376230.

47. Prevarskaya N, Ouadid-Ahidouch H, Skryma R, Shuba Y. Remodelling of Ca2+ transport in cancer: how it contributes to cancer hallmarks? Philosophical transactions of the Royal Society of London Series B, Biological sciences. 2014 Mar;369(1638):20130097. PubMed PMID: 24493745.

48. Radisky D, Muschler J, Bissell MJ. Order and disorder: the role of extracellular matrix in epithelial cancer. Cancer investigation. 2002 Jan;20(1):139-53. PubMed PMID: 11852996.

49. Wickstrom SA, Radovanac K, Fassler R. Genetic analyses of integrin signaling. Cold Spring Harb Perspect Biol. 2011 Feb;3(2). PubMed PMID: 21421914.

50. Easley CAt, Brown CM, Horwitz AF, Tombes RM. CaMK-II promotes focal adhesion turnover and cell motility by inducing tyrosine dephosphorylation of FAK and paxillin. Cell Motil Cytoskeleton. 2008 Aug;65(8):662-74. PubMed PMID: 18613116.

51. Kim MH, Lee YJ, Kim MO, Kim JS, Han HJ. Effect of leukotriene D4 on mouse embryonic stem cell migration and proliferation: involvement of PI3K/Akt as well as GSK-3beta/beta-catenin signaling pathways. J Cell Biochem. 2010 Oct;111(3):686-98. PubMed PMID: 20589831.

52. Giannone G, Ronde P, Gaire M, Beaudouin J, Haiech J, Ellenberg J, et al. Calcium rises locally trigger focal adhesion disassembly and enhance residency of focal adhesion kinase at focal adhesions. J Biol Chem. 2004 Jul 279(27):28715-23. PubMed PMID: 15102844.

53. Chan KT, Bennin DA, Huttenlocher A. Regulation of adhesion dynamics by calpain-mediated proteolysis of focal adhesion kinase (FAK). J Biol Chem. 2010 Apr;285(15):11418-26. PubMed PMID: 20150423.

54. Schneider M, Hansen JL, Sheikh SP. S100A4: a common mediator of epithelial-mesenchymal transition, fibrosis and regeneration in diseases? J Mol Med (Berl). 2008 May;86(5):507-22. PubMed PMID: 18322670.

55. Chen H, Xu C, Jin Q, Liu Z. S100 protein family in human cancer. American journal of cancer research. 2014 Mar;4(2):89-115. PubMed PMID: 24660101.

56. Lamouille S, Xu J, Derynck R. Molecular mechanisms of epithelial-mesenchymal transition. Nat Rev Mol Cell Biol. 2014 Mar;15(3):178-96. PubMed PMID: 24556840.

57. Carafoli E. The intracellular homeostasis of calcium: an overview. Ann N Y Acad Sci. 1988 Dec;551(1):147-57; discussion 57-8. PubMed PMID: 3072900.

58. Zhou Y, Xue S, Yang JJ. Calciomics: integrative studies of Ca2+-binding proteins and their interactomes in biological systems. Metallomics : integrated biometal science. 2013 Jan;5(1):29-42. PubMed PMID: 23235533.

59. Bootman MD, Collins TJ, Peppiatt CM, Prothero LS, MacKenzie L, De Smet P, et al. Calcium signalling--an overview. Semin Cell Dev Biol. 2001 Feb;12(1):3-10. PubMed PMID: 11162741.

60. Gomperts BD, Kramer IM, Tatham PER. Signal Transduction. 2nd ed. London: Elsevier; 2009. 576 p.

61. Alexander SP, Benson HE, Faccenda E, Pawson AJ, Sharman JL, McGrath JC, et al. The Concise Guide to PHARMACOLOGY 2013/14: overview. Br J Pharmacol. 2013 Dec;170(8):1449-58. PubMed PMID: 24528237.

62. Putney JW. Pharmacology of store-operated calcium channels. Mol Interv. 2010 Aug;10(4):209-18. PubMed PMID: 20729487.

63. Feske S, Gwack Y, Prakriya M, Srikanth S, Puppel SH, Tanasa B, et al. A mutation in Orai1 causes immune deficiency by abrogating CRAC channel function. Nature. 2006 May;441(7090):179-85. PubMed PMID: 16582901.

64. Yeromin AV, Zhang SL, Jiang W, Yu Y, Safrina O, Cahalan MD. Molecular identification of the CRAC channel by altered ion selectivity in a mutant of Orai. Nature. 2006 Sep;443(7108):226-9. PubMed PMID: 16921385.

65. Lewis RS. The molecular choreography of a store-operated calcium channel. Nature. 2007 Mar;446(7133):284-7. PubMed PMID: 17361175.

66. Liou J, Fivaz M, Inoue T, Meyer T. Live-cell imaging reveals sequential oligomerization and local plasma membrane targeting of stromal interaction molecule 1 after Ca2+ store depletion. Proc Natl Acad Sci U S A. 2007 May;104(22):9301-6. PubMed PMID: 17517596.

67. Park CY, Hoover PJ, Mullins FM, Bachhawat P, Covington ED, Raunser S, et al. STIM1 clusters and activates CRAC channels via direct binding of a cytosolic domain to Orai1. Cell. 2009 Mar;136(5):876-90. PubMed PMID: 19249086.

68. Yuan JP, Zeng W, Dorwart MR, Choi YJ, Worley PF, Muallem S. SOAR and the polybasic STIM1 domains gate and regulate Orai channels. Nat Cell Biol. 2009 Mar;11(3):337-43. PubMed PMID: 19182790.

69. McCarl CA, Picard C, Khalil S, Kawasaki T, Rother J, Papolos A, et al. ORAI1 deficiency and lack of store-operated Ca2+ entry cause immunodeficiency, myopathy, and ectodermal dysplasia. J Allergy Clin Immunol. 2009 Dec;124(6):1311-8 e7. PubMed PMID: 20004786.

70. Picard C, McCarl CA, Papolos A, Khalil S, Luthy K, Hivroz C, et al. STIM1 mutation associated with a syndrome of immunodeficiency and autoimmunity. N Engl J Med. 2009 May;360(19):1971-80. PubMed PMID: 19420366.

71. Yang S, Zhang JJ, Huang XY. Orai1 and STIM1 are critical for breast tumor cell migration and metastasis. Cancer Cell. 2009 Feb;15(2):124-34. PubMed PMID: 19185847.

72. McAndrew D, Grice DM, Peters AA, Davis FM, Stewart T, Rice M, et al. ORAI1-mediated calcium influx in lactation and in breast cancer. Mol Cancer Ther. 2011 Mar;10(3):448-60. PubMed PMID: 21224390.

73. Montell C. The TRP superfamily of cation channels. Sci STKE. 2005 Feb;2005(272):re3. PubMed PMID: 15728426.

74. Berridge MJ, Bootman MD, Roderick HL. Calcium signalling: dynamics, homeostasis and remodelling. Nat Rev Mol Cell Biol. 2003 Jul;4(7):517-29. PubMed PMID: 12838335.

75. Ramsey IS, Delling M, Clapham DE. An introduction to TRP channels. Annu Rev Physiol. 2006 Mar;68:619-47. PubMed PMID: 16460286.

76. Gees M, Colsoul B, Nilius B. The role of transient receptor potential cation channels in Ca2+ signaling. Cold Spring Harb Perspect Biol. 2010 Oct;2(10):a003962. PubMed PMID: 20861159.

77. Lanner JT, Georgiou DK, Joshi AD, Hamilton SL. Ryanodine receptors: structure, expression, molecular details, and function in calcium release. Cold Spring Harb Perspect Biol. 2010 Nov;2(11):a003996. PubMed PMID: 20961976.

78. Hisatsune C, Mikoshiba K. IP3 Receptor and Ca2+ Signaling. In: Lajtha A, Mikoshiba K, editors. Handbook of Neurochemistry and Molecular Neurobiology. New York: Springer US; 2009. p. 565-79.

79. Taylor CW, Taufiq Ur R, Pantazaka E. Targeting and clustering of IP3 receptors: key determinants of spatially organized Ca2+ signals. Chaos. 2009 Sep;19(3):037102. PubMed PMID: 19798811.

80. Berridge MJ, Irvine RF. Inositol phosphates and cell signalling. Nature. 1989 Sep;341(6239):197-205. PubMed PMID: 2550825.

81. Lino M. Biphasic Ca2+ dependence of inositol 1,4,5-trisphosphate-induced Ca release in smooth muscle cells of the guinea pig taenia caeci. J Gen Physiol. 1990 Jun;95(6):1103-22. PubMed PMID: 2373998.

82. Calcraft PJ, Ruas M, Pan Z, Cheng X, Arredouani A, Hao X, et al. NAADP mobilizes calcium from acidic organelles through two-pore channels. Nature. 2009 May 459(7246):596-600. PubMed PMID: 19387438.

83. Pitt SJ, Funnell TM, Sitsapesan M, Venturi E, Rietdorf K, Ruas M, et al. TPC2 is a novel NAADP-sensitive Ca2+ release channel, operating as a dual sensor of luminal pH and Ca2+. J Biol Chem. 2010 Nov;285(45):35039-46. PubMed PMID: 20720007.

84. Wang X, Zhang X, Dong XP, Samie M, Li X, Cheng X, et al. TPC proteins are phosphoinositide- activated sodium-selective ion channels in endosomes and lysosomes. Cell. 2012 Oct;151(2):372-83. PubMed PMID: 23063126.

85. Kirichok Y, Krapivinsky G, Clapham DE. The mitochondrial calcium uniporter is a highly selective ion channel. Nature. 2004 Jan;427(6972):360-4.

86. Marchi S, Pinton P. The mitochondrial calcium uniporter complex: molecular components, structure and physiopathological implications. J Physiol. 2014 Mar;592(Pt 5):829-39. PubMed PMID: 24366263.

87. Patron M, Raffaello A, Granatiero V, Tosatto A, Merli G, De Stefani D, et al. The mitochondrial calcium uniporter (MCU): molecular identity and physiological roles. J Biol Chem. 2013 Apr;288(15):10750-8. PubMed PMID: 23400777.

88. Raffaello A, De Stefani D, Sabbadin D, Teardo E, Merli G, Picard A, et al. The mitochondrial calcium uniporter is a multimer that can include a dominant-negative pore-forming subunit. EMBO J. 2013 Aug;32(17):2362-76. PubMed PMID: 23900286.

89. Curry MC, Peters AA, Kenny PA, Roberts-Thomson SJ, Monteith GR. Mitochondrial calcium uniporter silencing potentiates caspase-independent cell death in MDA-MB-231 breast cancer cells. Biochem Biophys Res Commun. 2013 May;434(3):695-700. PubMed PMID: 23602897.

90. Brini M. Plasma membrane Ca(2+)-ATPase: from a housekeeping function to a versatile signaling role. Pflugers Arch. 2009 Jan;457(3):657-64. PubMed PMID: 18548270.

91. Brini M, Carafoli E. Calcium pumps in health and disease. Physiol Rev. 2009 Oct;89(4):1341-78. PubMed PMID: 19789383.

92. Brini M, Cali T, Ottolini D, Carafoli E. The plasma membrane calcium pump in health and disease. The FEBS journal. 2013 Nov;280(21):5385-97. PubMed PMID: 23413890.

93. Strehler EE, Zacharias DA. Role of alternative splicing in generating isoform diversity among plasma membrane calcium pumps. Physiol Rev. 2001 Jan;81(1):21-50. PubMed PMID: 11152753.

94. Reinhardt TA, Filoteo AG, Penniston JT, Horst RL. Ca(2+)-ATPase protein expression in mammary tissue. Am J Physiol Cell Physiol. 2000 Nov;279(5):C1595-602. PubMed PMID: 11029307.

95. Okunade GW, Miller ML, Pyne GJ, Sutliff RL, O'Connor KT, Neumann JC, et al. Targeted ablation of plasma membrane Ca2+-ATPase (PMCA) 1 and 4 indicates a major housekeeping

function for PMCA1 and a critical role in hyperactivated sperm motility and male fertility for PMCA4. J Biol Chem. 2004 Aug;279(32):33742-50. PubMed PMID: 15178683.

96. Kozel PJ, Friedman RA, Erway LC, Yamoah EN, Liu LH, Riddle T, et al. Balance and hearing deficits in mice with a null mutation in the gene encoding plasma membrane Ca2+-ATPase isoform 2. J Biol Chem. 1998 Jul;273(30):18693-6. PubMed PMID: 9668038.

97. Oceandy D, Cartwright EJ, Emerson M, Prehar S, Baudoin FM, Zi M, et al. Neuronal nitric oxide synthase signaling in the heart is regulated by the sarcolemmal calcium pump 4b. Circulation. 2007 Jan;115(4):483-92. PubMed PMID: 17242280.

98. Lee WJ, Roberts-Thomson SJ, Monteith GR. Plasma membrane calcium-ATPase 2 and 4 in human breast cancer cell lines. Biochem Biophys Res Commun. 2005 Nov;337(3):779-83. PubMed PMID: 16216224.

99. Monteith GR, Davis FM, Roberts-Thomson SJ. Calcium channels and pumps in cancer: changes and consequences. J Biol Chem. 2012 Sep;287(38):31666-73. PubMed PMID: 22822055.

100. Aung CS, Kruger WA, Poronnik P, Roberts-Thomson SJ, Monteith GR. Plasma membrane Ca2+-ATPase expression during colon cancer cell line differentiation. Biochem Biophys Res Commun. 2007 Apr;355(4):932-6. PubMed PMID: 17321497.

101. Van Baelen K, Vanoevelen J, Missiaen L, Raeymaekers L, Wuytack F. The Golgi PMR1 P-type ATPase of Caenorhabditis elegans. Identification of the gene and demonstration of calcium and manganese transport. J Biol Chem. 2001 Apr;276(14):10683-91. PubMed PMID: 11134055.

102. Sudbrak R, Brown J, Dobson-Stone C, Carter S, Ramser J, White J, et al. Hailey-Hailey disease is caused by mutations in ATP2C1 encoding a novel Ca(2+) pump. Hum Mol Genet. 2000 Apr;9(7):1131-40. PubMed PMID: 10767338.

103. Lehotsky J, Racay P, Pavlikova M, Tatarkova Z, Urban P, Chomova M, et al. Cross-talk of intracellular calcium stores in the response to neuronal ischemia and ischemic tolerance. Gen Physiol Biophys. 2009;28 Spec No Focus:F104-14. PubMed PMID: 20093720.

104. Newbury DF, Monaco AP. Genetic advances in the study of speech and language disorders. Neuron. 2010 Oct;68(2):309-20. PubMed PMID: 20955937.

105. Baron S, Vangheluwe P, Sepulveda MR, Wuytack F, Raeymaekers L, Vanoevelen J. The secretory pathway Ca(2+)-ATPase 1 is associated with cholesterol-rich microdomains of human colon adenocarcinoma cells. Biochim Biophys Acta. 2010 Aug;1798(8):1512-21. PubMed PMID: 20363212.

106. Grice DM, Vetter I, Faddy HM, Kenny PA, Roberts-Thomson SJ, Monteith GR. Golgi calcium pump secretory pathway calcium ATPase 1 (SPCA1) is a key regulator of insulin-like growth factor receptor (IGF1R) processing in the basal-like breast cancer cell line MDA-MB-231. J Biol Chem. 2010 Nov;285(48):37458-66. PubMed PMID: 20837466.

107. Feng M, Grice DM, Faddy HM, Nguyen N, Leitch S, Wang Y, et al. Store-independent activation of Orai1 by SPCA2 in mammary tumors. Cell. 2010 Oct 143(1):84-98. PubMed PMID: 20887894.

108. Frasca F, Pandini G, Sciacca L, Pezzino V, Squatrito S, Belfiore A, et al. The role of insulin receptors and IGF-I receptors in cancer and other diseases. Arch Physiol Biochem. 2008 Feb;114(1):23-37. PubMed PMID: 18465356.

109. Peiro G, Adrover E, Sanchez-Tejada L, Lerma E, Planelles M, Sanchez-Paya J, et al. Increased insulin-like growth factor-1 receptor mRNA expression predicts poor survival in immunophenotypes of early breast carcinoma. Mod Pathol. 2011 Feb;24(2):201-8. PubMed PMID: 21057462.

110. Werner H, Bruchim I. The insulin-like growth factor-I receptor as an oncogene. Arch Physiol Biochem. 2009 May;115(2):58-71. PubMed PMID: 19485702.

111. Lytton J. Na+/Ca2+ exchangers: three mammalian gene families control Ca2+ transport. Biochem J. 2007 Sep;406(3):365-82. PubMed PMID: 17716241.

112. Jemal A, Bray F, Center MM, Ferlay J, Ward E, Forman D. Global cancer statistics. CA Cancer J Clin. 2011 Mar-Apr;61(2):69-90. PubMed PMID: 21296855.

113. DeSantis CE, Lin CC, Mariotto AB, Siegel RL, Stein KD, Kramer JL, et al. Cancer treatment and survivorship statistics, 2014. CA Cancer J Clin. 2014 Jul-Aug;64(4):252-71. PubMed PMID: 24890451.

114. GLOBOCAN. 2012 (IARC) [cited 2014 Dec]. Available from: http://globocan.iarc.fr/Pages/fact_sheets_population.aspx.

115. American Cancer Society. What are the risk factors for breast cancer? 2014 [cited 2014 Jan]. Available from: http://www.cancer.org/cancer/breastcancer/detailedguide/breast-cancer-risk-factors.

116. Song M, Lee KM, Kang D. Breast cancer prevention based on gene-environment interaction. Mol Carcinog. 2011 Apr;50(4):280-90. PubMed PMID: 21465576.

117. Florescu A, Amir E, Bouganim N, Clemons M. Immune therapy for breast cancer in 2010-hype or hope? Curr Oncol. 2011 Jan;18(1):e9-e18. PubMed PMID: 21331271.

118. Perou CM, Sorlie T, Eisen MB, van de Rijn M, Jeffrey SS, Rees CA, et al. Molecular portraits of human breast tumours. Nature. 2000 Aug;406(6797):747-52. PubMed PMID: 10963602.

119. Prat A, Perou CM. Deconstructing the molecular portraits of breast cancer. Mol Oncol. 2011 Feb;5(1):5-23. PubMed PMID: 21147047.

120. Weigel MT, Dowsett M. Current and emerging biomarkers in breast cancer: prognosis and prediction. Endocr Relat Cancer. 2010 Dec;17(4):R245-62. PubMed PMID: 20647302.

121. Sorlie T, Tibshirani R, Parker J, Hastie T, Marron JS, Nobel A, et al. Repeated observation of breast tumor subtypes in independent gene expression data sets. Proc Natl Acad Sci U S A. 2003 Jul;100(14):8418-23. PubMed PMID: 12829800.

122. Ross JS, Slodkowska EA, Symmans WF, Pusztai L, Ravdin PM, Hortobagyi GN. The HER-2 receptor and breast cancer: ten years of targeted anti-HER-2 therapy and personalized medicine. The oncologist. 2009 Apr;14(4):320-68. PubMed PMID: 19346299.

123. Wolff AC, Hammond ME, Hicks DG, Dowsett M, McShane LM, Allison KH, et al. Recommendations for human epidermal growth factor receptor 2 testing in breast cancer: American Society of Clinical Oncology/College of American Pathologists clinical practice guideline update. J Clin Oncol. 2013 Nov;31(31):3997-4013. PubMed PMID: 24101045.

124. Murphy CG, Morris PG. Recent advances in novel targeted therapies for HER2-positive breast cancer. Anti-cancer drugs. 2012 Sep;23(8):765-76. PubMed PMID: 22824822.

125. Mukai H. Treatment strategy for HER2-positive breast cancer. Int J Clin Oncol. 2010 Aug;15(4):335-40. PubMed PMID: 20632056.

126. Yardley DA, Tripathy D, Brufsky AM, Rugo HS, Kaufman PA, Mayer M, et al. Long-term survivor characteristics in HER2-positive metastatic breast cancer from registHER. Br J Cancer. 2014 May;110(11):2756-64. PubMed PMID: 24743708.

127. Roskoski R, Jr. The ErbB/HER family of protein-tyrosine kinases and cancer. Pharmacological research : the official journal of the Italian Pharmacological Society. 2014 Jan;79:34-74. PubMed PMID: 24269963.

128. Spector NL, Blackwell KL. Understanding the mechanisms behind trastuzumab therapy for human epidermal growth factor receptor 2-positive breast cancer. J Clin Oncol. 2009 Dec;27(34):5838-47. PubMed PMID: 19884552.

129. Nahta R, Esteva FJ. HER2 therapy: molecular mechanisms of trastuzumab resistance. Breast Cancer Res. 2006 Nov;8(6):215. PubMed PMID: 17096862.

130. Bacus SS, Altomare DA, Lyass L, Chin DM, Farrell MP, Gurova K, et al. AKT2 is frequently upregulated in HER-2/neu-positive breast cancers and may contribute to tumor aggressiveness by enhancing cell survival. Oncogene. 2002 May;21(22):3532-40. PubMed PMID: 12032855.

131. Makino K, Day CP, Wang SC, Li YM, Hung MC. Upregulation of IKKalpha/IKKbeta by integrin-linked kinase is required for HER2/neu-induced NF-kappaB antiapoptotic pathway. Oncogene. 2004 May;23(21):3883-7. PubMed PMID: 15021910.

132. Carter P, Presta L, Gorman CM, Ridgway JB, Henner D, Wong WL, et al. Humanization of an anti-p185HER2 antibody for human cancer therapy. Proc Natl Acad Sci U S A. 1992 May;89(10):4285-9. PubMed PMID: 1350088.

133. Romond EH, Perez EA, Bryant J, Suman VJ, Geyer CE, Jr., Davidson NE, et al. Trastuzumab plus adjuvant chemotherapy for operable HER2-positive breast cancer. N Engl J Med. 2005 Oct;353(16):1673-84. PubMed PMID: 16236738.

134. Slamon DJ, Leyland-Jones B, Shak S, Fuchs H, Paton V, Bajamonde A, et al. Use of chemotherapy plus a monoclonal antibody against HER2 for metastatic breast cancer that overexpresses HER2. N Engl J Med. 2001 Mar;344(11):783-92. PubMed PMID: 11248153.

135. Baselga J. Current and planned clinical trials with trastuzumab (Herceptin). Seminars in oncology. 2000 Oct;27(5 Suppl 9):27-32. PubMed PMID: 11049054.

136. Pegram MD, Konecny G, Slamon DJ. The molecular and cellular biology of HER2/neu gene amplification/overexpression and the clinical development of herceptin (trastuzumab) therapy for breast cancer. Advances in Breast Cancer Management. 103. 2000/08/19 ed. New York: Springer US; 2000. p. 57-75.

137. Verma S, Miles D, Gianni L, Krop IE, Welslau M, Baselga J, et al. Trastuzumab emtansine for HER2-positive advanced breast cancer. N Engl J Med. 2012 Nov;367(19):1783-91. PubMed PMID: 23020162.

138. O'Sullivan CC, Smith KL. Therapeutic Considerations in Treating HER2-Positive Metastatic Breast Cancer. Current breast cancer reports. 2014 Sep;6(3):169-82. PubMed PMID: 25285186.

139. Krop IE, LoRusso P, Miller KD, Modi S, Yardley D, Rodriguez G, et al. A phase II study of trastuzumab emtansine in patients with human epidermal growth factor receptor 2-positive metastatic breast cancer who were previously treated with trastuzumab, lapatinib, an anthracycline, a taxane, and capecitabine. J Clin Oncol. 2012 Sep;30(26):3234-41. PubMed PMID: 22649126.

140. Nahta R, Esteva FJ. Trastuzumab: triumphs and tribulations. Oncogene. 2007 May;26(25):3637-43. PubMed PMID: 17530017.

141. Holohan C, Van Schaeybroeck S, Longley DB, Johnston PG. Cancer drug resistance: an evolving paradigm. Nat Rev Cancer. 2013 Oct;13(10):714-26. PubMed PMID: 24060863.

142. Krishan A, Fitz CM, Andritsch I. Drug retention, efflux, and resistance in tumor cells. Cytometry. 1997 Dec 29(4):279-85. PubMed PMID: 9415409.

143. Gottesman MM. Mechanisms of cancer drug resistance. Annu Rev Med. 2002 Feb;53:615-27. PubMed PMID: 11818492.

144. Lissandron V, Podini P, Pizzo P, Pozzan T. Unique characteristics of Ca2+ homeostasis of the trans-Golgi compartment. Proc Natl Acad Sci U S A. 2010 May;107(20):9198-203. PubMed PMID: 20439740.

145. Solyanik GI. Multifactorial nature of tumor drug resistance. Exp Oncol. 2010 Sep;32(3):181-5. PubMed PMID: 21403614.

146. Nahta R, Esteva FJ. Herceptin: mechanisms of action and resistance. Cancer Lett. 2006 Feb;232(2):123-38. PubMed PMID: 16458110.

147. Brufsky A. Trastuzumab-based therapy for patients with HER2-positive breast cancer: from early scientific development to foundation of care. Am J Clin Oncol. 2010 Apr;33(2):186-95. PubMed PMID: 19675448.

148. Morrow PK, Wulf GM, Ensor J, Booser DJ, Moore JA, Flores PR, et al. Phase I/II study of trastuzumab in combination with everolimus (RAD001) in patients with HER2-overexpressing metastatic breast cancer who progressed on trastuzumab-based therapy. J Clin Oncol. 2011 Aug;29(23):3126-32. PubMed PMID: 21730275.

149. Tanner M, Kapanen AI, Junttila T, Raheem O, Grenman S, Elo J, et al. Characterization of a novel cell line established from a patient with Herceptin-resistant breast cancer. Mol Cancer Ther. 2004 Dec;3(12):1585-92. PubMed PMID: 15634652.

150. Hubalek M, Brunner C, Mattha K, Marth C. Resistance to HER2-targeted therapy: mechanisms of trastuzumab resistance and possible strategies to overcome unresponsiveness to treatment. Wien Med Wochenschr. 2010 Nov;160(19-20):506-12. PubMed PMID: 20972709.

151. Chung A, Cui X, Audeh W, Giuliano A. Current status of anti-human epidermal growth factor receptor 2 therapies: predicting and overcoming herceptin resistance. Clin Breast Cancer. 2013 Aug;13(4):223-32. PubMed PMID: 23829888.

152. Motoyama AB, Hynes NE, Lane HA. The efficacy of ErbB receptor-targeted anticancer therapeutics is influenced by the availability of epidermal growth factor-related peptides. Cancer Res. 2002 Jun;62(11):3151-8. PubMed PMID: 12036928.

153. Agus DB, Akita RW, Fox WD, Lewis GD, Higgins B, Pisacane PI, et al. Targeting ligand-activated ErbB2 signaling inhibits breast and prostate tumor growth. Cancer Cell. 2002 Aug;2(2):127-37. PubMed PMID: 12204533.

154. Gajria D, Chandarlapaty S. HER2-amplified breast cancer: mechanisms of trastuzumab resistance and novel targeted therapies. Expert review of anticancer therapy. 2011 Feb;11(2):263-75. PubMed PMID: 21342044.

155. Nahta R, Yuan LX, Zhang B, Kobayashi R, Esteva FJ. Insulin-like growth factor-I receptor/human epidermal growth factor receptor 2 heterodimerization contributes to trastuzumab resistance of breast cancer cells. Cancer Res. 2005 Dec;65(23):11118-28. PubMed PMID: 16322262.

156. O'Brien NA, Browne BC, Chow L, Wang Y, Ginther C, Arboleda J, et al. Activated phosphoinositide 3-kinase/AKT signaling confers resistance to trastuzumab but not lapatinib. Mol Cancer Ther. 2010 Jun;9(6):1489-502. PubMed PMID: 20501798.

157. Nagata Y, Lan KH, Zhou X, Tan M, Esteva FJ, Sahin AA, et al. PTEN activation contributes to tumor inhibition by trastuzumab, and loss of PTEN predicts trastuzumab resistance in patients. Cancer Cell. 2004 Aug;6(2):117-27. PubMed PMID: 15324695.

158. Huang X, Gao L, Wang S, McManaman JL, Thor AD, Yang X, et al. Heterotrimerization of the growth factor receptors erbB2, erbB3, and insulin-like growth factor-i receptor in breast cancer cells resistant to herceptin. Cancer Res. 2010 Feb 70(3):1204-14. PubMed PMID: 20103628.

159. Roberts-Thomson SJ, Curry MC, Monteith GR. Plasma membrane calcium pumps and their emerging roles in cancer. World J Biol Chem. 2010 Aug;1(8):248-53. PubMed PMID: 21537481.

160. Hoffmann EK, Lambert IH. Ion channels and transporters in the development of drug resistance in cancer cells. Philosophical transactions of the Royal Society of London Series B, Biological sciences. 2014 Mar;369(1638):20130109. PubMed PMID: 24493757.

161. Flourakis M, Lehen'kyi V, Beck B, Raphael M, Vandenberghe M, Abeele FV, et al. Orai1 contributes to the establishment of an apoptosis-resistant phenotype in prostate cancer cells. Cell Death Dis. 2010 Sep;1(9):e75. PubMed PMID: 21364678.

162. Yanamandra N, Buzzeo RW, Gabriel M, Hazlehurst LA, Mari Y, Beaupre DM, et al. Tipifarnib-induced apoptosis in acute myeloid leukemia and multiple myeloma cells depends on Ca2+ influx through plasma membrane Ca2+ channels. J Pharmacol Exp Ther. 2011 Jun;337(3):636-43. PubMed PMID: 21378206.

163. Lehen'kyi V, Flourakis M, Skryma R, Prevarskaya N. TRPV6 channel controls prostate cancer cell proliferation via Ca(2+)/NFAT-dependent pathways. Oncogene. 2007 Nov;26(52):7380-5. PubMed PMID: 17533368.

164. Monet M, Lehen'kyi V, Gackiere F, Firlej V, Vandenberghe M, Roudbaraki M, et al. Role of cationic channel TRPV2 in promoting prostate cancer migration and progression to androgen resistance. Cancer Res. 2010 Feb;70(3):1225-35. PubMed PMID: 20103638.

165. Liu G, Hu X, Varani J, Chakrabarty S. Calcium and calcium sensing receptor modulates the expression of thymidylate synthase, NAD(P)H:quinone oxidoreductase 1 and survivin in human colon carcinoma cells: promotion of cytotoxic response to mitomycin C and fluorouracil. Mol Carcinog. 2009 Mar;48(3):202-11. PubMed PMID: 18618519.

166. Shiota M, Tsunoda T, Song Y, Yokomizo A, Tada Y, Oda Y, et al. Enhanced S100 calcium-binding protein P expression sensitizes human bladder cancer cells to cisplatin. BJU Int. 2011 Apr;107(7):1148-53. PubMed PMID: 20726978.

167. Schrodl K, Oelmez H, Edelmann M, Huber RM, Bergner A. Altered Ca2+-homeostasis of cisplatin-treated and low level resistant non-small-cell and small-cell lung cancer cells. Cell Oncol. 2009 Jul;31(4):301-15. PubMed PMID: 19633366.

168. Chen Y, Tseng SH. The Potential of Tetrandrine against Gliomas. Anticancer Agents Med Chem. 2010 Sep;10(7):534-42. PubMed PMID: 20879981.

169. Lee EL, Hasegawa Y, Shimizu T, Okada Y. IK1 channel activity contributes to cisplatin sensitivity of human epidermoid cancer cells. Am J Physiol Cell Physiol. 2008 Jun;294(6):C1398-406. PubMed PMID: 18367588.

170. Savas S, Briollais L, Ibrahim-zada I, Jarjanazi H, Choi YH, Musquera M, et al. A whole-genome SNP association study of NCI60 cell line panel indicates a role of Ca2+ signaling in selenium resistance. PLoS One. 2010 Sep;5(9):e12601. PubMed PMID: 20830292.

171. Stevenson L, Allen WL, Proutski I, Stewart G, Johnston L, McCloskey K, et al. Calbindin 2 (CALB2) regulates 5-fluorouracil sensitivity in colorectal cancer by modulating the intrinsic apoptotic pathway. PLoS One. 2011 May;6(5):e20276. PubMed PMID: 21629658.

172. Peng X, Gong F, Xie G, Zhao Y, Tang M, Yu L, et al. A proteomic investigation into adriamycin chemo-resistance of human leukemia K562 cells. Mol Cell Biochem. 2011 May;351(1-2):233-41. PubMed PMID: 21243406.

173. He Q, Zhang G, Hou D, Leng A, Xu M, Peng J, et al. Overexpression of sorcin results in multidrug resistance in gastric cancer cells with up-regulation of P-gp. Oncol Rep. 2011 Jan;25(1):237-43. PubMed PMID: 21109982.

174. Qu Y, Yang Y, Liu B, Xiao W. Comparative proteomic profiling identified sorcin being associated with gemcitabine resistance in non-small cell lung cancer. Med Oncol. 2010 Dec;27(4):1303-8. PubMed PMID: 20012234.

175. Landriscina M, Laudiero G, Maddalena F, Amoroso MR, Piscazzi A, Cozzolino F, et al. Mitochondrial chaperone Trap1 and the calcium binding protein Sorcin interact and protect cells against apoptosis induced by antiblastic agents. Cancer Res. 2010 Aug;70(16):6577-86. PubMed PMID: 20647321.

176. Zhong F, Harr MW, Bultynck G, Monaco G, Parys JB, De Smedt H, et al. Induction of Ca(2)+-driven apoptosis in chronic lymphocytic leukemia cells by peptide-mediated disruption of Bcl-2-IP3 receptor interaction. Blood. 2011 Mar;117(10):2924-34. PubMed PMID: 21193695.

177. Li Z, Xu X, Bai L, Chen W, Lin Y. Epidermal growth factor receptor-mediated tissue transglutaminase overexpression couples acquired tumor necrosis factor-related apoptosis-inducing ligand resistance and migration through c-FLIP and MMP-9 proteins in lung cancer cells. J Biol Chem. 2011 Jun;286(24):21164-72. PubMed PMID: 21525012.

178. Liu G, Hu X, Chakrabarty S. Calcium sensing receptor down-regulates malignant cell behavior and promotes chemosensitivity in human breast cancer cells. Cell Calcium. 2009 Mar;45(3):216-25. PubMed PMID: 19038444.

179. Liu R, Zhang Y, Chen Y, Qi J, Ren S, Xushi MY, et al. A novel calmodulin antagonist O-(4-ethoxyl-butyl)-berbamine overcomes multidrug resistance in drug-resistant MCF-7/ADR breast carcinoma cells. J Pharm Sci. 2010 Jul;99(7):3266-75. PubMed PMID: 20112430.

180. McCubrey JA, Abrams SL, Stadelman K, Chappell WH, Lahair M, Ferland RA, et al. Targeting signal transduction pathways to eliminate chemotherapeutic drug resistance and cancer stem cells. Adv Enzyme Regul. 2010;50(1):285-307. PubMed PMID: 19895837.

181. McIlroy M, McCartan D, Early S, P OG, Pennington S, Hill AD, et al. Interaction of developmental transcription factor HOXC11 with steroid receptor coactivator SRC-1 mediates resistance to endocrine therapy in breast cancer [corrected]. Cancer Res. 2010 Feb;70(4):1585-94. PubMed PMID: 20145129.

182. VanHouten J, Sullivan C, Bazinet C, Ryoo T, Camp R, Rimm DL, et al. PMCA2 regulates apoptosis during mammary gland involution and predicts outcome in breast cancer. Proc Natl Acad Sci U S A. 2010 Jun;107(25):11405-10. PubMed PMID: 20534448.

183. Baggott RR, Mohamed TM, Oceandy D, Holton M, Blanc MC, Roux-Soro SC, et al. Disruption of the interaction between PMCA2 and calcineurin triggers apoptosis and enhances paclitaxel-induced cytotoxicity in breast cancer cells. Carcinogenesis. 2012 Dec;33(12):2362-8. PubMed PMID: 22962307.

184. Kim DS, Han BG, Park KS, Lee BI, Kim SY, Bae CD. I-kappaBalpha depletion by transglutaminase 2 and mu-calpain occurs in parallel with the ubiquitin-proteasome pathway. Biochem Biophys Res Commun. 2010 Aug;399(2):300-6. PubMed PMID: 20659425.

185. Xia W, Bacus S, Husain I, Liu L, Zhao S, Liu Z, et al. Resistance to ErbB2 tyrosine kinase inhibitors in breast cancer is mediated by calcium-dependent activation of RelA. Mol Cancer Ther. 2010 Feb;9(2):292-9. PubMed PMID: 20124457.

186. Adams TE, Epa VC, Garrett TP, Ward CW. Structure and function of the type 1 insulin-like growth factor receptor. Cellular and molecular life sciences : CMLS. 2000 Jul;57(7):1050-93. PubMed PMID: 10961344.

187. Ouban A, Muraca P, Yeatman T, Coppola D. Expression and distribution of insulin-like growth factor-1 receptor in human carcinomas. Human pathology. 2003 Aug;34(8):803-8. PubMed PMID: 14506643.

188. Yerushalmi R, Gelmon KA, Leung S, Gao D, Cheang M, Pollak M, et al. Insulin-like growth factor receptor (IGF-1R) in breast cancer subtypes. Breast Cancer Res Treat. 2012 Feb;132(1):131-42. PubMed PMID: 21574055.

189. Jin Q, Esteva FJ. Cross-talk between the ErbB/HER family and the type I insulin-like growth factor receptor signaling pathway in breast cancer. J Mammary Gland Biol Neoplasia. 2008 Dec;13(4):485-98. PubMed PMID: 19034632.

190. Browne BC, Crown J, Venkatesan N, Duffy MJ, Clynes M, Slamon D, et al. Inhibition of IGF1R activity enhances response to trastuzumab in HER-2-positive breast cancer cells. Ann Oncol. 2011 Jan;22(1):68-73. PubMed PMID: 20647220.

191. Kostler WJ, Hudelist G, Rabitsch W, Czerwenka K, Muller R, Singer CF, et al. Insulin-like growth factor-1 receptor (IGF-1R) expression does not predict for resistance to trastuzumab-based treatment in patients with Her-2/neu overexpressing metastatic breast cancer. Journal of cancer research and clinical oncology. 2006 Jan;132(1):9-18. PubMed PMID: 16184380.

192. Dokmanovic M, Shen Y, Bonacci TM, Hirsch DS, Wu WJ. Trastuzumab regulates IGFBP-2 and IGFBP-3 to mediate growth inhibition: implications for the development of predictive biomarkers for trastuzumab resistance. Mol Cancer Ther. 2011 Jun;10(6):917-28. PubMed PMID: 21487052.

193. Guha M, Srinivasan S, Biswas G, Avadhani NG. Activation of a novel calcineurin-mediated insulin-like growth factor-1 receptor pathway, altered metabolism, and tumor cell invasion in cells subjected to mitochondrial respiratory stress. J Biol Chem. 2007 May;282(19):14536-46. PubMed PMID: 17355970.

194. Gilmore TD. The Rel/NF-kappaB signal transduction pathway: introduction. Oncogene. 1999 Nov;18(49):6842-4. PubMed PMID: 10602459.

195. Prasad S, Ravindran J, Aggarwal BB. NF-kappaB and cancer: how intimate is this relationship. Mol Cell Biochem. 2010 Mar;336(1-2):25-37. PubMed PMID: 19823771.

196. Lilienbaum A, Israel A. From calcium to NF-kappa B signaling pathways in neurons. Mol Cell Biol. 2003 Apr;23(8):2680-98. PubMed PMID: 12665571.

197. Romieu-Mourez R, Landesman-Bollag E, Seldin DC, Traish AM, Mercurio F, Sonenshein GE. Roles of IKK kinases and protein kinase CK2 in activation of nuclear factor-kappaB in breast cancer. Cancer Res. 2001 May;61(9):3810-8. PubMed PMID: 11325857.

198. Huang WC, Chai CY, Chen WC, Hou MF, Wang YS, Chiu YC, et al. Histamine regulates cyclooxygenase 2 gene activation through Orai1-mediated NFkappaB activation in lung cancer cells. Cell Calcium. 2011 Jul;50(1):27-35. PubMed PMID: 21605904.

199. Schoolmeesters A, Brown DD, Fedorov Y. Kinome-wide functional genomics screen reveals a novel mechanism of TNFalpha-induced nuclear accumulation of the HIF-1alpha transcription factor in cancer cells. PLoS One. 2012 Feb;7(2):e31270. PubMed PMID: 22355351.

200. Mann AP, Verma A, Sethi G, Manavathi B, Wang H, Fok JY, et al. Overexpression of tissue transglutaminase leads to constitutive activation of nuclear factor-kappaB in cancer cells: delineation of a novel pathway. Cancer Res. 2006 Sep;66(17):8788-95. PubMed PMID: 16951195.

201. Storr SJ, Carragher NO, Frame MC, Parr T, Martin SG. The calpain system and cancer. Nat Rev Cancer. 2011 May;11(5):364-74. PubMed PMID: 21508973.

202. Storr SJ, Woolston CM, Barros FF, Green AR, Shehata M, Chan SY, et al. Calpain-1 expression is associated with relapse-free survival in breast cancer patients treated with trastuzumab following adjuvant chemotherapy. Int J Cancer. 2011 Oct;129(7):1773-80. PubMed PMID: 21140455.

203. Pianetti S, Arsura M, Romieu-Mourez R, Coffey RJ, Sonenshein GE. Her-2/neu overexpression induces NF-kappaB via a PI3-kinase/Akt pathway involving calpain-mediated degradation of IkappaB-alpha that can be inhibited by the tumor suppressor PTEN. Oncogene. 2001 Mar;20(11):1287-99. PubMed PMID: 11313873.

204. Kulkarni S, Reddy KB, Esteva FJ, Moore HC, Budd GT, Tubbs RR. Calpain regulates sensitivity to trastuzumab and survival in HER2-positive breast cancer. Oncogene. 2010 Mar;29(9):1339-50. PubMed PMID: 19946330.

205. Sareen D, Darjatmoko SR, Albert DM, Polans AS. Mitochondria, calcium, and calpain are key mediators of resveratrol-induced apoptosis in breast cancer. Mol Pharmacol. 2007 Dec;72(6):1466-75. PubMed PMID: 17848600.

206. Louis M, Zanou N, Van Schoor M, Gailly P. TRPC1 regulates skeletal myoblast migration and differentiation. J Cell Sci. 2008 Dec 121(Pt 23):3951-9. PubMed PMID: 19001499.

207. Chen YF, Chiu WT, Chen YT, Lin PY, Huang HJ, Chou CY, et al. Calcium store sensor stromal-interaction molecule 1-dependent signaling plays an important role in cervical cancer growth, migration, and angiogenesis. Proc Natl Acad Sci U S A. 2011 Sep;108(37):15225-30. PubMed PMID: 21876174.

208. Neve RM, Chin K, Fridlyand J, Yeh J, Baehner FL, Fevr T, et al. A collection of breast cancer cell lines for the study of functionally distinct cancer subtypes. Cancer Cell. 2006 Dec;10(6):515-27. PubMed PMID: 17157791.

209. Barok M, Isola J, Palyi-Krekk Z, Nagy P, Juhasz I, Vereb G, et al. Trastuzumab causes antibody-dependent cellular cytotoxicity-mediated growth inhibition of submacroscopic JIMT-1 breast cancer xenografts despite intrinsic drug resistance. Mol Cancer Ther. 2007 Jul;6(7):2065-72. PubMed PMID: 17620435.

210. ATCC. SKBR3 product description [cited 2011 Sep]. Available from: http://www.lgcstandards-atcc.org/Products/All/HTB-30.aspx.

211. Bacus SS, Kiguchi K, Chin D, King CR, Huberman E. Differentiation of cultured human breast cancer cells (AU-565 and MCF-7) associated with loss of cell surface HER-2/neu antigen. Mol Carcinog. 1990 Jul;3(6):350-62. PubMed PMID: 1980588.

212. Lasfargues EY, Coutinho WG, Redfield ES. Isolation of two human tumor epithelial cell lines from solid breast carcinomas. J Natl Cancer Inst. 1978 Oct;61(4):967-78. PubMed PMID: 212572.

213. Gazdar AF, Kurvari V, Virmani A, Gollahon L, Sakaguchi M, Westerfield M, et al. Characterization of paired tumor and non-tumor cell lines established from patients with breast cancer. Int J Cancer. 1998 Dec 78(6):766-74. PubMed PMID: 9833771.

214. Cailleau R, Young R, Olive M, Reeves WJ, Jr. Breast tumor cell lines from pleural effusions. J Natl Cancer Inst. 1974 Sep;53(3):661-74. PubMed PMID: 4412247.

215. Garcia R, Yu CL, Hudnall A, Catlett R, Nelson KL, Smithgall T, et al. Constitutive activation of Stat3 in fibroblasts transformed by diverse oncoproteins and in breast carcinoma cells. Cell Growth Differ. 1997 Dec;8(12):1267-76. PubMed PMID: 9419415.

216. Forozan F, Veldman R, Ammerman CA, Parsa NZ, Kallioniemi A, Kallioniemi OP, et al. Molecular cytogenetic analysis of 11 new breast cancer cell lines. Br J Cancer. 1999 Dec;81(8):1328-34. PubMed PMID: 10604729.

217. ATCC. UACC732 Product description [cited 2014 Jun]. Available from: http://www.lgcstandards-atcc.org/Products/All/CRL-3166.aspx.

218. Meltzer P, Leibovitz A, Dalton W, Villar H, Kute T, Davis J, et al. Establishment of two new cell lines derived from human breast carcinomas with HER-2/neu amplification. Br J Cancer. 1991 May;63(5):727-35. PubMed PMID: 1674877.

219. Engel LW, Young NA, Tralka TS, Lippman ME, O'Brien SJ, Joyce MJ. Establishment and characterization of three new continuous cell lines derived from human breast carcinomas. Cancer Res. 1978 Oct;38(10):3352-64. PubMed PMID: 688225.

220. Reid Y SD, authors; Riss T, Minor L. Authentication of Human Cell Lines by STR DNA Profiling Analysis. Assay Guidance Manual. Bethesda (MD): Eli Lilly & Company and the National Center for Advancing Translational Sciences; 2013.

221. Davis FM, Azimi I, Faville RA, Peters AA, Jalink K, Putney JW, Jr., et al. Induction of epithelial-mesenchymal transition (EMT) in breast cancer cells is calcium signal dependent. Oncogene. 2014 May;33(18):2307-16. PubMed PMID: 23686305.

222. de Cremoux P, Tran-Perennou C, Brockdorff BL, Boudou E, Brunner N, Magdelenat H, et al. Validation of real-time RT-PCR for analysis of human breast cancer cell lines resistant or sensitive to treatment with antiestrogens. Endocr Relat Cancer. 2003 Sep;10(3):409-18. PubMed PMID: 14503918.

223. Kutyavin IV, Afonina IA, Mills A, Gorn VV, Lukhtanov EA, Belousov ES, et al. 3'-minor groove binder-DNA probes increase sequence specificity at PCR extension temperatures. Nucleic acids research. 2000 Jan;28(2):655-61. PubMed PMID: 10606668.

224. Davis FM, Kenny PA, Soo ET, van Denderen BJ, Thompson EW, Cabot PJ, et al. Remodeling of purinergic receptor-mediated Ca2+ signaling as a consequence of EGF-induced epithelial-mesenchymal transition in breast cancer cells. PLoS One. 2011 Aug;6(8):e23464. PubMed PMID: 21850275.

225. Livak KJ, Schmittgen TD. Analysis of relative gene expression data using real-time quantitative PCR and the 2(-Delta Delta C(T)) Method. Methods (San Diego, Calif). 2001 Dec;25(4):402-8. PubMed PMID: 11846609.

226. Lee SH, Sinko PJ. siRNA--getting the message out. Eur J Pharm Sci. 2006 Apr;27(5):401-10. PubMed PMID: 16442784.

227. Anderson EM, Birmingham A, Baskerville S, Reynolds A, Maksimova E, Leake D, et al. Experimental validation of the importance of seed complement frequency to siRNA specificity. RNA. 2008 May;14(5):853-61. PubMed PMID: 18367722.

228. Lee WJ, Roberts-Thomson SJ, Holman NA, May FJ, Lehrbach GM, Monteith GR. Expression of plasma membrane calcium pump isoform mRNAs in breast cancer cell lines. Cell Signal. 2002 Dec;14(12):1015-22. PubMed PMID: 12359307.

229. Invitrogen. Click-iT® EdU Alexa Fluor® 555 Imaging Kit. July 2011.

230. Tanious FA, Veal JM, Buczak H, Ratmeyer LS, Wilson WD. DAPI (4',6-diamidino-2-phenylindole) binds differently to DNA and RNA: minor-groove binding at AT sites and intercalation at AU sites. Biochemistry. 1992 Mar;31(12):3103-12. PubMed PMID: 1372825.

231. Promega. CellTiter 96® AQueous Non-Radioactive Cell Proliferation Assay Technical Bulletin. 2012.

232. Putney JW. Calcium Signaling. 2nd ed. Boca Raton: CRC/Taylor & Francis; 2006. 536 p.

233. Gee KR, Brown KA, Chen WN, Bishop-Stewart J, Gray D, Johnson I. Chemical and physiological characterization of fluo-4 Ca(2+)-indicator dyes. Cell Calcium. 2000 Feb;27(2):97-106. PubMed PMID: 10756976.

234. Schroeder KS. FLIPR: A New Instrument for Accurate, High Throughput Optical Screening. Journal of Biomolecular Screening. 1996 Mar;1(2):75-80.

235. Takahashi A, Camacho P, Lechleiter JD, Herman B. Measurement of intracellular calcium. Physiol Rev. 1999 Oct;79(4):1089-125. PubMed PMID: 10508230.

236. Jacot JG, McCulloch AD, Omens JH. Substrate stiffness affects the functional maturation of neonatal rat ventricular myocytes. Biophys J. 2008 Oct;95(7):3479-87. PubMed PMID: 18586852.

237. Schmidt S, Mo M, Heidrich FM, Celic A, Ehrlich BE. C-terminal domain of chromogranin B regulates intracellular calcium signaling. J Biol Chem. 2011 Dec;286(52):44888-96. PubMed PMID: 22016391.

238. Davis FM, Peters AA, Grice DM, Cabot PJ, Parat MO, Roberts-Thomson SJ, et al. Non-stimulated, agonist-stimulated and store-operated Ca2+ influx in MDA-MB-468 breast cancer cells and the effect of EGF-induced EMT on calcium entry. PLoS One. 2012 May;7(5):e36923. PubMed PMID: 22666335.

239. Gronski MA, Kinchen JM, Juncadella IJ, Franc NC, Ravichandran KS. An essential role for calcium flux in phagocytes for apoptotic cell engulfment and the anti-inflammatory response. Cell Death Differ. 2009 Oct;16(10):1323-31. PubMed PMID: 19461656.

240. Towbin H, Staehelin T, Gordon J. Electrophoretic transfer of proteins from polyacrylamide gels to nitrocellulose sheets: procedure and some applications. Proc Natl Acad Sci U S A. 1979 Sep;76(9):4350-4. PubMed PMID: 388439.

241. Stauffer TP, Hilfiker H, Carafoli E, Strehler EE. Quantitative analysis of alternative splicing options of human plasma membrane calcium pump genes. J Biol Chem. 1993 Dec;268(34):25993-6003. PubMed PMID: 8245032.

242. Brailoiu E, Churamani D, Cai X, Schrlau MG, Brailoiu GC, Gao X, et al. Essential requirement for two-pore channel 1 in NAADP-mediated calcium signaling. J Cell Biol. 2009 Jul;186(2):201-9. PubMed PMID: 19620632.

243. Jahidin AH, Davis FM, Roberts-Thomson SJ, Monteith GR. Two-pore channels in breast cancer cells. 24 EORTC-NCI-AACR Symposium on Molecular Targets and Cancer Therapeutics; Nov; Dublin2012. p. 156.

244. Dhennin-Duthille I, Gautier M, Faouzi M, Guilbert A, Brevet M, Vaudry D, et al. High expression of transient receptor potential channels in human breast cancer epithelial cells and tissues: correlation with pathological parameters. Cellular physiology and biochemistry : international journal of experimental cellular physiology, biochemistry, and pharmacology. 2011 Nov;28(5):813-22. PubMed PMID: 22178934.

245. Middelbeek J, Kuipers AJ, Henneman L, Visser D, Eidhof I, van Horssen R, et al. TRPM7 is required for breast tumor cell metastasis. Cancer Res. 2012 Aug;72(16):4250-61. PubMed PMID: 22871386.

246. Bolanz KA, Hediger MA, Landowski CP. The role of TRPV6 in breast carcinogenesis. Mol Cancer Ther. 2008 Feb;7(2):271-9. PubMed PMID: 18245667.

247. Jung C, Fandos C, Lorenzo IM, Plata C, Fernandes J, Gene GG, et al. The progesterone receptor regulates the expression of TRPV4 channel. Pflugers Arch. 2009 Nov;459(1):105-13. PubMed PMID: 19701771.

248. Jamaludin SYN, Davis FM, Peters AA, Gonda TJ, Roberts-Thomson SJ, Monteith GR. TRPV4 channels in basal-like breast cancer cells. 24 EORTC-NCI-AACR Symposium on Molecular Targets and Cancer Therapeutics; Nov; Dublin2012. p. 155-6.

249. Aydar E, Yeo S, Djamgoz M, Palmer C. Abnormal expression, localization and interaction of canonical transient receptor potential ion channels in human breast cancer cell lines and tissues: a potential target for breast cancer diagnosis and therapy. Cancer cell international. 2009 Aug;9:23. PubMed PMID: 19689790.

250. Burnstock G, Di Virgilio F. Purinergic signalling and cancer. Purinergic signalling. 2013 Dec;9(4):491-540. PubMed PMID: 23797685.

251. Robinson JA, Jenkins NS, Holman NA, Roberts-Thomson SJ, Monteith GR. Ratiometric and nonratiometric Ca2+ indicators for the assessment of intracellular free Ca2+ in a breast cancer cell line using a fluorescence microplate reader. Journal of biochemical and biophysical methods. 2004 Mar;58(3):227-37. PubMed PMID: 15026209.

252. Fu T, Xu Y, Jiang W, Zhang H, Zhu P, Wu J. EGF receptor-mediated intracellular calcium increase in human hepatoma BEL-7404 cells. Cell Res. 1994 Dec;4(2):145-53.

253. Li YW, Zhu GY, Shen XL, Chu JH, Yu ZL, Fong WF. Furanodienone induces cell cycle arrest and apoptosis by suppressing EGFR/HER2 signaling in HER2-overexpressing human breast cancer cells. Cancer Chemother Pharmacol. 2011 Nov;68(5):1315-23. PubMed PMID: 21461888.

254. Yoshida J, Iwabuchi K, Matsui T, Ishibashi T, Masuoka T, Nishio M. Knockdown of stromal interaction molecule 1 (STIM1) suppresses store-operated calcium entry, cell proliferation and tumorigenicity in human epidermoid carcinoma A431 cells. Biochemical pharmacology. 2012 Dec;84(12):1592-603. PubMed PMID: 23022228.

255. Pereira GJ, Hirata H, Fimia GM, do Carmo LG, Bincoletto C, Han SW, et al. Nicotinic acid adenine dinucleotide phosphate (NAADP) regulates autophagy in cultured astrocytes. J Biol Chem. 2011 Aug;286(32):27875-81. PubMed PMID: 21610076.

256. Huang X, Godfrey TE, Gooding WE, McCarty KS, Jr., Gollin SM. Comprehensive genome and transcriptome analysis of the 11q13 amplicon in human oral cancer and synteny to the 7F5 amplicon in murine oral carcinoma. Genes, chromosomes & cancer. 2006 Nov;45(11):1058-69. PubMed PMID: 16906560.

257. Cui M, Honore P, Zhong C, Gauvin D, Mikusa J, Hernandez G, et al. TRPV1 receptors in the CNS play a key role in broad-spectrum analgesia of TRPV1 antagonists. The Journal of neuroscience : the official journal of the Society for Neuroscience. 2006 Sep;26(37):9385-93. PubMed PMID: 16971522.

258. Domotor A, Peidl Z, Vincze A, Hunyady B, Szolcsanyi J, Kereskay L, et al. Immunohistochemical distribution of vanilloid receptor, calcitonin-gene related peptide and substance P in gastrointestinal mucosa of patients with different gastrointestinal disorders. Inflammopharmacology. 2005 Aug;13(1-3):161-77. PubMed PMID: 16259736.

259. Hartel M, di Mola FF, Selvaggi F, Mascetta G, Wente MN, Felix K, et al. Vanilloids in pancreatic cancer: potential for chemotherapy and pain management. Gut. 2006 Apr;55(4):519-28. PubMed PMID: 16174661.

260. Lazzeri M, Vannucchi MG, Spinelli M, Bizzoco E, Beneforti P, Turini D, et al. Transient receptor potential vanilloid type 1 (TRPV1) expression changes from normal urothelium to transitional cell carcinoma of human bladder. European urology. 2005 Oct;48(4):691-8. PubMed PMID: 15992990.

261. Sanchez MG, Sanchez AM, Collado B, Malagarie-Cazenave S, Olea N, Carmena MJ, et al. Expression of the transient receptor potential vanilloid 1 (TRPV1) in LNCaP and PC-3 prostate cancer cells and in human prostate tissue. Eur J Pharmacol. 2005 May;515(1-3):20-7. PubMed PMID: 15913603.

262. Waning J, Vriens J, Owsianik G, Stuwe L, Mally S, Fabian A, et al. A novel function of capsaicin-sensitive TRPV1 channels: involvement in cell migration. Cell Calcium. 2007 Jul;42(1):17-25. PubMed PMID: 17184838.

263. Le XF, Vadlamudi R, McWatters A, Bae DS, Mills GB, Kumar R, et al. Differential signaling by an anti-p185(HER2) antibody and heregulin. Cancer Res. 2000 Jul 60(13):3522-31. PubMed PMID: 10910064.

264. Nahta R, Takahashi T, Ueno NT, Hung MC, Esteva FJ. P27(kip1) down-regulation is associated with trastuzumab resistance in breast cancer cells. Cancer Res. 2004 Jun;64(11):3981-6. PubMed PMID: 15173011.

265. Gallardo A, Lerma E, Escuin D, Tibau A, Munoz J, Ojeda B, et al. Increased signalling of EGFR and IGF1R, and deregulation of PTEN/PI3K/Akt pathway are related with trastuzumab resistance in HER2 breast carcinomas. Br J Cancer. 2012 Apr;106(8):1367-73. PubMed PMID: 22454081.

266. Bryant JA, Finn RS, Slamon DJ, Cloughesy TF, Charles AC. EGF activates intracellular and intercellular calcium signaling by distinct pathways in tumor cells. Cancer Biol Ther. 2004 Dec;3(12):1243-9. PubMed PMID: 15611621.

267. McAndrew D, Roberts-Thomson, S. J. and Monteith, G. R. TRPV1 and TRPV6 are upregulated in breast cancer cell lines. ComBio; Sep; Sydney2007.

268. Morgan AJ, Galione A. Two-pore channels (TPCs): current controversies. Bioessays. 2014 Feb;36(2):173-83. PubMed PMID: 24277557.

269. Vanoverberghe K, Lehen'kyi V, Thebault S, Raphael M, Vanden Abeele F, Slomianny C, et al. Cytoskeleton reorganization as an alternative mechanism of store-operated calcium entry control in neuroendocrine-differentiated cells. PLoS One. 2012 Sep;7(9):e45615. PubMed PMID: 23049826.

270. Guilbert A, Gautier M, Dhennin-Duthille I, Haren N, Sevestre H, Ouadid-Ahidouch H. Evidence that TRPM7 is required for breast cancer cell proliferation. Am J Physiol Cell Physiol. 2009 Sep;297(3):C493-502. PubMed PMID: 19515901.

271. Su LT, Agapito MA, Li M, Simonson WT, Huttenlocher A, Habas R, et al. TRPM7 regulates cell adhesion by controlling the calcium-dependent protease calpain. J Biol Chem. 2006 Apr;281(16):11260-70. PubMed PMID: 16436382.

272. Nahta R, Yu D, Hung MC, Hortobagyi GN, Esteva FJ. Mechanisms of disease: understanding resistance to HER2-targeted therapy in human breast cancer. Nat Clin Pract Oncol. 2006 May;3(5):269-80. PubMed PMID: 16683005.

273. Nahta R, Esteva FJ. In vitro effects of trastuzumab and vinorelbine in trastuzumab-resistant breast cancer cells. Cancer Chemother Pharmacol. 2004 Feb;53(2):186-90. PubMed PMID: 14605867.

274. Vazquez-Martin A, Oliveras-Ferraros C, Menendez JA. Autophagy facilitates the development of breast cancer resistance to the anti-HER2 monoclonal antibody trastuzumab. PLoS One. 2009 Jul;4(7):e6251. PubMed PMID: 19606230.

275. Ritter CA, Perez-Torres M, Rinehart C, Guix M, Dugger T, Engelman JA, et al. Human breast cancer cells selected for resistance to trastuzumab in vivo overexpress epidermal growth factor receptor and ErbB ligands and remain dependent on the ErbB receptor network. Clin Cancer Res. 2007 Aug;13(16):4909-19. PubMed PMID: 17699871.

276. Dua R, Zhang J, Nhonthachit P, Penuel E, Petropoulos C, Parry G. EGFR over-expression and activation in high HER2, ER negative breast cancer cell line induces trastuzumab resistance. Breast Cancer Res Treat. 2010 Aug;122(3):685-97. PubMed PMID: 19859802.

277. Henjes F, Bender C, von der Heyde S, Braun L, Mannsperger HA, Schmidt C, et al. Strong EGFR signaling in cell line models of ERBB2-amplified breast cancer attenuates response towards ERBB2-targeting drugs. Oncogenesis. 2012 Jul;1:e16. PubMed PMID: 23552733.

278. Xu H, Yu Y, Marciniak D, Rishi AK, Sarkar FH, Kucuk O, et al. Epidermal growth factor receptor (EGFR)-related protein inhibits multiple members of the EGFR family in colon and breast cancer cells. Mol Cancer Ther. 2005 Mar;4(3):435-42. PubMed PMID: 15767552.

279. Lu Y, Zi X, Zhao Y, Mascarenhas D, Pollak M. Insulin-like growth factor-I receptor signaling and resistance to trastuzumab (Herceptin). J Natl Cancer Inst. 2001 Dec;93(24):1852-7. PubMed PMID: 11752009.

280. Sehat B, Tofigh A, Lin Y, Trocme E, Liljedahl U, Lagergren J, et al. SUMOylation mediates the nuclear translocation and signaling of the IGF-1 receptor. Science signaling. 2010 Feb;3(108):ra10. PubMed PMID: 20145208.

281. Lorenzatti G, Huang W, Pal A, Cabanillas AM, Kleer CG. CCN6 (WISP3) decreases ZEB1-mediated EMT and invasion by attenuation of IGF-1 receptor signaling in breast cancer. J Cell Sci. 2011 May;124(Pt 10):1752-8. PubMed PMID: 21525039.

282. Giacomello M, Drago I, Bortolozzi M, Scorzeto M, Gianelle A, Pizzo P, et al. Ca2+ hot spots on the mitochondrial surface are generated by Ca2+ mobilization from stores, but not by activation of store-operated Ca2+ channels. Molecular cell. 2010 Apr;38(2):280-90. PubMed PMID: 20417605.

283. Sanchez-Hernandez Y, Laforenza U, Bonetti E, Fontana J, Dragoni S, Russo M, et al. Store-operated Ca(2+) entry is expressed in human endothelial progenitor cells. Stem cells and development. 2010 Dec;19(12):1967-81. PubMed PMID: 20677912.

284. Masters JR, Stacey GN. Changing medium and passaging cell lines. Nature protocols. 2007 Sep;2(9):2276-84. PubMed PMID: 17853884.

285. O'Driscoll L, Gammell P, McKiernan E, Ryan E, Jeppesen PB, Rani S, et al. Phenotypic and global gene expression profile changes between low passage and high passage MIN-6 cells. The Journal of endocrinology. 2006 Dec;191(3):665-76. PubMed PMID: 17170223.

286. Corcoran C, Rani S, Breslin S, Gogarty M, Ghobrial IM, Crown J, et al. miR-630 targets IGF1R to regulate response to HER-targeting drugs and overall cancer cell progression in HER2 over-expressing breast cancer. Molecular cancer. 2014 Mar;13:71. PubMed PMID: 24655723.

287. Rani S, Corcoran C, Shiels L, Germano S, Breslin S, Madden S, et al. Neuromedin U: a candidate biomarker and therapeutic target to predict and overcome resistance to HER-tyrosine kinase inhibitors. Cancer Res. 2014 Jul;74(14):3821-33. PubMed PMID: 24876102.

288. Scott GK, Robles R, Park JW, Montgomery PA, Daniel J, Holmes WE, et al. A truncated intracellular HER2/neu receptor produced by alternative RNA processing affects growth of human carcinoma cells. Mol Cell Biol. 1993 Apr;13(4):2247-57. PubMed PMID: 8096058.

289. Gackiere F, Bidaux G, Delcourt P, Van Coppenolle F, Katsogiannou M, Dewailly E, et al. CaV3.2 T-type calcium channels are involved in calcium-dependent secretion of neuroendocrine prostate cancer cells. J Biol Chem. 2008 Apr;283(15):10162-73. PubMed PMID: 18230611.

290. Findlay VJ, Wang C, Watson DK, Camp ER. Epithelial-to-mesenchymal transition and the cancer stem cell phenotype: insights from cancer biology with therapeutic implications for colorectal cancer. Cancer gene therapy. 2014 May;21(5):181-7. PubMed PMID: 24787239.

291. Mizuta E, Miake J, Yano S, Furuichi H, Manabe K, Sasaki N, et al. Subtype switching of T-type Ca 2+ channels from Cav3.2 to Cav3.1 during differentiation of embryonic stem cells to cardiac cell lineage. Circulation journal : official journal of the Japanese Circulation Society. 2005 Oct;69(10):1284-9. PubMed PMID: 16195632.

292. Yanagi K, Takano M, Narazaki G, Uosaki H, Hoshino T, Ishii T, et al. Hyperpolarization-activated cyclic nucleotide-gated channels and T-type calcium channels confer automaticity of

embryonic stem cell-derived cardiomyocytes. Stem cells (Dayton, Ohio). 2007 Nov;25(11):2712-9. PubMed PMID: 17656646.

293. Padar S, van Breemen C, Thomas DW, Uchizono JA, Livesey JC, Rahimian R. Differential regulation of calcium homeostasis in adenocarcinoma cell line A549 and its Taxol-resistant subclone. Br J Pharmacol. 2004 May;142(2):305-16. PubMed PMID: 15066902.

294. Henke N, Albrecht P, Bouchachia I, Ryazantseva M, Knoll K, Lewerenz J, et al. The plasma membrane channel ORAI1 mediates detrimental calcium influx caused by endogenous oxidative stress. Cell Death Dis. 2013 Jan;4:e470. PubMed PMID: 23348584.

295. Catterall WA, Perez-Reyes E, Snutch TP, Striessnig J. International Union of Pharmacology. XLVIII. Nomenclature and structure-function relationships of voltage-gated calcium channels. Pharmacol Rev. 2005 Dec;57(4):411-25. PubMed PMID: 16382099.

296. Cribbs LL, Lee JH, Yang J, Satin J, Zhang Y, Daud A, et al. Cloning and characterization of alpha1H from human heart, a member of the T-type Ca2+ channel gene family. Circulation research. 1998 Jul;83(1):103-9. PubMed PMID: 9670923.

297. Perez-Reyes E. Molecular physiology of low-voltage-activated t-type calcium channels. Physiol Rev. 2003 Jan;83(1):117-61. PubMed PMID: 12506128.

298. Gomora JC, Xu L, Enyeart JA, Enyeart JJ. Effect of mibefradil on voltage-dependent gating and kinetics of T-type Ca(2+) channels in cortisol-secreting cells. J Pharmacol Exp Ther. 2000 Jan;292(1):96-103. PubMed PMID: 10604935.

299. Khosravani H, Altier C, Simms B, Hamming KS, Snutch TP, Mezeyova J, et al. Gating effects of mutations in the Cav3.2 T-type calcium channel associated with childhood absence epilepsy. J Biol Chem. 2004 Mar;279(11):9681-4. PubMed PMID: 14729682.

300. Weiss N, Black SA, Bladen C, Chen L, Zamponi GW. Surface expression and function of Cav3.2 T-type calcium channels are controlled by asparagine-linked glycosylation. Pflugers Arch. 2013 Aug;465(8):1159-70. PubMed PMID: 23503728.

301. Orestes P, Osuru HP, McIntire WE, Jacus MO, Salajegheh R, Jagodic MM, et al. Reversal of neuropathic pain in diabetes by targeting glycosylation of Ca(V)3.2 T-type calcium channels. Diabetes. 2013 Nov;62(11):3828-38. PubMed PMID: 23835327.

302. Todorovic SM, Jevtovic-Todorovic V. Targeting of CaV3.2 T-type calcium channels in peripheral sensory neurons for the treatment of painful diabetic neuropathy. Pflugers Arch. 2014 Apr;466(4):701-6. PubMed PMID: 24482063.

303. Mariot P, Vanoverberghe K, Lalevee N, Rossier MF, Prevarskaya N. Overexpression of an alpha 1H (Cav3.2) T-type calcium channel during neuroendocrine differentiation of human prostate cancer cells. J Biol Chem. 2002 Mar;277(13):10824-33. PubMed PMID: 11799114.

304. Panner A, Cribbs LL, Zainelli GM, Origitano TC, Singh S, Wurster RD. Variation of T-type calcium channel protein expression affects cell division of cultured tumor cells. Cell Calcium. 2005 Feb;37(2):105-19. PubMed PMID: 15589991.

305. Hirooka K, Bertolesi GE, Kelly ME, Denovan-Wright EM, Sun X, Hamid J, et al. T-Type calcium channel alpha1G and alpha1H subunits in human retinoblastoma cells and their loss after differentiation. Journal of neurophysiology. 2002 Jul;88(1):196-205. PubMed PMID: 12091545.

306. Gray LS, Perez-Reyes E, Gomora JC, Haverstick DM, Shattock M, McLatchie L, et al. The role of voltage gated T-type Ca2+ channel isoforms in mediating "capacitative" Ca2+ entry in cancer cells. Cell Calcium. 2004 Dec;36(6):489-97. PubMed PMID: 15488598.

307. Asaga S, Ueda M, Jinno H, Kikuchi K, Itano O, Ikeda T, et al. Identification of a new breast cancer-related gene by restriction landmark genomic scanning. Anticancer Res. 2006 Jan-Feb;26(1A):35-42. PubMed PMID: 16475676.

308. Ohkubo T, Yamazaki J. T-type voltage-activated calcium channel Cav3.1, but not Cav3.2, is involved in the inhibition of proliferation and apoptosis in MCF-7 human breast cancer cells. Int J Oncol. 2012 Jul;41(1):267-75. PubMed PMID: 22469755.

309. Taylor JT, Huang L, Pottle JE, Liu K, Yang Y, Zeng X, et al. Selective blockade of T-type Ca2+ channels suppresses human breast cancer cell proliferation. Cancer Lett. 2008 Aug;267(1):116-24. PubMed PMID: 18455293.

310. Ranzato E, Martinotti S, Magnelli V, Murer B, Biffo S, Mutti L, et al. Epigallocatechin-3-gallate induces mesothelioma cell death via H2 O2 -dependent T-type Ca2+ channel opening. J Cell Mol Med. 2012 Nov;16(11):2667-78. PubMed PMID: 22564432.

311. Sorlie T, Perou CM, Tibshirani R, Aas T, Geisler S, Johnsen H, et al. Gene expression patterns of breast carcinomas distinguish tumor subclasses with clinical implications. Proc Natl Acad Sci U S A. 2001 Sep;98(19):10869-74. PubMed PMID: 11553815.

312. Martin-Castillo B, Oliveras-Ferraros C, Vazquez-Martin A, Cufi S, Moreno JM, Corominas-Faja B, et al. Basal/HER2 breast carcinomas: integrating molecular taxonomy with cancer stem cell dynamics to predict primary resistance to trastuzumab (Herceptin). Cell Cycle. 2013 Jan;12(2):225-45. PubMed PMID: 23255137.

313. Oliveras-Ferraros C, Vazquez-Martin A, Martin-Castillo B, Perez-Martinez MC, Cufi S, Del Barco S, et al. Pathway-focused proteomic signatures in HER2-overexpressing breast cancer with a basal-like phenotype: new insights into de novo resistance to trastuzumab (Herceptin). Int J Oncol. 2010 Sep;37(3):669-78. PubMed PMID: 20664936.

314. Oliveras-Ferraros C, Vazquez-Martin A, Martin-Castillo B, Cufi S, Del Barco S, Lopez-Bonet E, et al. Dynamic emergence of the mesenchymal CD44(pos)CD24(neg/low) phenotype in HER2-gene amplified breast cancer cells with de novo resistance to trastuzumab (Herceptin). Biochem Biophys Res Commun. 2010 Jun;397(1):27-33. PubMed PMID: 20470755.

315. Staaf J, Ringner M, Vallon-Christersson J, Jonsson G, Bendahl PO, Holm K, et al. Identification of subtypes in human epidermal growth factor receptor 2--positive breast cancer reveals a gene signature prognostic of outcome. J Clin Oncol. 2010 Apr;28(11):1813-20. PubMed PMID: 20231686.

316. Huang JB, Kindzelskii AL, Clark AJ, Petty HR. Identification of channels promoting calcium spikes and waves in HT1080 tumor cells: their apparent roles in cell motility and invasion. Cancer Res. 2004 Apr 64(7):2482-9. PubMed PMID: 15059902.

317. Applied-Biosystem. AB StepOne and StepOnePlus Real-Time PCR Systems - Relative Standard Curve and Comparative CT Experiments 2014.

318. Duggan DJ, Bittner M, Chen Y, Meltzer P, Trent JM. Expression profiling using cDNA microarrays. Nature genetics. 1999 Jan;21(1 Suppl):10-4. PubMed PMID: 9915494.

319. The Cancer Genome Atlas Network. Comprehensive molecular portraits of human breast tumours. Nature. 2012 Apr;490(7418):61-70.

320. Clozel JP, Ertel EA, Ertel SI. Voltage-gated T-type Ca2+ channels and heart failure. Proceedings of the Association of American Physicians. 1999 Sep-Oct;111(5):429-37. PubMed PMID: 10519164.

321. Bertolesi GE, Shi C, Elbaum L, Jollimore C, Rozenberg G, Barnes S, et al. The Ca2+ Channel Antagonists Mibefradil and Pimozide Inhibit Cell Growth via Different Cytotoxic Mechanisms. Molecular Pharmacology. 2002 Aug;62(2):210-9. PubMed PMID: 12130671.

322. Panner A, Wurster RD. T-type calcium channels and tumor proliferation. Cell Calcium. 2006 Aug;40(2):253-9. PubMed PMID: 16765439.

323. Jung HK, Doddareddy MR, Cha JH, Rhim H, Cho YS, Koh HY, et al. Synthesis and biological evaluation of novel T-type Ca2+ channel blockers. Bioorganic & medicinal chemistry. 2004 Aug 12(15):3965-70. PubMed PMID: 15246072.

324. Xiang Z, Thompson AD, Brogan JT, Schulte ML, Melancon BJ, Mi D, et al. The Discovery and Characterization of ML218: A Novel, Centrally Active T-Type Calcium Channel Inhibitor with Robust Effects in STN Neurons and in a Rodent Model of Parkinson's Disease. ACS chemical neuroscience. 2011 Dec;2(12):730-42. PubMed PMID: 22368764.

325. Xie X, Brogan JT, Schulte ML, Mi D, Yu H, Dawson ES, et al. Scaffold Hopping Affords a Highly Selective in vitro and in vivo T-Type Calcium Inhibitor Probe Free From IP Issues. Probe Reports from the NIH Molecular Libraries Program. Bethesda (MD)2010.

326. Varki A, Kannagi R, Toole BP. Glycosylation Changes in Cancer. In: Varki A, Cummings RD, Esko JD, Freeze HH, Stanley P, Bertozzi CR, et al., editors. Essentials of Glycobiology. 2nd ed. Cold Spring Harbor (NY): Cold Spring Harbor Laboratory Press; 2009.

327. Klimant E, Glurich I, Mukesh B, Onitilo AA. Blood type, hormone receptor status, HER2/neu status, and survival in breast cancer: a retrospective study exploring relationships in a phenotypically well-defined cohort. Clinical medicine & research. 2011 Nov;9(3-4):111-8. PubMed PMID: 21263059.

328. Chen L, Zhang W, Fregien N, Pierce M. The her-2/neu oncogene stimulates the transcription of N-acetylglucosaminyltransferase V and expression of its cell surface oligosaccharide products. Oncogene. 1998 Oct;17(16):2087-93. PubMed PMID: 9798679.

329. Dokmanovic MaW, Wen Jin Trastuzumab-Resistance and Breast Cancer. In: Gunduz PM, editor. Breast Cancer - Carcinogenesis, Cell Growth and Signalling Pathways2011.

330. Zhao Y, Liu H, Liu Z, Ding Y, Ledoux SP, Wilson GL, et al. Overcoming trastuzumab resistance in breast cancer by targeting dysregulated glucose metabolism. Cancer Res. 2011 Jul;71(13):4585-97. PubMed PMID: 21498634.

331. Yoshida M, Nosaka K, Yasunaga J, Nishikata I, Morishita K, Matsuoka M. Aberrant expression of the MEL1S gene identified in association with hypomethylation in adult T-cell leukemia cells. Blood. 2004 Apr;103(7):2753-60. PubMed PMID: 14656887.

332. Nadler MJ, Hermosura MC, Inabe K, Perraud AL, Zhu Q, Stokes AJ, et al. LTRPC7 is a Mg.ATP-regulated divalent cation channel required for cell viability. Nature. 2001 May;411(6837):590-5. PubMed PMID: 11385574.

333. Runnels LW, Yue L, Clapham DE. TRP-PLIK, a bifunctional protein with kinase and ion channel activities. Science. 2001 Feb;291(5506):1043-7. PubMed PMID: 11161216.

334. Ryazanov AG. Elongation factor-2 kinase and its newly discovered relatives. FEBS letters. 2002 Mar;514(1):26-9. PubMed PMID: 11904175.

335. Ryazanova LV, Pavur KS, Petrov AN, Dorovkov MV, Ryazanov AG. Novel Type of Signaling Molecules: Protein Kinases Covalently Linked with Ion Channels. Molecular Biology. 2001 Mar;35(2):271-83.

336. Perraud AL, Fleig A, Dunn CA, Bagley LA, Launay P, Schmitz C, et al. ADP-ribose gating of the calcium-permeable LTRPC2 channel revealed by Nudix motif homology. Nature. 2001 May;411(6837):595-9. PubMed PMID: 11385575.

337. Schlingmann KP, Weber S, Peters M, Niemann Nejsum L, Vitzthum H, Klingel K, et al. Hypomagnesemia with secondary hypocalcemia is caused by mutations in TRPM6, a new member of the TRPM gene family. Nature genetics. 2002 Jun;31(2):166-70. PubMed PMID: 12032568.

338. Penner R, Fleig A. The Mg2+ and Mg2+-Nucleotide-Regulated Channel-Kinase TRPM7. In: Flockerzi V, Nilius B, editors. Transient Receptor Potential (TRP) Channels. Handbook of Experimental Pharmacology. 179: Springer Berlin Heidelberg; 2007. p. 313-28.

339. Schmitz C, Perraud AL, Johnson CO, Inabe K, Smith MK, Penner R, et al. Regulation of vertebrate cellular Mg2+ homeostasis by TRPM7. Cell. 2003 Jul;114(2):191-200. PubMed PMID: 12887921.

340. Wu LJ, Sweet TB, Clapham DE. International Union of Basic and Clinical Pharmacology. LXXVI. Current progress in the mammalian TRP ion channel family. Pharmacol Rev. 2010 Sep;62(3):381-404. PubMed PMID: 20716668.

341. Matsushita M, Kozak JA, Shimizu Y, McLachlin DT, Yamaguchi H, Wei FY, et al. Channel function is dissociated from the intrinsic kinase activity and autophosphorylation of TRPM7/ChaK1. J Biol Chem. 2005 May;280(21):20793-803. PubMed PMID: 15781465.

342. Clark K, Langeslag M, van Leeuwen B, Ran L, Ryazanov AG, Figdor CG, et al. TRPM7, a novel regulator of actomyosin contractility and cell adhesion. EMBO J. 2006 Jan;25(2):290-301. PubMed PMID: 16407977.

343. Clark K, Middelbeek J, Dorovkov MV, Figdor CG, Ryazanov AG, Lasonder E, et al. The alpha-kinases TRPM6 and TRPM7, but not eEF-2 kinase, phosphorylate the assembly domain of myosin IIA, IIB and IIC. FEBS letters. 2008 Sep 582(20):2993-7. PubMed PMID: 18675813.

344. Clark K, Middelbeek J, Lasonder E, Dulyaninova NG, Morrice NA, Ryazanov AG, et al. TRPM7 regulates myosin IIA filament stability and protein localization by heavy chain phosphorylation. Journal of molecular biology. 2008 May;378(4):790-803. PubMed PMID: 18394644.

345. Dorovkov MV, Ryazanov AG. Phosphorylation of annexin I by TRPM7 channel-kinase. J Biol Chem. 2004 Dec;279(49):50643-6. PubMed PMID: 15485879.

346. Dorovkov MV, Kostyukova AS, Ryazanov AG. Phosphorylation of annexin A1 by TRPM7 kinase: a switch regulating the induction of an alpha-helix. Biochemistry. 2011 Mar;50(12):2187-93. PubMed PMID: 21280599.

347. Perraud AL, Zhao X, Ryazanov AG, Schmitz C. The channel-kinase TRPM7 regulates phosphorylation of the translational factor eEF2 via eEF2-k. Cell Signal. 2011 Mar;23(3):586-93. PubMed PMID: 21112387.

348. Ryazanova LV, Dorovkov MV, Ansari A, Ryazanov AG. Characterization of the protein kinase activity of TRPM7/ChaK1, a protein kinase fused to the transient receptor potential ion channel. J Biol Chem. 2004 Jan;279(5):3708-16. PubMed PMID: 14594813.

349. Bae CY, Sun HS. TRPM7 in cerebral ischemia and potential target for drug development in stroke. Acta Pharmacol Sin. 2011 Jun;32(6):725-33. PubMed PMID: 21552293.

350. Fonfria E, Murdock PR, Cusdin FS, Benham CD, Kelsell RE, McNulty S. Tissue distribution profiles of the human TRPM cation channel family. Journal of receptor and signal transduction research. 2006 Jan;26(3):159-78. PubMed PMID: 16777713.

351. Nilius B, Flockerzi V. Mammalian Transient Receptor Potential (TRP) Cation Channels. New York: Springer; 2014. 726 p.

352. Zierler S, Yao G, Zhang Z, Kuo WC, Porzgen P, Penner R, et al. Waixenicin A inhibits cell proliferation through magnesium-dependent block of transient receptor potential melastatin 7 (TRPM7) channels. J Biol Chem. 2011 Nov;286(45):39328-35. PubMed PMID: 21926172.

353. Ng NM, Jiang SP, Lv ZQ. Retrovirus-mediated siRNA targeting TRPM7 gene induces apoptosis in RBL-2H3 cells. European review for medical and pharmacological sciences. 2012 Sep;16(9):1172-8. PubMed PMID: 23047499.

354. Liu H, Li J, Huang Y, Huang C. Inhibition of transient receptor potential melastain 7 channel increases HSCs apoptosis induced by TRAIL. Life Sci. 2012 Apr;90(15-16):612-8. PubMed PMID: 22406504.

355. Lam DH, Grant CE, Hill CE. Differential expression of TRPM7 in rat hepatoma and embryonic and adult hepatocytes. Canadian journal of physiology and pharmacology. 2012 Apr;90(4):435-44. PubMed PMID: 22429021.

356. Jin J, Desai BN, Navarro B, Donovan A, Andrews NC, Clapham DE. Deletion of Trpm7 disrupts embryonic development and thymopoiesis without altering Mg2+ homeostasis. Science. 2008 Oct;322(5902):756-60. PubMed PMID: 18974357.

357. Sah R, Mesirca P, Mason X, Gibson W, Bates-Withers C, Van den Boogert M, et al. Timing of myocardial trpm7 deletion during cardiogenesis variably disrupts adult ventricular function, conduction, and repolarization. Circulation. 2013 Jul;128(2):101-14. PubMed PMID: 23734001.

358. Sun HS, Jackson MF, Martin LJ, Jansen K, Teves L, Cui H, et al. Suppression of hippocampal TRPM7 protein prevents delayed neuronal death in brain ischemia. Nature neuroscience. 2009 Oct;12(10):1300-7. PubMed PMID: 19734892.

359. Touyz RM, He Y, Montezano AC, Yao G, Chubanov V, Gudermann T, et al. Differential regulation of transient receptor potential melastatin 6 and 7 cation channels by ANG II in vascular smooth muscle cells from spontaneously hypertensive rats. American journal of physiology Regulatory, integrative and comparative physiology. 2006 Jan;290(1):R73-8. PubMed PMID: 16109804.

360. Sahni J, Tamura R, Sweet IR, Scharenberg AM. TRPM7 regulates quiescent/proliferative metabolic transitions in lymphocytes. Cell Cycle. 2010 Sep;9(17):3565-74. PubMed PMID: 20724843.

361. Rybarczyk P, Gautier M, Hague F, Dhennin-Duthille I, Chatelain D, Kerr-Conte J, et al. Transient receptor potential melastatin-related 7 channel is overexpressed in human pancreatic ductal adenocarcinomas and regulates human pancreatic cancer cell migration. Int J Cancer. 2012 Sep;131(6):E851-61. PubMed PMID: 22323115.

362. Meng X, Cai C, Wu J, Cai S, Ye C, Chen H, et al. TRPM7 mediates breast cancer cell migration and invasion through the MAPK pathway. Cancer Lett. 2013 Jun;333(1):96-102. PubMed PMID: 23353055.

363. Kim BJ, Park EJ, Lee JH, Jeon JH, Kim SJ, So I. Suppression of transient receptor potential melastatin 7 channel induces cell death in gastric cancer. Cancer science. 2008 Dec;99(12):2502-9. PubMed PMID: 19032368.

364. Jiang J, Li MH, Inoue K, Chu XP, Seeds J, Xiong ZG. Transient receptor potential melastatin 7-like current in human head and neck carcinoma cells: role in cell proliferation. Cancer Res. 2007 Nov;67(22):10929-38. PubMed PMID: 18006838.

365. Gao H, Chen X, Du X, Guan B, Liu Y, Zhang H. EGF enhances the migration of cancer cells by up-regulation of TRPM7. Cell Calcium. 2011 Dec;50(6):559-68. PubMed PMID: 21978419.

366. Chen JP, Luan Y, You CX, Chen XH, Luo RC, Li R. TRPM7 regulates the migration of human nasopharyngeal carcinoma cell by mediating Ca(2+) influx. Cell Calcium. 2010 May;47(5):425-32. PubMed PMID: 20363498.

367. Chubanov V, Mederos y Schnitzler M, Meissner M, Schafer S, Abstiens K, Hofmann T, et al. Natural and synthetic modulators of SK (K(ca)2) potassium channels inhibit magnesium-dependent activity of the kinase-coupled cation channel TRPM7. Br J Pharmacol. 2012 Jun;166(4):1357-76. PubMed PMID: 22242975.

368. Devkota AK, Tavares CD, Warthaka M, Abramczyk O, Marshall KD, Kaoud TS, et al. Investigating the kinetic mechanism of inhibition of elongation factor 2 kinase by NH125:

evidence of a common in vitro artifact. Biochemistry. 2012 Mar;51(10):2100-12. PubMed PMID: 22352903.

369. Jenkins DP, Strobaek D, Hougaard C, Jensen ML, Hummel R, Sorensen US, et al. Negative gating modulation by (R)-N-(benzimidazol-2-yl)-1,2,3,4-tetrahydro-1-naphthylamine (NS8593) depends on residues in the inner pore vestibule: pharmacological evidence of deep-pore gating of K(Ca)2 channels. Mol Pharmacol. 2011 Jun;79(6):899-909. PubMed PMID: 21363929.

370. Strobaek D, Hougaard C, Johansen TH, Sorensen US, Nielsen EO, Nielsen KS, et al. Inhibitory gating modulation of small conductance Ca2+-activated K+ channels by the synthetic compound (R)-N-(benzimidazol-2-yl)-1,2,3,4-tetrahydro-1-naphtylamine (NS8593) reduces afterhyperpolarizing current in hippocampal CA1 neurons. Mol Pharmacol. 2006 Nov;70(5):1771-82. PubMed PMID: 16926279.

371. Chen Z, Gopalakrishnan SM, Bui MH, Soni NB, Warrior U, Johnson EF, et al. 1-Benzyl-3-cetyl-2-methylimidazolium iodide (NH125) induces phosphorylation of eukaryotic elongation factor-2 (eEF2): a cautionary note on the anticancer mechanism of an eEF2 kinase inhibitor. J Biol Chem. 2011 Dec;286(51):43951-8. PubMed PMID: 22020937.

372. Arora S, Yang JM, Kinzy TG, Utsumi R, Okamoto T, Kitayama T, et al. Identification and characterization of an inhibitor of eukaryotic elongation factor 2 kinase against human cancer cell lines. Cancer Res. 2003 Oct;63(20):6894-9. PubMed PMID: 14583488.

373. Guilbert A, Gautier M, Dhennin-Duthille I, Rybarczyk P, Sahni J, Sevestre H, et al. Transient receptor potential melastatin 7 is involved in oestrogen receptor-negative metastatic breast cancer cells migration through its kinase domain. Eur J Cancer. 2013 Nov;49(17):3694-707. PubMed PMID: 23910495.

374. Cheng Y, Li H, Ren X, Niu T, Hait WN, Yang J. Cytoprotective effect of the elongation factor-2 kinase-mediated autophagy in breast cancer cells subjected to growth factor inhibition. PLoS One. 2010 Mar;5(3):e9715. PubMed PMID: 20300520.

375. McDermott MS, Browne BC, Conlon NT, O'Brien NA, Slamon DJ, Henry M, et al. PP2A inhibition overcomes acquired resistance to HER2 targeted therapy. Molecular cancer. 2014 Jun;13:157. PubMed PMID: 24958351.

376. Gschwendt M, Muller HJ, Kielbassa K, Zang R, Kittstein W, Rincke G, et al. Rottlerin, a novel protein kinase inhibitor. Biochem Biophys Res Commun. 1994 Feb;199(1):93-8. PubMed PMID: 8123051.

377. Song KS, Kim JS, Yun EJ, Kim YR, Seo KS, Park JH, et al. Rottlerin induces autophagy and apoptotic cell death through a PKC-delta-independent pathway in HT1080 human fibrosarcoma cells: the protective role of autophagy in apoptosis. Autophagy. 2008 Jul;4(5):650-8. PubMed PMID: 18424913.

378. Yin S, Sethi S, Reddy KB. Protein kinase Cdelta and caspase-3 modulate TRAIL-induced apoptosis in breast tumor cells. J Cell Biochem. 2010 Nov;111(4):979-87. PubMed PMID: 20665667.

379. Gschwendt M, Kittstein W, Marks F. Elongation factor-2 kinase: effective inhibition by the novel protein kinase inhibitor rottlerin and relative insensitivity towards staurosporine. FEBS letters. 1994 Jan;338(1):85-8. PubMed PMID: 8307162.

380. Zeng H, Lozinskaya IM, Lin Z, Willette RN, Brooks DP, Xu X. Mallotoxin is a novel human ether-a-go-go-related gene (hERG) potassium channel activator. J Pharmacol Exp Ther. 2006 Nov;319(2):957-62. PubMed PMID: 16928897.

381. Clements RT, Cordeiro B, Feng J, Bianchi C, Sellke FW. Rottlerin increases cardiac contractile performance and coronary perfusion through BKCa++ channel activation after

cold cardioplegic arrest in isolated hearts. Circulation. 2011 Sep;124(11 Suppl):S55-61. PubMed PMID: 21911819.

382. Macgregor PF, Squire JA. Application of microarrays to the analysis of gene expression in cancer. Clin Chem. 2002 Aug;48(8):1170-7. PubMed PMID: 12142369.

383. Russo G, Zegar C, Giordano A. Advantages and limitations of microarray technology in human cancer. Oncogene. 2003 Sep;22(42):6497-507. PubMed PMID: 14528274.

384. Kudoh K, Ramanna M, Ravatn R, Elkahloun AG, Bittner ML, Meltzer PS, et al. Monitoring the expression profiles of doxorubicin-induced and doxorubicin-resistant cancer cells by cDNA microarray. Cancer Res. 2000 Aug;60(15):4161-6. PubMed PMID: 10945624.

385. Sotiriou C, Powles TJ, Dowsett M, Jazaeri AA, Feldman AL, Assersohn L, et al. Gene expression profiles derived from fine needle aspiration correlate with response to systemic chemotherapy in breast cancer. Breast Cancer Res. 2002 Mar;4(3):R3. PubMed PMID: 12052255.

386. Wang Y, Klijn JG, Zhang Y, Sieuwerts AM, Look MP, Yang F, et al. Gene-expression profiles to predict distant metastasis of lymph-node-negative primary breast cancer. Lancet. 2005 Feb;365(9460):671-9. PubMed PMID: 15721472.

387. Liu R, Wang X, Chen GY, Dalerba P, Gurney A, Hoey T, et al. The prognostic role of a gene signature from tumorigenic breast-cancer cells. N Engl J Med. 2007 Jan;356(3):217-26. PubMed PMID: 17229949.

388. Chang HY, Nuyten DS, Sneddon JB, Hastie T, Tibshirani R, Sorlie T, et al. Robustness, scalability, and integration of a wound-response gene expression signature in predicting breast cancer survival. Proc Natl Acad Sci U S A. 2005 Mar;102(10):3738-43. PubMed PMID: 15701700.

389. Carter SL, Eklund AC, Kohane IS, Harris LN, Szallasi Z. A signature of chromosomal instability inferred from gene expression profiles predicts clinical outcome in multiple human cancers. Nature genetics. 2006 Sep;38(9):1043-8. PubMed PMID: 16921376.

390. Ong SE, Blagoev B, Kratchmarova I, Kristensen DB, Steen H, Pandey A, et al. Stable isotope labeling by amino acids in cell culture, SILAC, as a simple and accurate approach to expression proteomics. Molecular & cellular proteomics : MCP. 2002 May;1(5):376-86. PubMed PMID: 12118079.

391. Mann M. Functional and quantitative proteomics using SILAC. Nat Rev Mol Cell Biol. 2006 Dec;7(12):952-8. PubMed PMID: 17139335.

392. Sotoca AM, Gelpke MD, Boeren S, Strom A, Gustafsson JA, Murk AJ, et al. Quantitative proteomics and transcriptomics addressing the estrogen receptor subtype-mediated effects in T47D breast cancer cells exposed to the phytoestrogen genistein. Molecular & cellular proteomics : MCP. 2011 Jan;10(1):M110 002170. PubMed PMID: 20884965.

393. Hoedt E, Chaoui K, Huvent I, Mariller C, Monsarrat B, Burlet-Schiltz O, et al. SILAC-based proteomic profiling of the human MDA-MB-231 metastatic breast cancer cell line in response to the two antitumoral lactoferrin isoforms: the secreted lactoferrin and the intracellular delta-lactoferrin. PLoS One. 2014 Aug;9(8):e104563. PubMed PMID: 25116916.

394. Geiger T, Madden SF, Gallagher WM, Cox J, Mann M. Proteomic portrait of human breast cancer progression identifies novel prognostic markers. Cancer Res. 2012 May 72(9):2428-39. PubMed PMID: 22414580.

395. Chen H, Pimienta G, Gu Y, Sun X, Hu J, Kim MS, et al. Proteomic characterization of Her2/neu-overexpressing breast cancer cells. Proteomics. 2010 Nov;10(21):3800-10. PubMed PMID: 20960451.

396. Valabrega G, Capellero S, Cavalloni G, Zaccarello G, Petrelli A, Migliardi G, et al. HER2-positive breast cancer cells resistant to trastuzumab and lapatinib lose reliance upon HER2 and are sensitive to the multitargeted kinase inhibitor sorafenib. Breast Cancer Res Treat. 2011 Nov;130(1):29-40. PubMed PMID: 21153051.

397. Liu JC, Voisin V, Bader GD, Deng T, Pusztai L, Symmans WF, et al. Seventeen-gene signature from enriched Her2/Neu mammary tumor-initiating cells predicts clinical outcome for human HER2+:ERalpha- breast cancer. Proc Natl Acad Sci U S A. 2012 Apr;109(15):5832-7. PubMed PMID: 22460789.

398. Hoedt E, Zhang G, Neubert TA. Stable isotope labeling by amino acids in cell culture (SILAC) for quantitative proteomics. Adv Exp Med Biol. 2014 May;806:93-106. PubMed PMID: 24952180.

399. Boyer AP, Collier TS, Vidavsky I, Bose R. Quantitative proteomics with siRNA screening identifies novel mechanisms of trastuzumab resistance in HER2 amplified breast cancers. Molecular & cellular proteomics : MCP. 2013 Jan;12(1):180-93. PubMed PMID: 23105007.

400. Konecny GE, Pegram MD, Venkatesan N, Finn R, Yang G, Rahmeh M, et al. Activity of the dual kinase inhibitor lapatinib (GW572016) against HER-2-overexpressing and trastuzumab-treated breast cancer cells. Cancer Res. 2006 Feb;66(3):1630-9. PubMed PMID: 16452222.

401. Weisenberg RC. Microtubule formation in vitro in solutions containing low calcium concentrations. Science. 1972 Sep;177(4054):1104-5. PubMed PMID: 4626639.

402. Uetrecht AC, Bear JE. Coronins: the return of the crown. Trends Cell Biol. 2006 Aug;16(8):421-6. PubMed PMID: 16806932.

403. Bennett V, Baines AJ. Spectrin and ankyrin-based pathways: metazoan inventions for integrating cells into tissues. Physiol Rev. 2001 Jul;81(3):1353-92. PubMed PMID: 11427698.

404. Chiao YA, Ramirez TA, Zamilpa R, Okoronkwo SM, Dai Q, Zhang J, et al. Matrix metalloproteinase-9 deletion attenuates myocardial fibrosis and diastolic dysfunction in ageing mice. Cardiovascular research. 2012 Dec 96(3):444-55. PubMed PMID: 22918978.

405. Zhang H, Berezov A, Wang Q, Zhang G, Drebin J, Murali R, et al. ErbB receptors: from oncogenes to targeted cancer therapies. The Journal of clinical investigation. 2007 Aug;117(8):2051-8. PubMed PMID: 17671639.

406. Dumic J, Dabelic S, Flogel M. Galectin-3: an open-ended story. Biochim Biophys Acta. 2006 Apr;1760(4):616-35. PubMed PMID: 16478649.

407. Foulquier F, Amyere M, Jaeken J, Zeevaert R, Schollen E, Race V, et al. TMEM165 deficiency causes a congenital disorder of glycosylation. American journal of human genetics. 2012 Jul;91(1):15-26. PubMed PMID: 22683087.

408. Kometiani P, Tian J, Li J, Nabih Z, Gick G, Xie Z. Regulation of Na/K-ATPase beta1-subunit gene expression by ouabain and other hypertrophic stimuli in neonatal rat cardiac myocytes. Mol Cell Biochem. 2000 Dec;215(1-2):65-72. PubMed PMID: 11204457.

409. O'Brien CA, Kreso A, Dick JE. Cancer stem cells in solid tumors: an overview. Seminars in radiation oncology. 2009 Apr;19(2):71-7. PubMed PMID: 19249644.

410. Rhee DK, Park SH, Jang YK. Molecular signatures associated with transformation and progression to breast cancer in the isogenic MCF10 model. Genomics. 2008 Dec;92(6):419-28. PubMed PMID: 18804527.

411. McKiernan E, McDermott EW, Evoy D, Crown J, Duffy MJ. The role of S100 genes in breast cancer progression. Tumour biology : the journal of the International Society for Oncodevelopmental Biology and Medicine. 2011 Jun;32(3):441-50. PubMed PMID: 21153724.

412. Arumugam T, Logsdon CD. S100P: a novel therapeutic target for cancer. Amino acids. 2011 Oct;41(4):893-9. PubMed PMID: 20509035.

413. Xu C, Chen H, Wang X, Gao J, Che Y, Li Y, et al. S100A14, a member of the EF-hand calcium-binding proteins, is overexpressed in breast cancer and acts as a modulator of HER2 signaling. J Biol Chem. 2014 Jan;289(2):827-37. PubMed PMID: 24285542.

414. Putnam AJ, Schultz K, Mooney DJ. Control of microtubule assembly by extracellular matrix and externally applied strain. 2001 Mar;280(3):C556-C64. PubMed PMID: 11171575.

415. Ahmed AA, Mills AD, Ibrahim AE, Temple J, Blenkiron C, Vias M, et al. The extracellular matrix protein TGFBI induces microtubule stabilization and sensitizes ovarian cancers to paclitaxel. Cancer Cell. 2007 Dec;12(6):514-27. PubMed PMID: 18068629.

416. Cheetham P, Petrylak DP. Tubulin-targeted agents including docetaxel and cabazitaxel. Cancer journal (Sudbury, Mass). 2013 Jan-Feb;19(1):59-65. PubMed PMID: 23337758.

417. English DP, Roque DM, Santin AD. Class III b-tubulin overexpression in gynecologic tumors: implications for the choice of microtubule targeted agents? Expert review of anticancer therapy. 2013 Jan;13(1):63-74. PubMed PMID: 23259428.

418. Karki R, Mariani M, Andreoli M, He S, Scambia G, Shahabi S, et al. betaIII-Tubulin: biomarker of taxane resistance or drug target? Expert opinion on therapeutic targets. 2013 Apr;17(4):461-72. PubMed PMID: 23379899.

419. Das V, Kanakkanthara A, Chan A, Miller JH. Potential role of tubulin tyrosine ligase-like enzymes in tumorigenesis and cancer cell resistance. Cancer Lett. 2014 Aug;350(1-2):1-4. PubMed PMID: 24814394.

420. Stengel C, Newman SP, Leese MP, Potter BV, Reed MJ, Purohit A. Class III beta-tubulin expression and in vitro resistance to microtubule targeting agents. Br J Cancer. 2010 Jan;102(2):316-24. PubMed PMID: 20029418.

421. Paradiso A, Mangia A, Chiriatti A, Tommasi S, Zito A, Latorre A, et al. Biomarkers predictive for clinical efficacy of taxol-based chemotherapy in advanced breast cancer. Ann Oncol. 2005 May;16 Suppl 4(1569-8041 (Electronic)):iv14-9. PubMed PMID: 15923415.

422. Tommasi S, Mangia A, Lacalamita R, Bellizzi A, Fedele V, Chiriatti A, et al. Cytoskeleton and paclitaxel sensitivity in breast cancer: the role of beta-tubulins. Int J Cancer. 2007 May;120(10):2078-85. PubMed PMID: 17285590.

423. Jung M, Koo JS, Moon YW, Park BW, Kim SI, Park S, et al. Overexpression of class III beta tubulin and amplified HER2 gene predict good response to paclitaxel and trastuzumab therapy. PLoS One. 2012 Sep;7(9):e45127. PubMed PMID: 23028798.

424. Wojcechowskyj JA, Lee JY, Seeholzer SH, Doms RW. Quantitative phosphoproteomics of CXCL12 (SDF-1) signaling. PLoS One. 2011 Sep;6(9):e24918. PubMed PMID: 21949786.

425. Honjo Y, Nangia-Makker P, Inohara H, Raz A. Down-regulation of galectin-3 suppresses tumorigenicity of human breast carcinoma cells. Clin Cancer Res. 2001 Mar;7(3):661-8. PubMed PMID: 11297262.

426. Liu F-T, Rabinovich GA. Galectins as modulators of tumour progression. Nat Rev Cancer. 2005 Jan;5(1):29-41.

427. Reticker-Flynn NE, Malta DF, Winslow MM, Lamar JM, Xu MJ, Underhill GH, et al. A combinatorial extracellular matrix platform identifies cell-extracellular matrix interactions that correlate with metastasis. Nature communications. 2012 Jul;3:1122. PubMed PMID: 23047680.

428. Andre F, Dieci MV, Dubsky P, Sotiriou C, Curigliano G, Denkert C, et al. Molecular pathways: involvement of immune pathways in the therapeutic response and outcome in breast cancer. Clin Cancer Res. 2013 Jan;19(1):28-33. PubMed PMID: 23258741.

429. Papp B, Brouland JP. Altered Endoplasmic Reticulum Calcium Pump Expression during Breast Tumorigenesis. Breast cancer : basic and clinical research. 2011 Jul;5:163-74. PubMed PMID: 21863130.

430. Davis FM, Parsonage MT, Cabot PJ, Parat MO, Thompson EW, Roberts-Thomson SJ, et al. Assessment of gene expression of intracellular calcium channels, pumps and exchangers with epidermal growth factor-induced epithelial-mesenchymal transition in a breast cancer cell line. Cancer cell international. 2013 Jul;13(1):76. PubMed PMID: 23890218.

431. Gori S, Sidoni A, Colozza M, Ferri I, Mameli MG, Fenocchio D, et al. EGFR, pMAPK, pAkt and PTEN status by immunohistochemistry: correlation with clinical outcome in HER2-positive metastatic breast cancer patients treated with trastuzumab. Ann Oncol. 2009 Apr;20(4):648-54. PubMed PMID: 19188134.

432. Brini M, Ottolini D, Cali T, Carafoli E. Calcium in health and disease. Interrelations between Essential Metal Ions and Human Diseases. Met Ions Life Sci. 13: John Wiley & Sons. Ltd.; 2013. p. 81-137.

433. Valabrega G, Montemurro F, Aglietta M. Trastuzumab: mechanism of action, resistance and future perspectives in HER2-overexpressing breast cancer. Ann Oncol. 2007 Jun;18(6):977-84. PubMed PMID: 17229773.

9 Appendix

9.1 Appendix 1 – Solutions

Nominal Calcium Solution (pH 7.2)	Concentration
NaCl	140 mmol/L
glucose	11.5 mmol/L
HEPES	10 mmol/L
KCl	5.9 mmol/L
$MgCl_2$	1.4mmol/L
NaH_2PO_4	1.2 mmol/L
$NaHCO_3$	5 mmol/L

PSS Solution (pH 7.2)	Concentration
NaCl	140 mmol/L
glucose	11.5 mmol/L
$CaCl_2$	1.8 mmol/L
HEPES	10 mmol/L
KCl	5.9 mmol/L
$MgCl_2$	1.4mmol/L
NaH_2PO_4	1.2 mmol/L
$NaHCO_3$	5 mmol/L

9.2 Appendix 2 – Single bar graph for each target

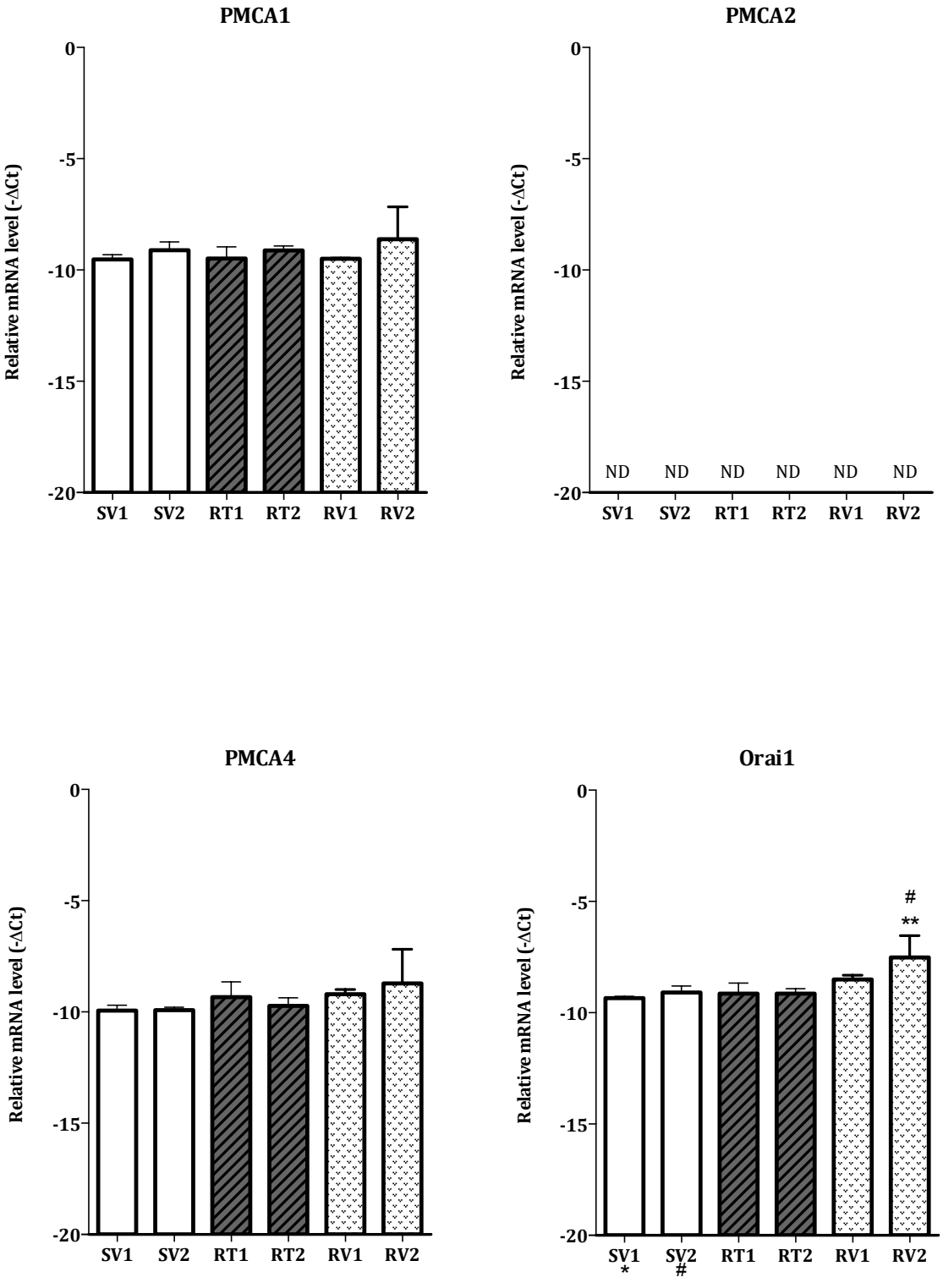

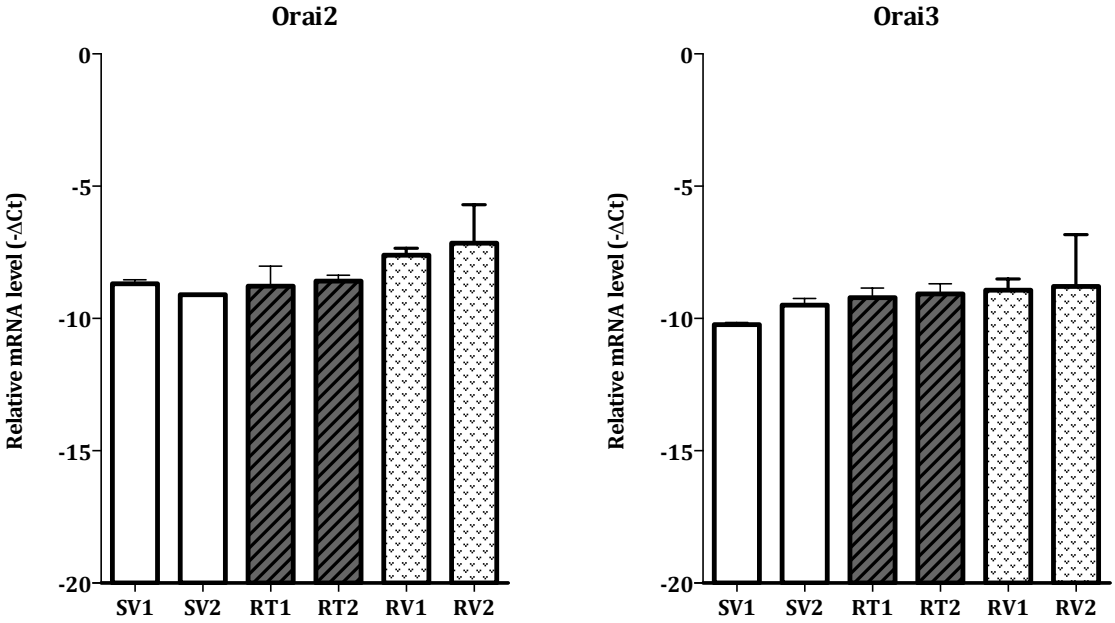
Orai2
Relative mRNA level (-ΔCt)
0
-5
-10
-15
-20
SV1
SV2
RT1
RT2
RV1
RV2

Orai3
Relative mRNA level (-ΔCt)
0
-5
-10
-15
-20
SV1
SV2
RT1
RT2
RV1
RV2

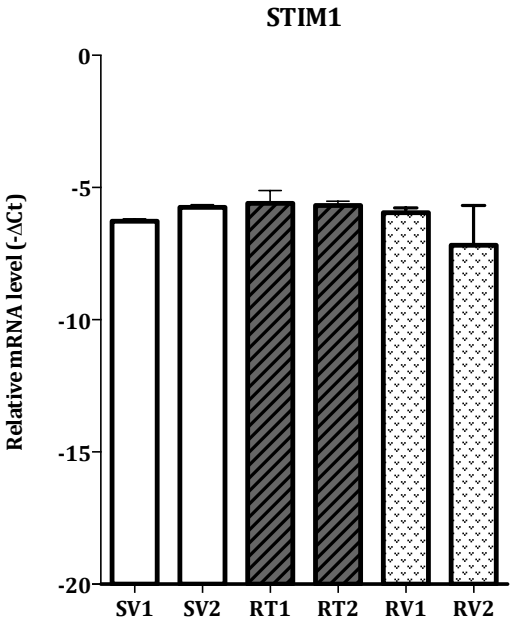
STIM1
Relative mRNA level (-ΔCt)
0
-5
-10
-15
-20
SV1
SV2
RT1
RT2
RV1
RV2

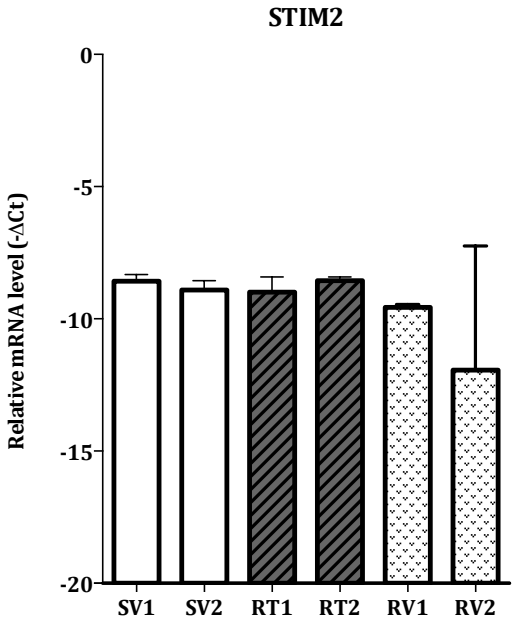
STIM2
Relative mRNA level (-ΔCt)
0
-5
-10
-15
-20
SV1
SV2
RT1
RT2
RV1
RV2

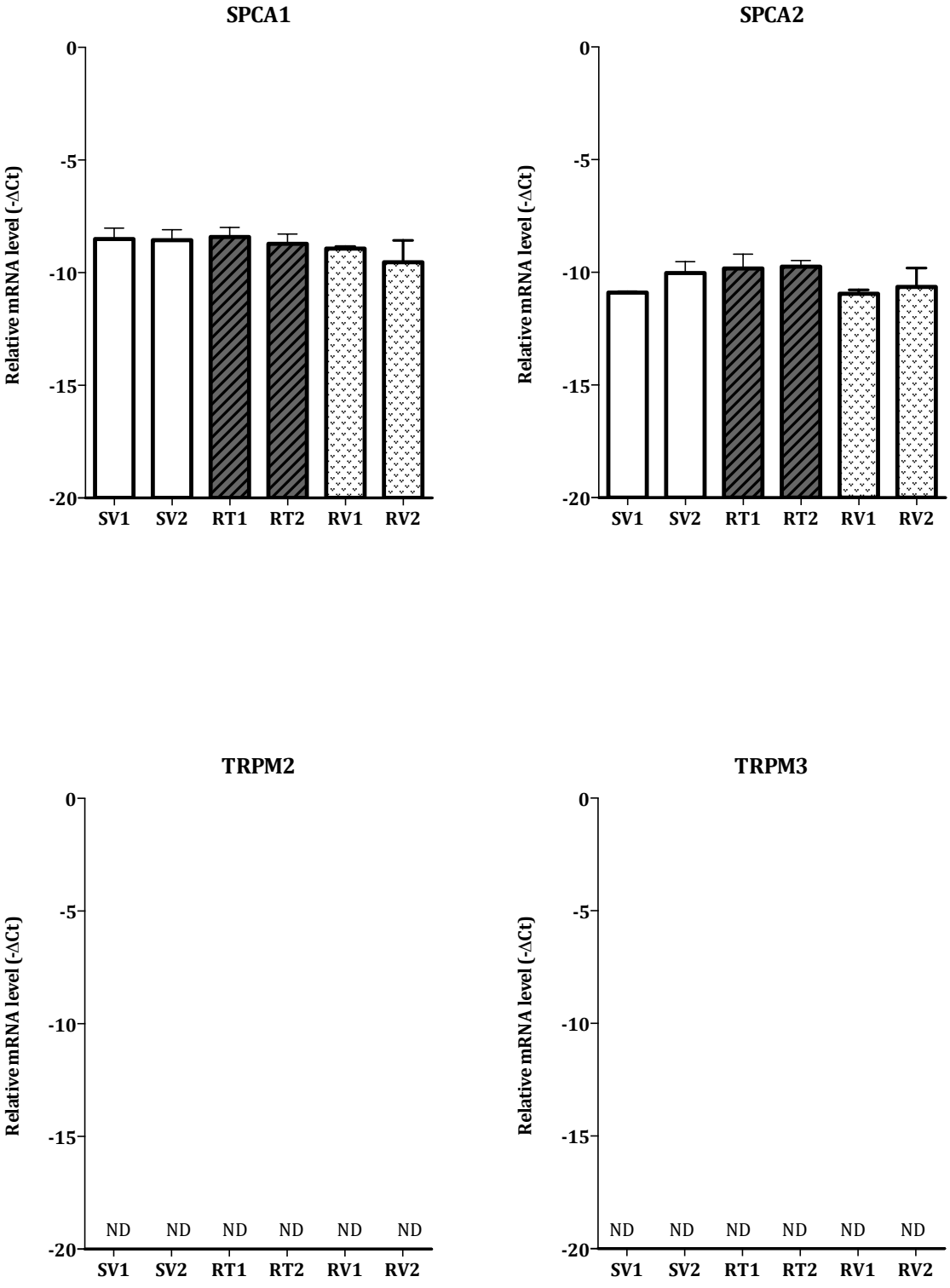
SPCA1
Relative mRNA level (-ΔCt)
0
-5
-10
-15
-20
SV1
SV2
RT1
RT2
RV1
RV2
SPCA2
Relative mRNA level (-ΔCt)
0
-5
-10
-15
-20
SV1
SV2
RT1
RT2
RV1
RV2
TRPM2
Relative mRNA level (-ΔCt)
0
-5
-10
-15
-20
ND
ND
ND
ND
ND
ND
SV1
SV2
RT1
RT2
RV1
RV2
TRPM3
Relative mRNA level (-ΔCt)
0
-5
-10
-15
-20
ND
ND
ND
ND
ND
ND
SV1
SV2
RT1
RT2
RV1
RV2

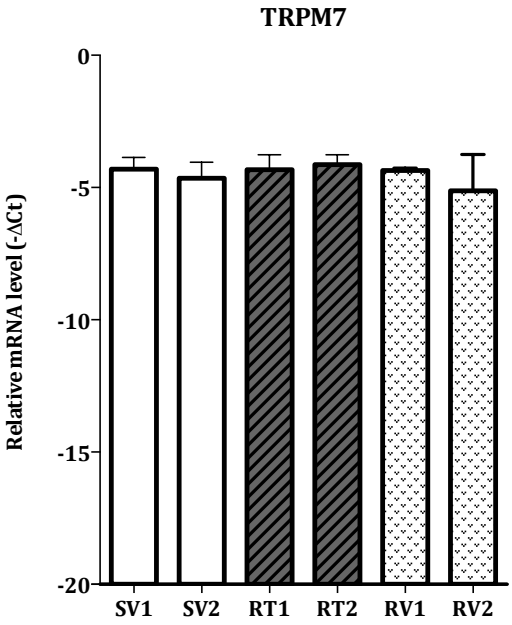
TRPM7
Relative mRNA level (-ΔCt)
0
-5
-10
-15
-20
SV1
SV2
RT1
RT2
RV1
RV2

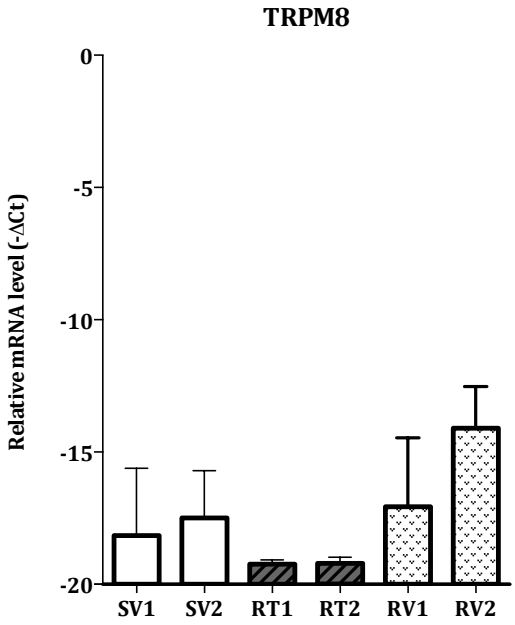
TRPM8
Relative mRNA level (-ΔCt)
0
-5
-10
-15
-20
SV1
SV2
RT1
RT2
RV1
RV2

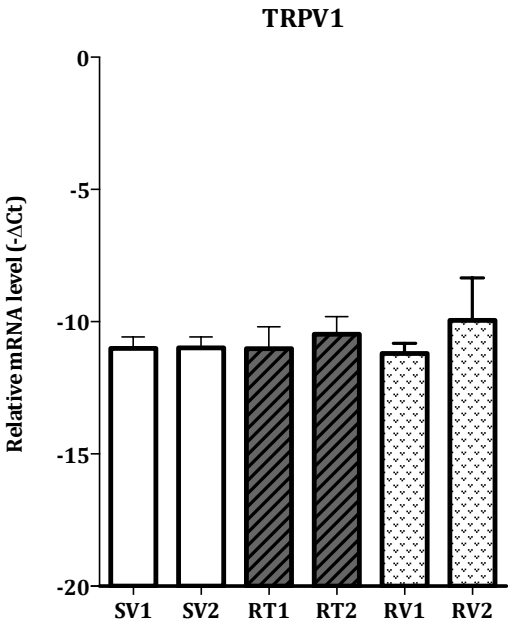
TRPV1
Relative mRNA level (-ΔCt)
0
-5
-10
-15
-20
SV1
SV2
RT1
RT2
RV1
RV2

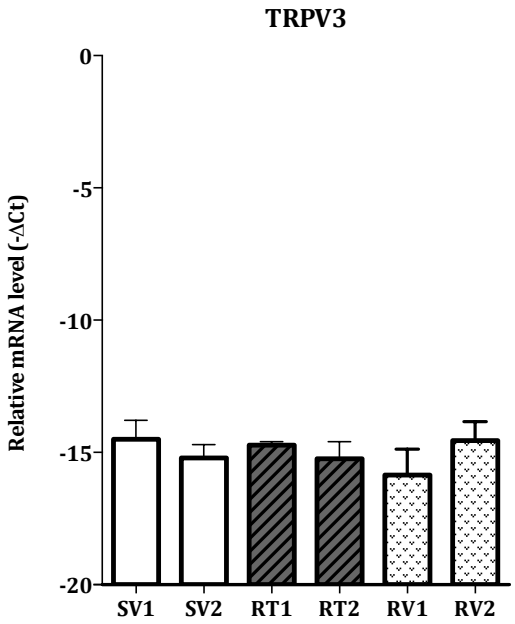
TRPV3
Relative mRNA level (-ΔCt)
0
-5
-10
-15
-20
SV1
SV2
RT1
RT2
RV1
RV2

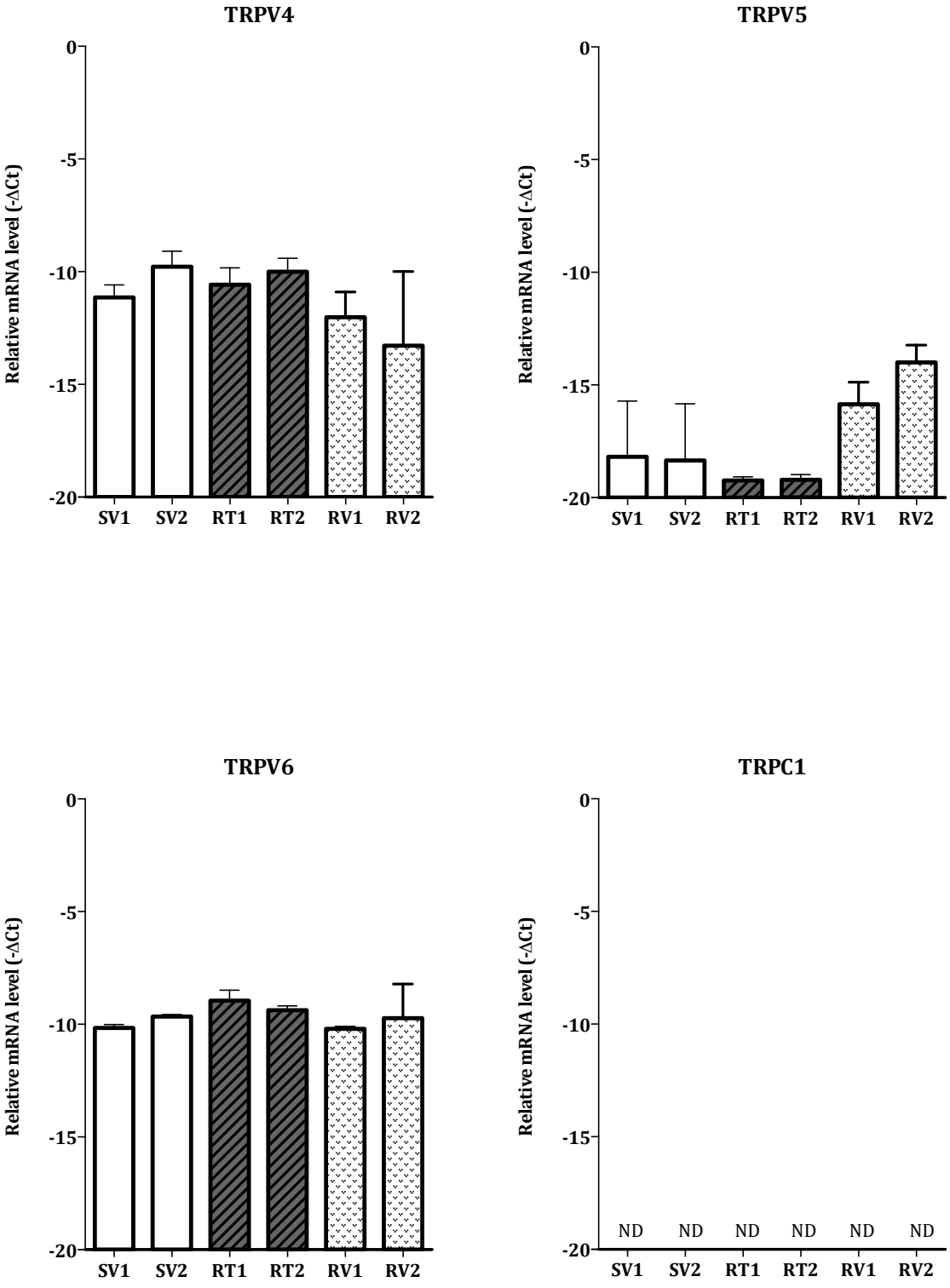
TRPV4
Relative mRNA level (-ΔCt)
0
-5
-10
-15
-20
SV1
SV2
RT1
RT2
RV1
RV2
TRPV5
Relative mRNA level (-ΔCt)
0
-5
-10
-15
-20
SV1
SV2
RT1
RT2
RV1
RV2
TRPV6
Relative mRNA level (-ΔCt)
0
-5
-10
-15
-20
SV1
SV2
RT1
RT2
RV1
RV2
TRPC1
Relative mRNA level (-ΔCt)
0
-5
-10
-15
-20
ND
ND
ND
ND
ND
ND
SV1
SV2
RT1
RT2
RV1
RV2

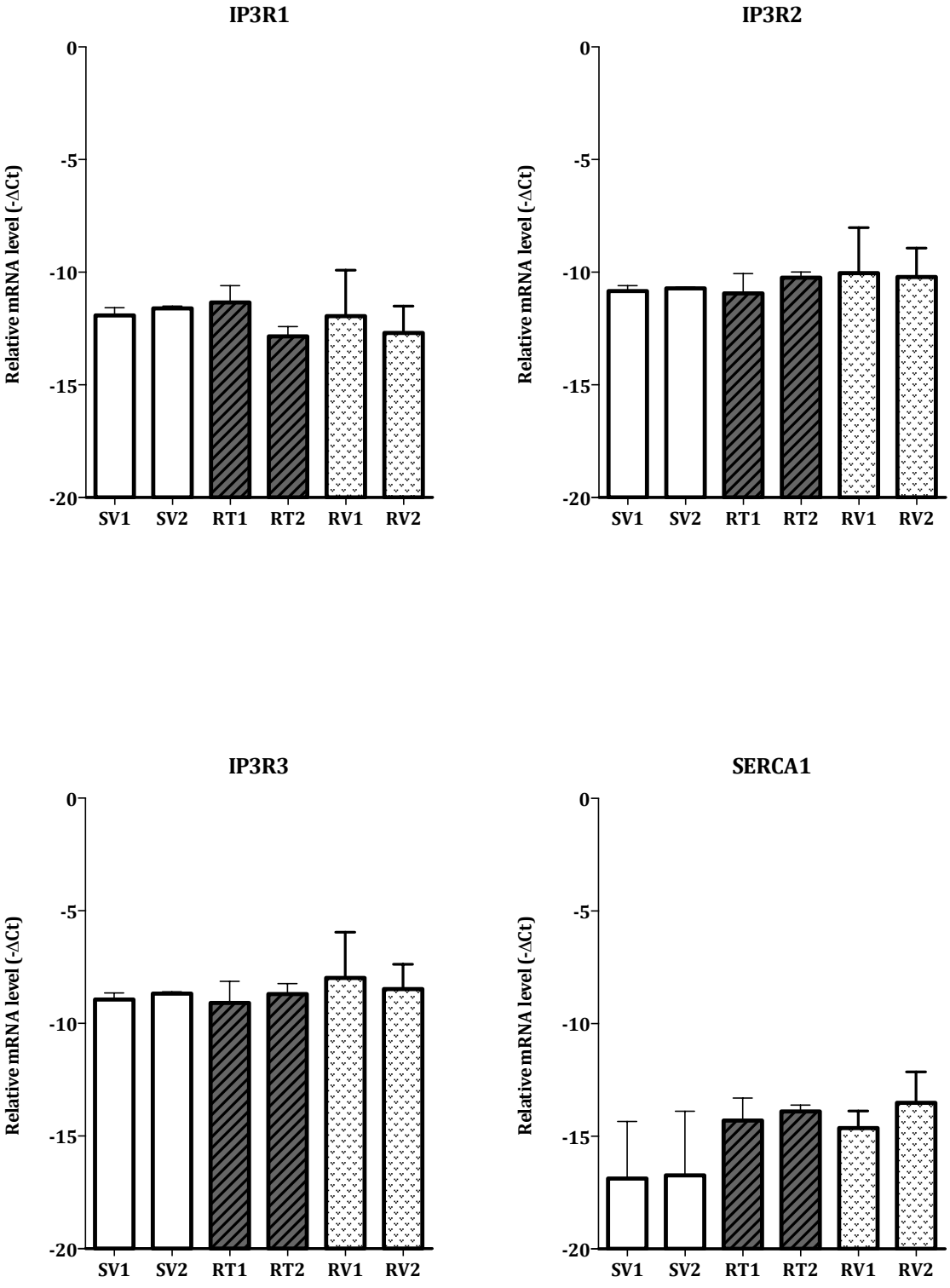
IP3R1
IP3R2
IP3R3
SERCA1
Relative mRNA level (-ΔCt)
0
-5
-10
-15
-20
SV1
SV2
RT1
RT2
RV1
RV2

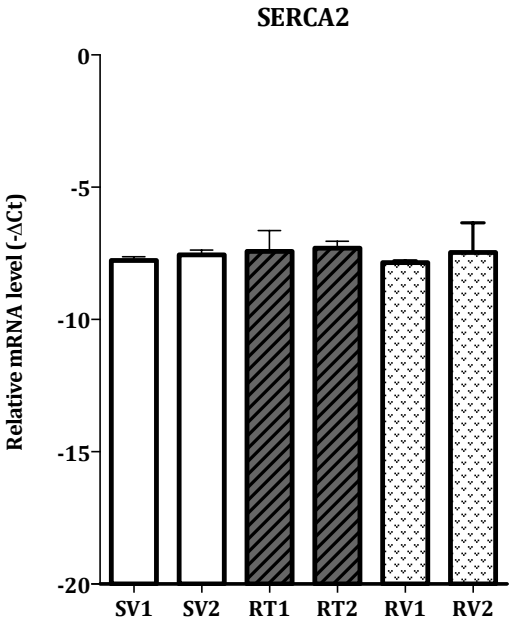
SERCA2
Relative mRNA level (-ΔCt)
0
-5
-10
-15
-20
SV1
SV2
RT1
RT2
RV1
RV2

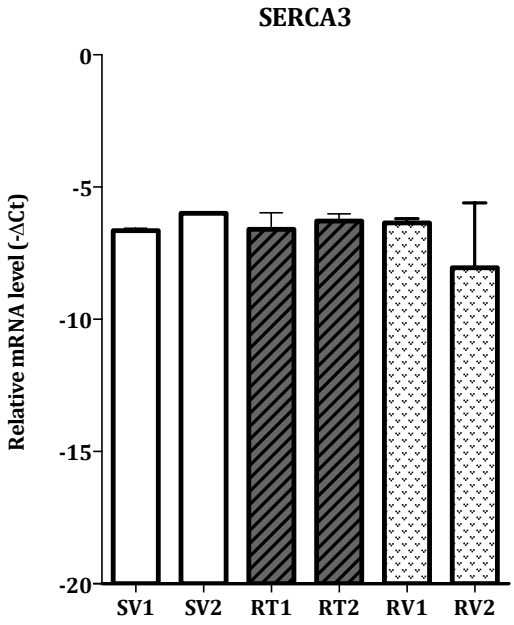
SERCA3
Relative mRNA level (-ΔCt)
0
-5
-10
-15
-20
SV1
SV2
RT1
RT2
RV1
RV2

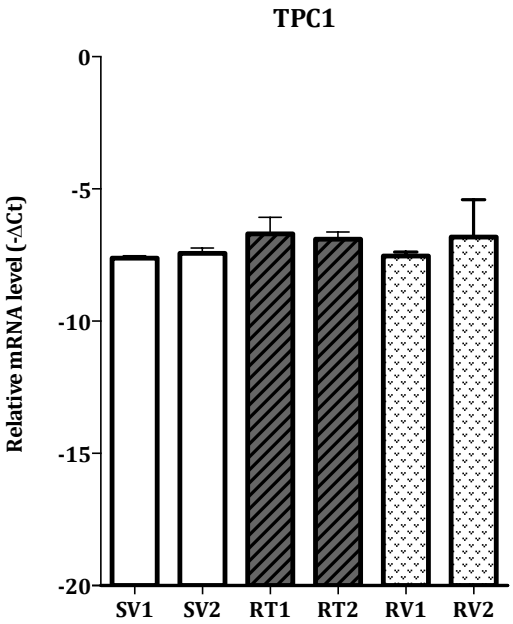
TPC1
Relative mRNA level (-ΔCt)
0
-5
-10
-15
-20
SV1
SV2
RT1
RT2
RV1
RV2

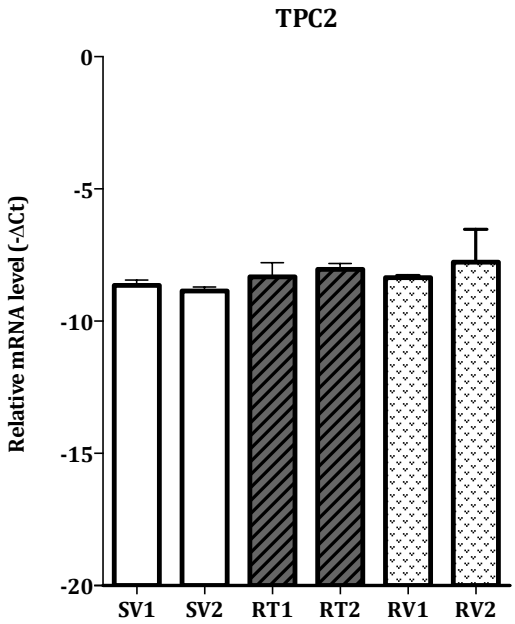
TPC2
Relative mRNA level (-ΔCt)
0
-5
-10
-15
-20
SV1
SV2
RT1
RT2
RV1
RV2

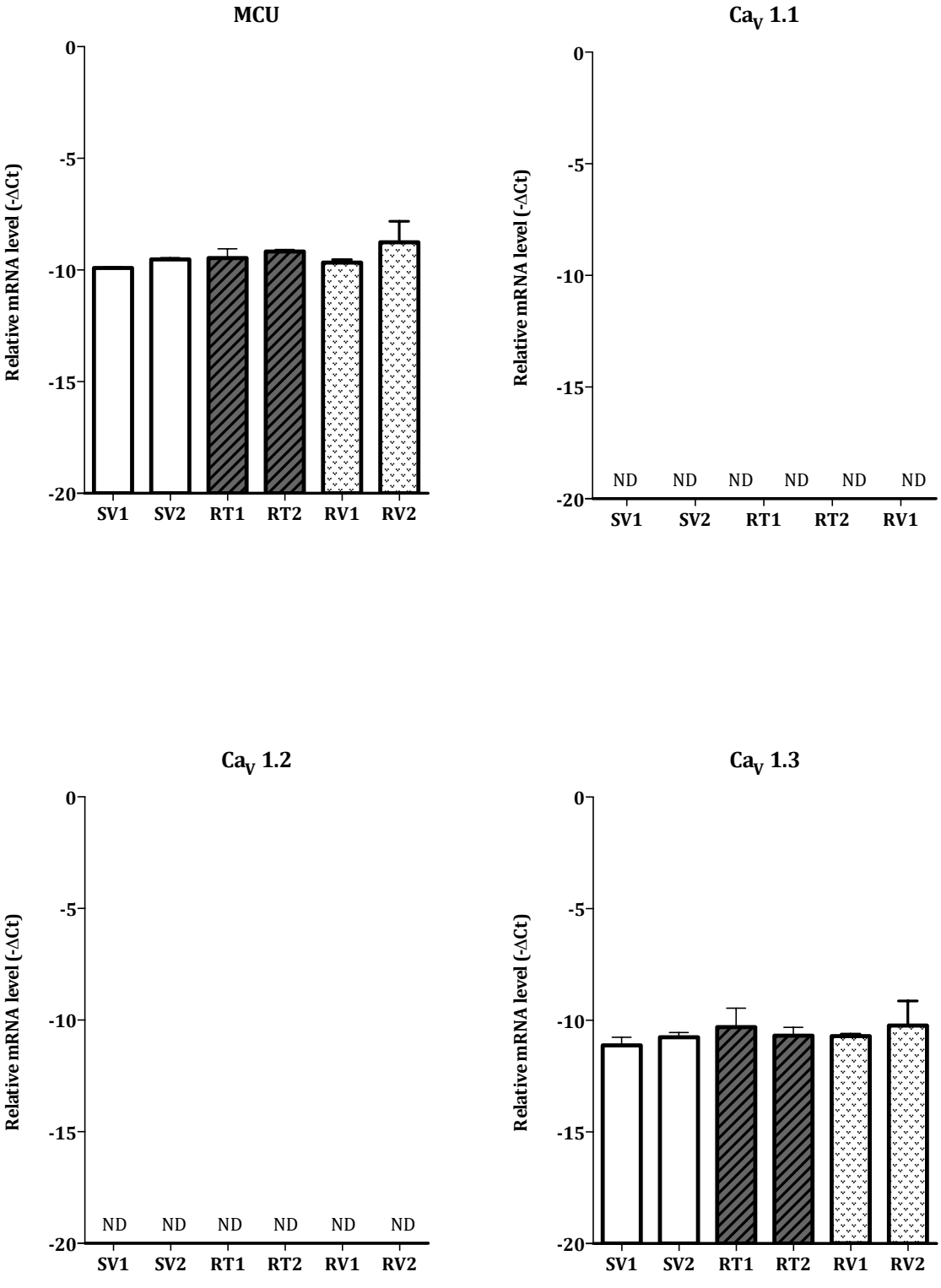
MCU
Relative mRNA level (-ΔCt)
0
-5
-10
-15
-20
SV1
SV2
RT1
RT2
RV1
RV2
Ca$_V$ 1.1
ND
ND
ND
ND
ND
ND
Ca$_V$ 1.2
ND
ND
ND
ND
ND
ND
Ca$_V$ 1.3

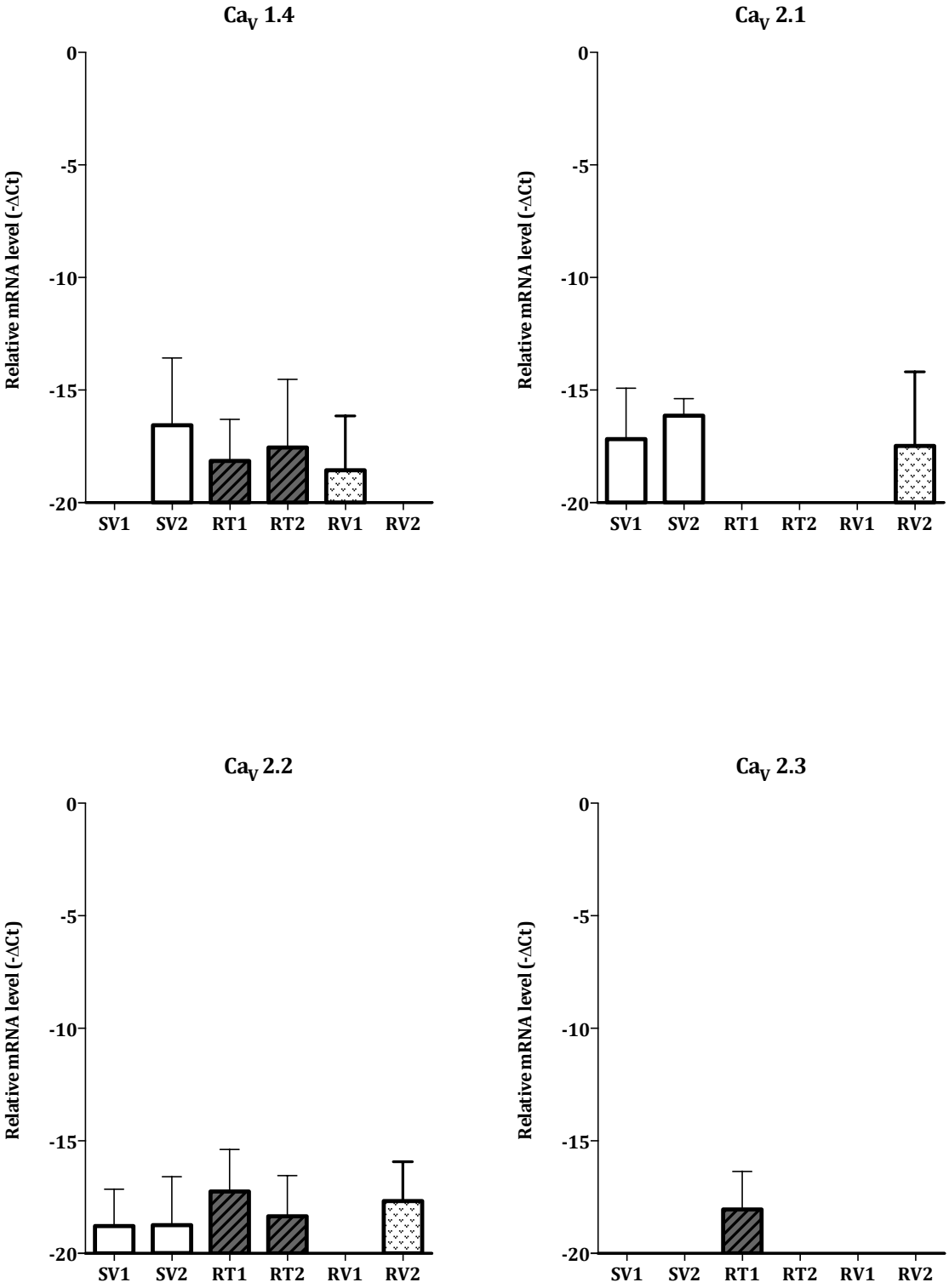
Ca_V 1.4
Ca_V 2.1
Ca_V 2.2
Ca_V 2.3
Relative mRNA level (-ΔCt)
0
-5
-10
-15
-20
SV1
SV2
RT1
RT2
RV1
RV2

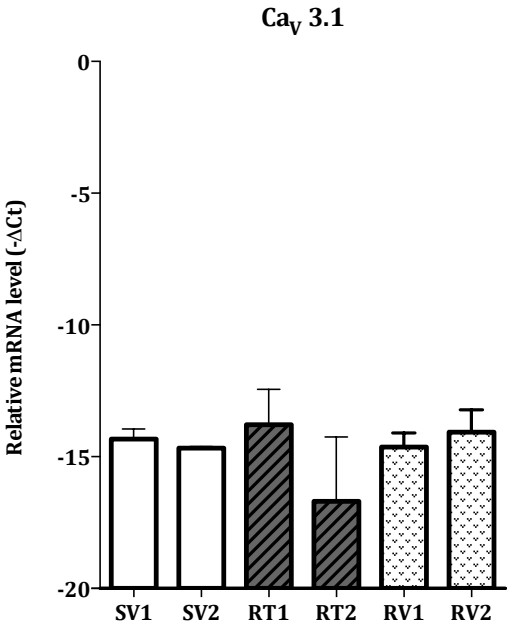
Ca_V 3.1
Relative mRNA level (-ΔCt)
0
-5
-10
-15
-20
SV1
SV2
RT1
RT2
RV1
RV2

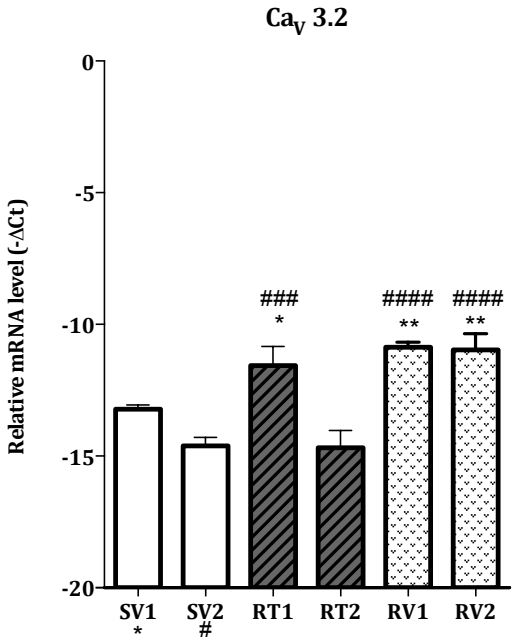
Ca_V 3.2
Relative mRNA level (-ΔCt)
0
-5
-10
-15
-20
###
*
####
**
####
**
SV1
*
SV2
#
RT1
RT2
RV1
RV2

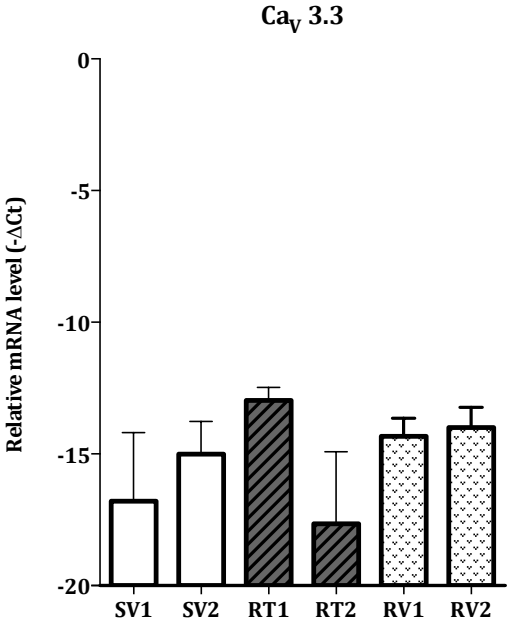
Ca_V 3.3
Relative mRNA level (-ΔCt)
0
-5
-10
-15
-20
SV1
SV2
RT1
RT2
RV1
RV2

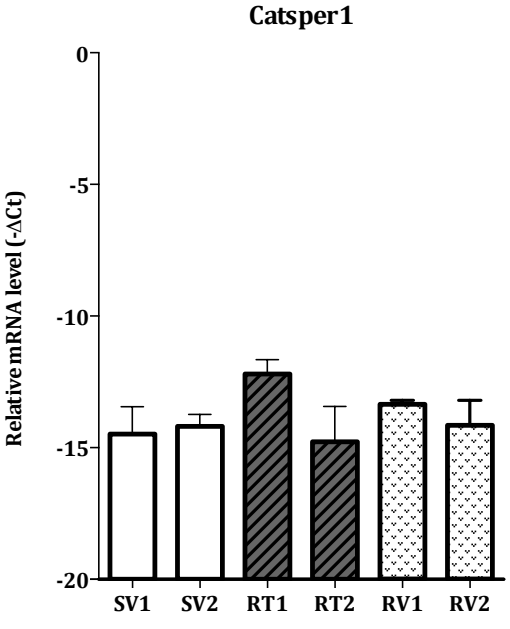
Catsper1
Relative mRNA level (-ΔCt)
0
-5
-10
-15
-20
SV1
SV2
RT1
RT2
RV1
RV2

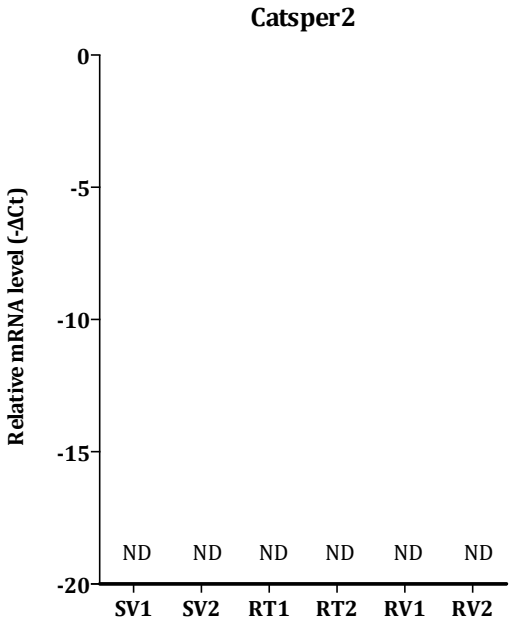
Catsper2
Relative mRNA level (-ΔCt)
0
-5
-10
-15
-20
ND ND ND ND ND ND
SV1 SV2 RT1 RT2 RV1 RV2

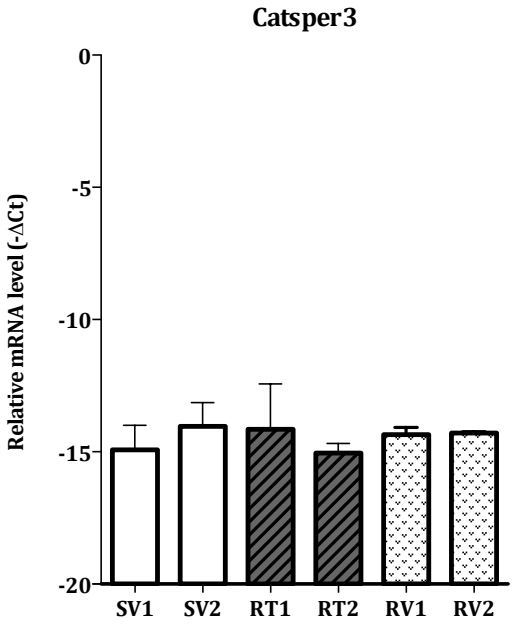
Catsper3
Relative mRNA level (-ΔCt)
0
-5
-10
-15
-20
SV1 SV2 RT1 RT2 RV1 RV2

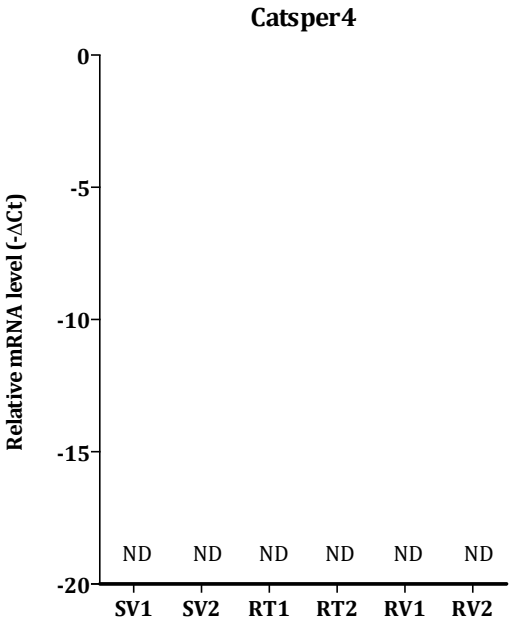
Catsper4
Relative mRNA level (-ΔCt)
0
-5
-10
-15
-20
ND ND ND ND ND ND
SV1 SV2 RT1 RT2 RV1 RV2

9.3 Appendix 3 – mRNA levels for each Ca^{2+} related genes assessed in this thesis

TARGET	SKBR3	SV1	SV2	RT1	RT2	RV1	RV2
HER2	nt	-2.726	-2.672	-2.817	-2.867	-2.816	-4.601
EGFR	nt	-9.909	-10.565	-9.581	-10.240	-11.949	-8.607
PMCA1	-7.397	-9.523	-9.107	-9.486	-9.123	-9.493	-8.618
PMCA2	nd	nd	nd	nd	nd	nd	nd
PMCA4	-8.567	-9.938	-9.918	-9.330	-9.723	-9.202	-8.715
Orai1	-10.059	-9.340	-9.087	-9.146	-9.139	-8.511	-7.516
Orai2	-13.918	-8.687	-9.100	-8.777	-8.584	-7.607	-7.157
Orai3	-12.788	-10.235	-9.496	-9.217	-9.070	-8.930	-8.783
STIM1	-11.101	-6.277	-5.748	-5.593	-5.684	-5.950	-7.180
STIM2	-14.010	-8.577	-8.905	-8.994	-8.558	-9.569	-11.941
SPCA1	-6.841	-8.506	-8.559	-8.416	-8.720	-8.931	-9.532
SPCA2	-7.648	-10.898	-10.029	-9.824	-9.751	-10.952	-10.649
TRPM2	nt	nd	nd	nd	nd	nd	nd
TRPM3	nt	nd	nd	nd	nd	nd	nd
TRPM7	-6.049	-4.305	-4.652	-4.327	-4.137	-4.360	-5.126
TRPM8	nt	-18.153	-17.494	-19.237	-19.220	-17.067	-14.095
TRPV1	-12.755	-11.014	-10.994	-11.021	-10.474	-11.205	-9.947
TRPV3	nt	-14.505	-15.206	-14.730	-15.242	-15.858	-14.549
TRPV4	-15.085	-11.145	-9.779	-10.574	-10.001	-12.018	-13.277
TRPV5	nt	-18.191	-18.353	-19.237	-19.220	-15.858	-13.995
TRPV6	-7.681	-10.165	-9.652	-8.953	-9.374	-10.199	-9.727
TRPC1	-16.072	nd	nd	nd	nd	nd	nd

IP3R1	nt	-11.916	-11.606	-11.342	-12.843	-11.949	-12.698
IP3R2	nt	-10.835	-10.719	-10.942	-10.243	-10.044	-10.208
IP3R3	nt	-8.939	-8.680	-9.091	-8.693	-7.977	-8.476
SERCA1	nt	-16.878	-16.734	-14.298	-13.894	-14.629	-13.510
SERCA2	nt	-7.774	-7.558	-7.429	-7.309	-7.845	-7.463
SERCA3	nt	-6.643	-5.987	-6.594	-6.287	-6.359	-8.055
TPC1	-9.229	-7.617	-7.432	-6.699	-6.903	-7.535	-6.819
TPC2	-12.738	-8.651	-8.854	-8.328	-8.040	-8.354	-7.767
MCU	nt	-9.909	-9.529	-9.469	-9.172	-9.663	-8.753
$Ca_V1.1$	nt	nd	nd	nd	nd	nd	nd
$Ca_V1.2$	nt	nd	nd	nd	nd	nd	nd
$Ca_V1.3$	nt	-11.123	-10.756	-10.300	-10.688	-10.716	-10.231
$Ca_V1.4$	nt	nd	-16.560	-18.147	-17.552	-18.559	nd
$Ca_V2.1$	nt	-17.177	-16.135	nd	nd	nd	-17.483
$Ca_V2.2$	nt	-18.781	-18.748	-17.248	-18.349	nd	-17.669
$Ca_V2.3$	nt	nd	nd	-18.047	nd	nd	nd
$Ca_V3.1$	nt	-14.332	-14.676	-13.781	-16.693	-14.630	-14.068
$Ca_V3.2$	nt	-13.222	-14.613	-11.563	-14.684	-10.867	-10.967
$Ca_V3.3$	nt	-16.790	-15.007	-12.969	-17.658	-14.332	-13.995
Catsper 1	nt	-14.483	-14.190	-12.202	-14.774	-13.363	-14.163
Catsper 2	nt	nd	nd	nd	nd	nd	nd
Catsper 3	nt	-14.923	-14.039	-14.148	-15.048	-14.355	-14.291
Catsper 4	nt	nd	nd	nd	nd	nd	nd

mRNA levels of all the Ca^{2+} related genes tested in the SKBR3 parental cell line, age-matched control and resistant cell lines in this thesis. The C_T values obtained for each target have been

normalized to a control gene, 18s rRNA. Data are shown as $-\Delta C_T$. The ΔC_T was calculated as the difference between the C_T value of the target and the 18s rRNA. A high $-\Delta C_T$ corresponds to an elevated mRNA level, while a low $-\Delta C_T$ to a low mRNA levels. (nt= not tested, nd= not detected).

9.4 Appendix 4 – Chemicals

Chemicals	Catalog Number	Suppliers
4',6-diamidino-2-phenylindole (DAPI)	D1306	Invitrogen
β-mercaptoethanol	M3148	Sigma Aldrich
Adenosine triphosphate (ATP)	A6419	Sigma Aldrich
BAPTA-AM	B6769	Invitrogen
BAPTA (tetra sodium)	B1214	Invitrogen
BioRad Coumassie Brilliant Blue based reagent	500-0006	BioRad Laboratories
Bovine serum albumin (BSA), essentially fatty-acid free (for FLIPR)	A3803	Sigma Aldrich
Bovine serum albumin (BSA), molecular grade	B4287	Sigma Aldrich
Calcium chloride (2H2O)	C7902	Sigma Aldrich
Cell titer 96 aqueous one solution cell proliferation assay	G5421	Promega
Click-iT® EdU Alexa Fluor 555 Imaging Kit	C10338	Invitrogen
Cyclopiazonic acid (CPA)	C1534	Sigma Aldrich
DharmaFECT 4 transfection reagent	T-2004-01	Dharmacon
Dimethyl sulfoxide (DMSO)	D8418	Sigma Aldrich
Distilled water (UltraPure, RNase/DNase free)	10977015	Invitrogen
EGTA-AM	E1219	Invitrogen
Epidermal growth factor (EGF)	E9644	Sigma Aldrich
Ethylenediamine tetraacetic acid (EDTA)	431788	Sigma Aldrich

Fetal bovine serum (FBS), batch number 7C0030	12003C	Sigma Aldrich
Fluo-4 AM	F14201	Invitrogen
Glucose powder	G7021	Sigma Aldrich
Goat serum	G9023	Sigma Aldrich
HEPES	H3375	Sigma Aldrich
iBlot gel transfer stacks PVDF regular	IB4010-01	Invitrogen
Magnesium chloride (anhydrous)	M8266	Sigma Aldrich
McCoy's A5 Modified media	1660	Invitrogen
Mibefradil	M5441	Sigma Aldrich
ML218	SML0385	Sigma Aldrich
MycoAlert Mycoplasma Detection kit	LT07-218	Lomb Scientific
NH125	3439	Tocris Bioscience
NS8593	N2538	Sigma Aldrich
NuPAGE 4-12% Bis-Tris gel	NP0321BOX	Invitrogen
NuPAGE antioxidant	NP0005	Invitrogen
NuPAGE LDS sample buffer (4X)	NP0007	Invitrogen
NuPAGE MOPS SDS running buffer (20X)	NP0001	Invitrogen
NuPAGE reducing agent	NP0004	Invitrogen
Omniscript RT kit	205113	Qiagen
PageRuler Plus prestained protein ladder	#26619	Thermo Fisher Scientific
Paraformaldehyde (16%)	15710	ProSciTech
Penicillin-streptomycin solution	15140	Invitrogen
Phosphate buffered saline (PBS)	P3813	Sigma Aldrich
PhosSTOP phosphatase inhibitor	04906845001	Roche

Potassium chloride	P5405	Sigma Aldrich
Protease inhibitor, complete mini	11836153	Roche
Random Primers	C1181	Promega
RNasin Ribonuclease inhibitor	N2111	Promega
RNeasy Plus mini kit	74104	Qiagen
siRNA buffer (5X)	B-002000-UB	Dharmacon
Sodium bicarbonate (NaHCO3)	S5761	Sigma Aldrich
Sodium chloride	S5886	Sigma Aldrich
SuperSignal west dura extended duration substrate	34076	Thermo Fisher Scientific
TaqMan FAST PCR master mix	4352042	Applied Biosystems
TaqMan universal PCR master mix	4324018	Applied Biosystems
Tris-HCl	T5941	Sigma Aldrich
Triton-X 100	T8787	Sigma Aldrich
Trypsin (0.25%)-EDTA (for cell culture)	25200	Invitrogen
Tween-20	P9416	Sigma Aldrich
96-well Cell-Bind (FLIPR) cell culture plates	3340	Corning
96-well clear, round-bottom (FLIPR) reagent plates	3797	Corning
96-well, FLIPR-TETRA black tips	90000762	Molecular Devices
96-well imaging grade (ImageXpress) plates	353219	BD Biosciences

9.5 Appendix 5 – Antibodies

Antibody	Catalog Number	Supplier
Anti-mouse horseradish peroxidase-conjugated secondary	170-6516	BioRad
Anti-rabbit horseradish peroxidase-conjugated secondary	170-6515	BioRad
β-Actin	AC-15	Sigma Aldrich
EGFR polyclonal rabbit (Tyr992)	#2232	Cell Signaling
HER2 polyclonal rabbit (Tyr1222)	#2242	Cell Signaling
IGF1R-β rabbit polyclonal (C-20)	sc-713	SantaCruz Technologies
IGF1R monoclonal XP® rabbit (IGF-I Receptor β, D23H3)	#9750	Cell Signaling

9.6 Appendix 6 – Gene expression assays

Gene name	Gene Expression ID
18s RNA (Control)	4319413E
Catsper 1	Hs00364950_m1
Catsper 2	Hs00542505_m1
Catsper 3	Hs00604374_m1
Catsper 4	Hs01374398_m1
$Ca_V1.1$	Hs00163885_m1
$Ca_V1.2$	Hs00167681_m1
$Ca_V1.3$	Hs01073321_m1
$Ca_V2.1$	Hs01579431_m1
$Ca_V2.2$	Hs01053090_m1
$Ca_V2.3$	Hs00167789_m1
$Ca_V3.1$	Hs00367969_m1
$Ca_V3.2$	Hs00234934_m1
$Ca_V3.3$	Hs00184168_m1
EGFR	Hs01076092_m1
HER2	Hs00170433_m1
IP3R1	Hs00181881_m1
IP3R2	Hs00181916_m1
IP3R3	Hs01573555_m1
MCU	Hs00293548_ml
Orai1	Hs00385627_m1
Orai2	Hs00259863_m1
Orai3	Hs00743683_s1

PMCA1	Hs00155949_m1
PMCA2	Hs00155975_m1
PMCA4	Hs00608066_m1
SERCA1	Hs01092295_m1
SERCA2	Hs00544877_m1
SERCA3	Hs00193090_m1
SPCA1	Hs00205122_m1
SPCA2	Hs00208296_m1
STIM1	Hs00162394_m1
STIM2	Hs00372712_m1
TPC1	Hs00330542_m1
TPC2	Hs01552063_m1
TRPC1	Hs01553152_m1
TRPM2	Hs01066085_m1
TRPM3	Hs00257553_m1
TRPM7	Hs00292383_m1
TRPM8	Hs00375481_m1
TRPV1	Hs00218912_m1
TRPV2	Hs00901640_m1
TRPV3	Hs00376854_ml
TRPV4	Hs01099348_m1
TRPV5	Hs00219765_m1
TRPV6	Hs00367960_m1

9.7 Appendix 7 – Dharmacon On Target Plus Pool siRNAs

Gene	Catalog number
$Ca_V3.2$	L-006128-00-0005
Non-targeting	D-001810-10-05
Orai1	L-014998-00-0005
Orai2	L-015012-00-0005
Orai3	L-015896-00-0005
PMCA1	L-006115-00-0005
PMCA4	L-006118-00-0005
SPCA1	L-006119-00-0005
SPCA2	L-006280-00-0005
STIM1	L-011785-00-0005
STIM2	L-013166-01-0005
TPC1	L-010710-00-0005
TPC2	L-006508-00-0005
TRPC1	L-004191-00-0005
TRPC4	L-006510-01-0003
TRPC5	L-006511-00-0003
TRPC6	L-004192-00-0003
TRPM6	L-005048-00-0003
TRPM7	L-005393-00-0003
TRPV1	L-006518-00-0005
TRPV4	L-005263-00-0003
TRPV6	L-003607-00-0005

9.8 Appendix 8 – Suppliers

Supplier	Address
Applied Biosystems (now Life Technologies)	30-32 Compark Circuit Mulgrave VIC 3170 AUSTRALIA
BD Biosciences (Becton, Dickinson and Company)	4 Research Park Drive Macquarie University Research Park North Ryde NSW 2113 AUSTRALIA
Bio-Rad Laboratories	446 Victoria Road Gladesville NSW 2111 AUSTRALIA
Genesearch	14 Technology Drive Arundel QLD 4214 AUSTRALIA
Invitrogen (now Life Technologies)	30-32 Compark Circuit Mulgrave VIC 3170 AUSTRALIA
Lomb Scientific (now Thermo Fisher Scientific)	5 Caribbean Drive Scoresby VIC 3179 AUSTRALIA
Millennium Science	PO BOX 49 Surrey Hills VIC 3027 AUSTRALIA
Molecular Devices Corporation	1311 Orleans Drive Sunnyvale CA 94089-1136 UNITED STATES OF AMERICA
Promega	75-85 O'Riordan Street Sydney Corporate Park Alexandria NSW 2015 AUSTRALIA
Qiagen	PO BOX 641

	Doncaster VIC 3108 AUSTRALIA
Quantum Scientific (now VWR International)	1/31 Archimedes Place Murarrie QLD 4172 AUSTRALIA
Roche Products	4-10 Inman Road Dee Why NSW 2099 AUSTRALIA
Sapphire Bioscience	126 Cope Street Waterloo NSW 2017 AUSTRALIA
Sigma Aldrich	PO BOX 970 Castle Hill NSW 1765 AUSTRALIA
Thermo Fisher Scientific	5 Caribbean Drive Scoresby VIC 2179 AUSTRALIA
Bio-Scientific	PO BOX 78 Gymnea NWS 2227 AUSTRALIA

9.9 Appendix 9 – Australian Distributors

Company	Australian Distributor
Abcam	Sapphire Bioscience
Cell Signaling	Genesearch
Corning	Sigma Aldrich
Dharmacon	Millennium Science
Santa Cruz	Quantum Scientific (now VWR International)
TPP	Lomb Scientific (now Thermo Fisher Scientific)
Tocris Bioscience	Bio-Scientific